Elucidating the role of the CCR4-NOT complex in miRNA-mediated gene silencing

Dissertation
der Mathematisch-Naturwissenschaftlichen Fakultät
der Eberhard Karls Universität Tübingen
zur Erlangung des Grades eines
Doktors der Naturwissenschaften
(Dr. rer. nat.)

vorgelegt von
Duygu Kuzuoğlu Öztürk
aus Istanbul

Tübingen
2015

Tag der mündlichen Qualifikation:	16.09.2015
Dekan:	Professor Dr. Wolfgang Rosenstiel
1. Berichterstatter:	Professor Dr. Elisa Izaurralde
2. Berichterstatter:	Professor Dr. Doron Rapaport

This thesis describes work conducted in Prof. Dr. Elisa Izaurralde's laboratory in the Department of Biochemistry at the Max Planck Institute for Developmental Biology, Tübingen, Germany from November 2010 to April 2015. It was further supervised by Prof. Dr. Doron Rapaport at the Eberhard Karls University Tübingen, Germany, and was supported by the International PhD program fellowship. I declare that this thesis is the product of my own work. The parts that have been published or where other sources had been used were cited accordingly. Work that was carried out by my colleagues was also indicated accordingly.

TABLE OF CONTENTS

ACKNOWLEDGEMENTS

A PhD program is not only about scientific progress. It is a life experience, which changed me deeply in many different aspects. The experiences and qualifications that I have gained during my doctoral studies would not be possible without help of colleagues and friends.

First of all, I would like to thank my supervisor Prof. Dr. Elisa Izaurralde for her infinite support and guidance during my studies. I am very grateful for her perfectionism, which pushed me only for the better. She was always supportive of my international travels to present my work, which were among the most important experiences I had during my studies. I also really appreciate all the time she has spent with me to go through the data, the presentations, the manuscripts and finally the thesis. Thank you for keeping your door open for everything!

I am very grateful to Prof. Dr. Doron Rapaport at Eberhard Karls University Tübingen for agreeing to be my supervisor. I would also like to thank the members of my PhD defense committee, Prof. Dr. Ralph Jansen and Dr. Adrian Streit.

I wish to thank Dr. Silke Hauf as a member of my advisor committee, whose support helped me especially in the beginning of my studies.

I would like to thank the PhD program coordinator Dr. Dagmar Sigurdardottir for her support from the day I came for the elections to the last day of my PhD.

I would like to thank all past and current members of Department II for the nice and friendly atmosphere. Specially, I am very grateful to Dr. Eric Huntzinger for his close supervision in the beginning of my PhD and collaboration in different projects. I have learned a lot from him. I want to express my deep gratitude to Dr. Catia Igreja, not only for the scientific discussions and suggestions but also for her precious friendship, which will always have a special place in my life. My special thanks goes to Dr. Oliver Weichenrieder for the discussions and his endless ideas. I would also like to thank all the lab members that I had chance to collaborate in different projects, namely, Dr. Praveen Bawankar, Dr. Dipankar Bhandari, Dr. Andreas Boland, Dr. Chung-Te Chang, Ying Chen, Dr. Stefanie Jonas, Tobias Raisch, Dr. Steffen Schmidt, Dr. Lara Wohlbold and Dr. Latifa Zekri. I also want to thank all the members of the lab, other than the ones that I have mentioned above, with whom I have shared memorable moments inside and outside of the lab, namely Annamaria Sgromo, Aoife

Hanet, Dr. Belinda Loh, Dr. Valentina Ahl, Dr. Anna Schneider, Dr. Natalia Bercovich, Dr. Joerg Braun, Dr. Tadashi Nishihara, Dr. Mary Christie, Dr. Elena Khazina. I would also like to thank Dr. Moritz Thran for his help on the German summary of the thesis.

My very special thanks go to our lovely technicians Maria Fauser and Sigrun Helms not only for their technical supports that immensely helped me in my projects, but also for their presence which truly felt like family. I also would like to thank Dr. Heike Budde for her endless support in every step of my PhD.

I also want to thank all my friends who live in different parts of the world. They always motivated and supported me during my PhD.

I would like to thank all my family for their support and unconditional faith. As we are a big family, it would not be possible to write out all the names, but I am very grateful to be a part of this family and I thank each of them for loving me and supporting me all the time, despite the physical distance.

I want to express my deepest gratitude to my husband, partner, friend, and love, Akın. I thank him for his unconditional support and willingness to take care of everything, without complaining a single day because I was late or because I had to do something in the lab. I believe that he earned this PhD as much as I did.

1A. SUMMARY

miRNAs are small non-coding RNAs involved in the regulation of almost all biological pathways in metazoans. miRNAs promote silencing of the mRNA targets by translational repression and mRNA degradation. They associate with Argonaute (AGO) proteins and bind to complementary mRNA targets. In animals, AGO interacts with GW182 family protein, which in turn recruits the main deadenylase complexes, the CCR4-NOT and PAN2-PAN3. These interactions trigger deadenylation which is followed by 5' decapping and finally by mRNA degradation.

GW182 proteins are essential for miRNA-mediated gene silencing. They are conserved in vertebrates and insects, and share a similar domain organization. By contrast, the *Caenorhabditis elegans* GW182 proteins, AIN-1 and AIN-2, are highly divergent and do not contain any identified domains. In the beginning of my doctoral studies, I investigated how *C. elegans* proteins mediate silencing and showed that only AIN-1, but not AIN-2, interacts with the deadenylases and poly(A)-binding protein (PABP). My studies demonstrated the evolutionary plasticity of GW182 proteins, which promote silencing via interaction with the deadenylase complexes and PABP across species. I used the information obtained from *C. elegans* proteins to design a functional GW182 protein, in order to understand the minimal requirements to mediate silencing. This study highlighted the importance of the CCR4-NOT complex and PABP for miRNA mediated translational repression and mRNA decay.

In order to understand the molecular mechanism of the CCR4-NOT complex in miRNA mediated gene silencing, I worked in collaborative projects where I first showed that the NOT module containing the NOT1,2,3 proteins, is required for the mRNA degradation mediated by the complex. Next, I demonstrated that GW182 proteins interact directly with CNOT9 (CAF40) subunit of the complex through two tryptophan-binding pockets. The collaborative structural project also revealed an uncharacterized direct interaction between the scaffold subunit of the complex, NOT1 and a DEAD-box helicase, DDX6, which functions as translational repressor and decapping activator. This interaction provides a direct link between deadenylation, decapping and translational repression.

Finally, I focused on the role of the CCR4-NOT complex in miRNA-mediated translational repression. Previous studies proposed that miRNAs inhibit translation

initiation by blocking ribosomal scanning through either the direct interaction between NOT1 and eIF4A2 or the displacement of eIF4A1 and eIF4A2 from the mRNA targets. By contrast, my studies demonstrated that miRNAs can repress translation independently of deadenylation and scanning. Moreover, I showed that DDX6, which is directly interacting with NOT1, is required for the translational repression activity of the CCR4-NOT complex. Overall, my studies placed the CCR4-NOT complex as a major effector complex in miRNA mediated gene silencing.

1B. ZUSAMMENFASSUNG

Mikro-RNAs sind kleine nicht-kodierende RNAs, die an der Regulation fast aller biologischen Prozesse in Metazoa beteiligt sind. Mikro-RNAs bewirken Gen-Silencing einer Ziel-mRNA entweder durch die Repression der Translation oder durch Degradation der Ziel-mRNA. Sie assoziieren mit Proteinen der Argonaut Familie (AGO) und binden an komplementäre Stellen in mRNAs. In tierischen Systemen interagiert AGO mit einem Protein der GW182 Familie, wodurch die Deadenylase-Komplexe CCR4-NOT und PAN2-PAN3 rekrutiert werden. Durch diese Interaktionen wird die Deadenylierung der mRNA ausgelöst worauf das Entfernen der 5‘ Kappe (5‘ CAP; auch als Decapping bezeichnet) folgt und letztlich die mRNA Degradation ermöglicht wird.

GW182 Proteine sind essentiell für das auf Mikro-RNA-basierende Gen-Silencing. Sie sind in Vertebraten und Insekten konserviert und besitzen eine ähnliche Organisation ihrer Proteindomänen. Im Gegensatz dazu sind die GW182 Proteine AIN-1 und AIN-2 aus *Caenorhabditis elegans* (*C. elegans*) sehr unterschiedlich. Zudem besitzen sie keine bislang identifizierte Proteindomäne.

Zu Beginn meiner Doktorarbeit untersuchte ich den Beitrag dieser Proteine aus *C. elegans* zu Gen-Silencing und beobachtete, dass nur AIN-1 mit Deadenylasen und dem Poly(A)-bindenden Protein (PABP) interagiert. Meine Untersuchungen demonstrierten eine evolutionäre Plastizität der GW182 Proteine, die Gen-Silencing durch diese Interaktionen artübergreifend fördern. Mithilfe, der aus diesen Daten, erworbenen Informationen konnte ich ein funktionales GW182 Protein entwerfen, um die minimalen Voraussetzungen für Gen-Silencing zu studieren. Meine Beobachtungen zeigten die Wichtigkeit des CCR4-Not-Komplexes und PABP für Mikro-RNA-basierende translationale Repression und mRNA Degradation.

Um die molekulare Grundlage für die Beteiligung des CCR4-NOT Komplexes am Mikro-RNA-basierenden Gen-Silencing zu verstehen arbeitete ich in verschiedenen kollaborativen Projekten. Zunächst konnte gezeigt werden, dass die Proteine NOT1, NOT2 und NOT3 ein NOT Modul bilden, das für die Degradation der mRNA durch den Komplex benötigt wird. Des Weiteren demonstrierte ich, dass GW182 Proteine direkt mit einer Untereinheit von NOT9 (auch als CAF40 bezeichnet) mittels zweier Tryptophan Bindetaschen interagieren. Darüber hinaus wurde in diesem strukturellem Projekt eine bislang unbekannte direkte Interaktion

zwischen dem Grundlage-Protein NOT1 und einer Helikase der DEAD-box Klasse, namens DDX6, beobachtet. Dieses Protein fungiert zum einen als Repressor der Translation und zum anderen als Aktivator des Decapping. Diese Interaktion ermöglicht eine Verbindung zwischen Deadenylierung, Decapping und translationale Repression.

Zuletzt fokussierte ich mich auf die Frage nach der Rolle des CCR4-NOT Komplexes in der, von Mikro-RNAs-vermittelten, translationalen Repression von mRNAs. In frühere Studien wurde vermutet, dass Mikro-RNAs das Scannen von Ribosomen blockieren. Dies sollte entweder durch eine direkte Interaktion zwischen NOT1 und dem eukaryotischen Initiationsfaktor A2 (eIF4A2) oder dem Verdrängen von den Faktoren eIF4A1 und eIFA2 von der Ziel-mRNA erfolgen. Im Gegensatz dazu ergaben meine Untersuchungen, dass die Repression unabhängig von Deadenylierung oder dem Scannen durch das Ribosom erfolgen kann. Außerdem konnte ich zeigen, dass DDX6, neben der direkten Interaktion mit NOT1, für die Repression der Translation durch den CCR4-NOT Komplex benötigt wird. Zusammenfassend konnte ich dem CCR4-NOT Komplex eine zentrale Bedeutung beim Mikro-RNA-basierenden Gen-Silencing in meinen Studien nachweisen.

2. INTRODUCTION

A messenger RNA (mRNA), which acts as an intermediate product between DNA and protein, is initially produced by transcription in the nucleus. Transcription is coupled with mRNA processing to produce a mature mRNA. mRNA processing includes 5'-end capping, splicing, 3'-end cleavage and polyadenylation. The mature mRNA is then exported to the cytoplasm where it associates with ribosomes to synthesize proteins and finally is degraded (Moore, 2005). There are other classes of RNAs, which do not code any protein but do have regulatory and modifying functions: the non-coding RNAs (ncRNA). The importance of ncRNAs is revealed by large scale transcriptome analyses showing that only ~1.2% of the human genome encodes proteins and 90% of disease-associated single nucleotide polymorphisms are located in the non-coding region of the human genome (Amaral et al., 2008; Hrdlickova et al., 2014). These numbers uncovered that the non-coding regions of the genome, also called as "junk DNA", are more important than previously anticipated. Several studies from various labs reported different regulatory functions for ncRNAs in almost all known species. Other than the known ncRNAs (transfer RNAs (tRNAs), ribosomal RNAs (rRNA), small nucleolar RNAs (snoRNAs) and small nuclear RNAs (snRNAs)), new classes of ncRNAs were also discovered during the last two decades. Their broad range of functions in gene regulation from transcription to translation also revealed their importance (Mattick and Makunin, 2006). The major ncRNAs classified according to their functions and sizes, are listed in Table 2.1.

The first microRNA (miRNA), lin-4, was characterized in *Caenorhabditis elegans* by Victor Ambros, Gary Ruvkun and their colleagues, while studying its key role in larval development in worms (Lee et al., 1993; Wightman et al., 1993). In 1998, the RNA interference mechanism was discovered by Andrew Fire, Craig Mello and their colleagues (Fire et al., 1998), who demonstrated that double-stranded RNA can induce gene silencing by base pairing with the target mRNA. A couple of years later, studies in plants and *Drosophila* cells showed that dsRNAs are cleaved to small-interfering RNAs (siRNAs) that mediate the recognition of the target mRNA to be silenced (Hamilton and Baulcombe, 1999; Hammond et al., 2000; Zamore et al., 2000). Meanwhile, another class of small RNAs present only in germ cells was discovered: the Piwi-interacting RNAs (piRNAs) (Kim, 2006; Aravin et al., 2007).

All these studies opened a new window in the RNA field and highlighted the importance of small RNAs in a very broad range of biological processes from cell proliferation to cell death (Bartel, 2004).

Table 2.1 Different classes of non-coding RNAs. Adapted from Cech and Steitz, 2014

Name	Definition	Function	Size
tRNA	Transfer RNA	Protein synthesis	70-90 nt
rRNA	Ribosomal RNA	Ribosome biogenesis	120, 160, 1868, 5025 nt in human
snRNA	Small nuclear RNA	Component of spliceosome	100-300 nt
snoRNA	Small nucleolar RNA	Pre-rRNA modification, processing and folding	70 nt
miRNA	Micro RNA	Gene silencing, translational repression and/or mRNA decay	22 nt
siRNA	Small interfering RNA	Gene silencing, mRNA decay	22 nt
piRNA	PIWI-associated RNA	Regulation of transcription, silencing of transposable elements	27 nt
lncRNA	Long non coding RNA	Various	>200 nt

2.1 microRNAs and their biogenesis

miRNAs are ~22 nucleotides long small RNAs encoded from introns or exons of non-coding or coding transcript units (Kim et al., 2009; Ha and Kim, 2014). Today, according to miRbase, there are more than 1800 miRNAs described in the human genome (Kozomara and Griffiths-Jones, 2014) and they are responsible for the regulation of more than 60% of all mammalian mRNAs (Friedman et al., 2009).

In general, miRNA genes are transcribed by RNA polymerase II into primary miRNA (pri-miRNA) (Cai et al., 2004; Lee et al., 2004), except some viral miRNAs transcribed by RNA polymerase III (Pfeffer et al., 2005). Consequently, pri-miRNAs have a 5' cap structure and a 3' poly(A) tail. They fold into 33-35 bp long stem loop structures and single stranded RNA segments at both 5' and 3' ends (Fig 2.1). The maturation of pri-miRNAs is initiated by the Microprocessor complex which consists

of an RNAse III-type endonuclease Drosha and its cofactor DGCR8 (DiGeorge syndrome critical region 8, Pasha in *Drosophila melanogaster*). Drosha contains two RNAse III domains (RIIIIDa and RIIIIDb), which cleave the 3' and 5' end of the pri-miRNA, respectively to a precursor miRNA (pre-miRNA) leaving a two nucleotides overhang at the 3' end (Blaszczyk et al., 2001; Han et al., 2004; Zhang et al., 2004). Drosha also contains a dsRNA binding domain (dsRBD) which interacts with the pri-miRNA. This interaction is also facilitated by the two dsRBDs of DGCR8 (Ha and Kim, 2014). Then, the pre-miRNA is exported by Exportin 5 (EXP5) from the nucleus to the cytoplasm for further maturation, in a GTP dependent manner (Yi et al., 2003; Bohnsack et al., 2004; Lund et al., 2004). EXP5 binds to the pre-miRNA and to the GTP-binding protein Ran-GTP to mediate the translocation of the pre-miRNA through the nuclear pore complex. GTP hydrolysis promotes dissociation of the complex and releases the pre-miRNA cargo, into the cytoplasm.

In the last step of maturation, the pre-miRNA binds the PAZ (PIWI-AGO-ZWILLE) domain of Dicer, another RNAse III endonuclease and is cleaved to produce the mature miRNA duplex (Bernstein et al., 2001; Grishok et al., 2001; Hutvágner et al., 2001; Ketting et al., 2001; Knight and Bass, 2001). Dicer associates with different dsRBD proteins involved in pre-miRNA processing. In *D. melanogaster*, Dicer-1 interacts with two isoforms of Loquacious (Loqs), Loq-PA and Loq-PB (Förstemann et al., 2005; Jiang et al., 2005; Saito et al., 2005). In human cells, Dicer binds to the trans-activation response RNA-binding protein, TRBP (a homologue of Loq-PB) (Chendrimada et al., 2005; Haase et al., 2005; Lee et al., 2006) and protein activator of PKR, PACT (Lee et al., 2006; 2013). Loqs and TRBP are important for Dicer cleavage site, they can tune the length of miRNAs (Fukunaga et al., 2012). Although the role of PACT is not completely understood, it acts together with TRBP on the production of miRNAs with different sizes (Lee et al., 2013).

Following the cleavage of the pre-miRNA, the miRNA duplex is first loaded onto an Argonaute (AGO) protein and then unwinded to form the RNA-induced silencing complex (RISC) (Kawamata and Tomari, 2010). The heat shock cognate 70 protein (HSC70)-heat shock protein 90 chaperone complex (HSP90) mediates the opening of AGO, in an ATP dependent manner, to provide a binding platform for the miRNA duplex. One strand of the miRNA duplex is then selected as the guide strand based on different criteria. According to the assymetry rule, the least thermodynamically stable strand at the 5' end, acts as the guide strand and the other

strand is degraded (Khvorova et al., 2003; Schwarz et al., 2003). Additionally, the strand containing uracil as the first nucleotide is also favored to be selected as guide strand (Lau et al., 2001; Czech et al., 2009; Hu et al., 2009; Okamura et al., 2009; Ghildiyal et al., 2010). Once the miRNA duplex is loaded onto AGO protein, the pre-RISC quickly removes the passenger strand. Since the miRNA duplex generally contains base pairing mismatches, the passenger strand can not be cleaved by AGO; instead it is removed (Ha and Kim, 2014) and quickly degraded by exonucleases from 5' to 3' (XRN1) or 3' to 5' (Exosome complex) (Rüegger and Großhans, 2012). The association with AGO protects miRNAs from degradation. miRNAs then recruit AGO to complementary mRNA targets to promote translational repression and mRNA degradation. The miRNA biogenesis is summarized in Fig 2.1.

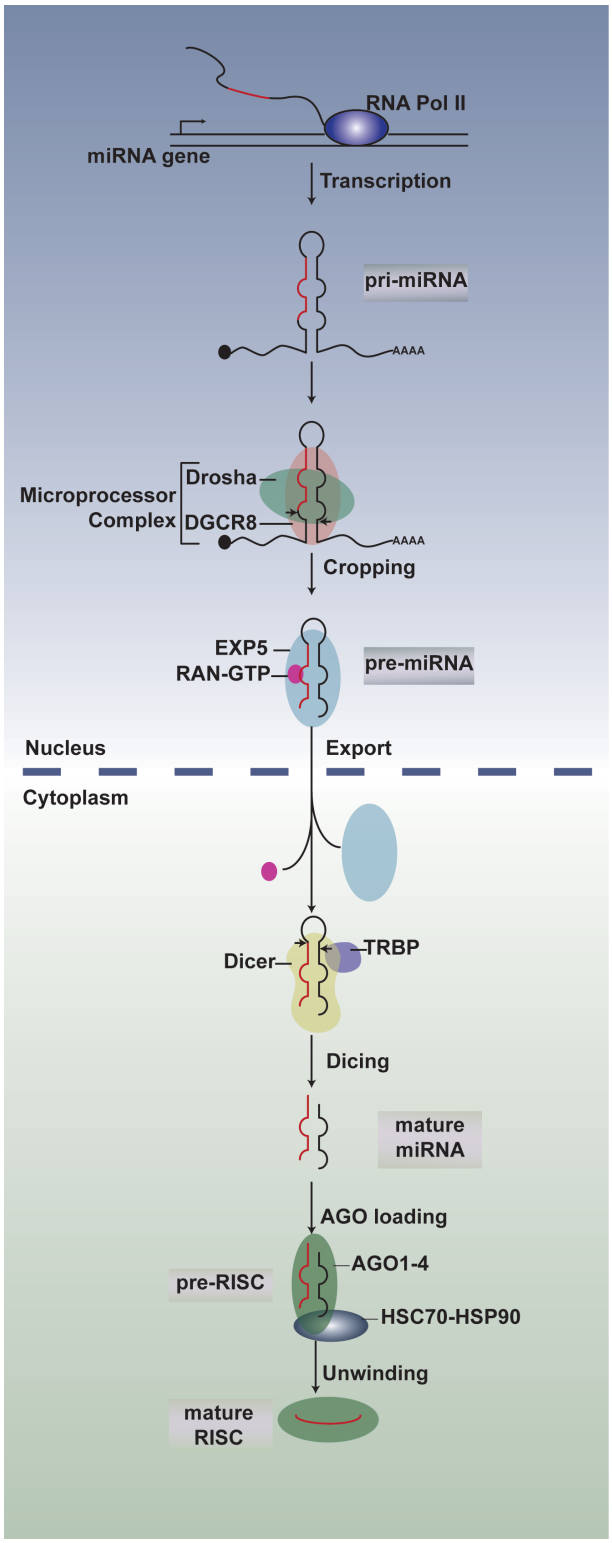

Figure 2.1 Schematic overview of miRNA biogenesis in humans. miRNAs are generally transcribed by RNA Polymerase II (RNA Pol II), processed by the Microprocessor complex (consisting of Drosha and DGCR8) and exported by Exportin 5 (EXP5) together with RAN-GTP. In the cytoplasm, the pre-miRNA is diced by Dicer, which associates with TRBP (TAR RNA-binding protein). The mature miRNA is then loaded onto AGO1-4, after the ATP hydrolysis by heat shock cognate 70 (HSC70)-heat shock protein 90 (HSP90) complex. After the release of the passenger strand, the guide miRNA (red) remains bound to the AGO protein as a member of mature RISC (RNA induced silencing complex). Modified from Ha and Kim, 2014.

2.2 miRNA target recognition

miRNAs recognize their target mRNAs by Watson-Crick base-pairing. In animals, in contrast to plants, miRNAs are generally not fully complementary to their targets. The "seed" region, including the 2-7 nucleotides (nt) from the 5' end of the miRNA, is sufficient to mediate silencing (Fig 2.2) (Huntzinger and Izaurralde, 2011).

In general, miRNAs bind to the 3' untranslated regions (3'UTRs) of the mRNA by complementarity to the seed sequence. The analyses of different types of miRNA target sites revealed that the seed sequence is crucial for binding to the target (Fig 2.2). Although the majority of miRNAs use the canonical 7-8 nt seed matched-sites, in some cases 6 nt complementarity is also enough to mediate miRNA binding (Bartel, 2009; Friedman et al., 2009). The context of the 3'UTR is important for miRNA silencing and the miRNA sites are more effective when located at least 15 nt downstream of the stop codon, to avoid the displacement by the ribosome, and are positioned away from the center of long UTRs (Bartel, 2009). Different studies showed that miRNAs can also bind to 5'UTRs, as well as to open reading frames (Kloosterman et al., 2004; Lytle et al., 2007).

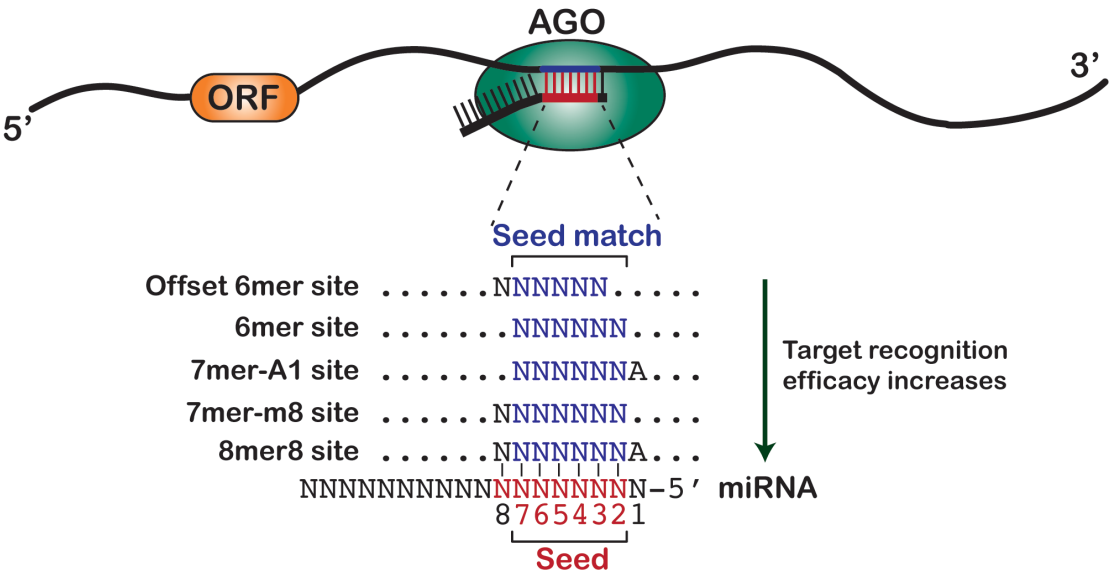

Figure 2.2 miRNA target recognition and seed matches. miRNAs generally target the 3' untranslated region, located downstream of the open reading frame (ORF). Except for the offset 6mer site, seed matches (blue) contain at least six Watson-Crick bases complementary to the miRNA seed (colored as red, nucleotides 2-7). The arrow indicates the increase in target recognition efficiency according to the complementarity. Modified from Friedman et al., 2009.

In the next sections, the key factors involved in miRNA-mediated gene silencing pathway will be described.

2.3 Argonaute Proteins

An Argonaute protein was originally described in a study performed in *Arabidopsis thaliana*. Since the phenotype of the mutant plant resembled a small squid, the corresponding gene was named after the octopus *Argonaute argo* (Bohmert et al., 1998). Further studies showed that the Argonaute proteins are highly conserved in prokaryotes and eukaryotes and can directly interact with small RNAs. The Argonaute family can be divided into two groups: AGO proteins (interacting with miRNAs and siRNAs) and PIWI proteins (interacting with piRNAs) (Meister, 2013). The number of AGO paralogs differs in each organism. In human, there are four AGO proteins, AGO1 to 4, which can function in miRNA-mediated gene silencing. Only AGO2 is catalytically active and can degrade the mRNA target by endonucleolytic cleavage (Liu et al., 2004; Song et al., 2004). In *C. elegans*, 27 different AGO proteins were identified, but only ALG-1 and ALG-2 are known to function in the miRNA pathway (Grishok et al., 2000; Yigit et al., 2006) and none of them has slicer activity (Tolia and Joshua-Tor, 2007). On the other hand, *D. melanogaster* contains two different AGOs, AGO1 and 2, both with slicer activity. However they play different roles: AGO1 is specific to miRNAs, whereas AGO2 to siRNAs (Höck and Meister, 2008).

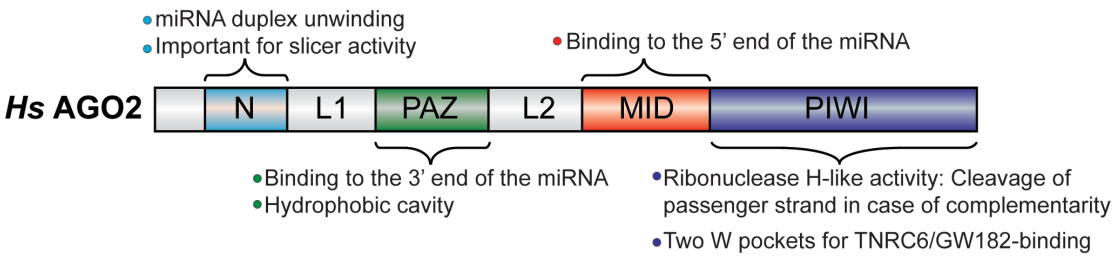

Figure 2.3 The domain organization of *Hs* AGO2. AGO2 contains four domains: N-terminal (N), PAZ (PIWI-ARGONAUTE-ZWILLE), MID and PIWI. L1 and L2 represent linker regions. The functional properties of each domain are summarized.

The AGO proteins are characterized by four structured domains (N, PAZ, MID, PIWI) connected by two linker regions (L1 and L2) (Song et al., 2004; Schirle and MacRae, 2012) (Fig 2.3). The N-terminal domain is critical for the miRNA duplex unwinding process. It was shown that after the loading of the RNA duplex, the N-terminal domain acts as a wedge to open the duplex in slicer-dependent or independent unwinding (Kwak and Tomari, 2012). Additionally, experiments performed with AGO3 protein fused to the N-terminal domain of AGO2 to become catalytically active, highlighted the role of the N-terminal domain in target cleavage (Faehnle et al., 2013; Hauptmann et al., 2013). The PAZ domain is responsible for nucleic acid binding. Structural studies revealed the presence of a specific binding pocket located in the PAZ domain which accomodates the 3' end of the small RNAs (Lingel et al., 2004; Ma et al., 2004; Wang et al., 2008) . The 5' end of the small RNA interacts with the basic nucleotide-binding pocket located in MID domain of AGO (Ma et al., 2005; Parker et al., 2005; Boland et al., 2010; Frank et al., 2010). The PIWI domain adopts a RNase H-like fold and is responsible for the slicing activity of AGOs (Song et al., 2004; Rivas et al., 2005; Nakanishi et al., 2012). It cleaves the target mRNA within the base-paired region opposite to nucleotides 10^{th} and 11^{th} from 5' end of the guide strand. The crystal structure of human AGO2 revealed the presence of two tryptophan-binding pockets in the PIWI domain, potentially important to mediate interaction with GW182 proteins (Schirle and MacRae, 2012).

2.4 GW182 Protein Family

Eystathioy and his colleagues identified GW182 proteins as antigens present in serum samples isolated from a patient affected by a motor and sensory neuropathy (Eystathioy et al., 2002). This protein is localized in cytoplasmic granules, known as GW-bodies or P-bodies. Subsequent studies demonstrated that the GW182 protein family interacts with AGO proteins and are essential for miRNA-mediated gene silencing (Ding et al., 2005; Jakymiw et al., 2005; Liu et al., 2005; Meister et al., 2005; Rehwinkel et al., 2005; Behm-Ansmant et al., 2006b).

GW182 proteins are a large family of proteins present in metazoans. Three paralogs, termed TNRC6A, TNRC6B and TNRC6C (trinucleotide repeat-containing gene protein 6) are present in vertebrates; one (GW182) in *D. melanogaster*, two

paralogs (AIN-1 and AIN-2) in *C. elegans* and none in fungi and plants (Huntzinger and Izaurralde, 2011). They are highly conserved in domain organization with the exception the *C. elegans* proteins (Fig 2.4).

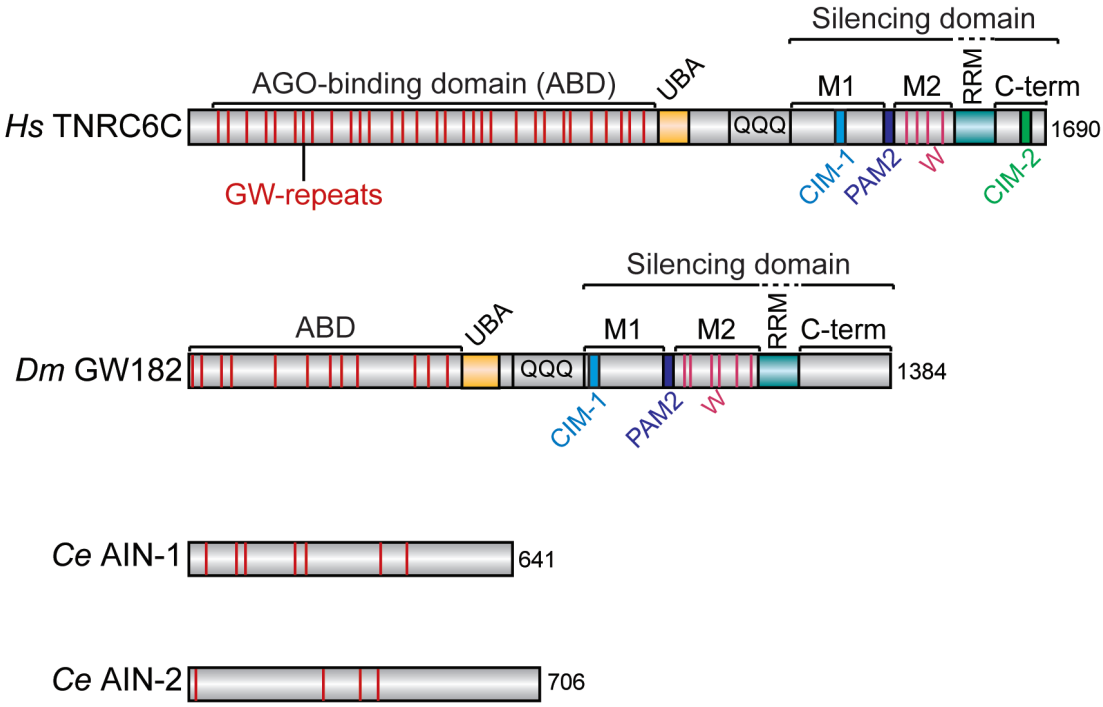

Figure 2.4 Domain organization of the GW182 protein family. GW182 proteins are highly conserved in animals. *H. sapiens* TNRC6C and *D. melanogaster* GW182 are shown as representative examples of the family. The structured domains, ubiquitin-associated (UBA) and RNA-recognition motif (RRM) are colored in yellow and green, respectively. The N-terminal part of the protein, the AGO-binding domain (ABD), contains several glycine-tryptophan (GW) repeats shown as red bars. The positions of the CCR4-interacting motifs (CIM-1 and CIM-2), the PABP-interacting motif 2 (PAM2) and tryptophan residues located in the M2 region (W) are indicated. *C. elegans* proteins, AIN-1 and AIN-2, do not contain any defined domains or motifs, except GW repeats shown as red bars. The numbers represent amino acid numbers. QQQ: glutamine-rich domain.

There are only two structured domains characterized in GW182 proteins: A central ubiquitin-associated (UBA) domain and an RNA recognition motif (RRM). The rest of the protein is predicted to be unstructured and contains several motifs, which are essential to mediate interactions with different binding partners (Braun et al., 2013). The N-terminal domain of GW182 proteins contains several glycine-tryptophan (GW) repeats, which mediate binding to AGOs and is termed the AGO-binding domain (ABD) (El-Shami et al., 2007; Till et al., 2007; Eulalio et al., 2009a; Lazzaretti et al., 2009; Takimoto et al., 2009). Additionally, the ABD is required for the localization of GW182 protein to P-bodies (Behm-Ansmant et al., 2006b; Eulalio et al., 2009a; Lazzaretti et al., 2009). The role of the UBA domain which was initially

identified in proteins involved in ubiquitination, is not clear and there is currently no evidence showing a contribution of this domain to gene silencing (Chekulaeva et al., 2009; Eulalio et al., 2009a; Lazzaretti et al., 2009; Zipprich et al., 2009). The Q-rich region is important for P-body localization in *D. melanogaster* (*Dm*) and human (*Hs*) cells; although the region itself is not sufficient for localization in P-bodies, its deletion prevents accumulation of GW182 proteins in P-bodies in *Dm* cells (Behm-Ansmant et al., 2006a; Eulalio et al., 2009a). The crystal structure of the RRM domain of *Dm* GW182 protein revealed an additional C-terminal α-helix that lies on the β-sheet surface which normally interacts with RNA in canonical RRMs. As such, binding to RNA by GW182 is unlikely to occur through the RRM domain (Eulalio et al., 2009c). Moreover the aromatic residues required for RNA binding are not present in this domain. Although deletion of the RRM domain has effects on some miRNA targets, in general this domain is not necessary for silencing and does not provide RNA binding activity (Eulalio et al., 2009c; Braun et al., 2013). The C-terminal region of GW182 proteins, termed the silencing domain (SD), is crucial for the silencing activity of the protein. Several studies showed that GW182 proteins lacking the SD are inactive in complementation assays, although they can still interact with AGOs. (Eulalio et al., 2009a; Zekri et al., 2009; Huntzinger et al., 2010). The SD acts as a binding platform for direct interactions with the poly(A)-binding protein (PABP) and mRNA deadenylases (Fabian et al., 2009; 2011; Zekri et al., 2009; Huntzinger et al., 2010; Jinek et al., 2010; Kozlov et al., 2010; Braun et al., 2011; Chekulaeva et al., 2011). In human cells, GW182 proteins directly interact with PABP through their PAM2 (PABP interacting motif 2) motif located between the M1 and M2 region of the SD (Jinek et al., 2010). Additionally to the PAM2 motif, M2 and C-terminal regions also contribute to the interaction with PABP in flies (Zekri et al., 2009; Huntzinger et al., 2010). Recent studies showed that tryptophan residues located in the SD mediate interactions with subunits of the CCR4-NOT and the PAN2-PAN3 deadenylase complexes. Two motifs, named as CCR4-NOT interacting motif 1 and 2 (CIM-1 and CIM-2) were identified in the SD of human GW182 proteins. In contrast to CIM-1, CIM-2 is not found in *Dm* GW182 (Fabian et al., 2011). Other tryptophan residues outside of the motifs also contribute to this interaction, as well as to the interaction with PAN2-PAN3 complex (Chekulaeva et al., 2011).

2.5 The CCR4-NOT Complex

The CCR4-NOT complex is a multi-subunit complex involved in the regulation of different steps of gene expression such as transcription, translation and mRNA decay. The complex was originally discovered as a transcription regulator; however further studies showed a role as the main mRNA deadenylase complex in different organisms (Collart and Panasenko, 2012; Wahle and Winkler, 2013; Chapat and Corbo, 2014). The conserved features of the complex are the NOT module (consisting of three subunits, NOT1, NOT2 and NOT3 proteins) and the catalytic module which contains two catalytically active proteins POP2 (CAF1) and CCR4. Additionally, CAF40 (NOT9, Rcd1 or RQCD1), CAF130, NOT4, NOT5, NOT10, NOT11 (C2orf29) and TAB182 are also subunits of the complex (Bawankar et al., 2013). The structured domains of each subunits, their conservation between species and their binding sites on NOT1 are summarized in Table 2.2.

Historically, the discovery of the CCR4-NOT complex starts with the characterization of NOT1 and NOT2 genes as CDC (Cell Division Cycle) genes (Reed, 1980). In 1984, another component, CCR4 (Carbon Catabolite Repressor 4), was identified, independently of the complex, as positive regulator of glucose-repressible enzymes in yeast (Denis, 1984). Eight years later, POP2 (PGK promoter directed over production) (Sakai et al., 1992) and one year after, NOT1,2,3 and 4 (Negative On TATA-less) proteins were identified as repressor of promoters lacking a canonical TATA box (Collart and Struhl, 1993; 1994) . It took three more years to understand that POP2 (CAF1, CCR4 associated factor 1) is in the same complex together with CCR4 (Draper et al., 1995). Finally in 1998, NOT proteins were discovered in the same complex with CCR4-CAF1 which was then named as the CCR4-NOT complex (Liu et al., 1998). Further studies showed the conservation of the complex in humans (Albert et al., 2000) and flies (Temme et al., 2004).

Table 2.2 The subunits of the CCR4-NOT complex. Adapted from Chapat and Corbo, 2014.

S. cerevisiae	*H. sapiens*	*D. melanogaster*	Domains	Binding sites on NOT1	References
NOT1	CNOT1	NOT1	Heat repeats MIF4G		(Maillet et al., 2000; Basquin et al., 2012; Petit et al., 2012)
NOT2	CNOT2	NOT2	Not-box	C-term of NOT1	(Zwartjes et al., 2004)
NOT3	CNOT3/5	NOT3/5	Not-box	C-term of NOT1	(Zwartjes et al., 2004)
NOT4	CNOT4	NOT4	RING E3 ligase		(Hanzawa et al., 2001; Albert et al., 2002)
NOT5	-	-	Not-box	C-term of NOT1	(Maillet et al., 2000)
CCR4	CNOT6/ CCR4a CNOT6L/ CCR4b	CCR4	EEP, LRR	POP2	(Malvar et al., 1992; Draper et al., 1995; Dupressoir et al., 2001;)
POP2/ CAF1	CNOT7/ CAF1a CNOT8/ POP2/ CAF1b	CAF1	DEDD	MIF4G domain of NOT1	(Bai et al., 1999; Schwede et al., 2008)
CAF40	CNOT9/ Rcd1/ RQCD1	CAF40	Armadillo Repeats	Mid part of NOT1	(Chen et al., 2001)
CAF130	-	-		N- and C-term of NOT1	(Chen et al., 2001)
-	CNOT10	NOT10		N-term of NOT1 and NOT11	(Bawankar et al., 2013; Mauxion et al., 2013)
-	CNOT11 (C2orf29)	NOT11		N-term of NOT1	(Lau et al., 2009; Bawankar et al., 2013; Mauxion et al., 2013)
-	TAB182	-			(Lau et al., 2009)

The CCR4-NOT complex was originally thought to be important only for transcription, until the discovery of its role as the major deadenylase complex in 2001 (Tucker et al., 2001). It was shown that CCR4-NOT can catalyze the removal of the poly(A) tail of the mRNA, the first step of bulk mRNA degradation. CCR4 and CAF1 (POP2) were identified as the catalytic subunits of the complex (Chen et al., 2002; Tucker et al., 2002; Thore et al., 2003). The experiments performed in yeast knock-out strains demonstrated that poly(A) tail length generally increases in the absence of CCR4 and CAF1 (Tucker et al., 2002). In addition to its role in deadenylation, the CCR4-NOT complex was also shown to be involved in nuclear quality control (Azzouz et al., 2009; Assenholt et al., 2011) and to be part of the mRNA export machinery (Kerr et al., 2011).

The importance of the CCR4-NOT complex in gene expression was further underlined with the discovery of its involvement in the miRNA pathway. Following the studies showing that miRNAs promote deadenylation of the mRNA target, the CCR4-NOT complex was demonstrated to be required for miRNA-mediated mRNA decay (Behm-Ansmant et al., 2006b; Giraldez et al., 2006; Eulalio et al., 2009b; Fabian et al., 2009) . However, it was not clear how it was recruited to miRNA targets until three independent studies reported the direct interaction between GW182 proteins and the CCR4-NOT complex (Braun et al., 2011; Chekulaeva et al., 2011; Fabian et al., 2011). In the mean time, several studies showed the role of the complex in translational repression independently of its deadenylation activity (Chekulaeva et al., 2009; Cooke et al., 2010; Bawankar et al., 2013). Overall, in the last decade, several studies were performed to elucidate the function and the assembly of the CCR4-NOT complex. The papers published after 2011 will be discussed in “Results&Discussion” section in the context of the thesis.

The major studies in the history of the CCR4-NOT complex are summarized in Fig 2.5.

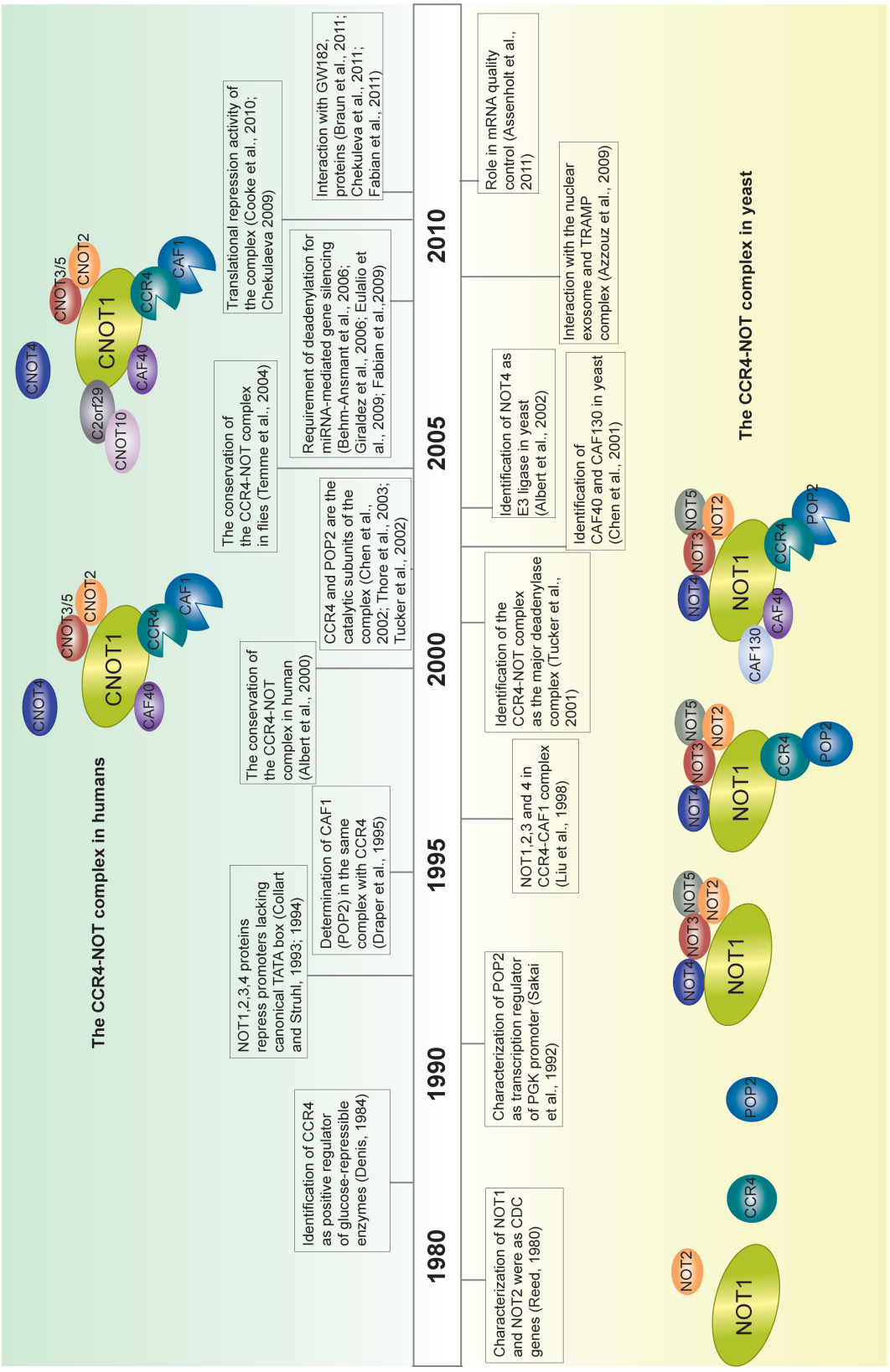

Figure 2.5 The history of the CCR4-NOT complex. The important studies from 1980 to 2011 are summarized. The positions of the papers and the cartoons correlate.

2.6 Translational Repression and mRNA degradation by miRNAs

miRNAs silence mRNA targets by promoting translational repression and mRNA degradation. Several studies provided evidence for the role of miRNAs on these two effects at a genome-wide level (Bagga et al., 2005; Farh et al., 2005; Lim et al., 2005; Wu and Belasco, 2005; Baek et al., 2008; Selbach et al., 2008; Hendrickson et al., 2009; Guo et al., 2010).

High throughput analyses demonstrated that miRNAs silence their target predominantly at the mRNA level (Selbach et al., 2008; Guo et al., 2010). miRNAs promote mRNA deadenylation through recruitment of the main deadenylase complex, the CCR4-NOT complex (Behm-Ansmant et al., 2006b; Wu et al., 2006; Chen et al., 2009; Piao et al., 2010). Following deadenylation, miRNAs promote 5' to 3' decay. Accordingly, miRNA targets are first deadenylated, then decapped by the decapping complex and finally degraded by the XRN1 exonuclease (Fig 2.6) (Rehwinkel et al., 2005; Eulalio et al., 2007; 2009b; Chen et al., 2009; Piao et al., 2010). Deadenylation occurs through the consecutive and partially redundant action of two deadenylase complexes: CCR4-NOT and PAN2-PAN3. Although depletion of PAN2-PAN3 complex does not have a general effect on miRNA-mediated mRNA decay (Braun et al., 2011), it is thought that PAN2-PAN3 complex initiates the deadenylation process which is then completed by the CCR4-NOT complex (Yamashita et al., 2005; Wahle and Winkler, 2013). Decapping, the removal of 5' cap by the decapping complex, follows deadenylation. The function of the catalytically active subunit of the complex, DCP2, is enhanced by additional proteins: DCP1, EDC3, EDC4 and DDX6 (Jonas and Izaurralde, 2013). Finally, the deadenylated and decapped miRNA target is degraded by the 5' to 3' exonuclease XRN1 (Huntzinger and Izaurralde, 2011). In 2011, it was shown that GW182 proteins are responsible for the direct recruitment of the CCR4-NOT and PAN2-PAN3 deadenylase complexes to promote mRNA deadenylation (Braun et al., 2011; Chekulaeva et al., 2011; Fabian et al., 2011). This observation demonstrated the main function of GW182 proteins as scaffold protein in the miRNA pathway.

In contrast to the general agreement about how miRNAs degrade their targets, the mechanism by which miRNAs repress translation is under debate. Several conflicting models have been proposed. These models involve inhibiting the initiation

or post-initiation steps of translation. (Eulalio et al., 2008; Huntzinger and Izaurralde, 2011; Fabian and Sonenberg, 2012).

Early studies performed in *C. elegans* showed that miRNAs repress translation at the elongation step, with negligible effect on mRNA levels (Olsen and Ambros, 1999; Seggerson et al., 2002). Studies using mammalian cultured cells have also confirmed this observation (Maroney et al., 2006; Nottrott et al., 2006; Petersen et al., 2006). All these studies demonstrated that miRNA targets associate with polysomes when cell lysates are fractionated through sucrose gradients. Moreover, the use of different translation inhibitors provided additional evidence showing that miRISC targets actively translated mRNAs (Maroney et al., 2006; Nottrott et al., 2006; Petersen et al., 2006). The data proposing active translation during miRNA targeting prompted the hypothesis of co-translational degradation of the nascent polypeptide chain (Nottrott et al., 2006). However, the protease responsible for the degradation of the polypeptide chain was not identified and more importantly, proteasome inhibitors do not have any effect on silencing.

Despite the studies proposing that miRNAs inhibit translation elongation, other studies indicated that miRNAs repress translation at the initiation step. These studies performed in mammalian cells and in cell-free extracts, showed that mRNAs targeted by miRNAs do not associate with polysomes and additionally in the presence of miRNAs, they shift towards to lighter fractions in polysome profiles. This observation indicated that miRNAs block the initiation step of translation (Humphreys et al., 2005; Pillai et al., 2005). In order to investigate the repression mechanism in details, several studies made use of reporters translated by cap-independent mechanisms. Viruses drive translation in their host cells by a phenomenon known as Internal Entry of the Ribosome (Deforges et al., 2014). They use sequences located upstream of the start codon, named as internal ribosome entry sites (IRES) to initiate translation independently of 5' cap structure. The IRES can interact with some of the initation factors or directly bind to the ribosomal subunits (Thompson, 2012). With this information, Pillai et al., Humphreys et al. and others used IRES-dependent reporters to test miRNA activity when translation is initiated in a cap-independent manner. They showed that miRNAs can not repress translation when it is driven by an IRES and concluded that miRNAs repress cap-dependent translation (Humphreys et al., 2005; Pillai et al., 2005; Mathonnet et al., 2007; Wakiyama et al., 2007). However Peterson et al. also used the same reporters and in

contrast to the other results, concluded that miRNAs do repress translation in a cap-independent manner by blocking translation elongation. All these contradictory observations highlighted the requirement for further studies to elucidate translational repression mechanism by miRNAs.

In 2007, two different studies proposed distinct mechanisms for miRNA-mediated inhibition of translation initiation. One suggested a competition between eukaryotic initiation factor 4E (eIF4E) and AGO2 for 5' cap binding (Kiriakidou et al., 2007). The authors identified a short sequence in AGO2, which is similar to eIF4E cap-binding domain and suggested that AGO2 promotes the removal of eIF4E from the cap structure and consequently inhibits translation. Another study (Chendrimada et al., 2007) provided evidence that AGO2 can bind to the large ribosomal subunit and to eIF6. They proposed that the recruitment of eIF6 by AGO2 blocks the association of the large and small ribosomal subunits. However, none of these proposals were supported by further studies.

In addition to the studies focusing on translation initiation complexes and potential interactions with different subunits of miRISC, the role of PABP was also investigated. PABP is crucial for efficient translation since it interacts with eukaryotic initiation factor 4G (eIF4G) which binds to eIF4E and connects the two ends of the mRNA promoting circularization (Gallie, 1991; Gingras et al., 1999; Kahvejian et al., 2005). A study proposed that miRNA-triggered deadenylation inhibits mRNA circularization. According to their model, the dissociation of PABP from deadenylated mRNAs disrupts the circular form of the mRNA and causes inhibition of translation (Wakiyama et al., 2007). Additional studies also supported the importance of PABP in miRNA-mediated gene silencing (Fabian et al., 2009; Huntzinger et al., 2010). However, further studies provide evidence that mRNAs lacking the poly(A) tail can still be repressed, showing that PABP may enhance silencing, but it is not essential for translational repression by miRNAs (Mishima et al., 2006; Mathonnet et al., 2007; Thermann and Hentze, 2007; Wakiyama et al., 2007; Zhang et al., 2007; Iwasaki et al., 2009; Zdanowicz et al., 2009; Fukaya and Tomari, 2011).

Overall, despite the fact that several studies were performed by different groups to understand how miRNAs repress translation; the mechanism remains elusive. However, most of the data supports a model in which miRNAs inhibit translation initiation.

During my PhD, from 2011 to 2015, additional studies were also published supporting that miRNAs repress translation initiation by blocking different steps. These studies will be discussed in "Results&Discussion" section, in the context of my results.

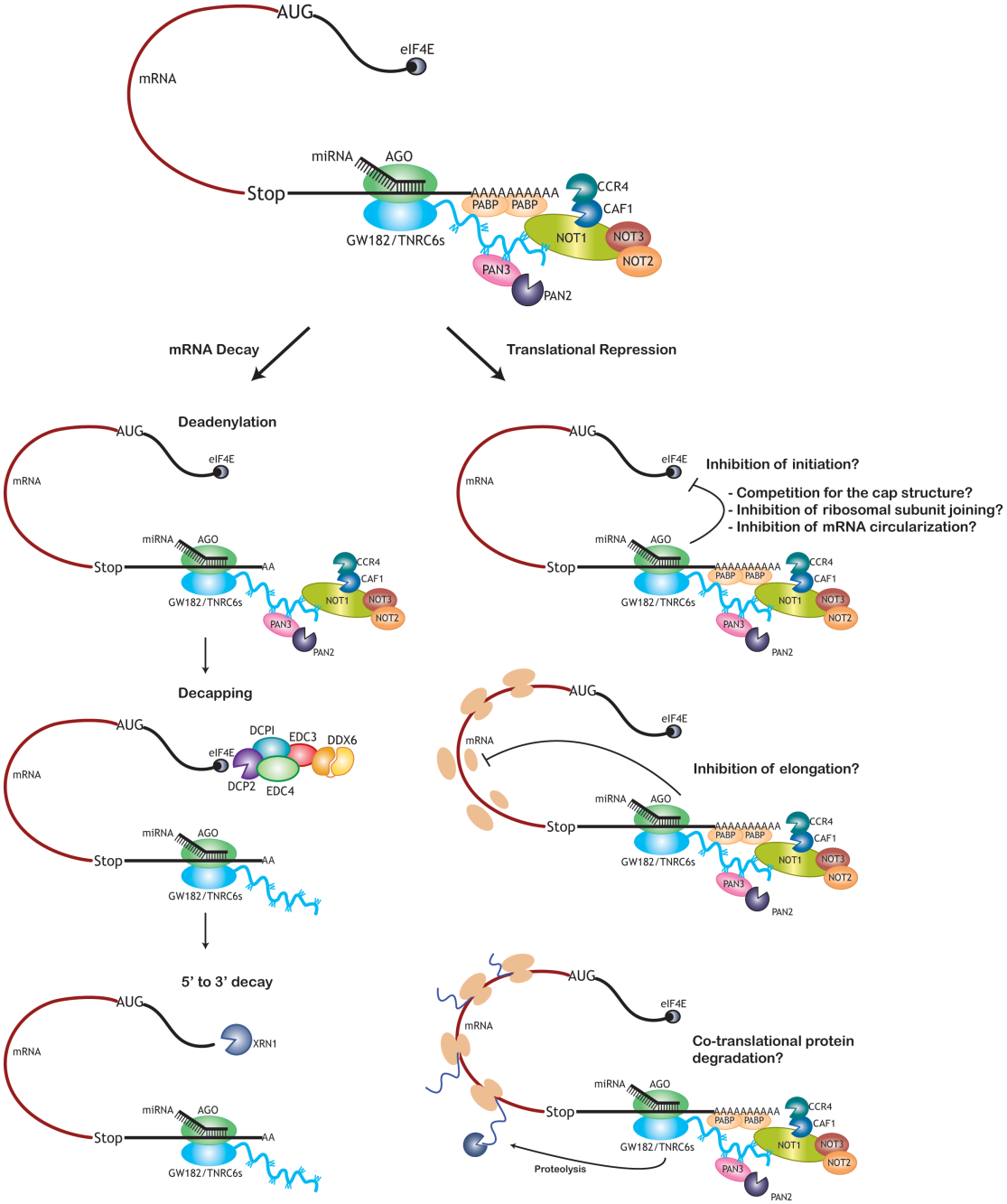

Figure 2.6 miRNA-mediated gene silencing. A miRNA bound to an Argonaute (AGO) protein binds to its mRNA target. AGO recruits the scaffold protein GW182 that directly interacts with PABP, the CCR4-NOT and the PAN2-PAN3 complexes. miRNAs promote mRNA decay via deadenylation followed by decapping and degradation by the 5'-3' exonuclease XRN1. The mechanism by which miRNAs repress translational is unkown. Here, several models are shown according to different studies providing evidence for inhibition of initiation, elongation or co-translational protein degradation (See text).

3. AIMS & OBJECTIVES

miRNAs regulate gene expression of several different mRNA targets and they are involved in the control of almost all known biological processes, such as development, apoptosis, cell growth and proliferation. Importantly, they are also associated with several diseases, causing changes in the expression of specific mRNAs. Their involvement in the regulation of all these processes highlights their importance.

In the last two decades, after their discovery, hundreds of studies focused on the mechanism of miRNA-mediated gene regulation. According to the current models, miRNAs together with AGOs bind to the mRNA target by sequence complementarity. AGO directly interacts with the scaffold protein GW182, which in turn recruits the main deadenylase complexes to the mRNA to promote mRNA deadenylation followed by decapping and finally mRNA degradation. In addition to mRNA degradation, miRNAs also trigger translational repression, but the mechanism remains unknown.

During my PhD, I investigated the mechanism of miRNA-mediated gene silencing and in particular the role of the CCR4-NOT complex in this pathway. At the beginning of my doctoral studies, I focused on the *C. elegans* GW182 proteins, AIN-1 and AIN-2, which are highly divergent from their human and fly orthologs. Previous studies demonstrated that GW182 proteins interact with PABP and the deadenylase complexes to trigger silencing in *Dm* and *Hs* cells. These interactions are mediated by the silencing domain located in the C-terminal region of *Hs* and *Dm* GW182 proteins. Sequence analyses could not identify such a domain in the *C. elegans* proteins. Whether AIN-1/2 interact with PABP and the PAN2-PAN3/CCR4-NOT deadenylase complexes was unknown. My aim was to identify the interactions required for AIN-1/2 to induce silencing and to investigate their mode of interaction. I showed that AIN-1, but not AIN-2, interacts with PABP and the deadenylase complexes to promote silencing. My work contributed to our understanding of the evolution and conservation of silencing mechanisms in metazoans.

I next examined the function of *Hs* and *Dm* GW182 proteins, which interact with PABP and the deadenylase complexes. Although the importance of these interactions for silencing was known, the contribution of each interaction was unclear. Additionally, the contribution of the N-terminal domain of GW182 to the binding to

the deadenylase complexes was also not clear. By using an engineered mini-GW182 protein, I aimed to define the minimal requirements for *Hs* and *Dm* proteins to mediate silencing. I demonstrated that the interaction with both PABP and the deadenylase complexes is required for miRNA-mediated translational repression and mRNA target degradation.

As the CCR4-NOT complex plays a main role in silencing, it was also important to understand how the complex degrades the mRNA targets, including miRNA targets. The complex consists of two main modules: The catalytic module containing the catalytically active subunits involved in deadenylation, and the NOT module containing NOT1,2,3 proteins. The NOT module is important for the recruitment of the complex to different mRNA targets, however the contribution of this module to mRNA decay was unclear. By using biochemical approaches, based on the information obtained from the crystal structure of the NOT module, I investigated the role of the NOT module in mRNA degradation. My results showed that the NOT module is essential for the assembly of the complex and therefore is required for the function of the complex in mRNA decay.

The next question I investigated during my PhD was the molecular mechanism of the recruitment of the CCR4-NOT complex to miRNA targets by GW182 proteins. GW182 proteins interact with the CCR4-NOT complex via W-containing motifs. However, the specific subunits of the CCR4-NOT complex that bind to GW182 were not known. I identified the subunits required for this interaction and the mode of binding in a collaborative project. The results indicated that CNOT9 (CAF40) interacts with GW182 through tandem W-binding pockets.

In the final part of my doctoral work, I focused on the mechanism of translational repression by miRNAs. miRNAs repress translation and promote degradation of the mRNA targets. However the mechanism of translational repression is not fully understood. Since the CCR4-NOT complex has the ability to repress translation independently of deadenylation, I investigated the contribution of the CCR4-NOT complex in miRNA mediated translational repression. My studies showed that NOT1, the scaffold subunit of the complex, directly interacts with a DEAD-box helicase DDX6, which functions as a translational repressor and decapping activator. I also showed that this interaction is required for miRNA-mediated translational repression.

4. RESULTS & DISCUSSION

4.1 The silencing mechanism is conserved across species

The work summarized in this section was published by Kuzuoglu-Ozturk et al., 2012 and the paper including detailed experimental data and methods is attached.

The GW182 protein family is highly conserved in metazoans with the exception of the *C. elegans* GW182 orthologous proteins, AIN-1 and AIN-2, which are highly divergent members of the family with less than 12% sequence identity. Their domain organization is completely different from other GW182 proteins: They do not contain any defined domains (UBA and RRM), or motifs (PAM2 and CIM-1/2) (Fig 2.4). AIN-1 and AIN-2 both interact with *Ce* Argonaute proteins, ALG-1 and ALG-2, and are involved in miRNA mediated gene silencing; however how they promote silencing remained unclear (Ding et al., 2005; Zhang et al., 2007; Ding and Großhans, 2009).

In order to understand how AIN-1 and AIN-2 trigger miRNA mediated gene silencing, I first cloned and expressed the proteins in *Dm* S2 cells. Using co-immunoprecipitation (co-IP) assays, I confirmed the interaction between AIN-1, AIN-2 and *Ce* ALG-1 and validated my approach of using S2 cells to study *Ce* proteins involved in silencing. I defined the AGO-binding domains (ABD) in AIN-1 and AIN-2, by aligning them with different GW182 proteins (Fig 4.1). The GW repeats located in the ABD of AIN-1 and AIN-2 mediate interaction with *Ce* ALG-1 and *Dm* AGO1. These results indicate that the mode of interaction of AIN-1 and AIN-2 with AGO proteins through GW repeats is highly conserved across species. Mutational analyses showed that each GW repeat located in the ABD contributes differently to AGO binding and more importantly, the GW repeats located outside of the ABD do not contribute to this interaction.

I next tested the binding between AIN-1, AIN-2 and the deadenylase complexes, as well as PABP, to investigate whether these interactions are conserved across species. In co-IP assays, only AIN-1, but not AIN-2, interacted with PABP, PAN3, NOT1 and NOT2. These results indicate a possible functional distinction between AIN-1 and AIN-2 in the silencing of miRNA targets. Accordingly, we can

speculate that AIN-2 does not promote mRNA degradation through mRNA deadenylation as GW182 proteins in flies and humans, however further experiments are necessary to make a clear conclusion. This observation is also consistent with the weak effect of AIN-2 depletion on the worms phenotype (Ding et al., 2005; Zhang et al., 2007). However, we cannot rule out the possibility of transient interactions of AIN-2 with PABP and the deadenylase complexes, which cannot be observed by co-IP assays.

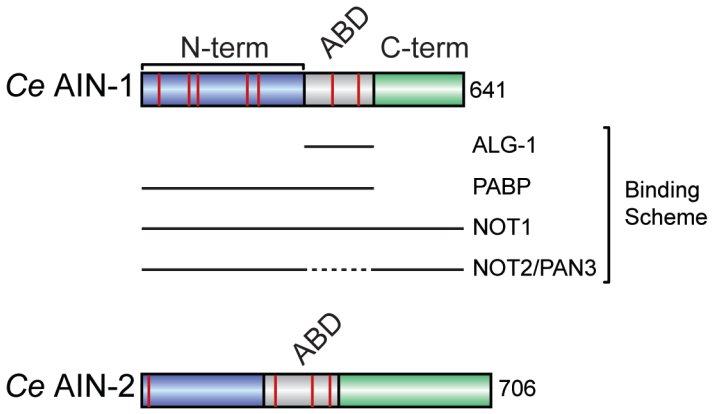

Figure 4.1 *C. elegans* GW182 proteins. AIN-1 and AIN-2 contain seven and four GW repeats presented as red bars, respectively. The AGO-binding domain (ABD) is labelled. The regions required for interaction with deadenylases and PABP are indicated in the binding scheme.

The interaction studies showed that AIN-1 interacts with *Dm* and *Ce* PABP, PAN3, NOT1 and NOT2 through several different binding regions. Although the interactions are conserved, the mode of binding is different compared to *Dm* and *Hs* proteins. The regions responsible for binding to each protein are shown in Fig 4.1. For the interaction with *Ce* NOT1, I could not define a single domain; the full-length protein is required for binding. Since *Dm* and *Hs* GW182 proteins contain W-rich CCR4-NOT interacting motifs (Chekulaeva et al., 2011; Fabian et al., 2011) to mediate interaction with the CCR4-NOT complex, I have also mutated all tryptophan residues (22 in total) to alanine in the AIN-1 protein. The mutant protein was unable to interact not only with *Ce* NOT1 and NOT2, but also with PABP and PAN3, which suggests non-specific disruption of protein-protein interaction. Nonetheless, W-residues can still be critical for interaction with the CCR4-NOT complex.

To test the activity of AIN-1 and AIN-2 in translational repression and mRNA degradation, I used two independent approaches: Tethering and complementation

assays. First, I tethered λN-tagged AIN-1 and AIN-2 to a reporter mRNA. The λN peptide binds with high affinity to the Box B hairpins located on the 3' UTR of the Firefly luciferase reporter (F-Luc-5BoxB). Surprisingly, direct tethering of both AIN-1 and AIN-2 to the 3' UTR of the reporter mRNA repressed translation and degraded the mRNA. Since AIN-1 associates with the deadenylase complexes, this effect was expected. However AIN-2, independently of the deadenylases, could still mediate degradation of the reporter. This result indicates that either AIN-2 interacts transiently with deadenylases and the interaction is not detectable by co-IPs, or it associates with an unknown partner, which promotes mRNA decay. In order to investigate whether AIN-2 uses the 5' to 3' decay pathway, which promotes deadenylation followed by decapping, different approaches can be applied: The subunits of deadenylation and decapping complexes could be knocked down or the catalytically inactive subunits of each complex could be overexpressed to replace the endogenous proteins. In both cases, the endogenous complexes would be blocked and under these conditions, the requirement of each complex could be investigated for AIN-2-mediated mRNA degradation. Additionally, the immunoprecipitation of AIN-2 followed by mass spectrometric analysis of associated partners, revealed a potential interaction with a micrococcal nuclease homolog TSN-1 (Zhang et al., 2007). TSN-1 was identified as a component of RISC in *C. elegans*, *D. melanogaster* and mammals. Its catalytic activity was shown to be crucial for mRNA degradation by siRNAs (Caudy et al., 2003). Here, we can speculate that the interaction of AIN-2 with TSN-1 can also trigger mRNA degradation of the reporter when AIN-2 is tethered. However, further studies are required to understand exactly how AIN-2 contributes to silencing.

In a second approach, I performed complementation assays. I knocked down endogenous *Dm* GW182 protein and transfected the cells with a F-Luc reporter containing the 3' UTR of the *Par-6* gene and a miR-1 plasmid, which regulates *Par-6* expression. Knocking down GW182 protein inhibited silencing of Par-6 mRNA by miR-1, as expected. Then, I transfected these cells with AIN-1 and AIN-2 to test whether they can complement GW182 depletion in *Dm* S2 cells. Unexpectedly, none of them rescued silencing. This observation demonstrated that although AIN-1 can interact with *Dm* and *Ce* PABP and deadenylase complexes, it is not sufficient to replace endogenous *Dm* GW182 protein. This result strengthened the hypothesis supporting different modes of interaction across species. Although AIN-1 can recruit all the partners required for silencing, it cannot promote silencing. It is possible that

an additional partner, which is not present in S2 cells, is required for AIN-1 and AIN-2 to mediate silencing.

My results revealed different mechanisms used by AIN-1 and AIN-2. One possible and simple explanation can be their localization. AIN-1 is localized in P-bodies and is proposed to target ALG-1 to P-bodies (Ding et al., 2005). However, AIN-2 localization was not investigated. Its localization together with AIN-1 in P-bodies is unlikely, since associated proteins identified in AIN-2 IP, did not reveal any P-body marker as the decapping factors (Zhang et al., 2007). Further investigation, especially performed in *C. elegans*, can identify the different mechanisms used by AIN-1 and AIN-2.

Overall, this study highlighted the conservation of the interactions between GW182 proteins with deadenylases and PABP across species. It showed that *C. elegans* GW182 protein AIN-1 can mediate these interactions despite its divergent sequence and pointed out that the mode of interaction has changed through evolution .

4.2 The interactions of GW182 proteins with PABP and the CCR4-NOT complex are required for both translational repression and degradation of miRNA targets

The work summarized in this section was published by Huntzinger et al., 2013 and the paper including detailed experimental data and methods is attached.

In this study, I created a chimeric and functional GW182 protein to understand the minimal sequence requirements to mediate silencing. When I started this project, it was known that the silencing domain (SD) of *Hs* TNRC6 proteins is sufficient to mediate the interaction with deadenylases (Braun et al., 2011; Chekulaeva et al., 2011; Fabian et al., 2011). However, co-IP assays also indicated additional binding sites, located outside of the SD in the *Dm* GW182 protein. Therefore, I first identified the regions of the *Dm* GW182 protein necessary to bind the deadenylase complexes. I showed that the Q-rich region together with the SD (i.e., residues between 635-1384) of *Dm* GW182 contributed to NOT1-binding.

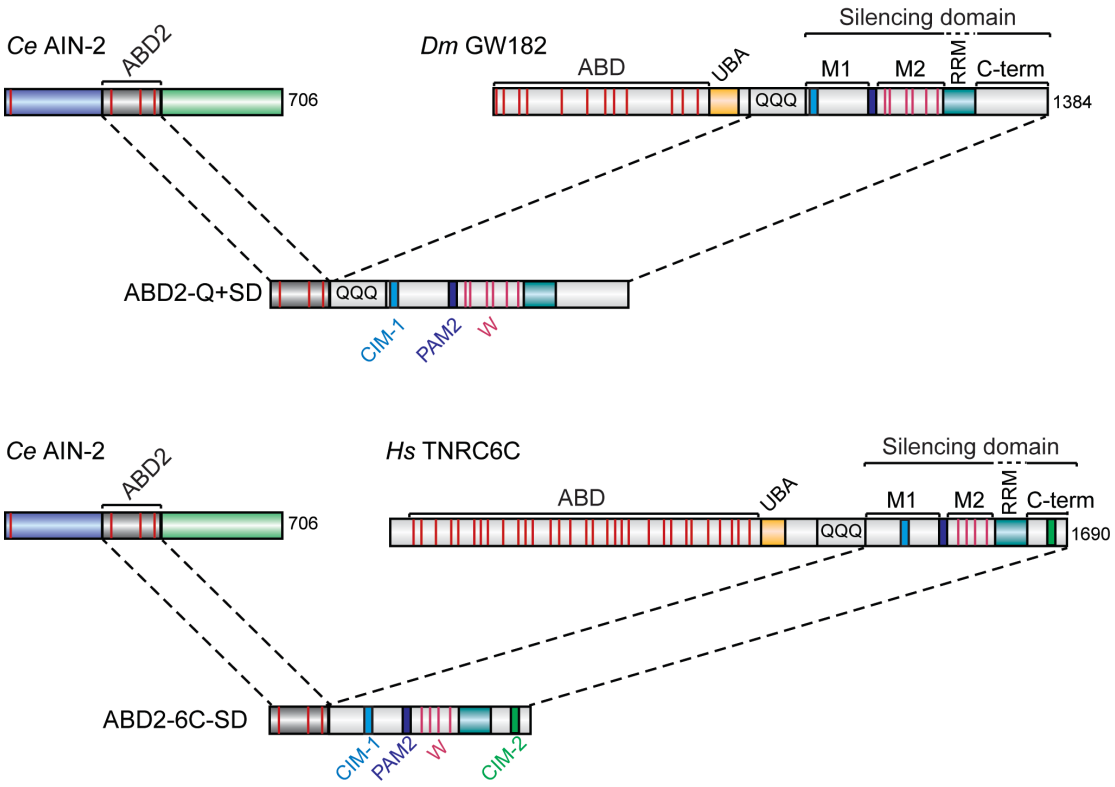

Figure 4.2 The schematic overview of the chimeric GW182 proteins. The mini GW182 proteins, labeled as ABD2-Q+SD or ABD2-6C-SD are constructed by the fusion of Ago-binding domain of *Ce* AIN-2 (ABD2) to the Q+SD region of *Dm* GW182 or to the SD of *Hs* TNRC6C, respectively. The motifs present in the SD are indicated. (CIM-1/2: CCR4-interacting motif 1/2, PAM2: PABP-interacting motif-2, W: Tryptophan residues located in M2 region).

To understand the contribution of N-terminal part of the *Dm* GW182 protein to silencing, I engineered a construct containing the ABD of *Ce* AIN-2 (ABD2) fused to the Q+SD region of *Dm* GW182. In this way, I bypassed the requirement of the N-terminal region of the *Dm* GW182 to interact with AGO1, and obtained a mini-GW182 protein, which can still interact with AGO1 (Fig 4.2). This chimeric protein gave me the chance to investigate more in detail the contribution of each fragment of the *Dm* GW182 protein in the context of silencing, by using them in complementation assays. I showed that although the ABD2 fused to the Q+SD domain of *Dm* GW182 rescues silencing, it was not as efficient as the wild-type protein. This result indicated that N-terminal region of *Dm* GW182 protein also contributes to silencing. With this construct in hand, we analyzed the contribution of each motif present in the SD. As discussed in section 2.4, the CIM-1 and PAM2 motifs located in the SD are important to mediate the interaction with the CCR4-NOT complex and PABP, respectively. In addition to these motifs, tryptophan residues (W) located in the M2 region of the SD

also contribute to binding to the deadenylase (Chekulaeva et al., 2011). We mutated these motifs individually or in combination and analyzed the effects of mutations in complementation assays. These experiments demonstrated that *Dm* GW182 requires the interactions with both PABP and deadenylases to mediate silencing.

Considering the conservation of the silencing machinery in flies and humans, I also generated a chimeric protein consisted of ABD2 fused to the SD of *Hs* TNRC6C (Fig 4.2). This construct was sufficient to rescue silencing in S2 cells and demonstrated that, in contrast to the *Dm* GW182 protein, which contains some minimal binding sites in the N-terminal, the *Hs* TNRC6C-SD alone is sufficient to mediate interaction with PABP and deadenylases. The analyses of mutated proteins demonstrated that PAM2, CIM-1, CIM-2 motifs and W residues in the M2 region of TNRC6C protein have different effect on silencing.

In summary, the approach of using chimeric proteins revealed differences between *Dm* and *Hs* GW182 proteins. This study demonstrated that although both *Dm* and *Hs* GW182 proteins require interactions with deadenylases and PABP to mediate silencing, their mode of interaction has changed through evolution, as observed in *C. elegans* proteins (Section 4.1). *Dm* GW182 has evolved additional binding sites located outside of the silencing domain and the Q-rich region, for the interaction with deadenylases. On the other hand, the SD of *Hs* TNRC6C is sufficient to mediate interactions with PABP and deadenylases. These differences in binding modes can be explained by the unstructured regions of GW182 proteins. GW182 proteins contain several intrinsically disordered regions and mediate their interactions via short linear motifs (SLiMs). SLiMs are small peptides, 3-10 amino acid in length, which can either act as sites for post-translational modifications (PTMs) or mediate interactions (Weatheritt and Gibson, 2012). The GW repeats located in the ABD and motifs (PAM2 and CIM-1/2) in the SD of GW182 proteins represent SLiMs. All these motifs mediate interaction with AGOs, PABP and the deadenylase complexes. One way to identify these motifs is to use a screen between overlapping peptides of interested protein vs interacting protein. This method was used to investigate the contribution of different GW repeats in the N-terminal domain of *Hs* TNRC6 protein for the interaction with AGO2 (Pfaff et al., 2013). A similar approach could be also used to investigate the contribution of the N-terminal domain of *Dm* GW182 protein to PABP and deadenylase complex binding.

4.3 The assembly of the NOT module of the CCR4-NOT complex is crucial for the mRNA degradation

The work summarized in this section was published by Boland et al., 2013 and the paper including detailed experimental data and methods is attached.

The CCR4-NOT complex consists of two modules: The NOT module containing NOT1,2,3 proteins and a catalytic module containing CAF1 (POP2) and CCR4 (Table 2.2). The specific role of the NOT module was not clear, although it was thought to be involved in the regulation of stability and activity of the catalytic module. In addition, the NOT module is also important for the recruitment of the CCR4-NOT complex to mRNA targets, since several RNA binding proteins (Nanos, Bicaudal-C, CUP, Smaug) interact with the CCR4-NOT complex through the subunits that form the NOT module (Barckmann and Simonelig, 2013).

To understand the contribution of this module to mRNA decay, we used a structural approach. The crystal structure of the human NOT module consisting of C-terminal regions of CNOT1, CNOT2 and CNOT3 proteins was solved in the lab (Fig 4.3). These highly conserved regions contain a NOT1 superfamily homology domain (NSHD) in CNOT1 and NOT-box domains in CNOT2 and CNOT3. The crystal structure revealed that NSHD consists of two perpendicular subdomains, which contain six and four heat-repeats, respectively. It also demonstrated that CNOT2 and CNOT3 heterodimerize through the NOT-box domains and interact with the CNOT1-SH domain via unstructured regions.

My role in this study was to evaluate the significance of the NOT module in mRNA degradation *in vivo*. Since the CCR4-NOT complex is highly conserved in human and flies, I tested the effects of mutations in the *Dm* proteins.

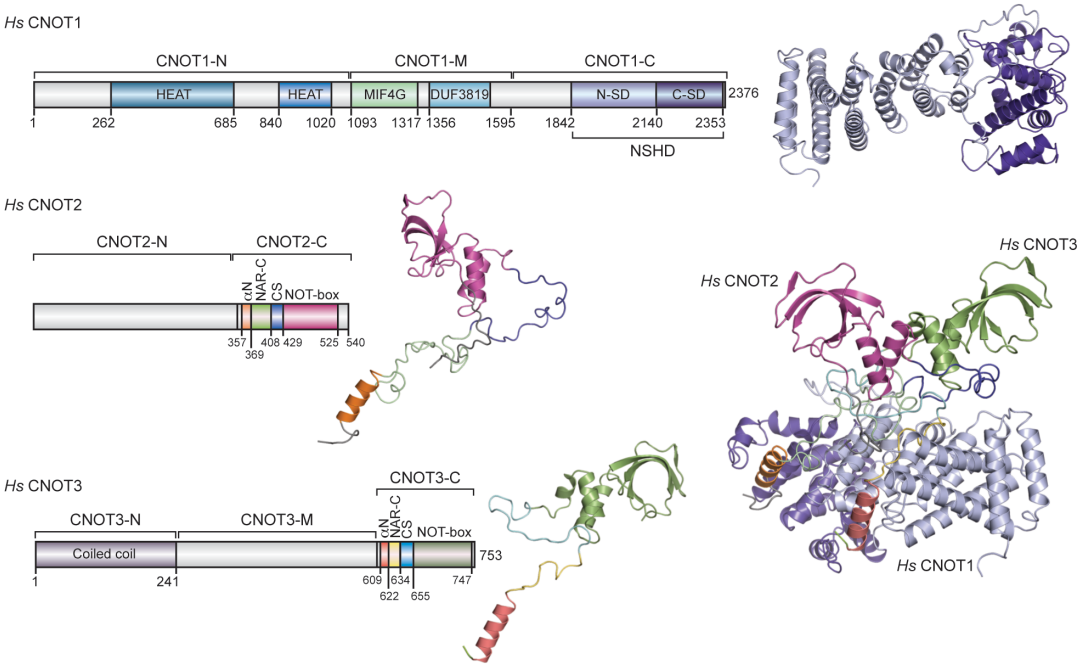

Figure 4.3 The domain organization and the structures of *Hs* NOT module. Domain organization of *Hs* CNOT1-3 proteins. *Hs* CNOT1 contains three regions: N-terminal (N), middle (M) and C-terminal (C). CNOT1-C contains the NOT1 superfamily homology domain (NSHD) consisting of N- and C-terminal subdomains (SD). The C-terminal regions of *Hs* CNOT2 and CNOT3 contain a NOT1 anchor region (NAR) consisting of an alpha-helix (αN) and NAR-C, a connector sequence (CS) and a NOT-box domain. The cartoon representations of each protein and the NOT module are shown. The numbers represent the amino acid positions at domain boundaries.

I designed the constructs according to the structure and investigated the interaction of the individual proteins with endogenous CCR4-NOT complex in S2 cells. First of all, I tested the interaction between HA-tagged overexpressed NOT1 protein with endogenous NOT2 and NOT3. As expected, deletion of the C-terminal NOT1 containing NSHD, abolished the interaction. This validated the structural data and showed that there are no additional binding sites on NOT1 for *Dm* NOT2 and NOT3 protein. Point mutations in NOT1 designed according to the crystal structure prevented the interaction with NOT2 and NOT3. Moreover, when I mutated the binding surface between NOT1 and NOT2, this NOT1 mutant was not able to bind to NOT3 and vice versa. This result indicated that three subunits exist as a complex *in vivo*. Further results also confirmed this conclusion. The structure demonstrated that NOT2 contacts NOT1 through several regions: NOT1 anchor region (NAR, consisting of an alpha-helix (αN) and C-terminal unstructured part (NAR-C)) and a connector sequence (CS, Fig 4.3). Deletion of each of these binding surfaces

prevented the binding of NOT2 to NOT1 and NOT3. I also obtained the same results, when NOT3 was mutated. Overall, these results showed that *in vivo*, each subunit of the NOT module requires interaction with other partners to be incorporated into the endogenous CCR4-NOT complex.

Finally, to understand the role of the NOT module in mRNA decay I used two different approaches: Overexpression and complementation assays. I used a reporter containing the coding sequence of the *Dm* alcohol dehydrogenase (*Adh*) gene fused to the 3' UTR of *hsp70* mRNA. It was previously shown that Hsp70 mRNA is rapidly deadenylated by the CCR4-NOT complex (Temme et al., 2004). I measured the half-life of this reporter under different conditions. First, I overexpressed the wild-type and the NOT1 mutant which does not interact with endogenous NOT2 and NOT3 proteins. The half-life of the reporter increased two fold in the presence of the NOT1 mutant. Since this NOT1 mutant is not incorporated into the endogenous complex, its effect is most likely explained by titration of the catalytic module from the active complex, causing inefficient mRNA decay. Second, I knocked-down endogenous NOT1, NOT2 and NOT3 proteins and performed complementation assays using different mutants. I showed that depletion of a single subunit (NOT1 or NOT3) co-depleted the others, in agreement with previous studies (Russell et al., 2002; Temme et al., 2010; Ito et al., 2011a; 2011b; Mauxion et al., 2013). Depletion of the different subunits had a similar effect on the half-life of the reporter, as expected. As a control, I transfected the cells with dsRNA-resistant versions of NOT1 or NOT3, they both restored the degradation of the reporter. However, the NOT1 or NOT3 mutants did not rescue degradation. These experiments demonstrated the requirement of a properly assembled NOT module for the activity and the recruitment of the CCR4-NOT complex.

In summary, this study demonstrated how the NOT module is assembled. In particular, the crystal structure showed the importance of NAR and CS for the assembly of the NOT module. The mutation analysis and functional studies highlighted the role of the NOT module for the activity of the CCR4-NOT complex.

4.4 CNOT9 contains tandem W-binding pockets that mediate the interaction with GW182 proteins

The work summarized in this section was published by Chen et al., 2014 and the paper including detailed experimental data and methods is attached.

The interaction between GW182/TNRC6 proteins and the CCR4-NOT complex is crucial for miRNA-mediated gene silencing. Although the relevance of this interaction was known, the mode of interaction remained unclear. Previous studies reported that tryptophan residues located in the SD of GW182/TNRC6 proteins were important for this interaction (Chekulaeva et al., 2011; Fabian et al., 2011; Huntzinger et al., 2013). Structural studies showed the presence of W-binding pockets in *Hs* AGO2 and *Dm* PAN3 homodimer, which mediate the interaction with W-containing motifs in GW182 proteins (Schirle and MacRae, 2012; Christie et al., 2013).

Previous work from our lab demonstrated that the NOT1 subunit of the CCR4-NOT complex interacts with TNRC6A-SD through a DUF domain (Fig 4.4). This domain also interacts with another subunit of the complex: CNOT9 (CAF40). In order to obtain detailed information about the molecular basis of this interaction, the DUF domain (hereby, referred as CNOT9 binding domain, CN9BD) was co-crystallized with the ARM (Armadillo repeats) domain of *Hs* CNOT9 in the absence or presence of L-tryptophan.

The crystal structure revealed the fold of CN9BD, which consists of seven α helices, arranged to locate the N- and C-termini of the domain into close proximity. The crystal structure also revealed the presence of two tandem W-binding pockets located in CNOT9. This information suggested a potential interaction between GW182/TNRC6 proteins and CNOT9. To investigate whether these pockets represent binding sites for GW182 proteins, I designed mutants and tested the interaction by co-IPs in human HEK293T cells. The IP results confirmed the binding between the proteins and showed that the point mutations designed to disrupt the W-binding pockets in CNOT9 abolished the interaction. To understand whether CNOT9 is the only subunit interacting with GW182/TNRC6 proteins, I designed mutations on CNOT1. A CNOT1 mutant, which does not interact with CNOT9, retains the ability

to interact with GW182/TNRC6, indicating the presence of additional binding sites in CNOT1.

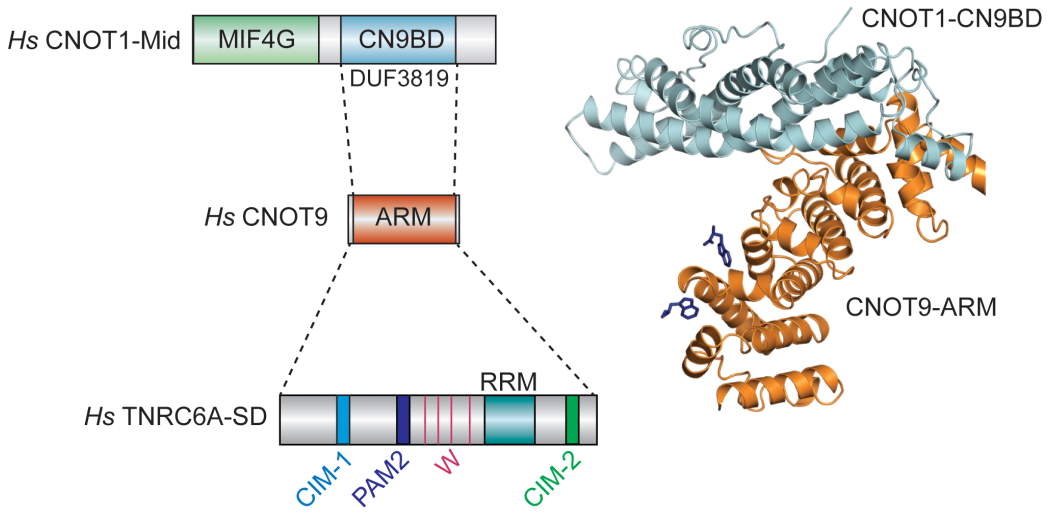

Figure 4.4 The domain organization of *Hs* CNOT1-Mid together with CNOT9 and TNRC6A-SD. The CNOT9 binding domain (CN9BD or DUF3819) of *Hs* CNOT1 interacts with armadillo repeat (ARM) domain of *Hs* CNOT9. The cartoon representations of CN9BD together with CNOT9-ARM highlight the presence of two W-binding pockets (represented as blue Ws) located on the CNOT9. These pockets mediate interaction with *Hs* TNRC6 proteins.

In order to investigate the role of the interaction between CNOT9 and TNRC6 proteins in silencing, I performed complementation assays in HeLa cells. I optimized the knock-down protocol in the lab and tested different miRNA reporters repressed by endogenous let-7. I could not observe any effect on silencing in *Hs* CNOT9 depleted cells, however depletion of *Hs* CNOT1 inhibited silencing in HeLa cells. Transfection of a shRNA-resistant version of wild-type CNOT1 restored silencing of the miRNA reporters. Then, I tested different mutants of CNOT1 and concluded that a CNOT1 mutant which does not interact with CNOT9 can still rescue silencing. This observation was in agreement with the results obtained from immunoprecipitation assays that revealed additional binding sites of GW182/TNRC6 proteins on CNOT1.

Overall, this study revealed the presence of two W-binding pockets on CNOT9 which mediate interaction with TNRC6 proteins. Although I could confirm the interaction *in vivo*, the functional significance of this interaction remains elusive. I could not observe any effect on silencing when CNOT9 was depleted in HEK293T or HeLa cells. Moreover, the results of immunoprecipitation assays showed that CNOT1, which does not bind to CNOT9 still interacts with TNRC6. This indicates

the presence of multiple binding sites for GW182 proteins on the CCR4-NOT complex, which mediate the recruitment of the complex to miRNA targets in a redundant manner. As miRNAs are crucial for the cell to regulate different pathways, we can expect that cells use more than one way to recruit the main effector complex, the CCR4-NOT complex, to the mRNA target. Moreover, the presence of multiple binding sites can facilitate the recruitment of the complex under specific conditions. CNOT9 is a highly conserved protein and is a core member of the CCR4-NOT complex. CNOT9 has been implicated in retinoic acid-induced cell differentiation (Hiroi et al., 2002) and is overexpressed in breast cancer (Ajiro et al., 2009). We can speculate that TNRC6 mediated recruitment of the CCR4-NOT complex is facilitated by CNOT9 when it is overexpressed. Further studies focusing on the differential expression of CNOT9 and its role in miRNA-mediated gene silencing in different tissues can provide more information.

4.5 The role of DDX6 in miRNA-mediated gene silencing

Part of the work summarized in this section was published by Chen et al., 2014 and the paper including detailed experimental data and methods is attached. The main part of the work is described in the manuscript attached Kuzuoglu-Ozturk et al., 2015, which is under review in Genes&Development.

In the last part of my PhD, I focused on the role of the CCR4-NOT complex in translational repression. My aim was to elucidate the translational repression mechanism employed by the deadenylase complex, which will consequently give information on how miRNAs repress translation. The studies published during my PhD supported the hypothesis of the CCR4-NOT complex is an effector complex in silencing, which can mediate the repressive activity of miRNAs as well as their effect on mRNA decay. Two studies, in one of which I was involved, showed that GW182 proteins dissociate PABP from their mRNA target which causes repression at the translational level (Moretti et al., 2012; Zekri et al., 2013). More importantly, it was demonstrated that GW182 proteins require the CCR4-NOT complex to dissociate PABP from the mRNA target (Zekri et al., 2013).

In order to elucidate the role of the CCR4-NOT complex in miRNA-mediated translational repression, I first investigated whether miRISC and the deadenylase complex use a similar mechanism to repress translation of miRNA targets. It was proposed that *Dm* AGO1 can repress translation independently of GW182 and the CCR4-NOT complex *in vitro* (Fukaya and Tomari, 2012). This study suggested that AGO1 requires GW182 to recruit the CCR4-NOT complex to mediate mRNA decay, but it could still repress translation of mRNA targets in the absence of mRNA deadenylation. In 2012, the crystal structure of *Hs* AGO2 was solved and it revealed the presence of two W-binding pockets in the PIWI domain, which can potentially mediate the interactions with GW182/TNRC6 proteins (Schirle and MacRae, 2012). I used this information to design *Dm* and *Hs* AGO1 and AGO2 mutants. The point mutations abolished the interaction with GW182. I confirmed the proper folding of the mutant proteins by miRNA IP; the mutants retained their ability to bind to miRNAs. I tested the activity of these mutants using either tethering or complementation assays. The different functional assays in S2 or HEK293T cells demonstrated that AGOs couldn't repress translation or promote mRNA degradation when their interaction with GW182 proteins was abolished.

Next, I focused on whether the miRISC and the CCR4-NOT complex use the same decay pathway. Since *Dm* AGO1 was proposed to act independently of GW182 proteins, I compared the activities of different proteins (AGO, GW182 and NOT1) in tethering assays in the presence of catalytically inactive decapping subunit DCP2. I observed that all proteins degrade mRNA targets using 5' to 3' decay machinery. These experiments also demonstrated that miRISC and the CCR4-NOT complex both repress and degrade their targets by a similar mechanism.

I next investigated whether all proteins use a similar mechanism to repress translation. Although different studies showed that the CCR4-NOT complex is important for translational repression by miRNAs, independently of its deadenylation activity, how this repression is achieved, remains unclear (Chekulaeva et al., 2009; Cooke et al., 2010; Bawankar et al., 2013; Zekri et al., 2013). One study reported that NOT1 blocks translation via interaction with the eukaryotic initiation factor eIF4A2 in human cells (Meijer et al., 2013). eIF4A is an RNA helicase responsible for unwinding secondary structures within the 5' UTR of the mRNA to allow the ribosome to scan and identify the first AUG to initiate translation. In human cells, two isoforms of eIF4A, eIF4A1 and eIF4A2, which share 91% of sequence identity, are

present. Meijer et al. demonstrated that miRNAs repress translation by recruiting eIF4A2 via NOT1. They proposed that eIF4A2, but not eIF4A1, interacts with NOT1 and this interaction locks eIF4A2 on the 5' UTR of the mRNA (Meijer et al., 2013). By contrast, two subsequent studies, proposed that miRNAs inhibit translation by causing dissociation of eIF4A1 and eIF4A2 from the mRNA target (Fukao et al., 2014; Fukaya et al., 2014).

In order to understand the role of the CCR4-NOT complex in miRNA-mediated translational repression, I generated different reporters. Briefly, I used a reporter containing a normal poly(A) tail, which is sensitive to mRNA deadenylation. I modified the 3' end of this parental reporter to generate a reporter, that is not deadenylated or degraded. For expression in human cells, I inserted the 3' end of the MALAT1 long non coding RNA which is processed by RNase P (Wilusz et al., 2012). For expression in *Dm* cells, I used a reporter containing an internal poly(A) stretch protected by a poly(C) stretch of seven residues followed by a self-cleaving Hammerhead ribozyme (HhR) sequence (Zekri et al., 2013). I obtained F-Luc or R-Luc reporters, which are independent of mRNA deadenylation, to express in *Dm* and human cells, respectively. This allowed me to study only translational repression, without any effect on mRNA levels. Additionally, I modified the 5' UTRs of the reporter to investigate the role of scanning in miRNA-mediated translational repression. I shortened the 5' UTR of the *Dm* reporter from 107 to 6 nucleotides to obtain a reporter translated independently of scanning. Similarly, I modified the 5' end of *Hs* reporter to insert a specific sequence (TISU: Translation initiator of short 5' UTR) found in very short 5' UTRs (Elfakess and Dikstein, 2008). TISU-driven translation is dependent on the 5' cap structure and independent of the eIF4A helicase activity (Elfakess and Dikstein, 2008; Elfakess et al., 2011; Sinvani et al., 2015). In both cases, I checked the translation efficiency of the reporters. I designed different control experiments to be sure that translation measured with the luciferase activity of the reporter is not due to leaky translation. In the case of leaky translation, ribosomes should initiate translation from the next start codon, which is located 30 residues downstream of the first AUG in the F-Luc reporter. When I deleted these 30 amino acids, I could not observe any luciferase activity. This showed that the first residues are crucial for the activity of the protein and in the case of leaky translation, I would not measure any luciferase activity, consistent with a previously published report (Sung and Kang, 1998). I also inserted a HA-tag on the 5'end of the R-Luc ORF and

translated it in the presence of TISU. I could observe HA-tagged R-Luc in western blot showing that translation starts at the first AUG without any scanning. In order to test the effect of scanning on silencing, I generated reporters containing different 5' UTRs for expression in human cells. I replaced the 5' UTR sequences with CAA stretches, which were shown to require less eIF4A activity because of their weak secondary structure or with CGG stretches, which form a highly structured 5' UTRs. The reporters used in this study are summarized in Table 4.1.

Table 4.1 Reporters used in this study. The length of the 5' untranslated regions (5' UTR) are given in nucleotide (nt) numbers. The presence of poly(A) tail is indicated. Deadenylation and scanning dependency of each reporter are represented.

	Name of the reporter	5'UTR	Poly(A)	Deadenylation dependent	Scanning dependent
Dm	F-Luc-5BoxB	107 nt	+	+	+
	F-Luc-5BoxB-A_{95}-C_7-HhR	107 nt	-	-	+
	6nt-F-Luc-5BoxB-A_{95}-C_7-HhR	6 nt	-	-	-
Hs	R-Luc-6MS2	219 nt	+	+	+
	R-Luc-6MS2-A_{95}-MALAT1	219 nt	-	-	+
	TISU-R-Luc-6MS2-A_{95}-MALAT1	12 nt	-	-	-
	CAA-R-Luc-6MS2-A_{95}-MALAT1	68 nt	-	-	+/-
	CGG-R-Luc-6MS2-A_{95}-MALAT1	123 nt	-	-	+

Next, I tested the effect of AGO, GW182 and the CCR4-NOT complex by tethering them directly to these reporters. The results demonstrated that none of the proteins require scanning or deadenylation to repress translation. This result was unexpected, since Meijer et al. showed that miRNAs repress translation by blocking scanning. I obtained similar results when I used reporters containing miRNA binding sites at their 3' UTRs and a TISU or short 5' UTRs. miRNAs also repressed translation of the reporters independently of scanning.

To confirm that the reporters do not require scanning, and consequently eIF4A activity, I treated human cells with silvestrol, which blocks eIF4A activity (Bordeleau

et al., 2008; Wolfe et al., 2014). The drug reduced the translation efficiency of all reporters, except the TISU-dependent reporters. This confirmed that TISU-mediated translation does not require eIF4A, as shown previously (Elfakess and Dikstein, 2008; Elfakess et al., 2011). In addition to the drug, I also analysed the association of eIF4A2 with different reporters. Briefly, endogenous eIF4A2 was immunoprecipitated with a specific antibody and total RNA was purified. By northern blotting, I analyzed the association of endogenous eIF4A2 with different reporters. This experiment demonstrated that the TISU-dependent mRNA reporter does not associate with eIF4A2. Overall, silencing of scanning-independent reporters by tethered AGO, GW182 and the CCR4-NOT complex or by miRNAs showed that scanning is not the step blocked by miRISC.

Since my results demonstrated that miRNAs does not require scanning or eIF4A activity to repress translation, it would be interesting to find out the mechanism of the CCR4-NOT-mediated translational repression. As mentioned above, Meijer et al. proposed that NOT1 interacts with eIF4A2 through its MIF4G domain, which is similar to the middle domain of the eIF4G protein. eIF4G interacts with eIF4A1/2 and eIF4E to form the eIF4F complex which is crucial for the initiation of translation. In the lab, we did not observe any interaction between NOT1 and eIF4A1/2 in human or *Dm* cells. On the other hand, our immunoprecipitation assays revealed another interacting partner of NOT1: A DEAD-box helicase DDX6 (named also as RCK, Me31B, Dhh1), which is involved in translational repression and decapping. We confirmed that this interaction is direct and the crystal structure of the C-terminal RecA domain of DDX6 bound to MIF4G domain of CNOT1 was solved in the lab, as shown in Fig 4.5.

In order to understand whether this interaction is required for silencing, the initial complementation assays performed in human cells demonstrated that DDX6 is required for silencing. Moreover, a DDX6 mutant which does not interact with NOT1 could not rescue silencing. This result indicated that the recruitment of DDX6 through NOT1 to miRNA targets is important for the activity of the protein. For further validation, I performed additional knock-down experiments. To understand the role of the interaction between NOT1 and DDX6 for the translation repression activity of the CCR4-NOT complex, I depleted endogenous DDX6 and tethered TNRC6 or NOT1 proteins to a reporter which is not deadenylated. In the absence of DDX6, none of the proteins could repress translation showing that NOT1/TNRC6-mediated translational

repression requires DDX6. In a different approach, I have also tethered a NOT1 mutant, which does not interact with DDX6 to a deadenylation-independent reporter. The result demonstrated that NOT1 requires the interaction with DDX6 to repress translation. Interestingly, when I repeated the same experiment with a reporter, that can be deadenylated, I could not observe any change between the wild-type and mutant NOT1. This showed that NOT1 degrades the mRNA target independently of DDX6; however it requires DDX6 for its repressive activity independently of deadenylation.

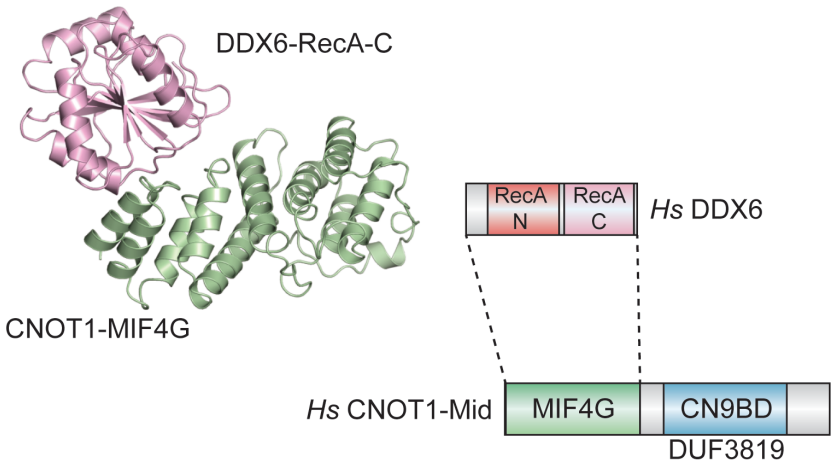

Figure 4.5 The domain organization of *Hs* CNOT1-Mid and DDX6. The middle domain of *Hs* CNOT1 contains MIF4G and CN9BD. *Hs* DDX6 is consisted of two RecA domains (RecA-N and RecA-C). MIF4G domain of *Hs* CNOT1 interacts with *Hs* DDX6. The crystal structure represented here contains RecA-C (pink) and MIF4G (green) domains.

DDX6 is involved in translational repression, however how it represses translation is not known. To address this question, I initially tested whether DDX6 requires deadenylation or scanning to promote translational repression. By using the same reporters that I have used for AGO, GW182 and the CCR4-NOT complex, I have tethered DDX6 and the DDX6 mutant which does not interact with NOT1. The wild-type protein repressed translation independently of scanning and deadenylation, as well as the mutant. This showed that DDX6 represses translation independently of NOT1. To investigate further this mechanism, I performed polysome profiling analysis in human cells. The analysis demonstrated that DDX6 tethering shifts the mRNA to the lighter fractions, which indicates that DDX6 inhibits translation initiation.

Overall, this study showed that miRISC containing a miRNA, AGO, GW182 and the CCR4-NOT complex use a similar mechanism for silencing. They all degrade the mRNA target via the 5' to 3' decay pathway. Although how they repress translation is not yet clear, this study showed that they do not require scanning or deadenylation to inhibit translation. The results demonstrated that the interaction between NOT1 and DDX6 is required for translational repression. This interaction also provides a direct link between deadenylation and decapping as well as translational repression.

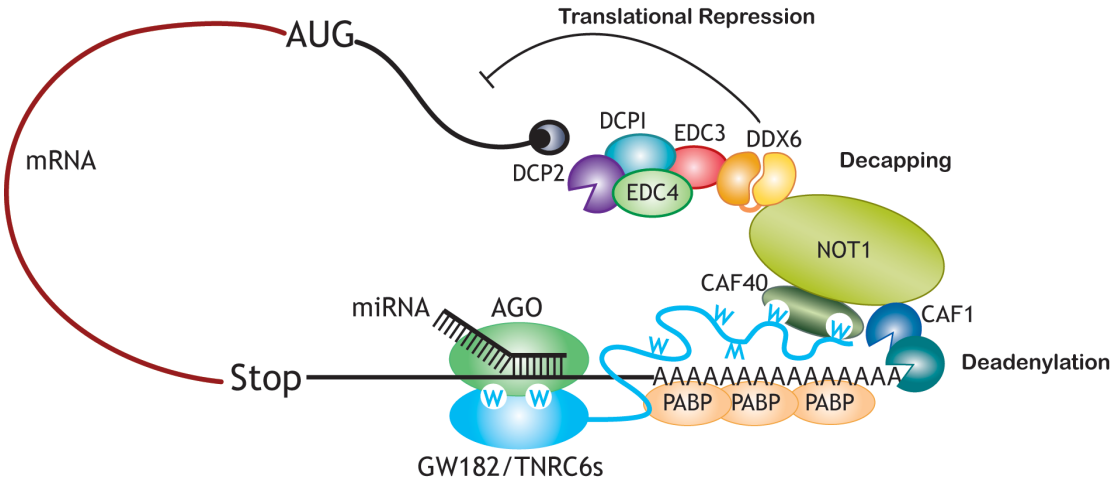

Figure 4.6 Model of miRNA mediated gene silencing. miRISC, consists of miRNA and an AGO protein, binds to the 3' UTR of the target mRNA. AGO recruits the GW182 protein. GW182 contains several W residues, represented as "W". The N-terminal part of the protein interacts with AGO and the C-tail mediate the recruitment of the main deadenylase complex, the CCR4-NOT complex. GW182 interacts directly with CAF40 (CNOT9) through two W-binding pockets. NOT1, the scaffold subunit of the CCR4-NOT complex, interacts with the decapping activator and translational repressor DDX6. This interaction bridges deadenylation to decapping and to translational repression.

5. CONCLUSION

miRNAs act as post-transcriptional gene regulators in almost all known biological pathways. GW182 proteins together with miRISC mediate silencing by promoting translational repression and mRNA decay. GW182 proteins are responsible for the recruitment of the main deadenylase complex, the CCR4-NOT complex, to miRNA targets. My doctoral studies, together with several studies mentioned in this thesis, identified the CCR4-NOT complex as a major effector complex in miRNA-mediated gene silencing. This complex is required for deadenylation, as well as translational repression. The data presented in this thesis highlighted the importance of the interaction between GW182 proteins and the CCR4-NOT complex for silencing by showing that the interaction is conserved across species. My initial studies were focused on the *C. elegans* GW182 proteins, AIN-1 and AIN-2, which are highly divergent in sequence from the other members of the family. My results demonstrated the conservation of the interactions with the deadenylases and PABP, which are essential for silencing, although the mode of binding has changed during evolution. I next investigated minimal requirements of *Hs* and *Dm* GW182 proteins to mediate silencing and showed that the interaction of GW182 with both PABP and deadenylases are required to promote translational repression and mRNA degradation. In order to understand how GW182 recruits the CCR4-NOT complex to miRNA target, I was involved in a collaborative project. In this project, we identified two W-binding pockets in the CNOT9 (CAF40) subunit of the CCR4-NOT complex. These W-binding pockets mediate the interaction with GW182 proteins. My results showed additional binding sites on the CCR4-NOT complex for GW182, which remain to be identified by further studies. Additionally, this study revealed a direct link between deadenylation and decapping pathways, by showing a direct interaction between MIF4G domain of NOT1 and DDX6, a translational repressor and decapping activator. Importantly, this link also connects the CCR4-NOT complex to translational repression.

In the last part of my PhD, I focused on the translational repression activity of the CCR4-NOT complex. My studies demonstrated that the CCR4-NOT complex requires the interaction with DDX6 to repress translation of the miRNA targets in human cells. However how DDX6 represses translation is still not clear. Previous studies performed in yeast showed conflicting results: DDX6 was shown to inhibit the

assembly of 43S complex on mRNA (Coller and Parker, 2005) as well as to slow down the translation rate thereby causing the accumulation of ribosomes on mRNA (Sweet et al., 2012). The *Xenopus* ortholog of DDX6, Xp54, was also proposed to inhibit translation via the interaction with 4E-Transporter (4E-T), a 4E-binding protein which competes with eIF4G to bind to eIF4E and therefore represses translation (Kamenska et al., 2014). Human DDX6 was reported to be involved in translational repression by miRNAs, specially through the interaction with AGO (Chu and Rana, 2006). The polysome profiling experiments that I performed indicated that DDX6 inhibits translation initiation. However there are still several unanswered questions. Although we have showed that the CCR4-NOT complex and miRISC require DDX6 to repress translation, whether its helicase activity is necessary remains unclear. One recent study reported that NOT1 binding stimulates ATPase activity of DDX6 (Mathys et al., 2014). Further *in vitro* studies, for example toe-printing analyses, can provide more information about the contribution of the interaction between NOT1 and DDX6 to translational repression. Another question is whether DDX6 requires other decapping subunits to inhibit translation. It has previously been shown that DDX6 can repress translation of different mRNAs in yeast strain lacking Dcp2 (Sweet et al., 2012). In order to address this question in a more direct way, point mutations could be introduced in DDX6 to abolish the interaction with other decapping factors and test the effect of the protein in different assays.

The mechanism of translation could differentiate in various cell types and distinct requirements could be necessary. As an example, the length of poly(A) tail, was shown not to correlate with translation efficiency in the beginning at gastrulation (Subtelny et al., 2014). This result showed that translation is differentially regulated under distinct conditions. We can also speculate that miRNA-mediated repression and the contribution of DDX6 also vary according to cell or environmental conditions. Future studies focusing on these questions will provide information to understand exactly how miRNAs promote translational repression.

In conclusion, my doctoral studies highlighted the importance of the CCR4-NOT complex as a main effector complex in miRNA-mediate gene silencing. My results contributed to our understanding of miRNA pathway by showing that the CCR4-NOT complex does not only promote deadenylation followed by decapping but also triggers translational repression of miRNA targets thorough its direct interaction with the translational repressor DDX6.

6. AUTHOR CONTRIBUTIONS

In this section, the contribution of each author is described for the papers discussed in this thesis.

6.1 The *Caenorhabditis elegans* GW182 protein AIN-1 interacts with PAB-1 and subunits of the PAN2-PAN3 and CCR4-NOT deadenylase complexes

Kuzuoglu-Ozturk, D., Huntzinger, E., Schmidt, S., & Izaurralde, E. (2012). The *Caenorhabditis elegans* GW182 protein AIN-1 interacts with PAB-1 and subunits of the PAN2-PAN3 and CCR4-NOT deadenylase complexes. Nucleic Acids Res., *40*(12), 5651–5665.

D.K.-Ö performed all the experiments. E.H. and D.K.-Ö. designed the experiments and analyzed the results. S.S. performed the alignments. E.I. conceived, supervised the project and wrote the manuscript. All authors corrected the manuscript.

6.2 The interactions of GW182 proteins with PABP and deadenylases are required for both translational repression and degradation of miRNA targets

Huntzinger, E*., **Kuzuoglu-Ozturk, D***., Braun, J. E., Eulalio, A., Wohlbold, L., & Izaurralde, E. (2013). The interactions of GW182 proteins with PABP and deadenylases are required for both translational repression and degradation of miRNA targets. Nucleic Acids Res., *41*(2), 978–994.

E.H. and D.K.-Ö. contributed equally to this work. E.H. performed the complementation assays in *Dm* and *Hs* cells. D.K.-Ö designed the chimeric constructs and performed coimmunoprecipitations in *Dm* cells. J.E.B. performed initial coimmunoprecipitations and A.E. performed screens with different miRNA reporters. L.W. prepared the constructs for CNOT1 and CNOT7. E.I conceived, supervised the project and wrote the manuscript. All authors corrected the manuscript.

6.3 Structure and assembly of the NOT module of the human CCR4-NOT complex

Boland, A*., Chen, Y*., Raisch, T*., Jonas, S*., **Kuzuoglu-Ozturk, D**., Wohlbold, L., Weichenrieder, O., and Izaurralde, E. (2013). Structure and assembly of the NOT module of the human CCR4-NOT complex. Nat. Struct. Mol. Biol. *20*(11), 1289–1297.

A.B., Y.C., T.R. and S.J. contributed equally to this work. A.B. and Y.C. purified, crystallized and solved the structures of CNOT3 and CNOT2 oligomers and of *Ct* NOT1. A.B. and Y.C. cloned, expressed and established the purification protocol for the ternary complex. T.R. purified and crystallized the ternary complex. T.R. and S.J. solved the structure of the ternary complex. A.B., Y.C., T.R., S.J. and O.W. collected and analyzed diffraction data. L.W. performed pulldowns and coimmunprecipitations in human cells. D.K.-Ö. performed coimmunprecipitations and functional assays in S2 cells. E.I. conceived of the project. E.I. and O.W. supervised the project. All authors contributed to the writing of the manuscript.

6.4 A DDX6-CNOT1 complex and W-binding pockets in CNOT9 reveal direct links between miRNA target recognition and silencing

Chen, Y*., Boland, A*., **Kuzuoglu-Ozturk, D***., Bawankar, P., Loh, B., Chang, C.-T., Weichenrieder, O., and Izaurralde, E. (2014). A DDX6-CNOT1 complex and W-binding pockets in CNOT9 reveal direct links between miRNA target recognition and silencing. Mol. Cell *54*(5), 737–750.

Y.C., A.B., and D.K.-Ö. contributed equally to this work. Y.C. and A.B. purified, crystallized, and solved the structures of CNOT1-CN9BD bound to the CNOT9 ARM repeat and of the CNOT1 MIF4G bound to DDX6 RecA-C domain. Y.C., A.B., and O.W. collected and analyzed diffraction data. Y.C. and A.B. performed pulldowns in vitro. D.K.-Ö. performed coimmunoprecipitations and functional assays in human cells. P.B. performed coimmunoprecipitation assays in S2 cells. B.L. performed the DDX6 complementation assays. C.-T.C. performed DDX6 coimmunoprecipitation assays in human cells. E.I. conceived and supervised the project. A.B., E.I., and O.W. wrote the manuscript. All authors corrected the manuscript.

6.5 miRISC and the CCR4-NOT complex repress and degrade mRNA targets independently of 43S ribosomal scanning

Kuzuoglu-Ozturk D., Bhandari D., Huntzinger E., Fauser M., Helms S., and Izaurralde E. (2015). miRISC and the CCR4-NOT complex repress and degrade mRNA targets independently of 43S ribosomal scanning. Submitted to Genes Dev.

D.K.-Ö planned and performed almost all the experiments. D.B performed some of the tethering assays and experiments with reporters containing miRNA binding sites in *Dm* cells. E.H. performed initial complementation assays. M.F generated many of the DNA constructs used in this study and S.H performed western blots. E.I supervised the project. D.K-Ö, D.B and E.I wrote the manuscript.

7. REFERENCES

Ajiro, M., Katagiri, T., Ueda, K., Nakagawa, H., Fukukawa, C., Lin, M.-L., Park, J.-H., Nishidate, T., Daigo, Y., and Nakamura, Y. (2009). Involvement of RQCD1 overexpression, a novel cancer-testis antigen, in the Akt pathway in breast cancer cells. Int. J. Oncol. *35*, 673–681.

Albert, T.K., Hanzawa, H., Legtenberg, Y.I.A., de Ruwe, M.J., van den Heuvel, F.A.J., Collart, M.A., Boelens, R., and Timmers, H.T.M. (2002). Identification of a ubiquitin-protein ligase subunit within the CCR4-NOT transcription repressor complex. EMBO J. *21*, 355–364.

Albert, T.K., Lemaire, M., van Berkum, N.L., Gentz, R., Collart, M.A., and Timmers, H.T. (2000). Isolation and characterization of human orthologs of yeast CCR4-NOT complex subunits. Nucleic Acids Res. *28*, 809–817.

Amaral, P.P., Dinger, M.E., Mercer, T.R., and Mattick, J.S. (2008). The eukaryotic genome as an RNA machine. Science *319*, 1787–1789.

Aravin, A.A., Hannon, G.J., and Brennecke, J. (2007). The Piwi-piRNA pathway provides an adaptive defense in the transposon arms race. Science *318*, 761–764.

Assenholt, J., Mouaikel, J., Saguez, C., Rougemaille, M., Libri, D., and Jensen, T.H. (2011). Implication of Ccr4-Not complex function in mRNA quality control in Saccharomyces cerevisiae. RNA *17*, 1788–1794.

Azzouz, N., Panasenko, O.O., Colau, G., and Collart, M.A. (2009). The CCR4-NOT complex physically and functionally interacts with TRAMP and the nuclear exosome. PLoS ONE *4*, e6760.

Baek, D., Villén, J., Shin, C., Camargo, F.D., Gygi, S.P., and Bartel, D.P. (2008). The impact of microRNAs on protein output. Nature *455*, 64–71.

Bagga, S., Bracht, J., Hunter, S., Massirer, K., Holtz, J., Eachus, R., and Pasquinelli, A.E. (2005). Regulation by let-7 and lin-4 miRNAs results in target mRNA degradation. Cell *122*, 553–563.

Bai, Y., Salvadore, C., Chiang, Y.C., Collart, M.A., Liu, H.Y., and Denis, C.L. (1999). The CCR4 and CAF1 proteins of the CCR4-NOT complex are physically and functionally separated from NOT2, NOT4, and NOT5. Mol. Cell. Biol. *19*, 6642–6651.

Barckmann, B., and Simonelig, M. (2013). Control of maternal mRNA stability in germ cells and early embryos. Biochim. Biophys. Acta *1829*, 714–724.

Bartel, D.P. (2004). MicroRNAs: genomics, biogenesis, mechanism, and function. Cell *116*, 281–297.

Bartel, D.P. (2009). MicroRNAs: Target Recognition and Regulatory Functions. Cell *136*, 215–233.

Basquin, J., Roudko, V.V., Rode, M., Basquin, C., Séraphin, B., and Conti, E. (2012). Architecture of the Nuclease Module of the Yeast Ccr4-Not Complex: the Not1-Caf1-Ccr4 Interaction. Mol. Cell *48*, 207–218.

Bawankar, P., Loh, B., Wohlbold, L., Schmidt, S., and Izaurralde, E. (2013). NOT10 and C2orf29/NOT11 form a conserved module of the CCR4-NOT complex that docks onto the NOT1 N-terminal domain. RNA Biol. *10*, 228–244.

Behm-Ansmant, I., Rehwinkel, J., and Izaurralde, E. (2006a). MicroRNAs silence gene expression by repressing protein expression and/or by promoting mRNA decay. Cold Spring Harb. Symp. Quant. Biol. *71*, 523–530.

Behm-Ansmant, I., Rehwinkel, J., Doerks, T., Stark, A., Bork, P., and Izaurralde, E. (2006b). mRNA degradation by miRNAs and GW182 requires both CCR4:NOT deadenylase and DCP1:DCP2 decapping complexes. Genes Dev. *20*, 1885–1898.

Bernstein, E., Caudy, A.A., Hammond, S.M., and Hannon, G.J. (2001). Role for a bidentate ribonuclease in the initiation step of RNA interference. Nature *409*, 363–366.

Blaszczyk, J., Tropea, J.E., Bubunenko, M., Routzahn, K.M., Waugh, D.S., Court, D.L., and Ji, X. (2001). Crystallographic and modeling studies of RNase III suggest a mechanism for double-stranded RNA cleavage. Structure *9*, 1225–1236.

Bohmert, K., Camus, I., Bellini, C., Bouchez, D., Caboche, M., and Benning, C. (1998). AGO1 defines a novel locus of Arabidopsis controlling leaf development. EMBO J. *17*, 170–180.

Bohnsack, M.T., Czaplinski, K., and Gorlich, D. (2004). Exportin 5 is a RanGTP-dependent dsRNA-binding protein that mediates nuclear export of pre-miRNAs. RNA *10*, 185–191.

Boland, A., Chen, Y., Raisch, T., Jonas, S., Kuzuoglu-Ozturk, D., Wohlbold, L., Weichenrieder, O., and Izaurralde, E. (2013). Structure and assembly of the NOT module of the human CCR4-NOT complex. Nat. Struct. Mol. Biol. *20*, 1289–1297.

Boland, A., Tritschler, F., Heimstädt, S., Izaurralde, E., and Weichenrieder, O. (2010). Crystal structure and ligand binding of the MID domain of a eukaryotic Argonaute protein. EMBO Rep. *11*, 522–527.

Bordeleau, M.-E., Robert, F., Gerard, B., Lindqvist, L., Chen, S.M.H., Wendel, H.-G., Brem, B., Greger, H., Lowe, S.W., Porco, J.A., et al. (2008). Therapeutic suppression of translation initiation modulates chemosensitivity in a mouse lymphoma model. J. Clin. Invest. *118*, 2651–2660.

Braun, J.E., Huntzinger, E., and Izaurralde, E. (2013). The role of GW182 proteins in miRNA-mediated gene silencing. Adv. Exp. Med. Biol. *768*, 147–163.

Braun, J.E., Huntzinger, E., Fauser, M., and Izaurralde, E. (2011). GW182 proteins directly recruit cytoplasmic deadenylase complexes to miRNA targets. Mol. Cell *44*, 120–133.

Cai, X., Hagedorn, C.H., and Cullen, B.R. (2004). Human microRNAs are processed from capped, polyadenylated transcripts that can also function as mRNAs. RNA *10*, 1957–1966.

Caudy, A.A., Ketting, R.F., Hammond, S.M., Denli, A.M., Bathoorn, A.M.P., Tops, B.B.J., Silva, J.M., Myers, M.M., Hannon, G.J., and Plasterk, R.H.A. (2003). A micrococcal nuclease homologue in RNAi effector complexes. Nature *425*, 411–414.

Cech, T.R., and Steitz, J.A. (2014). The noncoding RNA revolution-trashing old rules to forge new ones. Cell *157*, 77–94.

Chapat, C., and Corbo, L. (2014). Novel roles of the CCR4-NOT complex. WIREs RNA *5*, 883–901.

Chekulaeva, M., Filipowicz, W., and Parker, R. (2009). Multiple independent domains of dGW182 function in miRNA-mediated repression in Drosophila. RNA *15*, 794–803.

Chekulaeva, M., Mathys, H., Zipprich, J.T., Attig, J., Colic, M., Parker, R., and Filipowicz, W. (2011). miRNA repression involves GW182-mediated recruitment of CCR4-NOT through conserved W-containing motifs. Nat. Struct. Mol. Biol. *18*, 1218–1226.

Chen, C.-Y.A., Zheng, D., Xia, Z., and Shyu, A.-B. (2009). Ago-TNRC6 triggers microRNA-mediated decay by promoting two deadenylation steps. Nat. Struct. Mol. Biol. *16*, 1160–1166.

Chen, J., Rappsilber, J., Chiang, Y.C., Russell, P., Mann, M., and Denis, C.L. (2001). Purification and characterization of the 1.0 MDa CCR4-NOT complex identifies two novel components of the complex. J. Mol. Biol. *314*, 683–694.

Chen, J., Chiang, Y.-C., and Denis, C.L. (2002). CCR4, a 3“-5” poly(A) RNA and ssDNA exonuclease, is the catalytic component of the cytoplasmic deadenylase. EMBO J. *21*, 1414–1426.

Chen, Y., Boland, A., Kuzuoglu-Ozturk, D., Bawankar, P., Loh, B., Chang, C.-T., Weichenrieder, O., and Izaurralde, E. (2014). A DDX6-CNOT1 complex and W-binding pockets in CNOT9 reveal direct links between miRNA target recognition and silencing. Mol. Cell *54*, 737–750.

Chendrimada, T.P., Finn, K.J., Ji, X., Baillat, D., Gregory, R.I., Liebhaber, S.A., Pasquinelli, A.E., and Shiekhattar, R. (2007). MicroRNA silencing through RISC recruitment of eIF6. Nature *447*, 823–828.

Chendrimada, T.P., Gregory, R.I., Kumaraswamy, E., Norman, J., Cooch, N., Nishikura, K., and Shiekhattar, R. (2005). TRBP recruits the Dicer complex to Ago2 for microRNA processing and gene silencing. Nature *436*, 740–744.

Christie, M., Boland, A., Huntzinger, E., Weichenrieder, O., and Izaurralde, E. (2013). Structure of the PAN3 pseudokinase reveals the basis for interactions with the PAN2 deadenylase and the GW182 proteins. Mol. Cell *51*, 360–373.

Chu, C.-Y., and Rana, T.M. (2006). Translation Repression in Human Cells by MicroRNA-Induced Gene Silencing Requires RCK/p54. PLoS Biol. *4*, e210.

Collart, M.A., and Struhl, K. (1993). CDC39, an essential nuclear protein that negatively regulates transcription and differentially affects the constitutive and inducible HIS3 promoters. EMBO J. *12*, 177–186.

Collart, M.A., and Struhl, K. (1994). NOT1(CDC39), NOT2(CDC36), NOT3, and NOT4 encode a global-negative regulator of transcription that differentially affects TATA-element utilization. Genes Dev. *8*, 525–537.

Collart, M.A., and Panasenko, O.O. (2012). The Ccr4–Not complex. Gene *492*, 42–53.

Coller, J., and Parker, R. (2005). General translational repression by activators of mRNA decapping. Cell *122*, 875–886.

Cooke, A., Prigge, A., and Wickens, M. (2010). Translational repression by deadenylases. J. Biol. Chem. *285*, 28506–28513.

Czech, B., Zhou, R., Erlich, Y., Brennecke, J., Binari, R., Villalta, C., Gordon, A., Perrimon, N., and Hannon, G.J. (2009). Hierarchical rules for Argonaute loading in Drosophila. Mol. Cell *36*, 445–456.

Deforges, J., Locker, N., and Sargueil, B. (2014). mRNAs that specifically interact with eukaryotic ribosomal subunits. Biochimie. doi:10.1016/j.biochi.2014.12.008

Denis, C.L. (1984). Identification of new genes involved in the regulation of yeast alcohol dehydrogenase II. Genetics *108*, 833–844.

Ding, L., Spencer, A., Morita, K., and Han, M. (2005). The Developmental Timing Regulator AIN-1 Interacts with miRISCs and May Target the Argonaute Protein ALG-1 to Cytoplasmic P Bodies in C. elegans. Mol. Cell *19*, 437–447.

Ding, X.C., and Großhans, H. (2009). Repression of C. elegans microRNA targets at the initiation level of translation requires GW182 proteins. EMBO J. *28*, 213–222.

Draper, M.P., Salvadore, C., and Denis, C.L. (1995). Identification of a mouse protein whose homolog in Saccharomyces cerevisiae is a component of the CCR4 transcriptional regulatory complex. Mol. Cell. Biol. *15*, 3487–3495.

Dupressoir, A., Morel, A.-P., Barbot, W., Loireau, M.-P., Corbo, L., and Heidmann, T. (2001). Identification of four families of yCCR4- and Mg2+-dependent endonuclease-related proteins in higher eukaryotes, and characterization of orthologs of yCCR4 with a conserved leucine-rich repeat essential for hCAF1/hPOP2 binding. BMC Genomics *2*, 9.

El-Shami, M., Pontier, D., Lahmy, S., Braun, L., Picart, C., Vega, D., Hakimi, M.-A., Jacobsen, S.E., Cooke, R., and Lagrange, T. (2007). Reiterated WG/GW motifs form functionally and evolutionarily conserved ARGONAUTE-binding platforms in RNAi-related components. Genes Dev. *21*, 2539–2544.

Elfakess, R., and Dikstein, R. (2008). A translation initiation element specific to mRNAs with very short 5'UTR that also regulates transcription. PLoS ONE *3*, e3094.

Elfakess, R., Sinvani, H., Haimov, O., Svitkin, Y., Sonenberg, N., and Dikstein, R. (2011). Unique translation initiation of mRNAs-containing TISU element. Nucleic Acids Res. *39*, 7598–7609.

Eulalio, A., Helms, S., Fritzsch, C., Fauser, M., and Izaurralde, E. (2009a). A C-terminal silencing domain in GW182 is essential for miRNA function. RNA *15*, 1067–1077.

Eulalio, A., Huntzinger, E., and Izaurralde, E. (2008). Getting to the Root of miRNA-Mediated Gene Silencing. Cell *132*, 9–14.

Eulalio, A., Huntzinger, E., Nishihara, T., Rehwinkel, J., Fauser, M., and Izaurralde, E. (2009b). Deadenylation is a widespread effect of miRNA regulation. RNA *15*, 21–32.

Eulalio, A., Rehwinkel, J., Stricker, M., Huntzinger, E., Yang, S.-F., Doerks, T., Dorner, S., Bork, P., Boutros, M., and Izaurralde, E. (2007). Target-specific requirements for enhancers of decapping in miRNA-mediated gene silencing. Genes Dev. *21*, 2558–2570.

Eulalio, A., Tritschler, F., Büttner, R., Weichenrieder, O., Izaurralde, E., and Truffault, V. (2009c). The RRM domain in GW182 proteins contributes to miRNA-mediated gene silencing. Nucleic Acids Res. *37*, 2974–2983.

Eystathioy, T., Chan, E.K.L., Tenenbaum, S.A., Keene, J.D., Griffith, K., and Fritzler, M.J. (2002). A phosphorylated cytoplasmic autoantigen, GW182, associates with a unique population of human mRNAs within novel cytoplasmic speckles. Mol. Biol. Cell *13*, 1338–1351.

Fabian, M.R., and Sonenberg, N. (2012). The mechanics of miRNA-mediated gene silencing: a look under the hood of miRISC. Nat. Struct. Mol. Biol. *19*, 586–593.

Fabian, M.R., Cieplak, M.K., Frank, F., Morita, M., Green, J., Srikumar, T., Nagar, B., Yamamoto, T., Raught, B., Duchaine, T.F., et al. (2011). miRNA-mediated deadenylation is orchestrated by GW182 through two conserved motifs that interact with CCR4–NOT. Nat. Struct. Mol. Biol. *18*, 1211–1217.

Fabian, M.R., Mathonnet, G., Sundermeier, T., Mathys, H., Zipprich, J.T., Svitkin, Y.V., Rivas, F., Jinek, M., Wohlschlegel, J., Doudna, J.A., et al. (2009). Mammalian miRNA RISC recruits CAF1 and PABP to affect PABP-dependent deadenylation. Mol. Cell *35*, 868–880.

Faehnle, C.R., Elkayam, E., Haase, A.D., Hannon, G.J., and Joshua-Tor, L. (2013). The making of a slicer: activation of human Argonaute-1. Cell Rep. *3*, 1901–1909.

Farh, K.K.-H., Grimson, A., Jan, C., Lewis, B.P., Johnston, W.K., Lim, L.P., Burge, C.B., and Bartel, D.P. (2005). The widespread impact of mammalian MicroRNAs on mRNA repression and evolution. Science *310*, 1817–1821.

Fire, A., Xu, S., Montgomery, M.K., Kostas, S.A., Driver, S.E., and Mello, C.C. (1998). Potent and specific genetic interference by double-stranded RNA in Caenorhabditis elegans. Nature *391*, 806–811.

Förstemann, K., Tomari, Y., Du, T., Vagin, V.V., Denli, A.M., Bratu, D.P., Klattenhoff, C., Theurkauf, W.E., and Zamore, P.D. (2005). Normal microRNA maturation and germ-line stem cell maintenance requires Loquacious, a double-stranded RNA-binding domain protein. PLoS Biol. *3*, e236.

Frank, F., Sonenberg, N., and Nagar, B. (2010). Structural basis for 5'-nucleotide base-specific recognition of guide RNA by human AGO2. Nature *465*, 818–822.

Friedman, R.C., Farh, K.K.-H., Burge, C.B., and Bartel, D.P. (2009). Most mammalian mRNAs are conserved targets of microRNAs. Genome Res. *19*, 92–105.

Fukao, A., Mishima, Y., Takizawa, N., Oka, S., Imataka, H., Pelletier, J., Sonenberg, N., Thoma, C., and Fujiwara, T. (2014). MicroRNAs trigger dissociation of eIF4AI and eIF4AII from target mRNAs in humans. Mol. Cell *56*, 79–89.

Fukaya, T., and Tomari, Y. (2011). PABP is not essential for microRNA-mediated translational repression and deadenylation in vitro. EMBO J. *30*, 4998–5009.

Fukaya, T., and Tomari, Y. (2012). MicroRNAs Mediate Gene Silencing via Multiple Different Pathways in Drosophila. Mol. Cell *48*, 825–836.

Fukaya, T., Iwakawa, H.-O., and Tomari, Y. (2014). MicroRNAs block assembly of eIF4F translation initiation complex in Drosophila. Mol. Cell *56*, 67–78.

Fukunaga, R., Han, B.W., Hung, J.-H., Xu, J., Weng, Z., and Zamore, P.D. (2012). Dicer partner proteins tune the length of mature miRNAs in flies and mammals. Cell *151*, 533–546.

Gallie, D.R. (1991). The cap and poly(A) tail function synergistically to regulate mRNA translational efficiency. Genes Dev. *5*, 2108–2116.

Ghildiyal, M., Xu, J., Seitz, H., Weng, Z., and Zamore, P.D. (2010). Sorting of Drosophila small silencing RNAs partitions microRNA* strands into the RNA interference pathway. RNA *16*, 43–56.

Gingras, A.C., Raught, B., and Sonenberg, N. (1999). eIF4 initiation factors: effectors of mRNA recruitment to ribosomes and regulators of translation. Annu. Rev. Biochem. *68*, 913–963.

Giraldez, A.J., Mishima, Y., Rihel, J., Grocock, R.J., Van Dongen, S., Inoue, K., Enright, A.J., and Schier, A.F. (2006). Zebrafish MiR-430 promotes deadenylation and clearance of maternal mRNAs. Science *312*, 75–79.

Grishok, A., Pasquinelli, A.E., Conte, D., Li, N., Parrish, S., Ha, I., Baillie, D.L., Fire, A., Ruvkun, G., and Mello, C.C. (2001). Genes and mechanisms related to RNA interference regulate expression of the small temporal RNAs that control C. elegans developmental timing. Cell *106*, 23–34.

Grishok, A., Tabara, H., and Mello, C.C. (2000). Genetic requirements for inheritance of RNAi in C. elegans. Science *287*, 2494–2497.

Guo, H., Ingolia, N.T., Weissman, J.S., and Bartel, D.P. (2010). Mammalian microRNAs predominantly act to decrease target mRNA levels. Nature *466*, 835–840.

Ha, M., and Kim, V.N. (2014). Regulation of microRNA biogenesis. Nat. Rev. Mol. Cell Biol. *15*, 509–524.

Haase, A.D., Jaskiewicz, L., Zhang, H., Lainé, S., Sack, R., Gatignol, A., and Filipowicz, W. (2005). TRBP, a regulator of cellular PKR and HIV-1 virus expression, interacts with Dicer and functions in RNA silencing. EMBO Rep. *6*, 961–967.

Hamilton, A.J., and Baulcombe, D.C. (1999). A species of small antisense RNA in posttranscriptional gene silencing in plants. Science *286*, 950–952.

Hammond, S.M., Bernstein, E., Beach, D., and Hannon, G.J. (2000). An RNA-directed nuclease mediates post-transcriptional gene silencing in Drosophila cells. Nature *404*, 293–296.

Han, J., Lee, Y., Yeom, K.-H., Kim, Y.K., Jin, H., and Kim, V.N. (2004). The Drosha-DGCR8 complex in primary microRNA processing. Genes Dev. *18*, 3016–3027.

Hanzawa, H., de Ruwe, M.J., Albert, T.K., van Der Vliet, P.C., Timmers, H.T., and Boelens, R. (2001). The structure of the C4C4 ring finger of human NOT4 reveals features distinct from those of C3HC4 RING fingers. J. Biol. Chem. *276*, 10185–10190.

Hauptmann, J., Dueck, A., Harlander, S., Pfaff, J., Merkl, R., and Meister, G. (2013). Turning catalytically inactive human Argonaute proteins into active slicer enzymes. Nat. Struct. Mol. Biol. *20*, 814–817.

Hendrickson, D.G., Hogan, D.J., McCullough, H.L., Myers, J.W., Herschlag, D., Ferrell, J.E., and Brown, P.O. (2009). Concordant regulation of translation and mRNA abundance for hundreds of targets of a human microRNA. PLoS Biol. *7*, e1000238.

Hiroi, N., Ito, T., Yamamoto, H., Ochiya, T., Jinno, S., and Okayama, H. (2002). Mammalian Rcd1 is a novel transcriptional cofactor that mediates retinoic acid-induced cell differentiation. EMBO J. *21*, 5235–5244.

Höck, J., and Meister, G. (2008). The Argonaute protein family. Genome Biol. *9*, 210.

Hrdlickova, B., de Almeida, R.C., Borek, Z., and Withoff, S. (2014). Genetic variation in the non-coding genome: Involvement of micro-RNAs and long non-coding RNAs in disease. Biochim. Biophys. Acta *1842*, 1910–1922.

Hu, H.Y., Yan, Z., Xu, Y., Hu, H., Menzel, C., Zhou, Y.H., Chen, W., and Khaitovich, P. (2009). Sequence features associated with microRNA strand selection in humans and flies. BMC Genomics *10*, 413.

Humphreys, D., Westman, B.J., Martin, D.I., and Preiss, T. (2005). MicroRNAs control translation initiation by inhibiting eukaryotic initiation factor 4E/cap and poly(A) tail function. Proc. Natl. Acad. Sci. USA 1–6.

Huntzinger, E., and Izaurralde, E. (2011). Gene silencing by microRNAs: contributions of translational repression and mRNA decay. Nat. Rev.Genet. *12*, 99–110.

Huntzinger, E., Braun, J.E., Heimstädt, S., Zekri, L., and Izaurralde, E. (2010). Two PABPC1-binding sites in GW182 proteins promote miRNA-mediated gene silencing. EMBO J. *29*, 4146–4160.

Huntzinger, E., Kuzuoglu-Ozturk, D., Braun, J.E., Eulalio, A., Wohlbold, L., and Izaurralde, E. (2013). The interactions of GW182 proteins with PABP and deadenylases are required for both translational repression and degradation of miRNA targets. Nucleic Acids Res. *41*, 978–994.

Hutvágner, G., McLachlan, J., Pasquinelli, A.E., Bálint, E., Tuschl, T., and Zamore, P.D. (2001). A cellular function for the RNA-interference enzyme Dicer in the maturation of the let-7 small temporal RNA. Science *293*, 834–838.

Ito, K., Inoue, T., Yokoyama, K., Morita, M., Suzuki, T., and Yamamoto, T. (2011a). CNOT2 depletion disrupts and inhibits the CCR4-NOT deadenylase complex and induces apoptotic cell death. Genes Cells *16*, 368–379.

Ito, K., Takahashi, A., Morita, M., Suzuki, T., and Yamamoto, T. (2011b). The role of the CNOT1 subunit of the CCR4-NOT complex in mRNA deadenylation and cell viability. Protein Cell *2*, 755–763.

Iwasaki, S., Kawamata, T., and Tomari, Y. (2009). Drosophila argonaute1 and argonaute2 employ distinct mechanisms for translational repression. Mol. Cell *34*, 58–67.

Jakymiw, A., Lian, S., Eystathioy, T., Li, S., Satoh, M., Hamel, J.C., Fritzler, M.J., and Chan, E.K.L. (2005). Disruption of GW bodies impairs mammalian RNA interference. Nat. Cell Biol. *7*, 1267–1274.

Jiang, F., Ye, X., Liu, X., Fincher, L., McKearin, D., and Liu, Q. (2005). Dicer-1 and R3D1-L catalyze microRNA maturation in Drosophila. Genes Dev. *19*, 1674–1679.

Jinek, M., Fabian, M.R., Coyle, S.M., Sonenberg, N., and Doudna, J.A. (2010). Structural insights into the human GW182-PABC interaction in microRNA-mediated deadenylation. Nat. Struct. Mol. Biol. *17*, 238–240.

Jonas, S., and Izaurralde, E. (2013). The role of disordered protein regions in the assembly of decapping complexes and RNP granules. Genes Dev. *27*, 2628–2641.

Kahvejian, A., Svitkin, Y.V., Sukarieh, R., M'Boutchou, M.-N., and Sonenberg, N. (2005). Mammalian poly(A)-binding protein is a eukaryotic translation initiation factor, which acts via multiple mechanisms. Genes Dev. *19*, 104–113.

Kamenska, A., Lu, W.-T., Kubacka, D., Broomhead, H., Minshall, N., Bushell, M.,

and Standart, N. (2014). Human 4E-T represses translation of bound mRNAs and enhances microRNA-mediated silencing. Nucleic Acids Res. *42*, 3298–3313.

Kawamata, T., and Tomari, Y. (2010). Making RISC. Trends Biochem. Sci. *35*, 368–376.

Kerr, S.C., Azzouz, N., Fuchs, S.M., Collart, M.A., Strahl, B.D., Corbett, A.H., and Laribee, R.N. (2011). The Ccr4-Not Complex Interacts with the mRNA Export Machinery. PLoS ONE *6*, e18302.

Ketting, R.F., Fischer, S.E., Bernstein, E., Sijen, T., Hannon, G.J., and Plasterk, R.H. (2001). Dicer functions in RNA interference and in synthesis of small RNA involved in developmental timing in C. elegans. Genes Dev. *15*, 2654–2659.

Khvorova, A., Reynolds, A., and Jayasena, S.D. (2003). Functional siRNAs and miRNAs exhibit strand bias. Cell *115*, 209–216.

Kim, V.N. (2006). Small RNAs just got bigger: Piwi-interacting RNAs (piRNAs) in mammalian testes. Genes Dev. *20*, 1993–1997.

Kim, V.N., Han, J., and Siomi, M.C. (2009). Biogenesis of small RNAs in animals. Nat. Rev. Mol. Cell Biol. *10*, 126–139.

Kiriakidou, M., Tan, G.S., Lamprinaki, S., De Planell-Saguer, M., Nelson, P.T., and Mourelatos, Z. (2007). An mRNA m7G Cap Binding-like Motif within Human Ago2 Represses Translation. Cell *129*, 1141–1151.

Kloosterman, W.P., Kloos, Wienholds, E., Wien, RF, K., and Plasterk, R.H.A. (2004). Substrate requirements for let-7 function in the developing zebrafish embryo. Nucleic Acids Res. *32*, 6284–6291.

Knight, S.W., and Bass, B.L. (2001). A role for the RNase III enzyme DCR-1 in RNA interference and germ line development in Caenorhabditis elegans. Science *293*, 2269–2271.

Kozlov, G., Safaee, N., Rosenauer, A., and Gehring, K. (2010). Structural basis of binding of P-body-associated proteins GW182 and ataxin-2 by the Mlle domain of poly(A)-binding protein. J. Biol. Chem. *285*, 13599–13606.

Kozomara, A., and Griffiths-Jones, S. (2014). miRBase: annotating high confidence microRNAs using deep sequencing data. Nucleic Acids Res. *42*, D68–D73.

Kuzuoglu-Ozturk, D., Huntzinger, E., Schmidt, S., and Izaurralde, E. (2012). The Caenorhabditis elegans GW182 protein AIN-1 interacts with PAB-1 and subunits of the PAN2-PAN3 and CCR4-NOT deadenylase complexes. Nucleic Acids Res. *40*, 5651–5665.

Kwak, P.B., and Tomari, Y. (2012). The N domain of Argonaute drives duplex unwinding during RISC assembly. Nat. Struct. Mol. Biol. *19*, 145–151.

Lau, N.C., Lim, L.P., Weinstein, E.G., and Bartel, D.P. (2001). An abundant class of tiny RNAs with probable regulatory roles in Caenorhabditis elegans. Science *294*,

858–862.

Lau, N.-C., Kolkman, A., van Schaik, F.M.A., Mulder, K.W., Pijnappel, W.W.M.P., Heck, A.J.R., and Timmers, H.T.M. (2009). Human Ccr4-Not complexes contain variable deadenylase subunits. Biochem. J. *422*, 443–453.

Lazzaretti, D., Tournier, I., and Izaurralde, E. (2009). The C-terminal domains of human TNRC6A, TNRC6B, and TNRC6C silence bound transcripts independently of Argonaute proteins. RNA *15*, 1059–1066.

Lee, H.Y., Zhou, K., Smith, A.M., Noland, C.L., and Doudna, J.A. (2013). Differential roles of human Dicer-binding proteins TRBP and PACT in small RNA processing. Nucleic Acids Res. *41*, 6568–6576.

Lee, R.C., Feinbaum, R.L., and Ambros, V. (1993). The C. elegans heterochronic gene lin-4 encodes small RNAs with antisense complementarity to lin-14. Cell *75*, 843–854.

Lee, Y., Hur, I., Park, S.Y., Kim, Y.K., Suh, M.R., and Kim, V.N. (2006). The role of PACT in the RNA silencing pathway. EMBO J. *25*, 522–532.

Lee, Y., Kim, M., Han, J., Yeom, K.-H., Lee, S., Baek, S.H., and Kim, V.N. (2004). MicroRNA genes are transcribed by RNA polymerase II. EMBO J. *23*, 4051–4060.

Lim, L.P., Lau, N.C., Garrett-Engele, P., Grimson, A., Schelter, J.M., Castle, J., Bartel, D.P., Linsley, P.S., and Johnson, J.M. (2005). Microarray analysis shows that some microRNAs downregulate large numbers of target mRNAs. Nature *433*, 769–773.

Lingel, A., Simon, B., Izaurralde, E., and Sattler, M. (2004). Nucleic acid 3'-end recognition by the Argonaute2 PAZ domain. Nat. Struct. Mol. Biol. *11*, 576–577.

Liu, H.Y., Badarinarayana, V., Audino, D.C., Rappsilber, J., Mann, M., and Denis, C.L. (1998). The NOT proteins are part of the CCR4 transcriptional complex and affect gene expression both positively and negatively. EMBO J. *17*, 1096–1106.

Liu, J., Carmell, M.A., Rivas, F.V., Marsden, C.G., Thomson, J.M., Song, J.-J., Hammond, S.M., Joshua-Tor, L., and Hannon, G.J. (2004). Argonaute2 is the catalytic engine of mammalian RNAi. Science *305*, 1437–1441.

Liu, J., Rivas, F.V., Wohlschlegel, J., Yates, J.R., Parker, R., and Hannon, G.J. (2005). A role for the P-body component GW182 in microRNA function. Nat. Cell Biol. *7*, 1261–1266.

Lund, E., Güttinger, S., Calado, A., Dahlberg, J.E., and Kutay, U. (2004). Nuclear export of microRNA precursors. Science *303*, 95–98.

Lytle, J.R., Lytle, Yario, T.A., A, T., Steitz, J.A., Steitz (2007). Target mRNAs are repressed as efficiently by microRNA-binding sites in the 5′ UTR as in the 3′ UTR. Proc. Natl. Acad. Sci. USA *104*, 9667–9672.

Ma, J.-B., Ye, K., and Patel, D.J. (2004). Structural basis for overhang-specific small

interfering RNA recognition by the PAZ domain. Nature *429*, 318–322.

Ma, J.-B., Yuan, Y.-R., Meister, G., Pei, Y., Tuschl, T., and Patel, D.J. (2005). Structural basis for 5'-end-specific recognition of guide RNA by the A. fulgidus Piwi protein. Nature *434*, 666–670.

Maillet, L., Tu, C., Hong, Y.K., Shuster, E.O., and Collart, M.A. (2000). The essential function of Not1 lies within the Ccr4-not complex. J. Mol. Biol. *303*, 131–143.

Malvar, T., Biron, R.W., Kaback, D.B., and Denis, C.L. (1992). The CCR4 protein from Saccharomyces cerevisiae contains a leucine-rich repeat region which is required for its control of ADH2 gene expression. Genetics *132*, 951–962.

Maroney, P.A., Yu, Y., Fisher, J., and Nilsen, T.W. (2006). Evidence that microRNAs are associated with translating messenger RNAs in human cells. Nat. Struct. Mol. Biol. *13*, 1102–1107.

Mathonnet, G., Fabian, M.R., Svitkin, Y.V., Parsyan, A., Huck, L., Murata, T., Biffo, S., Merrick, W.C., Darzynkiewicz, E., Pillai, R.S., et al. (2007). MicroRNA inhibition of translation initiation in vitro by targeting the cap-binding complex eIF4F. Science *317*, 1764–1767.

Mathys, H., Basquin, J., Ozgur, S., Czarnocki-Cieciura, M., Bonneau, F., Aartse, A., Dziembowski, A., Nowotny, M., Conti, E., and Filipowicz, W. (2014). Structural and biochemical insights to the role of the CCR4-NOT complex and DDX6 ATPase in microRNA repression. Mol. Cell *54*, 751–765.

Mattick, J.S., and Makunin, I.V. (2006). Non-coding RNA. Hum. Mol. Genet. *15*, R17–R29.

Mauxion, F., Prève, B., and Séraphin, B. (2013). C2ORF29/CNOT11 and CNOT10 form a new module of the CCR4-NOT complex. RNA Biol. *10*, 267–276.

Meijer, H.A., Kong, Y.W., Lu, W.T., Wilczynska, A., Spriggs, R.V., Robinson, S.W., Godfrey, J.D., Willis, A.E., and Bushell, M. (2013). Translational Repression and eIF4A2 Activity Are Critical for MicroRNA-Mediated Gene Regulation. Science *340*, 82–85.

Meister, G. (2013). Argonaute proteins: functional insights and emerging roles. Nat. Rev.Genet. *14*, 447–459.

Meister, G., Landthaler, M., Peters, L., Chen, P.Y., Urlaub, H., Lührmann, R., and Tuschl, T. (2005). Identification of novel argonaute-associated proteins. Curr. Biol. *15*, 2149–2155.

Mishima, Y., Giraldez, A.J., Takeda, Y., Fujiwara, T., Sakamoto, H., Schier, A.F., and Inoue, K. (2006). Differential regulation of germline mRNAs in soma and germ cells by zebrafish miR-430. Curr. Biol. *16*, 2135–2142.

Moore, M.J. (2005). From birth to death: the complex lives of eukaryotic mRNAs. Science *309*, 1514–1518.

Moretti, F., Kaiser, C., Zdanowicz-Specht, A., and Hentze, M.W. (2012). PABP and the poly(A) tail augment microRNA repression by facilitated miRISC binding. Nat. Struct. Mol. Biol. *19*, 603–608.

Nakanishi, K., Weinberg, D.E., Bartel, D.P., and Patel, D.J. (2012). Structure of yeast Argonaute with guide RNA. Nature *486*, 368–374.

Nottrott, S., Simard, M.J., and Richter, J.D. (2006). Human let-7a miRNA blocks protein production on actively translating polyribosomes. Nat. Struct. Mol. Biol. *13*, 1108–1114.

Okamura, K., Liu, N., and Lai, E.C. (2009). Distinct Mechanisms for MicroRNA Strand Selection by Drosophila Argonautes. Mol. Cell *36*, 431–444.

Olsen, P.H., and Ambros, V. (1999). The lin-4 regulatory RNA controls developmental timing in Caenorhabditis elegans by blocking LIN-14 protein synthesis after the initiation of translation. Dev. Biol. *216*, 671–680.

Parker, J.S., Roe, S.M., and Barford, D. (2005). Structural insights into mRNA recognition from a PIWI domain-siRNA guide complex. Nature *434*, 663–666.

Petersen, C.P., Bordeleau, M.-E., Pelletier, J., and Sharp, P.A. (2006). Short RNAs Repress Translation after Initiation in Mammalian Cells. Mol. Cell *21*, 533–542.

Petit, A.-P., Wohlbold, L., Bawankar, P., Huntzinger, E., Schmidt, S., Izaurralde, E., and Weichenrieder, O. (2012). The structural basis for the interaction between the CAF1 nuclease and the NOT1 scaffold of the human CCR4-NOT deadenylase complex. Nucleic Acids Res. *40*, 11058–11072.

Pfaff, J., Hennig, J., Herzog, F., Aebersold, R., Sattler, M., Niessing, D., and Meister, G. (2013). Structural features of Argonaute-GW182 protein interactions. Proc. Natl. Acad. Sci. USA *110*, E3770–E3779.

Pfeffer, S., Sewer, A., Lagos-Quintana, M., Sheridan, R., Sander, C., Grässer, F.A., van Dyk, L.F., Ho, C.K., Shuman, S., Chien, M., et al. (2005). Identification of microRNAs of the herpesvirus family. Nat. Methods *2*, 269–276.

Piao, X., Zhang, X., Wu, L., and Belasco, J.G. (2010). CCR4-NOT deadenylates mRNA associated with RNA-induced silencing complexes in human cells. Mol. Cell. Biol. *30*, 1486–1494.

Pillai, R.S., Bhattacharyya, S.N., Artus, C.G., Zoller, T., Cougot, N., Basyuk, E., Bertrand, E., and Filipowicz, W. (2005). Inhibition of translational initiation by Let-7 MicroRNA in human cells. Science *309*, 1573–1576.

Reed, S.I. (1980). The selection of amber mutations in genes required for completion of start, the controlling event of the cell division cycle of S. cerevisiae. Genetics *95*, 579–588.

Rehwinkel, J., Behm-Ansmant, I., Gatfield, D., and Izaurralde, E. (2005). A crucial role for GW182 and the DCP1:DCP2 decapping complex in miRNA-mediated gene silencing. RNA *11*, 1640–1647.

Rivas, F.V., Tolia, N.H., Song, J.-J., Aragon, J.P., Liu, J., Hannon, G.J., and Joshua-Tor, L. (2005). Purified Argonaute2 and an siRNA form recombinant human RISC. Nat. Struct. Mol. Biol. *12*, 340–349.

Russell, P., Benson, J.D., and Denis, C.L. (2002). Characterization of Mutations in NOT2 Indicates that it Plays an Important Role in Maintaining the Integrity of the CCR4–NOT Complex. J. Mol. Biol. *322*, 27–39.

Rüegger, S., and Großhans, H. (2012). MicroRNA turnover: when, how, and why. Trends Biochem. Sci. *37*, 436–446.

Saito, K., Ishizuka, A., Siomi, H., and Siomi, M.C. (2005). Processing of pre-microRNAs by the Dicer-1-Loquacious complex in Drosophila cells. PLoS Biol. *3*, e235.

Sakai, A., Chibazakura, T., Shimizu, Y., and Hishinuma, F. (1992). Molecular analysis of POP2 gene, a gene required for glucose-derepression of gene expression in Saccharomyces cerevisiae. Nucleic Acids Res. *20*, 6227–6233.

Schirle, N.T., and MacRae, I.J. (2012). The crystal structure of human Argonaute2. Science *336*, 1037–1040.

Schwarz, D.S., Hutvágner, G., Du, T., Xu, Z., Aronin, N., and Zamore, P.D. (2003). Asymmetry in the assembly of the RNAi enzyme complex. Cell *115*, 199–208.

Schwede, A., Ellis, L., Luther, J., Carrington, M., Stoecklin, G., and Clayton, C. (2008). A role for Caf1 in mRNA deadenylation and decay in trypanosomes and human cells. Nucleic Acids Res. *36*, 3374–3388.

Seggerson, K., Tang, L., and Moss, E.G. (2002). Two genetic circuits repress the Caenorhabditis elegans heterochronic gene lin-28 after translation initiation. Dev. Biol. *243*, 215–225.

Selbach, M., Schwanhäusser, B., Thierfelder, N., Fang, Z., Khanin, R., and Rajewsky, N. (2008). Widespread changes in protein synthesis induced by microRNAs. Nature *455*, 58–63.

Sinvani, H., Haimov, O., Svitkin, Y., Sonenberg, N., Tamarkin-Ben-Harush, A., Viollet, B., and Dikstein, R. (2015). Translational Tolerance of Mitochondrial Genes to Metabolic Energy Stress Involves TISU and eIF1-eIF4GI Cooperation in Start Codon Selection. Cell Metab. *21*, 479–492.

Song, J.-J., Smith, S.K., Hannon, G.J., and Joshua-Tor, L. (2004). Crystal structure of Argonaute and its implications for RISC slicer activity. Science *305*, 1434–1437.

Subtelny, A.O., Eichhorn, S.W., Chen, G.R., Sive, H., and Bartel, D.P. (2014). Poly(A)-tail profiling reveals an embryonic switch in translational control. Nature *508*, 66–71.

Sung, D., and Kang, H. (1998). The N-terminal amino acid sequences of the firefly luciferase are important for the stability of the enzyme. Photochem. Photobiol. *68*, 749–753.

Sweet, T., Kovalak, C., and Coller, J. (2012). The DEAD-box protein Dhh1 promotes decapping by slowing ribosome movement. PLoS Biol. *10*, e1001342.

Takimoto, K., Wakiyama, M., and Yokoyama, S. (2009). Mammalian GW182 contains multiple Argonaute-binding sites and functions in microRNA-mediated translational repression. RNA *15*, 1078–1089.

Temme, C., Zaessinger, S., Meyer, S., Simonelig, M., and Wahle, E. (2004). A complex containing the CCR4 and CAF1 proteins is involved in mRNA deadenylation in Drosophila. EMBO J. *23*, 2862–2871.

Temme, C., Zhang, L., Kremmer, E., Ihling, C., Chartier, A., Sinz, A., Simonelig, M., and Wahle, E. (2010). Subunits of the Drosophila CCR4-NOT complex and their roles in mRNA deadenylation. RNA *16*, 1356–1370.

Thermann, R., and Hentze, M.W. (2007). Drosophila miR2 induces pseudo-polysomes and inhibits translation initiation. Nature *447*, 875–878.

Thompson, S.R. (2012). So you want to know if your message has an IRES? WIREs RNA *3*, 697–705.

Thore, S., Mauxion, F., Séraphin, B., and Suck, D. (2003). X-ray structure and activity of the yeast Pop2 protein: a nuclease subunit of the mRNA deadenylase complex. EMBO Rep. *4*, 1150–1155.

Till, S., Lejeune, E., Thermann, R., Bortfeld, M., Hothorn, M., Enderle, D., Heinrich, C., Hentze, M.W., and Ladurner, A.G. (2007). A conserved motif in Argonaute-interacting proteins mediates functional interactions through the Argonaute PIWI domain. Nat. Struct. Mol. Biol. *14*, 897–903.

Tolia, N.H., and Joshua-Tor, L. (2007). Slicer and the Argonautes. Nature Chemical Biology *3*, 36–43.

Tucker, M., Valencia-Sanchez, M.A., Staples, R.R., Chen, J., Denis, C.L., and Parker, R. (2001). The transcription factor associated Ccr4 and Caf1 proteins are components of the major cytoplasmic mRNA deadenylase in Saccharomyces cerevisiae. Cell *104*, 377–386.

Tucker, M., Staples, R.R., Valencia-Sanchez, M.A., Muhlrad, D., and Parker, R. (2002). Ccr4p is the catalytic subunit of a Ccr4p/Pop2p/Notp mRNA deadenylase complex in Saccharomyces cerevisiae. EMBO J. *21*, 1427–1436.

Wahle, E., and Winkler, G.S. (2013). RNA decay machines: deadenylation by the Ccr4-not and Pan2-Pan3 complexes. Biochim. Biophys. Acta *1829*, 561–570.

Wakiyama, M., Takimoto, K., Ohara, O., and Yokoyama, S. (2007). Let-7 microRNA-mediated mRNA deadenylation and translational repression in a mammalian cell-free system. Genes Dev. *21*, 1857–1862.

Wang, Y., Juranek, S., Li, H., Sheng, G., Tuschl, T., and Patel, D.J. (2008). Structure of an argonaute silencing complex with a seed-containing guide DNA and target RNA duplex. Nature *456*, 921–926.

Weatheritt, R.J., and Gibson, T.J. (2012). Linear motifs: lost in (pre)translation. Trends Biochem. Sci. *37*, 333–341.

Wightman, B., Ha, I., and Ruvkun, G. (1993). Posttranscriptional regulation of the heterochronic gene lin-14 by lin-4 mediates temporal pattern formation in C. elegans. Cell *75*, 855–862.

Wilusz, J.E., JnBaptiste, C.K., Lu, L.Y., Kuhn, C.-D., Joshua-Tor, L., and Sharp, P.A. (2012). A triple helix stabilizes the 3' ends of long noncoding RNAs that lack poly(A) tails. Genes Dev. *26*, 2392–2407.

Wolfe, A.L., Singh, K., Zhong, Y., Drewe, P., Rajasekhar, V.K., Sanghvi, V.R., Mavrakis, K.J., Jiang, M., Roderick, J.E., Van der Meulen, J., et al. (2014). RNA G-quadruplexes cause eIF4A-dependent oncogene translation in cancer. Nature *513*, 65–70.

Wu, L., and Belasco, J.G. (2005). Micro-RNA regulation of the mammalian lin-28 gene during neuronal differentiation of embryonal carcinoma cells. Mol. Cell. Biol. *25*, 9198–9208.

Wu, L., Fan, J., and Belasco, J.G. (2006). MicroRNAs direct rapid deadenylation of mRNA. Proc. Natl. Acad. Sci. USA *103*, 4034–4039.

Yamashita, A., Chang, T.-C., Yamashita, Y., Zhu, W., Zhong, Z., Chen, C.-Y.A., and Shyu, A.-B. (2005). Concerted action of poly(A) nucleases and decapping enzyme in mammalian mRNA turnover. Nat. Struct. Mol. Biol. *12*, 1054–1063.

Yi, R., Qin, Y., Macara, I.G., and Cullen, B.R. (2003). Exportin-5 mediates the nuclear export of pre-microRNAs and short hairpin RNAs. Genes Dev. *17*, 3011–3016.

Yigit, E., Batista, P.J., Bei, Y., Pang, K.M., Chen, C.-C.G., Tolia, N.H., Joshua-Tor, L., Mitani, S., Simard, M.J., and Mello, C.C. (2006). Analysis of the C. elegans Argonaute family reveals that distinct Argonautes act sequentially during RNAi. Cell *127*, 747–757.

Zamore, P.D., Tuschl, T., Sharp, P.A., and Bartel, D.P. (2000). RNAi: double-stranded RNA directs the ATP-dependent cleavage of mRNA at 21 to 23 nucleotide intervals. Cell *101*, 25–33.

Zdanowicz, A., Thermann, R., Kowalska, J., Jemielity, J., Duncan, K., Preiss, T., Darzynkiewicz, E., and Hentze, M.W. (2009). Drosophila miR2 Primarily Targets the m7GpppN Cap Structure for Translational Repression. Mol. Cell *35*, 881–888.

Zekri, L., Huntzinger, E., Heimstädt, S., and Izaurralde, E. (2009). The silencing domain of GW182 interacts with PABPC1 to promote translational repression and degradation of microRNA targets and is required for target release. Mol. Cell. Biol. *29*, 6220–6231.

Zekri, L., Kuzuoglu-Ozturk, D., and Izaurralde, E. (2013). GW182 proteins cause PABP dissociation from silenced miRNA targets in the absence of deadenylation. EMBO J. 1–14.

Zhang, H., Kolb, F.A., Jaskiewicz, L., Westhof, E., and Filipowicz, W. (2004). Single processing center models for human Dicer and bacterial RNase III. Cell *118*, 57–68.

Zhang, L., Ding, L., Cheung, T.H., Dong, M.-Q., Chen, J., Sewell, A.K., Liu, X., Yates, J.R., III, and Han, M. (2007). Systematic Identification of C. elegans miRISC Proteins, miRNAs, and mRNA Targets by Their Interactions with GW182 Proteins AIN-1 and AIN-2. Mol. Cell *28*, 598–613.

Zipprich, J.T., Bhattacharyya, S., Mathys, H., and Filipowicz, W. (2009). Importance of the C-terminal domain of the human GW182 protein TNRC6C for translational repression. RNA *15*, 781–793.

Zwartjes, C.G.M., Jayne, S., van den Berg, D.L.C., and Timmers, H.T.M. (2004). Repression of promoter activity by CNOT2, a subunit of the transcription regulatory Ccr4-not complex. J. Biol. Chem. *279*, 10848–10854.

8. ABBREVIATIONS

4E-T	4E-Transporter
ABD	AGO-binding domain
Adh	*Alcohol dehydrogenase*
AGO	Argonaute
AIN	ALG-1 interacting protein
ALG	Argonaute-like
ARM	Armadillo repeats
At	*Arabidopsis thaliana*
C-term	C-terminal
C2orf29	Chromosome 2 open reading frame 29
CAF	CCR4 associated factor
CCR4	Carbon catabolite repressor 4
CDC	Cell cycle division
Ce	*Caenorhabditis elegans*
CIM	CCR4-NOT interacting motif
CN9BD	CNOT9 binding domain
Co-IP	Co-immunoprecipitation
CS	Connector sequence
DCP	Decapping protein
DDX6	DEAD box protein 6
DEED	Asp-Glu-Asp-Asp
DGCR8	DiGeorge syndrome critical region 8
Dhh1	DexD7H-box helicase 1
Dm	*Drosophila melanogaster*
DNA	Deoxyribonucleic acid
dsRBD	Double-stranded RNA binding domain
dsRNA	Double-stranded RNA
DUF	Domain of unknown function
EDC	Enhancer of decapping
EEP	Endonuclease-exonuclease-phosphatase
eIF	Eukaryotic initiation factor
EXP5	Exportin 5

GW	Glycine-tryptophan
GW182	Glycine-tryptophan repeat containing protein of 182 kDa size, Gawky
HA	Hemagglutinin
HEAT	Huntingtin, elongation factor 3, protein phosphatase 2A, TOR1
HEK293T	Human embryonic kidney 293T cells
HeLa	Henrietta Lacks
HhR	Hammerhead ribozyme
Hs	*Homo sapiens*
HSC70	Heat shock cognate 70 protein
HSP90	Heat shock protein 90 chaperone complex
IP	Immunoprecipitation
IRES	Internal ribosome entry site
lncRNA	Long non-coding RNA
Loq	Loquacious
LRR	Leucine rich repeat
MALAT1	Metastasis associated lung adenocarcinoma transcript 1
Me31B	Maternal expression at 31B
Mid	Middle
MIF4G	Middle domain of eukaryotic initiation factor 4G
miRISC	miRNA induced silencing complex
miRNA	Micro RNA
mRNA	Messanger RNA
mRNP	Messanger ribonucleoprotein
N-term	N-terminal
NAR	NOT anchor region
ncRNA	Non-coding RNA
NOT	Negative on TATA-less
NSHD	NOT1 superfamily homology domain
Nt	Nucleotides
ORF	Open reading frame
PABP	Poly(A) binding protein
PACT	Protein activator of PKR
PAM2	Poly(A) binding motif 2

PAN	Poly(A) nuclease
PAZ	Piwi-Ago-Zwille
piRNA	Piwi-interacting RNA
PIWI	P-element induced wimpy testis
POP2	PGK promoter directed over production
pre-miRNA	Precursor micro RNA
pri-miRNA	Primary micro RNA
PTM	Post-translational modification
Q-rich	Glutamine-rich
Rcd1	Cell differentiation protein
RIIID	RNase III domain
RISC	RNA-induced silencing complex
RNA	Ribonucleic acid
RQCD1	Required for cell differentiation 1
RRM	RNA-recognition motif
rRNA	Ribosomal RNA
S2	Schneider 2 cells
SD	Silencing domain
siRNA	Small interfering RNA
SLiM	Short linear motif
snoRNA	Small nucleolar RNA
snRNA	Small nuclear RNA
TAB182	Tankyrase-binding protein 182
TISU	Translation initiator of short 5’ UTR
TNRC6	Trinucleotide repeat containing gene protein 6
TRBP	Trans-activation response RNA-binding protein
tRNA	Transfer RNA
UBA	Ubiquitin-associated
UTR	Untranslated region
XRN1	5’-3’ exoribonuclease 1

9. APPENDIX

9.1 List of Publication

9.1.1 Discussed Publications

The original manuscripts of the publications listed in this section are attached.

1. The *Caenorhabditis elegans* GW182 protein AIN-1 interacts with PAB-1 and subunits of the PAN2-PAN3 and CCR4-NOT deadenylase complexes.

Kuzuoglu-Ozturk, D., Huntzinger, E., Schmidt, S., and Izaurralde, E.

Nucleic Acids Res. 2012 July; *40*(12), 5651–5665.

2. The interactions of GW182 proteins with PABP and deadenylases are required for both translational repression and degradation of miRNA targets.

Huntzinger, E*., Kuzuoglu-Ozturk, D*., Braun, J.E., Eulalio, A., Wohlbold, L., and Izaurralde, E.

Nucleic Acids Res. 2013 Jan; *41*(2), 978–994. *equal contributions

3. Structure and assembly of the NOT module of the human CCR4-NOT complex.

Boland, A*., Chen, Y*., Raisch, T*., Jonas, S*., Kuzuoglu-Ozturk, D., Wohlbold, L., Weichenrieder, O., and Izaurralde, E.

Nat. Struct. Mol. Biol. 2013 Nov, *20*(11), 1289–1297. *equal contributions

4. A DDX6-CNOT1 complex and W-binding pockets in CNOT9 reveal direct links between miRNA target recognition and silencing.

Chen, Y*., Boland, A*., Kuzuoglu-Ozturk, D*., Bawankar, P., Loh, B., Chang, C.-T., Weichenrieder, O., and Izaurralde, E.

Mol. Cell 2014, *54*(5), 737–750. *equal contributions

5. miRISC and the CCR4-NOT complex repress and degrade mRNA targets independently of 43S ribosomal scanning.

Kuzuoglu-Ozturk D., Bhandari D., Huntzinger E., Fauser M., Helms S., and Izaurralde E.

Genes Dev. 2015, under review

9.1.2 Additional Publications (during PhD)

6. GW182 proteins cause PABP dissociation from silenced miRNA targets in the absence of deadenylation.

Zekri L., Kuzuoglu-Ozturk, D., and Izaurralde, E.

EMBO J. 2013, *32*(7), 1052-1065.

9.1.3 Additional Publications (prior PhD)

7. Autophagy-related gene, TdAtg8, in wild emmer wheat plays a role in drought and osmotic stress response.

Kuzuoglu-Ozturk D*., Cebeci Yalcinkaya O*., Akpinar B.A., Mitou G., Korkmaz G., Gozuacik D., and Budak H.

Planta 2012 Oct; *236*(4), 1081-92. *equal contributions

8. The prevalence of Behcet's syndrome, familial Mediterranean fever, HLA-B51 and MEFV gene mutations among ethic Armenians living in Istanbul, Turkey.

Seyahi E., Tahir Turanli E., Mangan M.S., Celikyapi G., Oktay V., Cevirgen D., Kuzuoglu D., Ozoglu S., and Yazici H.

Clin Exp Rheumatol. 2010 Jul-Aug; *28*, 67-75.

9.2 Original manuscripts of the discussed publications

Published online 7 March 2012

Nucleic Acids Research, 2012, Vol. 40, No. 12 ***5651–5665***
doi:10.1093/nar/gks218

The *Caenorhabditis elegans* GW182 protein AIN-1 interacts with PAB-1 and subunits of the PAN2-PAN3 and CCR4-NOT deadenylase complexes

Duygu Kuzuoğlu-Öztürk, Eric Huntzinger, Steffen Schmidt and Elisa Izaurralde*

Department of Biochemistry, Max Planck Institute for Developmental Biology, Spemannstrasse 35, D-72076 Tübingen, Germany

Received January 14, 2012; Revised February 18, 2012; Accepted February 21, 2012

ABSTRACT

GW182 family proteins are essential for miRNA-mediated gene silencing in animal cells. They are recruited to miRNA targets via interactions with Argonaute proteins and then promote translational repression and degradation of the miRNA targets. The human and *Drosophila melanogaster* GW182 proteins share a similar domain organization and interact with PABPC1 as well as with subunits of the PAN2-PAN3 and CCR4-NOT deadenylase complexes. The homologous proteins in *Caenorhabditis elegans*, AIN-1 and AIN-2, lack most of the domains present in the vertebrate and insect proteins, raising the question as to how AIN-1 and AIN-2 contribute to silencing. Here, we show that both AIN-1 and AIN-2 interact with Argonaute proteins through GW repeats in the middle region of the AIN proteins. However, only AIN-1 interacts with *C. elegans* and *D. melanogaster* PABPC1, PAN3, NOT1 and NOT2, suggesting that AIN-1 and AIN-2 are functionally distinct. Our findings reveal a surprising evolutionary plasticity of the GW182 protein interaction network and demonstrate that binding to PABPC1 and deadenylase complexes has been maintained throughout evolution, highlighting the significance of these interactions for silencing.

INTRODUCTION

The proteins AIN-1 and AIN-2 have important and partially redundant functions in the miRNA pathway in *Caenorhabditis elegans* (*Ce*) (1–4). They are highly divergent members of the GW182 protein family, which plays an essential role in miRNA-mediated gene silencing in animals (5). In vertebrates and several invertebrate species, there are up to three GW182 paralogs with partially redundant functions, whereas there is only one orthologous protein in *Drosophila melanogaster* (*Dm* GW182).

GW182 family proteins are characterized by an N-terminal region (N-term) containing multiple glycine–tryptophan repeats (GW repeats), a central ubiquitin-associated (UBA) domain and a C-terminal RNA recognition motif (RRM) (Figure 1A) (2,6–9). Additional regions of the protein include a glutamine-rich (Q-rich) region, which is located between the UBA domain and the RRM, and a middle (Mid) and C-terminal (C-term) regions containing few or none GW repeats (Figure 1A) (6–9).

The N-term GW repeat region of the proteins mediates binding to the Argonaute (AGO) proteins and thus is essential for miRNA-mediated gene silencing (7,10–15). The Mid and C-term regions (collectively termed the silencing domain, SD) are also required for silencing (12,13,16,17). Indeed, GW182 protein mutants lacking the silencing domain fail to rescue silencing of several miRNA reporters in cells lacking endogenous GW182, even though these proteins interact with AGO proteins and are active in tethering assays (12,17–21).

The precise mechanism by which GW182 proteins mediate silencing is not completely understood. However, important insight was provided by the observation that these proteins interact with the cytoplasmic poly(A)-binding protein (PABPC1) and with subunits of the two major cytoplasmic deadenylase complexes (the PAN2-PAN3 and CCR4-NOT complexes) both in *D. melanogaster* and human cells (17,19–25).

Binding to PABPC1 is mediated by a conserved PAM2 motif (PABP-binding motif 2) located in the Mid region. This motif directly binds to the C-term MLLE domain of PABPC1 (17,22–24). Moreover, the protein sequences downstream of the PAM2 motif (termed M2) together with the C-term region mediate indirect binding to PABPC1 *in vivo* (17).

*To whom correspondence should be addressed. Tel: +49 7071 601 1350; Fax: +49 7071 601 1353; Email: elisa.izaurralde@tuebingen.mpg.de

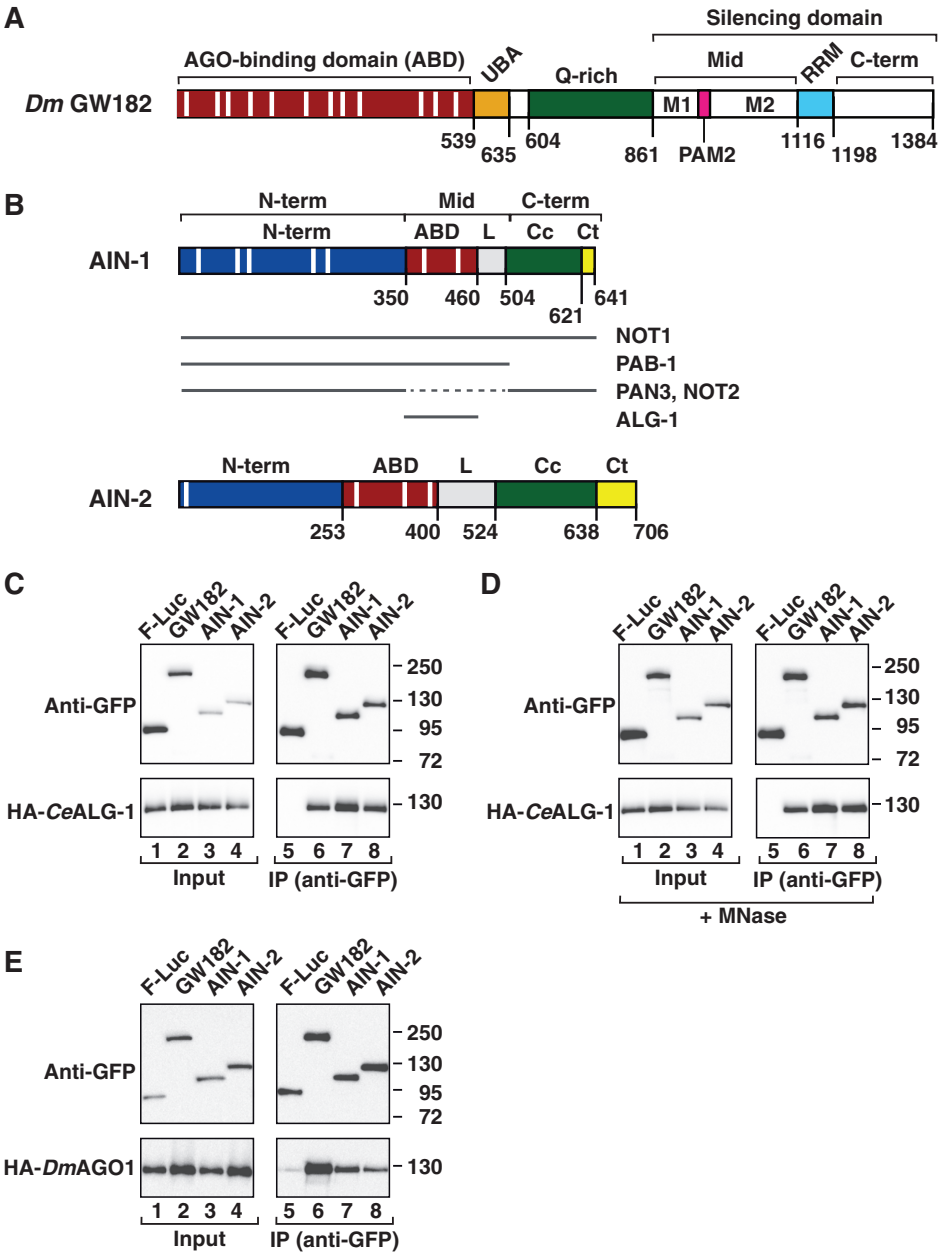

Figure 1. Interaction of AIN-1 and AIN-2 proteins with ALG-1. (**A**) Domain organization of *Dm* GW182. The N-term ABD is shown in red, with GW repeats shown as white vertical bars; Mid, Middle domain with PAM2 motif, M1 and M2 regions; The silencing domain includes the Mid and C-term regions but not the RRM, which is dispensable for silencing (38). (**B**) Domain organization of AIN-1 and AIN-2. Regions colored in red and green show limited similarity to the corresponding regions in *Dm* GW182. Cc, region with helical propensity. Gray lines underneath AIN-1 schematic represent protein fragments required for the interaction with the indicated partners. (**C–E**) S2 cells were cotransfected with plasmids expressing GFP-tagged *Dm* GW182, AIN-1 or AIN-2, and HA-tagged *Ce* ALG-1 or *Dm* AGO1. Cell lysates were immunoprecipitated using a polyclonal anti-GFP antibody. GFP-tagged firefly luciferase served as a negative control. For the HA-tagged proteins, inputs (1%) and immunoprecipitates (35%) were analyzed. For the GFP-tagged proteins, 3.5% of the inputs and 8% of the IPs were loaded. In panel D, cell lysates were treated with Micrococcal nuclease (MNase).

In addition to PABPC1, the silencing domains of human GW182 proteins (known as TNRC6A, B and C) confer direct binding to PAN3 and NOT1, which are subunits of the PAN2-PAN3 and CCR4-NOT deadenylase complexes, respectively (20,21,25). Binding to PAN3 is mediated by the M2- and C-term regions of the silencing domain (20), whereas NOT1 binding requires W-containing motifs in the M1, M2 and C-term regions (Figure 1A) (20,21,25). The interactions with the deadenylase complex subunits are conserved in *Dm* (20,21).

Remarkably, the *Ce* proteins AIN-1 and AIN-2 show <12% global sequence identity to *Dm* GW182 and human TNRC6s and do not contain sequences homologous to the

silencing domain (Figure 1B) (2,8,9). They also lack UBA and RRM domains, a PAM2 motif, as well as a defined Q-rich region. One common feature between AIN-1, AIN-2 and other GW182 proteins is the presence of GW repeats, which are dispersed within the N-term and Mid regions of AIN-1 and AIN-2. Accordingly, AIN-1 and AIN-2 coimmunoprecipitate *Ce* AGO-like proteins 1 and 2 (ALG-1 and ALG-2) (1,3). However, it is not known which GW repeats in AIN-1 and AIN-2 contribute to ALG-1 and ALG-2 binding.

The highly divergent sequences of AIN-1 and AIN-2 raise the question regarding how these proteins contribute to silencing and whether there are differences in the mechanisms of silencing between species. One possibility is that AIN-1 and AIN-2 perform similar functions as their vertebrate and insect homologs but have evolved different modes of interaction with PABPC1 and deadenylase complexes. Alternatively, AIN-1 and AIN-2 may serve as adaptor proteins between ALG-1,2 and other protein(s), which in turn mediate binding to PABPC1 and deadenylase complexes. Finally, miRNA-mediated gene silencing in *Ce* may occur by a different mechanism that does not require interactions with PABPC1 or deadenylase complexes, although miRNA targets have also been reported to undergo deadenylation in *Ce* (26).

In this study, we identified the GW repeats that are required for AIN-1 and AIN-2 to interact with ALG-1. Despite the low sequence conservation with *Drosophil*a and human GW182 proteins, we found that AIN-1 interacts with *Ce* PABPC1 (PAB-1), PAN3, NOT1 and NOT2, whereas AIN-2 showed no significant interaction. Thus, despite strong sequence divergence, the interaction of AIN-1 with PABPC1 and deadenylase complexes has been conserved throughout evolution, underscoring their importance for miRNA-mediated gene silencing.

MATERIALS AND METHODS

Sequence analysis

Ce AIN-1 (WBGene00015547) and AIN-2 (WBGene00015007) sequences were analyzed using sensitive methods such as PSI-BLAST and HHpred (27,28). The sequence identity of the paralogous sequences of AIN-1 and AIN-2 is ~12%, but the Mid and C-term regions show some common features, as depicted in Figure 1A and B. Sequence homology to the AGO-binding region of *Dm* GW182 was detected using extensive PSI-BLAST searches (red region). Sequence homology for another region (green) to a region in *Dm* GW182 (amino acids 721–795) was also detected using HHpred. This region shows helical propensity and is annotated as Q-rich in *Dm* GW182.

Plasmids

Luciferase reporters and plasmids for expression of miRNAs, *Dm* AGO1, *Dm* GW182, *Dm* PABPC1 and subunits of the *Drosophila* deadenylase complexes were described before (7,19,20,29). The AGO1 F2V2 mutant carries valine substitutions of phenylalanines 594 (F594V) and 629 (F629V) (11). For expression of *Ce* proteins, the corresponding cDNAs were cloned into the pAc5.1A–λN-HA or pAc5.1–EGFP vectors as described in Supplementary Table S1. Mutations in AIN-1 and AIN-2 were generated by site-directed mutagenesis using the QuickChange mutagenesis kit from Stratagene.

Coimmunoprecipitations and western blots

Coimmunoprecipitations were performed as previously described (17). Briefly, S2 cells were transfected in six-well plates using the Effectene Transfection Reagent (Qiagen). The transfection mixtures contained 1, 0.2 and 1 μg of plasmid expressing GFP-tagged *Dm* GW182, AIN-1 and AIN-2, respectively, or the corresponding mutants, and 0.5 μg of HA-tagged proteins (*Ce* PABP, *Ce* ALG-1, *Dm* AGO1 or deadenylation factors). *Dm* PABPC1 was expressed with a C-term V5 tag. Cells ($10–12 \times 10^6$ cells) were harvested 3 days after transfection, washed with PBS and lysed on ice in 0.5 ml of NET buffer [50 mM Tris (pH 7.4), 150 mM NaCl, 1 mM EDTA and 0.1% Triton X-100] containing a protease inhibitor cocktail for 30 min. Cell lysates were supplemented with 2.5 mM $CaCl_2$ and treated with micrococcal nuclease for 30 min. After removal of insoluble proteins, cell lysates were incubated with homemade rabbit polyclonal anti-GFP antibodies (2 μl) for 1 h. Subsequently, Protein A-Sepharose beads (GE HealthCare, 50 μl) were added and samples were gently rotated for 1 h at 4°C. Beads were washed 3 times with NET buffer and once with NET buffer without Triton X-100. Proteins were eluted with SDS–PAGE sample buffer and analyzed by western blotting using conventional procedures. Small aliquots from cell lysates prior and after Micrococcal nuclease treatment were analyzed by native agarose gel electrophoresis to confirm that rRNA was efficiently degraded.

HA- and GFP-tagged proteins were detected using HRP-conjugated monoclonal anti-HA (Roche 3F10; 1:5000) and anti-GFP antibodies (Roche 11 814 460 001; 1:2000), respectively. V5-tagged proteins were detected with anti-V5 antibodies (Invitrogen, 1:5000). All western blots were developed with the ECL western blotting detection system (GE Healthcare) as recommended by the manufacturer.

Complementation and tethering assays in S2 cells

S2 cells were transfected in 24- or 6-well plates using Effectene transfection reagent (Qiagen). For the tethering assay, the following plasmids were cotransfected (amounts are given for six-well plates): 0.1 μg reporter plasmid (F-Luc-5BoxB or F-Luc without 5BoxB), 0.4 μg pAc5.1–R–Luc as transfection control and various amounts of plasmids expressing λN-HA-protein fusions (adjusted to obtain equal expression levels for all proteins tested). Firefly and *Renilla* luciferase activities were measured 3 days after transfection using the Dual-Luciferase Reporter Assay System (Promega).

AGO1 complementation assays were performed as described before (11). The following siRNAs were used: AGO1 5′-CGAAGGAGAUCAAGGGUUUUU-3′ and β-Gal 5′-CUACACAAAUCAGCGAUUUUU-3′; Dharmacon). GW182 complementation assays were performed

as previously described (12). For miRNA-mediated silencing assays, the transfection mixtures contained (amounts given for 24-well plates): 20 ng of firefly luciferase reporter plasmid, 80 ng of the *Renilla* transfection control and 40 ng of plasmids expressing miRNA primary transcripts or the corresponding vector without insert. When indicated, 10–100 ng of plasmid expressing recombinant protein was cotransfected.

Firefly and *Renilla* luciferase activities were measured 4 (AGO1 complementation) or 3 (GW182 complementation) days after transfection using the Dual-Luciferase Reporter Assay System (Promega). Total RNA was isolated using TriFast (Peqlab Biotechnologies) and analyzed as previously described (12).

RESULTS

AIN-1 and AIN-2 interact with ALG-1 through GW repeats in the Mid region

Sequence comparison and secondary structure predictions indicated that AIN-1 and AIN-2 consist of five different regions (Figure 1B): an N-term low-complexity region containing 5 and 1 GW repeats, respectively; a region of homology to the AGO-binding domain (ABD) of human TNRC6s and *Dm* GW182, containing additional 2 and 3 GW repeats, respectively; a linker region (L) rich in serine and glycine residues; a region with limited similarity to the Q-rich region of *Dm* GW182 (Cc), which exhibits helical propensity; and a C-terminal tail (Ct). Overall, the sequence identity between AIN-1 and AIN-2 and orthologous vertebrate and insect proteins is <12%, whereas AIN-1 and AIN-2 exhibit 22.4% identity (Supplementary Table S2).

To analyze the interaction of AIN-1 and AIN-2 with potential-binding partners, we used a heterologous system based on *Dm* S2 cells. We validated this approach by showing that AIN-1 and AIN-2 interacted with ALG-1 in these cells. Indeed, GFP-tagged versions of AIN-1 and AIN-2 coimmunoprecipitated HA-tagged ALG-1 in lysates from S2 cells coexpressing these proteins (Figure 1C and D, lanes 7 and 8). Interestingly, *Dm* GW182 also bound to ALG-1 (Figure 1C and D, lane 6), indicating that the mode of interaction is conserved. Conversely, both AIN-1 and AIN-2 coimmunoprecipitated *Dm* AGO1 (Figure 1E), consistent with the observation that ALG-1 and AGO1 exhibit 61% identity (Supplementary Table S3). The interactions with ALG-1 were observed in cell lysates treated with Micrococcal nuclease, suggesting that they are not mediated by RNA (Figure 1D, MNase).

To define the regions in AIN-1 required for ALG-1 binding, we generated mutants lacking either the N-term, Mid or C-term regions (Figure 1B) and tested them in coimmunoprecipitation assays. We observed that deletion of the AIN-1 Mid region abolished ALG-1 binding, whereas deletion of the N-term or C-term regions had no effect (Figure 2A). Furthermore, protein fragments containing only the AIN-1 Mid region or the Mid region without the linker (hereafter termed the AGO-binding domain, ABD) were sufficient for binding to ALG-1 (Figure 2A, lane 11; Figure 2B, lanes 7 and 8). These results indicate that the N-term GW repeats do not significantly contribute to the AIN-1/ALG-1 interaction.

The ABD of AIN-1 contains two GW repeats; to examine their contribution to ALG-1 binding, we substituted the tryptophan residues in each repeat with alanines. These substitutions slightly reduced AIN-1 binding to ALG-1 (Figure 2C, lanes 10 and 11). A stronger reduction was observed when the substitutions were combined (Figure 2C, lane 12). However, the AIN-1 double mutant retained some residual ALG-1 binding relative to the AIN-1 mutant lacking the entire Mid region (Figure 2C, lane 12 versus 9), indicating that additional residues in the Mid region contribute to the interaction.

A similar analysis of the interaction of AIN-2 with ALG-1 revealed that the corresponding ABD is essential for this interaction (Figure 2D, lane 13). The AIN-2 ABD contains 3 GW repeats. We observed that alanine substitution of the tryptophan residue in the first repeat (GW1-A) reduced binding to ALG-1, whereas substitutions in repeats 2 and 3 had no effect (Figure 2D, lanes 14–16). ALG1 binding was abolished when repeats 1 and 2 were substituted simultaneously (Figure 2D, lane 17), whereas substitutions in repeats 1 and 3 or 2 and 3 reduced but did not abolish binding (Figure 2D, lanes 18 and 19). We conclude that the GW repeats in the ABD are essential for AIN-2 to interact with ALG-1. These repeats contribute to ALG-1 binding in an additive manner as previously observed for the human and *Dm* GW182 proteins (10,12,13,15,30). These results also indicate that a GW repeat present in the AIN-2 N-term region does not detectably contribute to the interaction with ALG-1.

AIN-1 interacts with the RRM domains of PAB-1

We next tested whether AIN-1 and AIN-2 interact with *Ce* PAB-1. Remarkably, only AIN-1 coimmunoprecipitated HA-tagged *Ce* PAB-1 (Figure 3A and B, lane 7). In contrast, AIN-2 did not detectably interact with PAB-1, although it was expressed at similar levels (Figure 3A and B, lane 8). Interestingly, although *Ce* and *Dm* PABPC1 exhibit 51.5% identity (Supplementary Table S3), *Dm* GW182 did not interact with *Ce* PAB-1 (Figure 3A and B, lane 6). In contrast, AIN-1 interacted with *Dm* PABPC1 (Figure 3C, lanes 11 and 15). The interaction of AIN-1 with *Ce* or *Dm* PABPC1 was observed in extracts treated with Micrococcal nuclease, suggesting that this association is not mediated by RNA (Figure 3B and C).

PABPC1 contains four N-term RRM1–4, a proline-rich unstructured linker, and a C-term domain [termed PABC or MLLE because of a conserved KITGMLLE signature motif in this domain; Figure 3D; (24)]. Human TNRC6 and *Dm* GW182 interact directly with the C-term MLLE domain of PABPC1 through a conserved PAM2 motif located in the Mid region of the silencing domain [see Figure 1A; (17,22–24)]. However, we could not identify a PAM2 motif in AIN-1. To map the sequences in AIN-1 required for PAB-1 binding, we performed coimmunoprecipitations using the deletion mutants

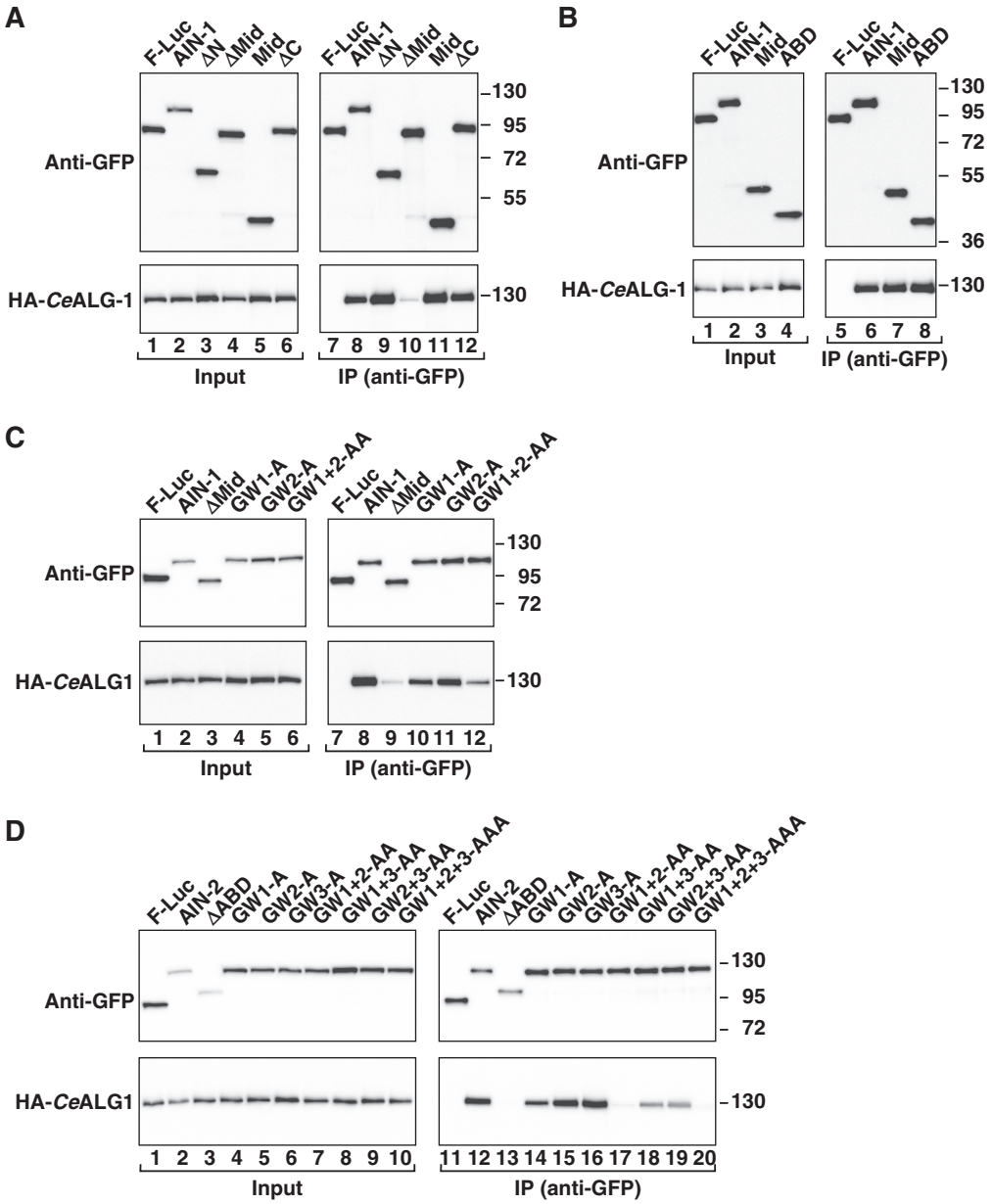

Figure 2. GW repeats in the ABD domains of AIN-1 and AIN-2 mediate binding to ALG-1. (**A–D**) S2 cells coexpressing HA-ALG-1 together with GFP-tagged AIN-1 or AIN-2 (wild-type or mutants) were lysed 3 days after transfection. Cell lysates were immunoprecipitated with a polyclonal anti-GFP antibody and analyzed as described in Figure 1. In panel (C), AIN-1 mutants GW1-A, GW2-A and GW1+2-AA carry alanine substitutions of tryptophan residues in the first, second or both GW repeats, respectively, of the ABD. The same nomenclature was used to describe AIN-2 mutants in panel (D).

described above. We observed that deletion of the N-term or Mid regions of AIN-1 reduced the interaction with PAB-1, whereas deletion of the C-term region was inconsequential (Figure 3E, lanes 9, 10 and 12). However, neither the N-term nor the Mid regions in isolation were sufficient for binding (Figure 3E and F). Thus, both the N-term and Mid regions contribute to PAB-1 binding (Figure 1B).

We next investigated whether AIN-1 interacts with the MLLE domain of PAB-1 despite the lack of a PAM2 motif. We observed that AIN-1 interacted preferentially with the RRM domains of PAB-1 but not with the MLLE domain (Figure 3G). We conclude that the interaction of GW182 proteins with PABP is conserved, although the interaction mode may differ between species.

AIN-1 interacts with the PAN3 C-term kinase-like domain

We next studied whether AIN-1 and AIN-2 interact with *Ce* PAN3. As observed for PAB-1, only AIN-1 interacted with *Ce* PAN3 in an RNA-independent manner (Figure 4A and B, lane 7), whereas AIN-2 or GW182 did not bind (Figure 4A and B, lanes 6 and 8). In

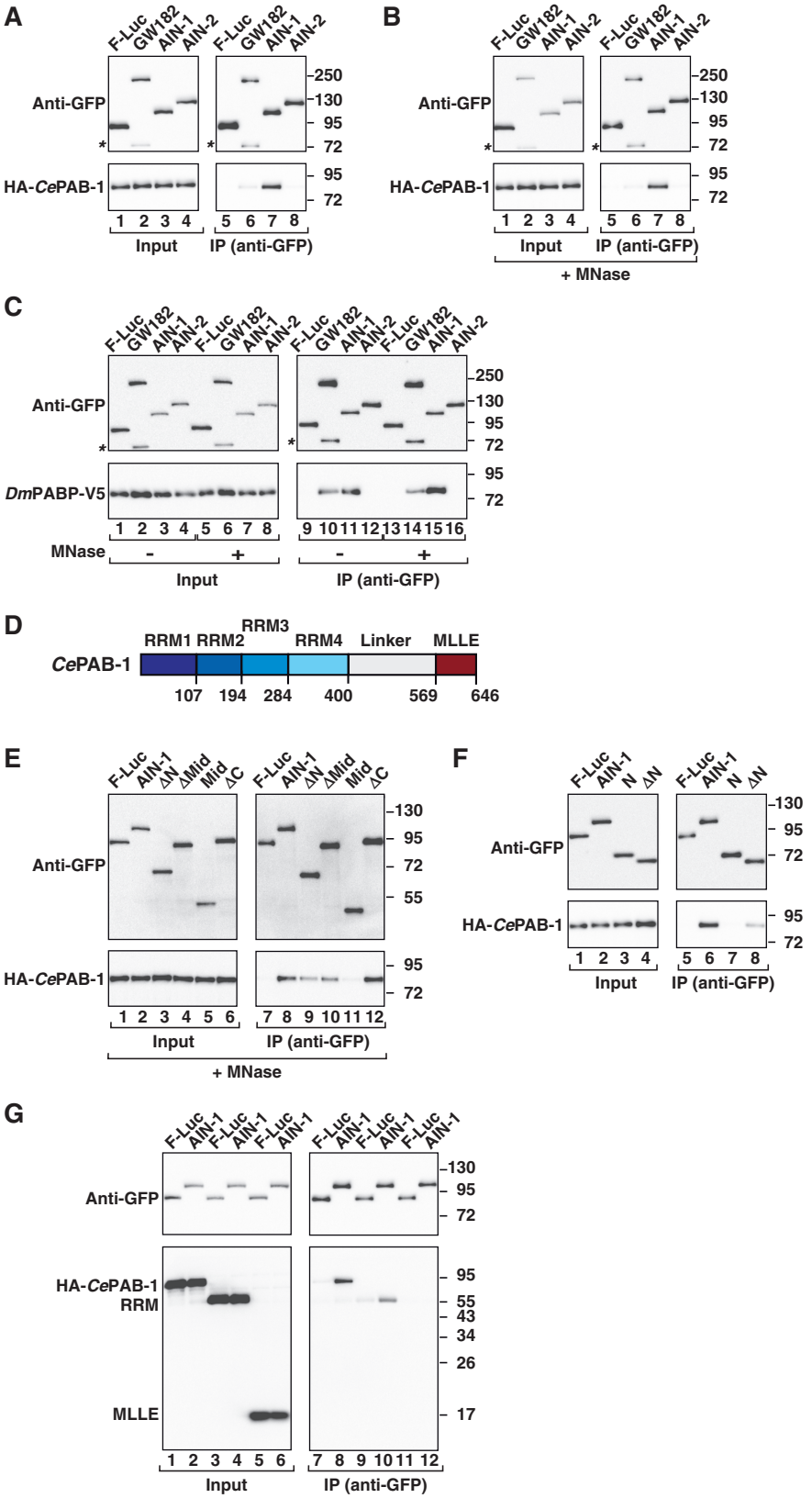

Figure 3. AIN-1 interacts with the RRM domains of PAB-1. (**A–C**) S2 cells were cotransfected with plasmids expressing GFP-tagged GW182, AIN-1 or AIN-2, and HA-tagged *Ce* PAB-1 or V5-tagged *Dm* PABP as indicated. Cell lysates were immunoprecipitated and analyzed as described in Figure 1. Asterisks indicate a *Dm* GW182 degradation product. (**D**) Domain organization of *Ce* PAB-1. PAB-1 consists of four N-term RRM1–4, a proline-rich unstructured linker, and a conserved C-term domain, termed MLLE. (**E–G**) The interaction of GFP-tagged AIN-1 (wild type or mutants) with full-length HA-tagged *Ce* PAB-1 or fragments was analyzed as described in Figure 1. In panels B and E, cell lysates were treated with Micrococcal nuclease.

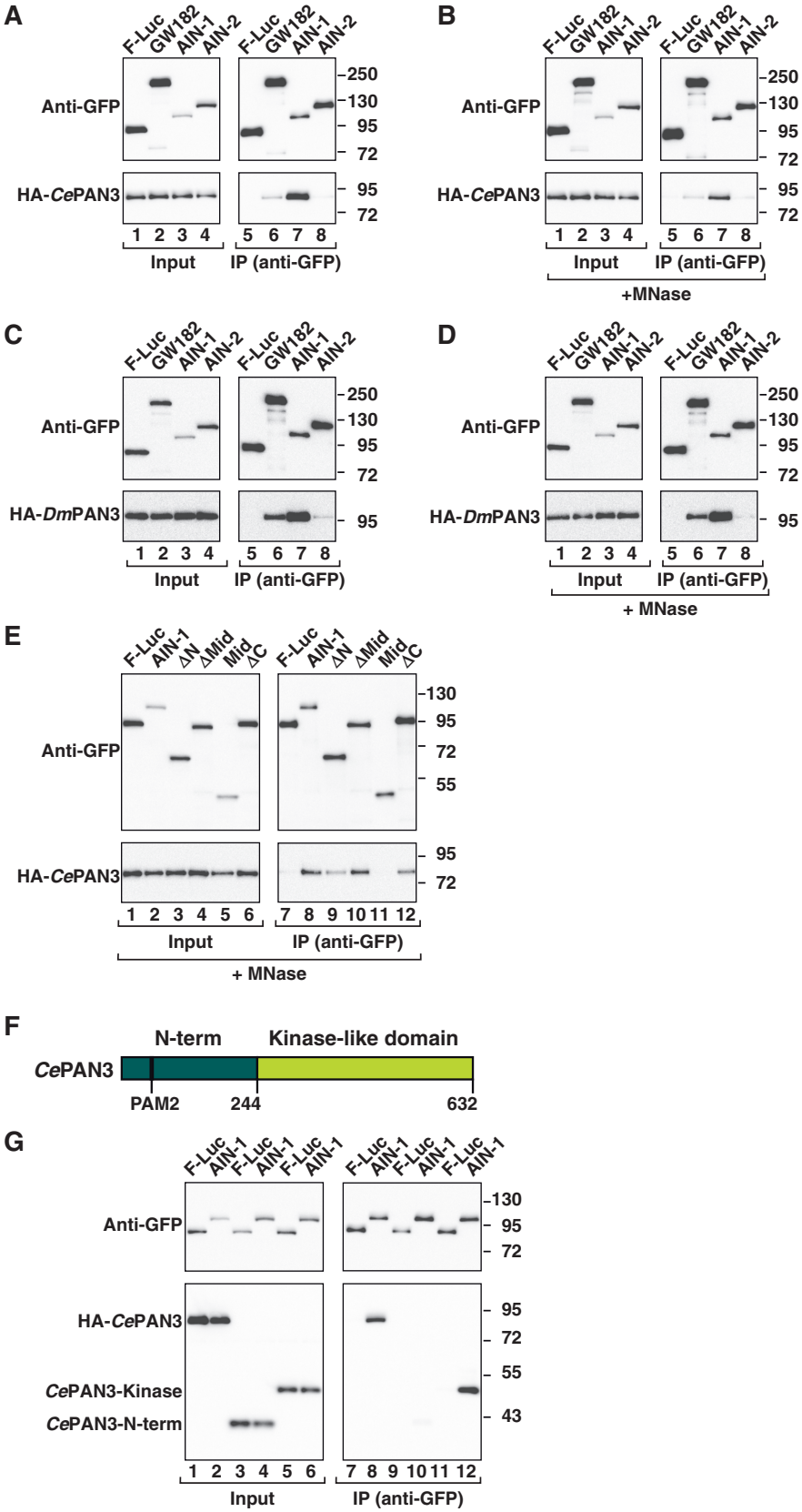

Figure 4. AIN-1 interacts with the PAN3 kinase-like domain. (**A–D**) The interaction of GFP-tagged GW182, AIN-1 or AIN-2 with HA-tagged *Ce* or *Dm* PAN3 was analyzed as described in Figure 1. (**E**) Interaction of GFP-tagged AIN-1 wild type or mutants, and HA-tagged *Ce* PAN3. (**F**) Domain organization of *Ce* PAN3. PAN3 consists of an N-term region containing a PAM2 motif, and a conserved C-term domain related to protein kinases. (**G**) Interaction of GFP-tagged AIN-1 with HA-tagged wild-type *Ce* PAN3 or deletion mutants.

contrast, AIN-1 coimmunoprecipitated *Dm* PAN3 more efficiently than *Dm* GW182 (Figure 4C and D).

Our previous studies showed that human TNRC6 proteins interact with PAN3 through the M2 and C-term regions of the silencing domains (20). We observed that deletion of either the N-term or C-term regions of AIN-1 reduced binding to PAN3 (Figure 4E and Supplementary Figure S1A). In contrast, a protein fragment containing both the N-term and C-term regions but lacking the Mid region (ΔMid) interacted with PAN3 to a similar extent as full-length AIN-1 (Figure 4E, lane 10 and Supplementary Figure S1A), indicating that the N-term and C-term regions both contribute to the interaction. Accordingly, the isolated N-term or C-term regions did not interact with PAN3 (Supplementary Figure S1A).

PAN3 proteins contain an N-term region and a C-term domain with homology to protein kinases (Figure 4F). The PAN3 N-term region contains a canonical PAM2 motif and interacts with PABPC1, whereas the C-term kinase-like domain is required for PAN3 binding to PAN2, the catalytic subunit of the PAN2–PAN3 deadenylase complex (31–33). Our previous studies showed a direct interaction between human TNRC6 proteins and the kinase-like domain of PAN3 (20). Likewise, AIN-1 interacted with the PAN3 kinase-like domain but not with the N-term region (Figure 4G). Thus, the interaction of GW182 proteins with the kinase-like domain of PAN3 is conserved. Since the PAN3 kinase-like domain does not interact with PABPC1, we conclude that AIN-1 interacts with PAN3 independently of PABPC1, as previously reported for human TNRC6s (20).

AIN-1 interacts with NOT1 and NOT2

We also examined the interaction of AIN-1 and AIN-2 with NOT1 and NOT2, which are the subunits of the CCR4-NOT complex that exhibit the strongest interaction with *Dm* GW182 (20). We observed that AIN-1 interacted with *Ce* NOT1 and *Ce* NOT2 (a.k.a. NTL-2) (Figure 5A–C, lane 7), as well as with *Dm* NOT1 and *Dm* NOT2 (Figure 5D and E), whereas AIN-2 showed very weak binding to *Ce* NOT1 (Figure 5B, lane 8). Immunoprecipitations with AIN-1 deletion mutants, revealed that full-length AIN-1 is required for binding to NOT1, as deletion of either the N-term, Mid or C-term regions reduced binding and none of these regions in isolation was sufficient for binding (Figure 5F). In contrast, the AIN-1 interaction with NOT2 is mediated by the N-term and C-term regions, as an AIN-1 mutant lacking the Mid domain coimmunoprecipitated NOT2 to a similar extent as the full-length protein (Figure 5G, lane 14 versus 10; see Figure 1B).

Recent work showed that the interaction of human TNRC6s with NOT1 is mediated by W-containing motifs in the M1, M2 and C-term regions of the silencing domains (21,25). These motifs contribute to the affinity of the interaction in an additive manner. AIN-1 contains a total of 22 tryptophan residues (of which 7 are in GW repeats) in the N-term and Mid regions, whereas the C-term region lacks tryptophan residues. To investigate the potential contribution of W-containing motifs to deadenylase binding, we generated an AIN-1 mutant in which all tryptophan residues were substituted with alanines (AIN-1-22×W-A). This mutant displayed lower mobility in SDS–PAGE and no longer interacted with NOT1 and NOT2 (Supplementary Figure S1B and S1C). As expected, the substitutions abrogated AGO1 and ALG-1 binding (Supplementary Figure S1D and S1E). Unexpectedly, interaction with PAB-1 and PAN3 was also abolished (Supplementary Figure S1F and S1G), suggesting that simultaneous substitution of 22 tryptophan residues by alanines non-specifically disrupted protein–protein interactions. Nevertheless, our data do not rule out that a subset of tryptophan residues is involved in mediating NOT1 binding, as shown recently (21, 25).

ALG-1 rescues silencing in cells depleted of AGO1

Given that the interactions of GW182 proteins with AGOs are conserved and that *Dm* GW182 interacts with *Ce* ALG-1, we tested if ALG-1 could rescue silencing in S2 cells depleted of AGO1, which is the AGO protein dedicated to the miRNA pathway in *D. melanogaster* (34). To this end, we made use of a complementation assay as previously described (11). In this assay, S2 cells were transfected with either siRNA specific to AGO1 or a control siRNA against β-Gal. We then tested ALG-1 for its ability to restore silencing in AGO1-depleted cells.

We monitored miRNA activity using previously characterized firefly luciferase reporters, including the F-Luc-Par-6 reporter (silenced by miR-1) and the F-Luc-Nerfin-1 reporter [silenced by miR-9b; (7,29)]. Depletion of endogenous AGO1 suppressed silencing of the reporters, leading to a 6- to 7-fold increase in firefly luciferase expression (Figure 6A–D). Transfecting AGO1-depleted cells with a plasmid expressing a siRNA-resistant form of AGO1 fully restored silencing (Figure 6A–D) as reported previously (11). Interestingly, ALG-1 also restored silencing in AGO1-depleted cells (Figure 6A–D) when expressed at similar levels (Figure 6E). In contrast, neither ALG-1 nor AGO1 rescued silencing in cells in which AGO1 and *Dm* GW182 were codepleted (Figure 6F and G), indicating that both AGO1 and ALG-1 interact with *Dm* GW182 to silence miRNA targets. Accordingly, coexpression of AGO1 or ALG-1 with a dsRNA-resistant form of *Dm* GW182 rescued silencing in cells codepleted of AGO1 and GW182 (Figure 6F and G). These results indicate conservation in the mechanisms of miRNA loading and target silencing.

AIN-1 and AIN-2 repress expression of bound mRNAs

To investigate the conservation of the pathway downstream of AGOs, we tested whether AIN-1 and AIN-2 could repress expression of target mRNAs using a tethering assay as previously described (35). AIN-1 and AIN-2 were expressed with two tags: a peptide derived from the bacteriophage λ N protein (λN tag) to enable tethering to a firefly luciferase (F-Luc) reporter and an HA tag (hemagglutinin) to allow detection of the expressed protein by western blot. The F-Luc reporter contains five Box B hairpins (5BoxB) inserted in the 3′-UTR; these bind the λN tag with high affinity and

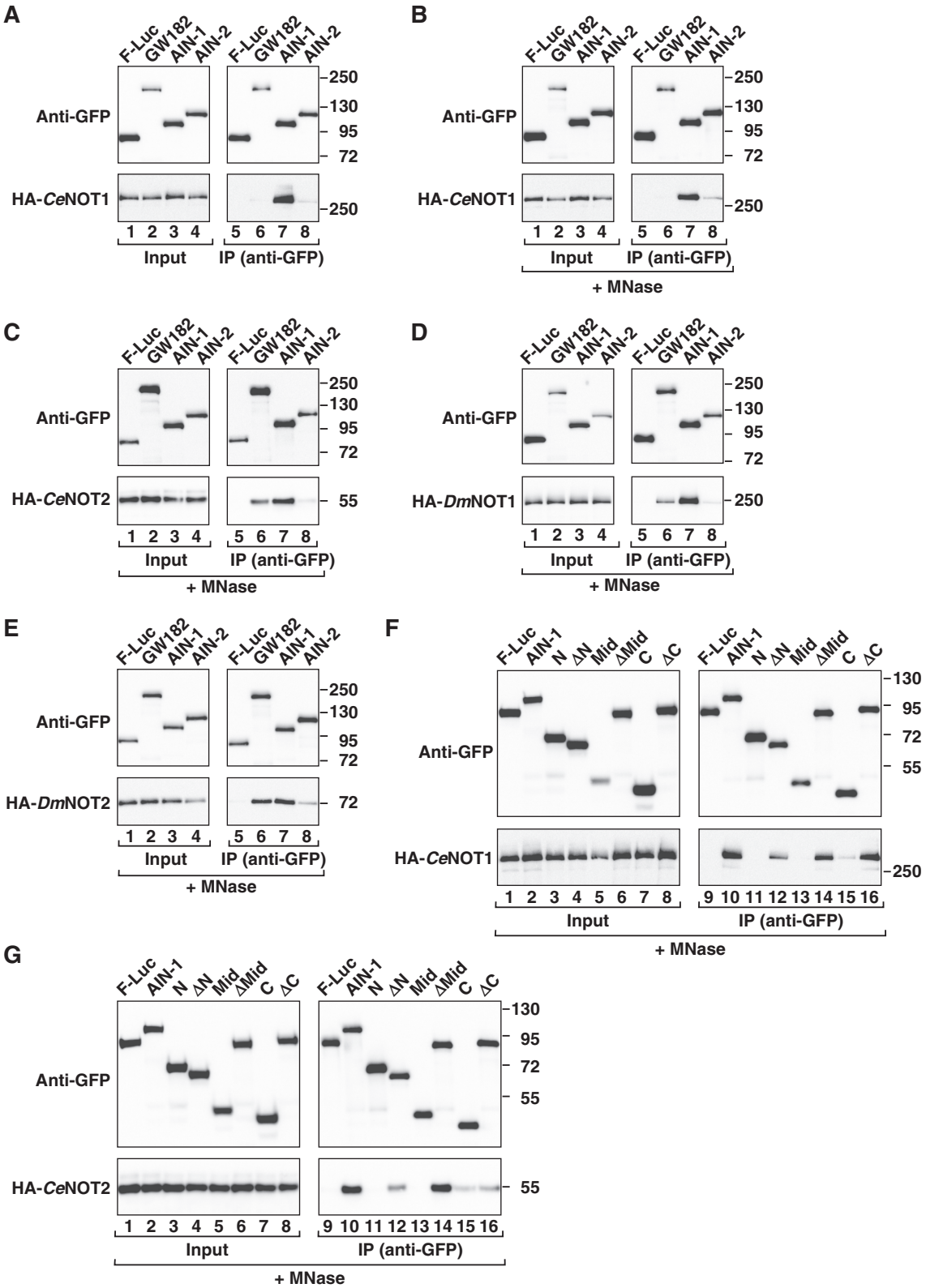

Figure 5. AIN-1 interacts with NOT1 and NOT2. (**A–E**) Interaction of GFP-tagged GW182, AIN-1 or AIN-2 with HA-tagged NOT1 or NOT2. For *Ce* NOT1 and *Ce* NOT2, 1% of the input and 30% of the IPs were loaded. (**F** and **G**) Interaction of GFP-tagged AIN-1 (wild-type or mutants) with HA-tagged *Ce* NOT1 or *Ce* NOT2. Cell lysates were treated with Micrococcal nuclease as indicated.

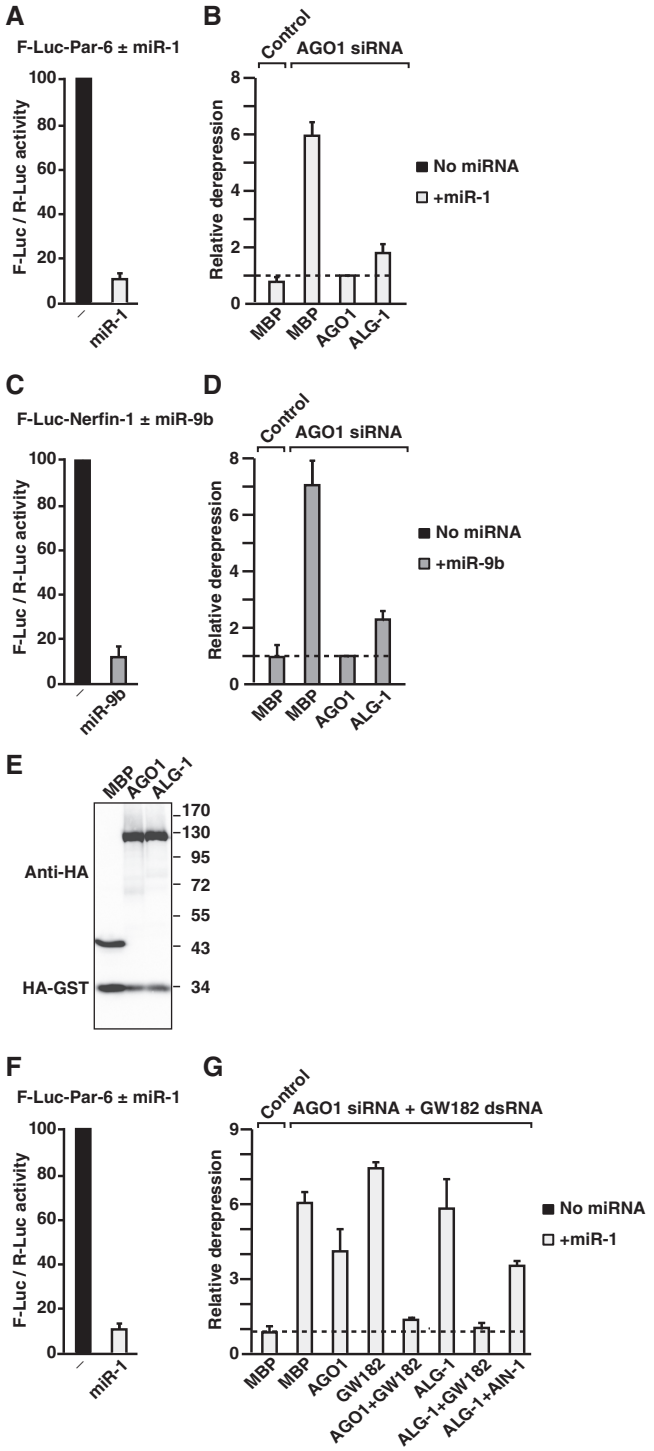

Figure 6. ALG-1 rescues silencing in S2 cells depleted of AGO1. (**A–D**) S2 cells were transfected with a siRNA targeting *AGO1* mRNA. Control cells were treated with an siRNA targeting *β-Gal*. The siRNAs were cotransfected with a mixture of three plasmids: one expressing the indicated F-Luc reporters; another expressing miRNA primary transcripts or the corresponding empty vector (−); and a third expressing *Renilla* luciferase (R-Luc). Plasmids expressing HA-AGO1 (siRNA resistant), HA-ALG-1 or HA-MBP (Maltose-binding protein) were included in the transfection mixtures as indicated. Firefly luciferase activities were normalized to those of the *Renilla* luciferase transfection control and set to 100 in cells transfected with the empty vector (i.e. in the absence of miRNA) for each condition. Panels (A and C) show normalized firefly luciferase activities in the absence or presence of miRNAs in control cells (i.e. cells treated with β-Gal siRNA and expressing MBP). (B and D) show the relative fold derepression for each condition. Mean values ± standard deviations from three independent experiments are shown. (**E**) Western blot analysis showing equivalent expression of the HA-tagged proteins. (**F** and **G**) S2 cells were codepleted of AGO1 and GW182, transfected with the indicated plasmids and analyzed as described in panels (A–D).

thus recruit AIN-1 or AIN-2 to the F-Luc-5BoxB mRNA. A plasmid encoding *Renilla* luciferase served as a transfection control (R-Luc).

We observed that both AIN-1 and AIN-2 repressed expression of the F-Luc-5BoxB reporter relative to the λN-HA tag or a negative mutant of *Dm* AGO1 termed F2V2 [Figure 7A–C; (11)]. The repression was similar to that observed with *Dm* GW182, which served as the positive control (Figure 7A–C). Furthermore, the repression was specific; the expression of an F-Luc reporter lacking the BoxB hairpins was unaffected by *Dm* GW182, AIN-1 or AIN-2 expression (Supplementary Figure S2A–C). Importantly, AIN-1 and AIN-2 silenced the F-Luc-5BoxB reporter in AGO1-depleted cells, indicating that their activity in tethering assays is not mediated by AGO1 (Supplementary Figure S2D and E). These results are not due to inefficient depletion because silencing of the F-Luc-Par-6 reporter by miR-1 was completely suppressed in these cells (Supplementary Figure S2E). To confirm that AIN-1 and AIN-2 activities are independent of AGO proteins, we tested protein mutants that do not interact with ALG1 (i.e. carrying deletions of the Mid domain or mutations in the GW repeats of the ABD). All mutants repressed the F-Luc-5BoxB reporter similar to the wild-type protein (Figure 7D and Supplementary Figure S2F), but did not affect the expression of a reporter lacking the BoxB hairpins (Supplementary Figure S2G–S2I). In contrast, the AIN-1 mutant with 22 tryptophan-to-alanine substitutions was inactive in this assay (Figure 7D, 22 × W-A).

Northern blot analysis of the F-Luc-5BoxB mRNA revealed that both AIN-1 and AIN-2 reduced the abundance of the F-Luc-5BoxB mRNA by ∼2.5-fold relative to the R-Luc mRNA transfection control (Figure 7A and B). Remarkably, all of the tested AIN-1 or AIN-2 protein fragments that were active in the tethering assays promoted mRNA degradation (Figure 7D and E). However, the decrease in mRNA levels was smaller than the reduction observed in firefly luciferase activity, suggesting a net contribution of translational repression. Similarly, previous studies showed that almost all fragments of *Dm* GW182 promoted translational repression and mRNA degradation in tethering assays, including N-term fragments that do not interact with PABPC1 (18,21,36). Therefore, we conclude that the activity of the GW182 protein fragments in tethering assays is not correlated with AGO, deadenylase or PABPC1 binding in coimmunoprecipitation assays. However, we cannot rule out that transient and weak interactions occur *in vivo* that are not detectable under the conditions used for coimmunoprecipitations.

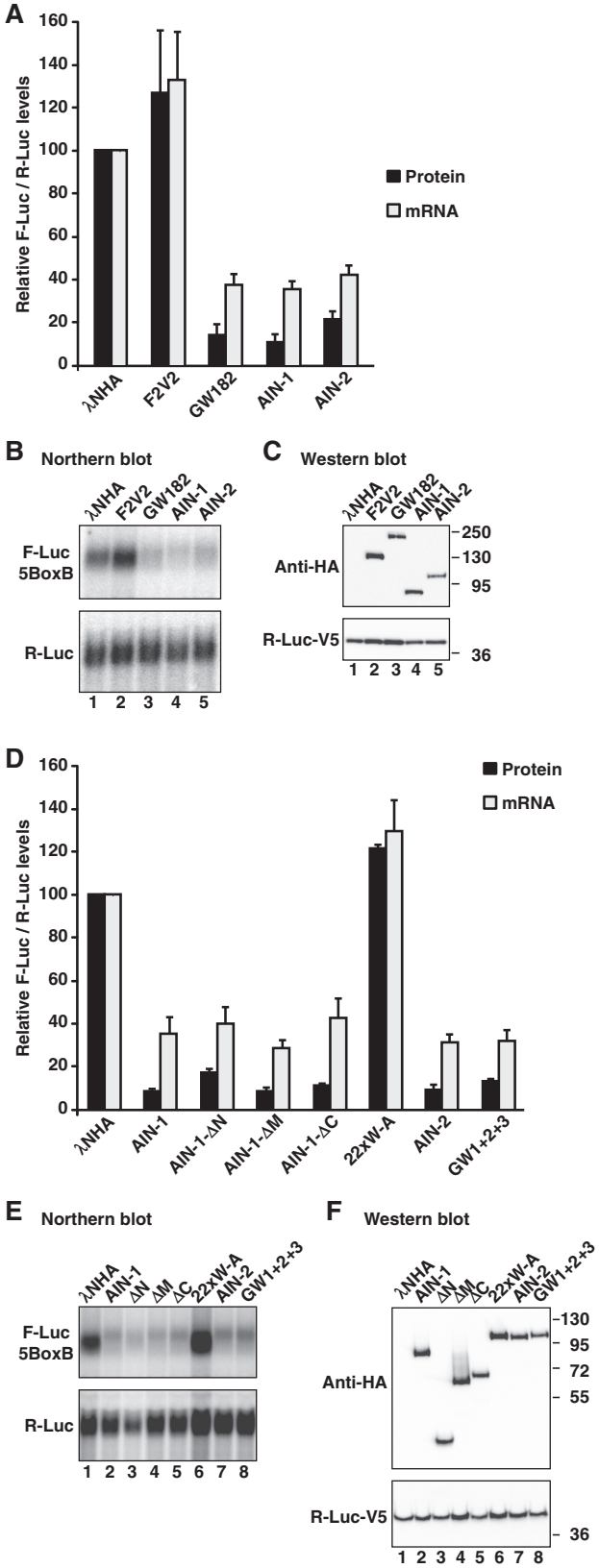

Figure 7. AIN-1 and AIN-2 promote degradation of bound mRNAs. (**A–F**) S2 cells were transfected with a mixture of three plasmids: one expressing the F–Luc-5BoxB reporter; another expressing the λN-HA peptide or the indicated λN-HA-tagged proteins; and a third expressing *Renilla* luciferase (R–Luc). Firefly luciferase activity and mRNA levels were normalized to those of *Renilla* luciferase. The normalized values of F–Luc activity and mRNA levels were set to 100 in the presence of the λN-HA peptide. Mean values ± standard deviations from three independent experiments are shown. Panels (B and E) show a northern blot of representative RNA samples quantified in panels (A) and (D). Panels (C and F) show equivalent expression of the λN-HA-tagged proteins. 22×W-A: AIN-1 mutant in which all tryptophan residues were substituted with alanines. GW1+2+3: AIN-2 mutant in which tryptophan residues in the three GW repeats of the ABD were substituted with alanine.

AIN-1 and AIN-2 do not rescue silencing in cells depleted of GW182

As mentioned above, previous reports documented that multiple and non-overlapping fragments of *Dm* GW182 are active in tethering assays including N-term fragments (18,21,36). However, despite their activity in tethering assays, GW182 N-term protein fragments did not rescue silencing in cells lacking endogenous GW182 in complementation assays (except for the Nerfin reporter silenced by miR-9b), but rather inhibited silencing in a dominant-negative manner (12,18). Therefore, we next tested the silencing activity of AIN-1 and AIN-2 in complementation assays.

Knockdown of endogenous *Dm* GW182 in S2 cells was achieved using dsRNA targeting *GW182* mRNA. This depletion inhibited silencing of the reporters tested, leading to a 2.5- to 3-fold increase in firefly luciferase expression (Figure 8A–D). GW182-depleted cells were then transfected with a plasmid expressing a dsRNA-resistant version of GW182, which restored silencing (Figure 8A–D) as previously reported (12). Despite similar expression levels, neither AIN-1 nor AIN-2 restored silencing in GW182-depleted cells (Figure 8A–E and Supplementary Figure S3A–S3D). Moreover, coexpression of AIN-1 and AIN-2 also failed to rescue silencing (Figure 8A–D). Likewise, coexpression of AIN-1 with *Ce* ALG-1, PAN3, NOT1 or PAB-1 did not rescue silencing (Supplementary Figure S3A–S3D). Additionally, both AIN-1 and AIN-2 inhibited silencing in a dominant-negative manner in control cells (Supplementary Figure S4A and S4B). This dominant-negative effect was reduced when AIN-1 and AIN-2 mutants that do not interact with ALG-1 were tested (Supplementary Figure S4A), suggesting that AIN-1 and AIN-2 inhibit silencing at least in part by competing with GW182 for AGO1 binding.

Finally, coexpression of AIN-1 and ALG-1 did not rescue silencing in S2 cells codepleted of *Dm* GW182 and AGO1, whereas coexpression of *Dm* GW182 with ALG-1 did (Figure 6F and G). Thus, although AIN-1 and AIN-2 were active in tethering assays (Figure 7), both proteins were inactive in complementation assays (Figure 8).

Together, our results indicate that AIN-1 and AIN-2 are probably too divergent to rescue silencing in GW182-depleted cells despite that AIN-1 interacts with *Dm* AGO1, PABPC1, NOT1, NOT2 and PAN3.

DISCUSSION

GW182 proteins play a central role in the miRNA pathway in animal cells. Vertebrate and insect members

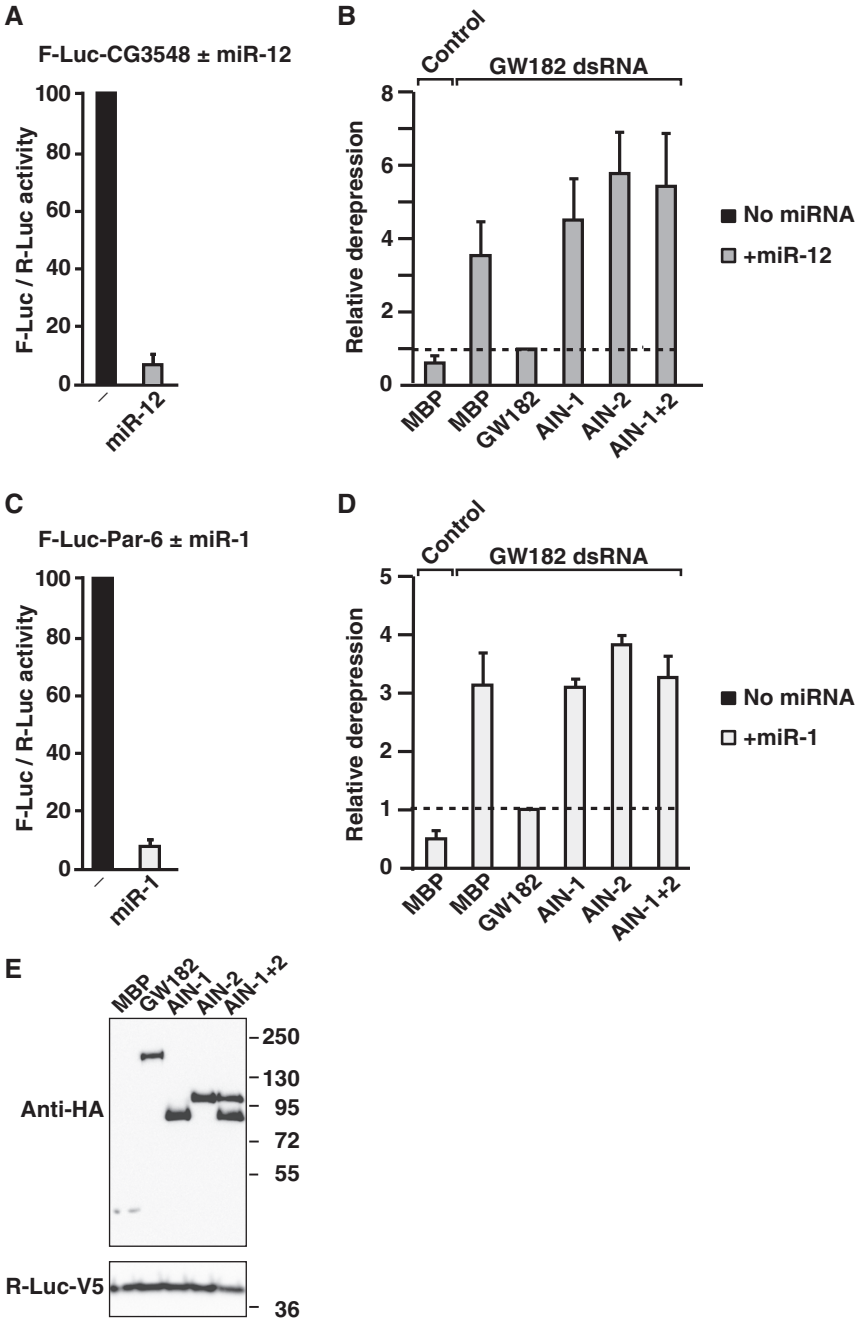

Figure 8. AIN-1 does not rescue silencing in S2 cells depleted of GW182. (**A–D**) S2 cells were treated with a dsRNA targeting *GW182* mRNA. Control cells were treated with *GFP* dsRNA. These cells were subsequently transfected with a mixture of three plasmids: one expressing the indicated F-Luc reporters; another expressing miRNA primary transcripts or the corresponding empty vector (–); and a third expressing *Renilla* luciferase (R-Luc). Plasmids expressing wild-type HA-GW182 (dsRNA resistant), HA-AIN-1, HA-AIN-2 or HA-MBP were included in the transfection mixtures, as indicated. Firefly luciferase activities were normalized to those of the *Renilla* luciferase transfection control and set to 100 in cells transfected with the empty vector (i.e. in the absence of miRNAs) for each condition. Panels (A and C) show normalized firefly luciferase activities in the absence or presence of miRNAs in control cells (i.e. cells treated with *GFP* dsRNA and expressing MBP). Panels (B and D) show the relative fold derepression for each condition. Mean values ± standard deviations from three independent experiments are shown. (**E**) Western blot showing that the HA-tagged proteins were expressed to equivalent levels.

of the family interact with the AGO proteins, PABPC1 and subunits of the two cytoplasmic deadenylase complexes (the PAN2-PAN3 and the CCR4-NOT complexes) (5,20,21,25). Despite strong sequence divergence, we demonstrated that *Ce* AIN-1 interacts with *Ce* or *Dm* PABPC1, PAN3, NOT1 and NOT2, whereas AIN-2 shows no significant interactions. In contrast, both AIN-1 and AIN-2 interact with ALG-1, as previously reported (1,3). Our findings suggest that AIN-1 and AIN-2 are functionally distinct and may silence

miRNA targets using different mechanisms. Indeed, AIN-2 may not promote miRNA target deadenylation and subsequent degradation, potentially explaining why AIN-2 depletion has no overt phenotype but enhances the delayed heterochronic phenotype observed in worms lacking AIN-1 (2,3). This phenotype includes defects in alae formation, drastic increase in seam-cell numbers and protruding vulva (2,3). Alternatively, AIN-2 may be expressed at lower levels and/or regulate fewer targets. Finally, AIN-2 may use a similar mechanism but may recruit PABPC1 and deadenylases through transient low-affinity interactions or through an adaptor protein(s).

Evolutionary plasticity of the GW182 protein interaction network

The finding that AIN-1 interacts with PABPC1, PAN3, NOT1 and NOT2 is surprising given that AIN-1 shows <12% sequence identity with *Dm* GW182 or human TNRC6s, whereas the binding partners (e.g. PABPC1, PAN3, NOT1 and NOT2) are conserved (Supplementary Tables S2 and S3). However, although the interactions of GW182 proteins with PABPC1, NOT1 and PAN3 are conserved in humans and *D. melanogaster*, the mode of interaction is not. For example, human TNRC6s interact with PABPC1 through a PAM2 motif in the silencing domain (17,22–24). This motif is also present in *Dm* GW182 and interacts with PABPC1 *in vitro*; nevertheless, deletion of the *Dm* GW182 PAM2 motif does not abrogate PABPC1 binding *in vivo* (17). In our previous studies, we showed that *Dm* GW182 interacts with PABPC1 through additional regions in the silencing domain. Although indirect, this interaction is dominant over that mediated by the PAM2 motif *in vivo* (17,19).

Another example of change in the binding mode is the interaction of GW182 proteins with NOT1. Indeed, recent work showed that binding of human TNRC6s to NOT1 is mediated by short motifs in the M1, M2 and C-term regions of the silencing domains, which contribute to the interaction in an additive manner (20,21,25). The motif in the M1 region (termed CCR4-interacting motif 1, CIM-1) is conserved in *Dm* GW182 (25). However, in contrast to human TNRC6s, the silencing domain of *Dm* GW182 is not sufficient for binding to NOT1 (our unpublished results), suggesting that additional motifs upstream of the silencing domain are present in *Dm* GW182.

Finally, although the interaction of GW182 proteins with AGOs is mediated by GW repeats (i.e. GW, WG or GWG), the exact location and number of repeats is not conserved (10,12,13,15,30). Here, we show that only a few repeats in the Mid region of AIN-1 and AIN-2 contribute to their interaction with ALG-1; in contrast, 12 and >20 GW repeats in the N-term regions of *Dm* GW182 and human TNRC6s, respectively, contribute to AGO protein binding (12,13).

How can the GW182 protein interaction network be conserved while the location of the binding sites appears to be rapidly evolving? The regions of GW182 proteins mediating the interactions with AGO1, PABPC1 and deadenylase subunits are predicted to be unstructured. These unstructured regions interact with (predicted or known) globular domains in AGO1, PABPC1, PAN3, NOT1 and NOT2, suggesting that the interactions might be mediated by short linear motifs [SLiMs; (37)] in the GW182 unstructured regions. This provides one explanation for why the location of the binding sites is rapidly evolving. Linear motifs are evolutionarily plastic, as only a small number of point mutations in a disordered region of a protein sequence are required to relocate these motifs. In doing so, the interactions between GW182 and binding partners can be maintained, but the details can change during evolution. Additionally, the possibility that GW182 proteins interact with their partners via SLiMs, potentially explains why the binding of AIN-1 to PABPC1, PAN3, NOT1 and NOT2 requires multiple protein regions (Figure 1B), as SLiMs may be dispersed along the protein sequence and collectively contribute to high-affinity interactions. In this context, we can envision a scenario in which nematode AIN-1 proteins gained additional motifs to interact with PABP and deadenylases, so that the silencing domain became progressively redundant and was eventually lost.

Conservation of silencing mechanisms

The present work shows that ALG-1 can rescue silencing in *Drosophila* cells depleted of AGO1, demonstrating conservation in the miRNA pathway including the mechanism of AGO loading, target recognition and target silencing. However, despite conservation of the basic interactions, AIN-1 could not rescue silencing in cells depleted of *Dm* GW182. Furthermore, both AIN-1 and AIN-2 inhibited silencing in a dominant-negative manner in wild-type cells. This effect was at least in part mediated by the ABD, suggesting that these proteins compete with GW182 for binding to AGO1 but assemble non-functional miRISC complexes. Why are these complexes non-functional? One possibility is that the assembly of functional silencing complexes requires GW182 proteins to interact with unknown partners (other than PABPC1 and deadenylase complexes), and that these interactions are not conserved. Alternatively, changes in protein conformation may be required to activate silencing complexes but may not occur for complexes assembled with AIN-1 or AIN-2 proteins in S2 cells.

An important message from our study is that AIN-1 and AIN-2 do not complement the *Dm* GW182 depletion, although both proteins silence an mRNA reporter to which they are artificially tethered. Furthermore, there is no correlation between activity in tethering assays and binding to AGO, deadenylases or PABPC1. Similarly, non-overlapping fragments of *Dm* GW182, including N-term fragments that do not interact with PABPC1, have been shown to be active in tethering assays (18,21,36). These results were interpreted as evidence that interactions of GW182 proteins with PABPC1 are not required for silencing (36). However, in complementation assays, TNRC6 mutants that do not interact with PABPC1 (i.e. PAM2 mutants) are impaired in silencing both in human and S2 cells, indicating that the PABPC1 interaction is critical for silencing *in vivo* (17,20). One possible explanation for the discrepancies between

tethering assays and complementation assays is that tethering assays involve direct high-affinity binding of multiple GW182 proteins to the mRNA target and thus bypass upstream steps in the silencing pathway. Therefore, although tethering assays are an invaluable tool in the dissection of the role of GW182 protein domains in silencing, conclusions from these assays should be validated in complementation assays.

In summary, our work extends and confirms the evolutionary conservation of GW182 interactions with PABPC1 and deadenylase complexes, unveiling their importance for silencing. Further elucidating the molecular basis for these interactions will be key to understanding their roles in both miRNA-mediated translational repression and mRNA target degradation.

SUPPLEMENTARY DATA

Supplementary Data are available at NAR Online: Supplementary Tables S1–S3 and Supplementary Figures S1–S4.

ACKNOWLEDGEMENTS

We are grateful to A. Streit for the kind gift of *C. elegans* cDNA.

FUNDING

The Max Planck Society; The Deutsche Forschungsgemeinschaft (DFG, FOR855 and the Gottfried Wilhelm Leibniz Program awarded to E.I.); The Sixth Framework Programme of the European Commission through the SIROCCO Integrated Project LSHG-CT-2006-037900. Funding for open access charge: Max Planck Society.

Conflict of interest statement. None declared.

REFERENCES

1. Ding,L., Spencer,A., Morita,K. and Han,M. (2005) The developmental timing regulator AIN-1 interacts with miRISCs and may target the Argonaute protein ALG-1 to cytoplasmic P bodies in *C. elegans*. *Mol. Cell*, **19**, 437–447.
2. Ding,L. and Han,M. (2007) GW182 family proteins are crucial for microRNA-mediated gene silencing. *Trends Cell. Biol.*, **17**, 411–416.
3. Zhang,L., Ding,L., Cheung,T.H., Dong,M.-Q., Che,J., Sewell,A.K., Liu,X., Yates,J.R. and Han,M. (2007) Systematic identification of *C. elegans* miRISC proteins, miRNAs, and mRNA targets by their interactions with GW182 proteins AIN-1 and AIN-2. *Mol. Cell*, **28**, 598–613.
4. Ding,X.C. and Großhans,H. (2009) Repression of *C. elegans* microRNA targets at the initiation level of translation requires GW182 proteins. *EMBO J.*, **28**, 213–222.
5. Huntzinger,E. and Izaurralde,E. (2011) Gene silencing by microRNAs, contributions of translational repression and mRNA decay. *Nat. Rev. Genet.*, **12**, 99–110.
6. Eystathioy,T., Chan,E.K., Tenenbaum,S.A., Keene,J.D., Griffith,K. and Fritzler,M.J. (2002) A phosphorylated cytoplasmic autoantigen, GW182, associates with a unique population of human mRNAs within novel cytoplasmic speckles. *Mol. Biol. Cell.*, **13**, 1338–1351.
7. Behm-Ansmant,I., Rehwinkel,J., Doerks,T., Stark,A., Bork,P. and Izaurralde,E. (2006) mRNA degradation by miRNAs and GW182 requires both CCR4:NOT deadenylase and DCP1:DCP2 decapping complexes. *Genes Dev.*, **20**, 1885–1898.
8. Eulalio,A., Tritschler,F. and Izaurralde,E. (2009) The GW182 protein family in animal cells: new insights into domains required for miRNA mediated gene silencing. *RNA*, **15**, 1433–1442.
9. Tritschler,F., Huntzinger,E. and Izaurralde,E. (2010) Role of GW182 proteins and PABPC1 in the miRNA pathway: a sense of déjà vu. *Nat. Rev. Mol. Cell. Biol.*, **11**, 379–384.
10. Till,S., Lejeune,E., Thermann,R., Bortfeld,M., Hothorn,M., Enderle,D., Heinrich,C., Hentze,M.W. and Ladurner,A.G. (2007) A conserved motif in Argonaute-interacting proteins mediates functional interactions through the Argonaute PIWI domain. *Nat. Struct. Mol. Biol.*, **14**, 897–903.
11. Eulalio,A., Huntzinger,E. and Izaurralde,E. (2008) GW182 interaction with Argonaute is essential for miRNA-mediated translational repression and mRNA decay. *Nat. Struct. Mol. Biol.*, **15**, 346–353.
12. Eulalio,A., Helms,S., Fritzsch,C., Fauser,M. and Izaurralde,E. (2009) A C-terminal silencing domain in GW182 is essential for miRNA function. *RNA*, **15**, 1067–1077.
13. Lazzaretti,D., Tournier,I. and Izaurralde,E. (2009) The C-terminal domains of human TNRC6A, B and C silence bound transcripts independently of the Argonaute proteins. *RNA*, **15**, 1059–1066.
14. Lian,S.L., Abadal,G.X., Pauley,B.A., Fritzler,M.J. and Chan,E.K.L. (2009) The C-terminal half of human Ago2 binds to multiple GW-rich regions of GW182 and requires GW182 to mediate silencing. *RNA*, **15**, 804–813.
15. Takimoto,K., Wakiyama,M. and Yokoyama,S. (2009) Mammalian GW182 contains multiple Argonaute binding sites and functions in microRNA-mediated translational repression. *RNA*, **15**, 1078–1089.
16. Zipprich,J.T., Bhattacharyya,S., Mathys,H. and Filipowicz,W. (2009) Importance of the C-terminal domain of the human GW182 protein TNRC6C for translational repression. *RNA*, **15**, 781–793.
17. Huntzinger,E., Braun,E.J., Heimstädt,S., Zekri,L. and Izaurralde,E. (2010) Two PABPC-binding sites in GW182 proteins promote miRNA-mediated gene silencing. *EMBO J.*, **29**, 4146–4160.
18. Chekulaeva,M., Filipowicz,W. and Parker,R. (2009) Multiple independent domains of dGW182 function in miRNA-mediated repression in Drosophila. *RNA*, **15**, 794–803.
19. Zekri,L., Huntzinger,E., Heimstädt,S. and Izaurralde,E. (2009) The silencing domain of GW182 interacts with PABPC1 to promote translational repression and degradation of miRNA targets and is required for target release. *Mol. Cell. Biol.*, **29**, 6220–6231.
20. Braun,J.E., Huntzinger,E., Fauser,M. and Izaurralde,E. (2011) GW182 proteins recruit cytoplasmic deadenylase complexes to miRNA targets. *Mol. Cell*, **44**, 120–133.
21. Chekulaeva,M., Mathys,H., Zipprich,J.T., Attig,J., Colic,M., Parker,R. and Filipowicz,W. (2011) miRNA repression involves GW182-mediated recruitment of CCR4-NOT through conserved W-containing motifs. *Nat. Struct. Mol. Biol.*, **18**, 1218–1226.
22. Fabian,M.R., Mathonnet,G., Sundermeier,T., Mathys,H., Zipprich,J.T., Svitkin,Y.V., Rivas,F., Jinek,M., Wohlschlegel,J. and Doudna,J.A. (2009) Mammalian miRNA RISC recruits CAF1 and PABP to affect PABP-dependent deadenylation. *Mol. Cell*, **35**, 868–880.
23. Jinek,M., Fabian,M.R., Coyle,S.M., Sonenberg,N. and Doudna,J.A. (2010) Structural insights into the human GW182-PABC interaction in microRNA-mediated deadenylation. *Nat. Struct. Mol. Biol.*, **17**, 238–240.
24. Kozlov,G., Safaee,N., Rosenauer,A. and Gehring,K. (2010) Structural basis of binding of P-body associated protein GW182 and Ataxin-2 by the MLLE domain of poly(A)-binding protein. *J. Biol. Chem.*, **285**, 13599–13606.
25. Fabian,M.R., Cieplak,M.K., Frank,F., Morita,M., Green,J., Srikumar,T., Nagar,B., Yamamoto,T., Raught,B. and Duchaine,T.F. (2011) miRNA-mediated deadenylation is orchestrated by GW182 through two conserved motifs that interact with CCR4–NOT. *Nat. Struct. Mol. Biol.*, **18**, 1211–1217.

26. Wu,E., Thivierge,C., Flamand,M., Mathonnet,G., Vashisht,A.A., Wohlschlegel,J., Fabian,M.R., Sonenberg,N. and Duchaine,T.F. (2010) Pervasive and cooperative deadenylation of 3′UTRs by embryonic microRNA families. *Mol. Cell*, **40**, 558–570.
27. Altschul,S.F., Madden,T.L., Schäffer,A.A., Zhang,J., Zhang,Z., Miller,W. and Lipman,D.J. (1997) Gapped BLAST and PSI-BLAST: a new generation of protein database search programs. *Nucleic Acids Res.*, **25**, 3389–402.
28. Söding,J., Biegert,A. and Lupas,A.N. (2005) The HHpred interactive server for protein homology detection and structure prediction. *Nucleic Acids Res.*, **33**, W244–W288.
29. Eulalio,A., Rehwinkel,J., Stricker,M., Huntzinger,E., Yang,S.F., Doerks,T., Dorner,S., Bork,P., Boutros,M. and Izaurralde,E. (2007) Target-specific requirements for enhancers of decapping in miRNA-mediated gene silencing. *Genes Dev.*, **21**, 2558–2570.
30. El-Shami,M., Pontier,D., Lahmy,S., Braun,L., Picart,C., Vega,D., Hakimi,M.A., Jacobsen,S.E., Cooke,R. and Lagrange,T. (2007) Reiterated WG/GW motifs form functionally and evolutionarily conserved ARGONAUTE-binding platforms in RNAi-related components. *Genes Dev.*, **21**, 2539–2544.
31. Mangus,D.A., Evans,M.C., Agrin,N.S., Smith,M., Gongidi,P. and Jacobson,A. (2004) Positive and negative regulation of poly(A) nuclease. *Mol. Cell. Biol.*, **24**, 5521–5533.
32. Uchida,N., Hoshino,S. and Katada,T. (2004) Identification of a human cytoplasmic poly(A) nuclease complex stimulated by poly(A)-binding protein. *J. Biol. Chem.*, **279**, 1383–1389.
33. Siddiqui,N., Mangus,D.A., Chang,T.C., Palermino,J.M., Shyu,A.B. and Gehring,K. (2007) Poly(A) nuclease interacts with the C-terminal domain of polyadenylate-binding protein domain from poly(A)-binding protein. *J. Biol. Chem.*, **282**, 25067–25075.
34. Okamura,K., Ishizuka,A., Siomi,H. and Siomi,M.C. (2004) Distinct roles for Argonaute proteins in small RNA-directed RNA cleavage pathways. *Genes Dev.*, **18**, 1655–1666.
35. Rehwinkel,J., Behm-Ansmant,I., Gatfield,D. and Izaurralde,E. (2005) A crucial role for GW182 and the DCP1:DCP2 decapping complex in miRNA-mediated gene silencing. *RNA*, **11**, 1640–1647.
36. Fukaya,T. and Tomari,Y. (2011) PABP is not essential for microRNA-mediated translational repression and deadenylation *in vitro*. *EMBO J.*, **30**, 4998–5009.
37. Davey,N.E., Van Roey,K., Weatheritt,R.J., Toedt,G., Uyar,B., Altenberg,B., Budd,A., Diella,F., Dinkel,H. and Gibson,T.J. (2012) Attributes of shirt linear motifs. *Mol. Biosyst.*, **8**, 268–281.
38. Eulalio,A., Tritschler,F., Büttner,R., Weichenrieder,O., Izaurralde,E. and Truffault,V. (2009) The RRM domain in GW182 proteins contributes to miRNA-mediated gene silencing. *Nucleic Acids Res.*, **37**, 2974–2983.

SUPPLEMENTARY DATA

The *C. elegans* GW182 protein AIN-1 interacts with PAB-1 and subunits of the PAN2-PAN3 and CCR4-NOT deadenylase complexes

Duygu Kuzuoğlu-Öztürk, Eric Huntzinger, Steffen Schmidt and Elisa Izaurralde

Supplementary Figure S1. AIN-1 interactions with binding partners. (**A**) Interaction of GFP-tagged AIN-1 (wild type or mutants) with HA-tagged *Ce* PAN3. Cell lysates were treated with Micrococcal nuclease. (**B**, **C**, **D**, **E**, **F** and **G**) Substitution of all tryptophan residues in AIN-1 by alanines nonspecifically abolished all protein-protein interactions. S2 cells were cotransfected with plasmids expressing the indicated HA-tagged proteins and wild type GFP-tagged AIN-1 or the 22xW-A mutant (in which all tryptophan residues were substituted with alanines). Cell lysates were immunoprecipitated using a polyclonal anti-GFP antibody. GFP-tagged firefly luciferase served as a negative control. Samples were analyzed as described in Figure 1. The AIN-1 22xW-A mutant exhibited a lower mobility in SDS-PAGE.

Supplementary Figure S2. AIN-1 and AIN-2 silence bound mRNAs in tethering assays. **(A**, **B** and **C)** S2 cells were transfected with a mixture of three plasmids: one expressing a control F-Luc reporter (without Box B hairpins); another expressing the λN-HA peptide or the indicated λN-HA-tagged proteins; and a third expressing *Renilla* luciferase (R-Luc). Firefly luciferase activity and mRNA levels were normalized to those of *Renilla* luciferase. The normalized values of F-Luc activity and mRNA levels were set to 100 in the presence of the λN-HA peptide. Mean values ± standard deviations from three independent experiments are shown. Panel (B),

Northern blot analysis of representative RNA samples quantified in panel (A). Panel (C) shows the expression levels of the λN-HA-tagged proteins. (**D** and **E**) S2 cells were transfected with an siRNA targeting *AGO1* mRNA. Control cells were treated with a control siRNA targeting *β-Gal*. The siRNAs were cotransfected with a mixture of three plasmids: one expressing the F-Luc-5BoxB reporter; another expressing the λN-HA peptide or the indicated λN-HA-tagged proteins; and a third expressing *Renilla* luciferase (R-Luc). Firefly luciferase activity was normalized to that of *Renilla* luciferase. For each condition, the normalized values of F-Luc activity and mRNA levels were set to 100 in the presence of the λN-HA peptide. Mean values ± standard deviations from three independent experiments are shown. To monitor in parallel the efficiency of the depletion, the siRNAs were cotransfected with the F-Luc-Par-6 reporter, a plasmid expressing the miR-1 primary transcript or the corresponding empty vector (-); and a third expressing *Renilla* luciferase (R-Luc). Firefly luciferase activities were normalized to those of the *Renilla* luciferase transfection control and set to 100 in cells transfected with the empty vector (i.e., in the absence of miR-1) for each condition (black bars). (**F**) S2 cells were transfected with a mixture of three plasmids: one expressing the F-Luc-5BoxB reporter; another expressing the λN-HA peptide or the indicated λN-HA-tagged proteins; and a third expressing *Renilla* luciferase (R-Luc). Firefly luciferase activity and mRNA levels were normalized to those of *Renilla* luciferase. The normalized values of F-Luc activity and mRNA levels were set to 100 in the presence of the λN-HA peptide. (**G**, **H** and **I**) AIN-1 and AIN-2 mutants were tested for nonspecific activity using the F-Luc reporter lacking the Box B hairpins as described in (A–C).

Supplementary Figure S3. AIN-1 does not complement *Dm* GW182 depletion. (**A**,

B, **C** and **D**) S2 cells were treated with a dsRNA targeting *GW182* mRNA. Control cells were treated with *GFP* dsRNA. These cells were subsequently transfected with a mixture of three plasmids: one expressing the indicated F-Luc reporters; another expressing miRNA primary transcripts or the corresponding empty vector (-); and a third expressing *Renilla* luciferase (R-Luc). Plasmids expressing the indicated *C. elegans* HA-tagged proteins were included in the transfection mixtures. Firefly luciferase activities were normalized to those of the *Renilla* luciferase transfection control and set to 100 in cells transfected with the empty vector (i.e., in the absence of the miRNAs) for each condition. Panels (A and C) show normalized firefly luciferase activities in the absence or presence of miRNAs in control cells (i.e., cells treated with GFP dsRNA and expressing MBP). Panels (B and D) show relative fold derepression for each condition. Mean values ± standard deviations from three independent experiments are shown.

Supplementary Figure S4. AIN-1 and AIN-2 inhibit silencing in a dominant-negative manner in S2 cells. (**A** and **B**) S2 cells were transfected with a mixture of three plasmids: one expressing the indicated F-Luc-Par-6 reporter; another expressing the miR-1 primary transcript or the corresponding empty vector (-); and a third expressing *Renilla* luciferase (R-Luc). Increasing amounts of plasmids expressing HA-tagged proteins were included in the transfection mixtures as indicated. Firefly luciferase activities were normalized to those of the *Renilla* luciferase transfection control and set to 100 in cells transfected with the empty vector (i.e., in the absence of miR-1) for each condition (shown only for control cells expressing MBP, black bar). Mean values ± standard deviations from technical replicates are shown. Panel (B) shows the expression levels of the λN-HA-tagged proteins.

Kuzuoglu et al. Figure S1

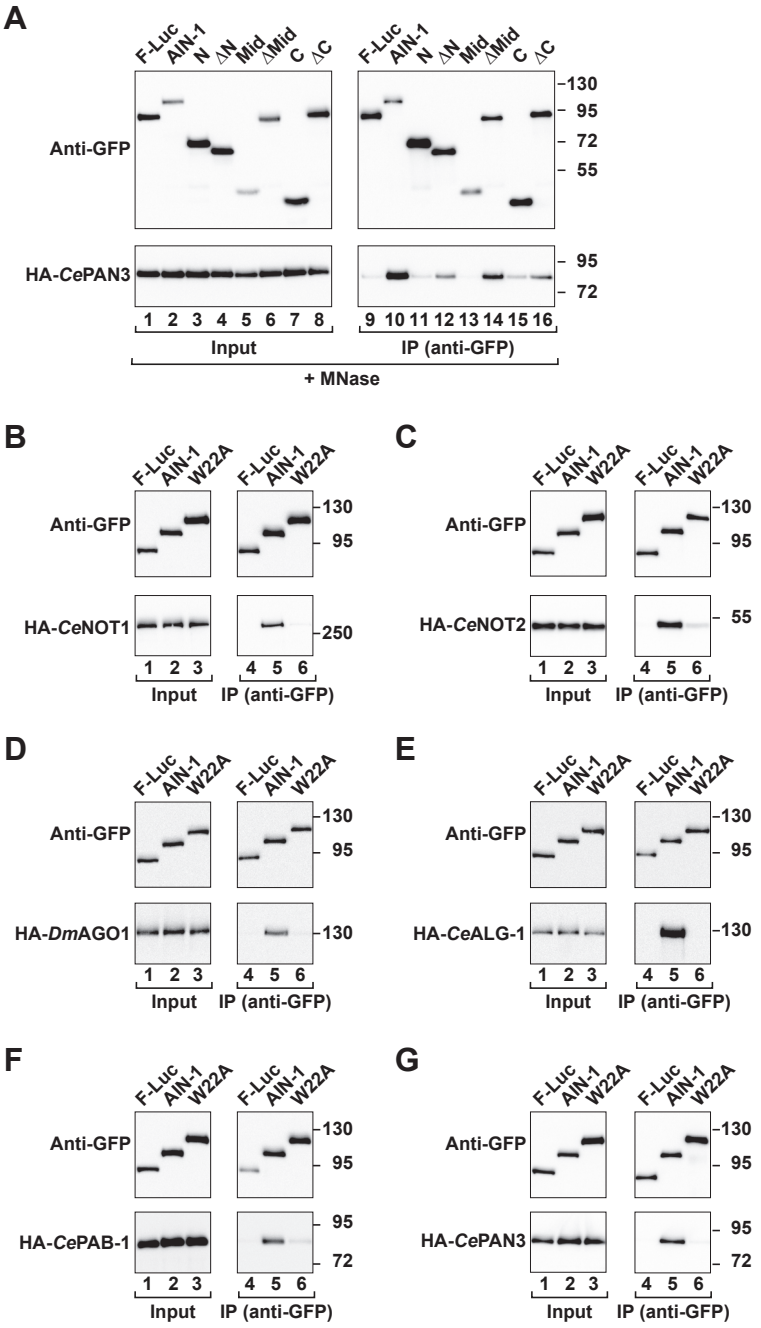

Kuzuoglu et al. Figure S2

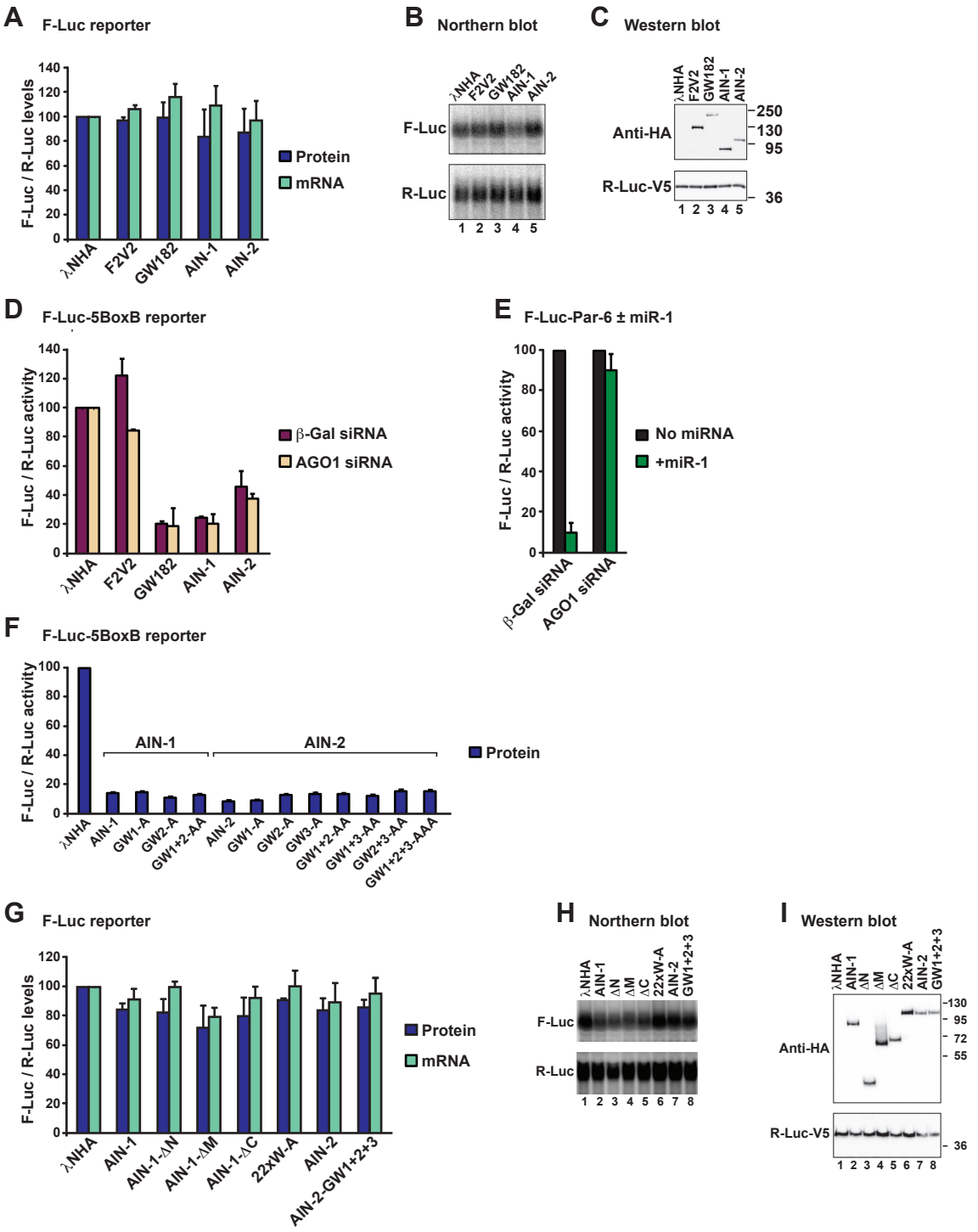

Kuzuoglu et al. Figure S3

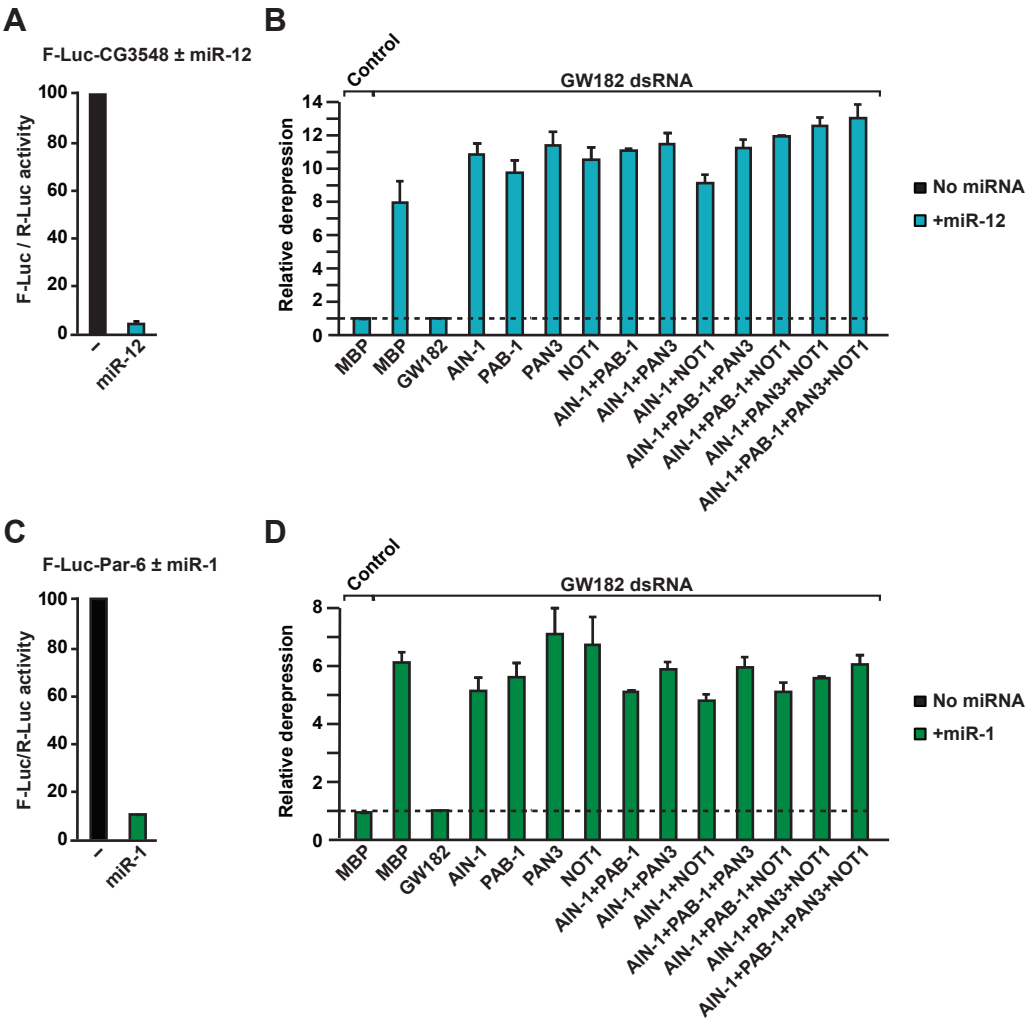

Kuzuoglu et al. Figure S4

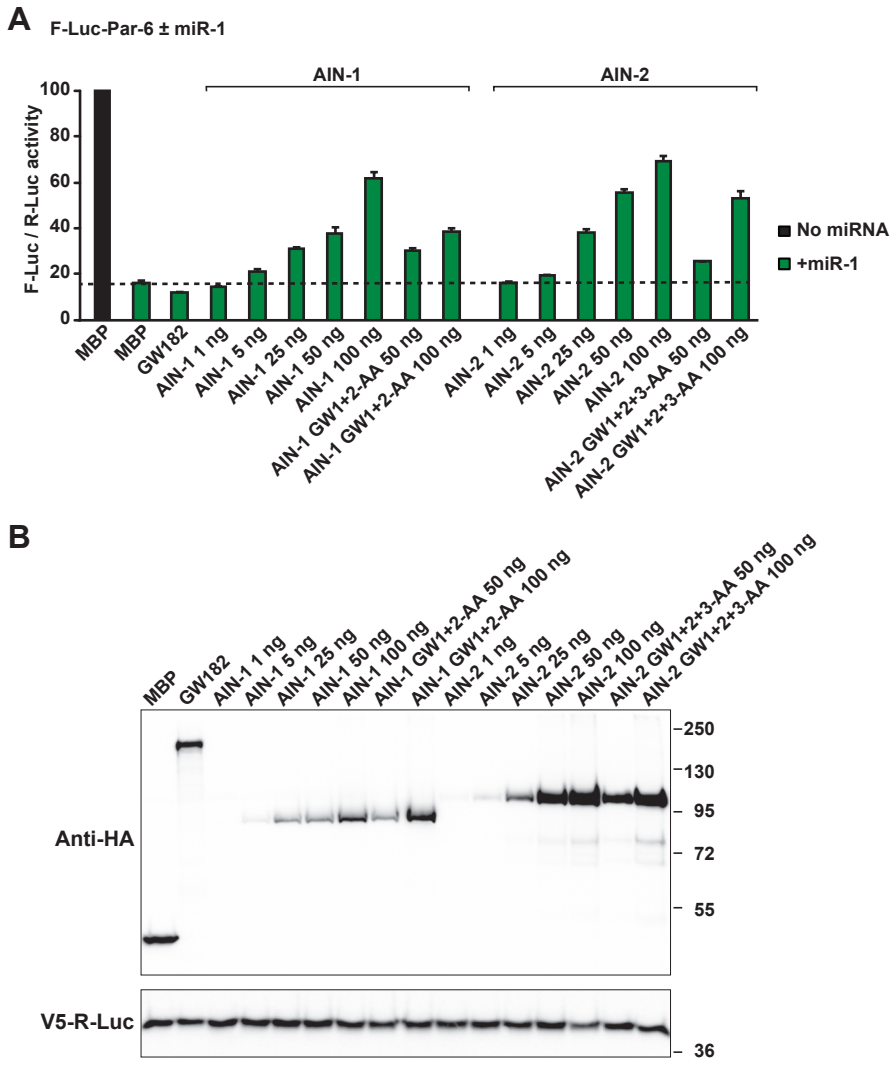

Supplementary Table S1. DNA constructs

Protein /ORF length in amino acids / accession	**Cloning sites**
AIN-1 / 1-641 / NP_510687.2	Cloned EcoRI-XhoI into pAc5.1-λN-HA and pAc5.1-GFP
AIN-1 - ΔN / 351-641	Cloned EcoRI-XhoI into pAc5.1-λN-HA and pAc5.1-GFP
AIN-1 - N-term / 1-350	Cloned EcoRI-XhoI into pAc5.1-λN-HA and pAc5.1-GFP
AIN-1 - ΔMid / Δ351-504	Cloned into pAc5.1-λN-HA and pAc5.1-GFP
AIN-1-Mid / 351-504	Cloned EcoRI-XhoI into pAc5.1-λN-HA and pAc5.1-GFP
AIN-1-ΔC / 1-504	Cloned EcoRI-XhoI into pAc5.1-λN-HA and pAc5.1-GFP
AIN-1-C / 505–641	Cloned EcoRI-XhoI into pAc5.1-λN-HA and pAc5.1-GFP
AIN-1- W378A	Mutagenesis using pAc5.1-λN-HA-AIN-1 and pAc5.1-GFP-AIN-1 as templates
AIN-1- W437A	Mutagenesis using pAc5.1-λN-HA-AIN-1 and pAc5.1-GFP-AIN-1 as templates
AIN-1- W378A+W437A	Mutagenesis using pAc5.1-λN-HA-AIN-1 and pAc5.1-GFP-AIN-1 as templates
AIN-2 / 1-706 / AAC24251.2	Cloned NotI-XhoI into pAc5.1-λN-HA and pAc5.1-GFP
AIN2-ΔABD /Δ254-400	Mutagenesis using pAc5.1-λN-HA-AIN-2 and pAc5.1-GFP-AIN-2 as templates
AIN-2- W282A	Mutagenesis using pAc5.1-λN-HA-AIN-2 and pAc5.1-GFP-AIN-2 as templates
AIN-2- W366A	Mutagenesis using pAc5.1-λN-HA-AIN-2 and pAc5.1-GFP-AIN-2 as templates
AIN-2- W390A	Mutagenesis using pAc5.1-λN-HA-AIN-2 and pAc5.1-GFP-AIN-2 as templates
AIN-2- W282A+W366A	Mutagenesis using AIN-2-W282A as template
AIN-2- W282A+W390A	Mutagenesis using AIN-2-W282A as template
AIN-2- W366A+W390A	Mutagenesis using AIN-2-W366A as template
AIN-2- W282A+W366A+W390A	Mutagenesis using AIN-2-W282A+W366A as template
ALG1 / 1-1002 / CAA93496.2	Cloned NotI-SacII into pAc5.1-λN-HA
Ce PAB-1 / 1-646 / AAA65224.1	Cloned NotI-XbaI into pAc5.1-λN-HA
Ce PAB-1-RRM / 1-400	Cloned NotI-XbaI into pAc5.1-λN-HA
Ce PAB-1-MLLE / 569-646	Cloned NotI-XbaI into pAc5.1-λN-HA
Ce PAN3 / 1-632 / NP_499177/ WP:CE37601	Cloned NotI-XbaI into pAc5.1-λN-HA
Ce PAN3-N term / 1-244	Cloned NotI-XbaI into pAc5.1-λN-HA
Ce PAN3-C term / 245-632	Cloned NotI-XbaI into pAc5.1-λN-HA
Ce NOT1 / 1-2527 / AAA21168.2 (GB) WP:CE28239	Cloned HindIII-SacII into pAc5.1-λN-HA
Ce NOT2 (NTL-2) / 1-444 / NP_494772.1	Cloned NotI-XbaI into pAc5.1-λN-HA

Supplementary Table S2. Amino acid sequence identities (similarities) between *Dm* and *Ce* GW182 proteins.

	***Ce* AIN-1**	***Ce* AIN-2**
***Dm* GW182**	11.9 (19)	11.7 (18.8)
***Ce* AIN-1**		22.4 (31.9)

The pairwise identities (similarities) were calculated using the global alignment tool "needle" from the European Molecular Biology Open Software Suite (EMBOSS).

Supplementary Table S3. Amino acid sequence identities (similarities) between *Dm* and *Ce* PABP and deadenylase subunits.

	***Ce* ALG1**	***Ce* PAB1**	***Ce* PAN3**	***Ce* NOT1**	***Ce* NOT2**
***Drosophila* orthologs**	61.1 (72.7)	51.5 (62.4)	28 (40.2)	29.1 (44.3)	21.8 (32.6)

The pairwise identities (similarities) were calculated using the global alignment tool "needle" from the European Molecular Biology Open Software Suite (EMBOSS).

978–994 *Nucleic Acids Research, 2013, Vol. 41, No. 2* *Published online 21 November 2012*
doi:10.1093/nar/gks1078

The interactions of GW182 proteins with PABP and deadenylases are required for both translational repression and degradation of miRNA targets

Eric Huntzinger, Duygu Kuzuoğlu-Öztürk, Joerg E. Braun, Ana Eulalio, Lara Wohlbold and Elisa Izaurralde*

Department of Biochemistry, Max Planck Institute for Developmental Biology, Spemannstrasse 35, D-72076 Tübingen, Germany

Received July 6, 2012; Accepted October 15, 2012

ABSTRACT

Animal miRNAs silence the expression of mRNA targets through translational repression, deadenylation and subsequent mRNA degradation. Silencing requires association of miRNAs with an Argonaute protein and a GW182 family protein. In turn, GW182 proteins interact with poly(A)-binding protein (PABP) and the PAN2–PAN3 and CCR4–NOT deadenylase complexes. These interactions are required for the deadenylation and decay of miRNA targets. Recent studies have indicated that miRNAs repress translation before inducing target deadenylation and decay; however, whether translational repression and deadenylation are coupled or represent independent repressive mechanisms is unclear. Another remaining question is whether translational repression also requires GW182 proteins to interact with both PABP and deadenylases. To address these questions, we characterized the interaction of *Drosophila melanogaster* GW182 with deadenylases and defined the minimal requirements for a functional GW182 protein. Functional assays in *D. melanogaster* and human cells indicate that miRNA-mediated translational repression and degradation are mechanistically linked and are triggered through the interactions of GW182 proteins with PABP and deadenylases.

INTRODUCTION

miRNAs belong to a large family of non-coding RNAs that post-transcriptionally silence the expression of mRNAs containing fully or partially complementary binding sites. To exert their regulatory functions, miRNAs assemble into miRNA-induced silencing complexes (miRISCs), minimally comprising an Argonaute protein (AGO) and a protein of the GW182 family (1,2). GW182 proteins function downstream of AGOs and play an essential role in miRNA-mediated gene silencing in animal cells (1,2).

Three GW182 paralog proteins (termed TNRC6A, B and C) exist in vertebrates and various invertebrate species; however, only one family member exists in ***Drosophila*** *melanogaster* [GW182 (1,2)]. These proteins typically contain an N-terminal (N-term) Argonaute-binding domain (ABD) and a C-terminal (C-term) silencing domain (SD) [Figure 1 (1,2)]. The SDs of the human proteins are required for silencing and serve as binding platforms for the cytoplasmic poly(A)-binding protein (PABP), as well as PAN3 and NOT1, which are subunits of the PAN2–PAN3 and CCR4–NOT deadenylase complexes, respectively (3–10).

The SD is bipartite and comprises the middle (Mid) and C-term regions of the GW182 proteins that flank an RNA-recognition motif (RRM). The Mid region is further divided into the M1 and M2 regions (Figure 1), which, together with the C-term, contribute to the interactions with deadenylases in an additive manner (8–10). For example, the interaction between human TNRC6 SDs and PAN3 requires both the M2 and C-term regions of the SD (8,9). NOT1 binding is mediated through tryptophan-containing sequences in the M1, M2 and C-term regions of the SD [Figure 1 (9,10)]. The motifs in the M1 and C-term regions were termed CCR4–NOT-interacting motifs 1 and 2 (CIM-1 and CIM-2), respectively [Figure 1 (10)]. However, in addition to the CIM-1 and CIM-2 motifs, tryptophan residues in the M2 region of the SD contribute

*To whom correspondence should be addressed. Tel: +49 7071 601 1350; Fax: +49 7071 601 1353; Email: elisa.izaurralde@tuebingen.mpg.de
Present address:
Ana Eulalio, Institute for Molecular Infection Biology (IMIB), University of Würzburg, Würzburg, Germany.

The author wish it to be known that in their opinion the first two authors should be regarded as the joint First Authors.

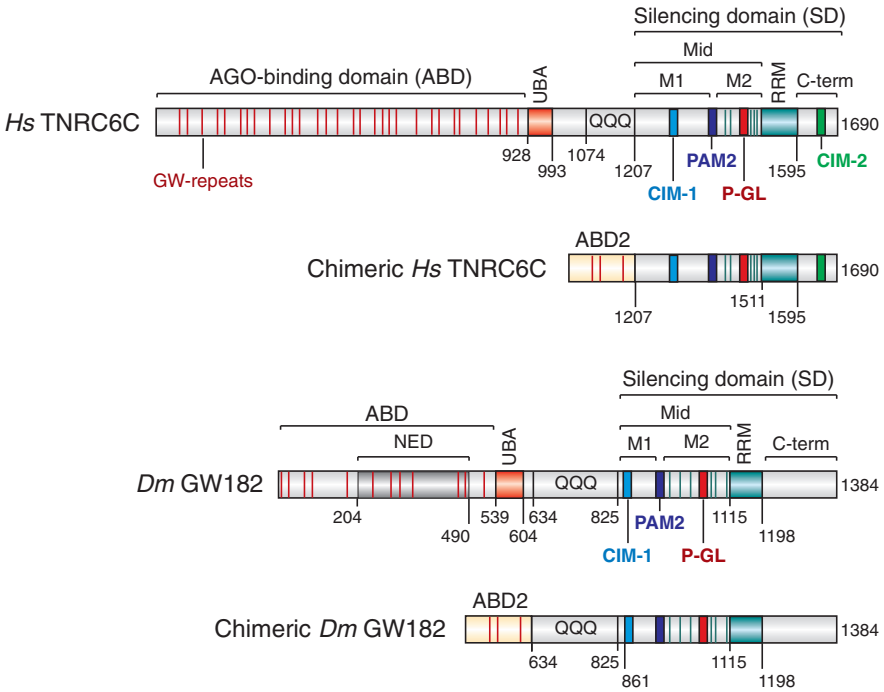

Figure 1. Domain organization of *Drosophila melanogaster* GW182, *Hs* TNRC6C and the corresponding chimeric proteins. ABD, AGO-binding domain; ABD2, AGO-binding domain from *Caenorhabditis elegans* AIN-2; NED, N-terminal effector domain; UBA, ubiquitin associated-like domain; QQQ, region rich in glutamine; Mid, middle region containing the PAM2 motif (dark blue), which divides the Mid region into the M1 and M2 regions; RRM, RNA recognition motif; C-term, C-terminal region; SD, silencing domain. The position of the conserved CIM-1, CIM-2 and P-GL motifs are indicated. Amino acid positions at domain boundaries are indicated below the protein outlines. Vertical red lines indicate the positions of GW repeats. Vertical green lines indicate the positions of tryptophan residues in the M2 region that are involved in NOT1-binding (9). Sequence alignments of the PAM2, CIM-1, CIM-2 and P-GL motifs and the amino acids mutated in this study are shown in Supplementary Figure S7.

to interactions with NOT1 and PAN3 (9). Finally, PABP binds directly to a conserved PAM2 motif (PABP-interacting motif 2) located between the M1 and M2 regions of the SD (Figure 1 (3–7)).

Remarkably, although the interactions between GW182 proteins and PABP and deadenylase complexes are conserved in *D. melanogaster,* the mode of interaction differs (5,8). For example, the CIM-2 motif is absent in *D. melanogaster* GW182 (9,10). Moreover, in contrast to the human SDs, which are necessary and sufficient for NOT1 and PAN3 binding, the deletion of the SD from *D. melanogaster* GW182 reduces but does not abolish binding to deadenylases (8), indicating that sequences upstream of the SD contribute to these interactions (8,9). Finally, in contrast to the human proteins, *D. melanogaster* GW182 also indirectly interacts with PABP through the M2 and C-term regions in cultured cells (4,5). Consequently, the *D. melanogaster* GW182 PAM2 motif is dispensable for PABP binding and silencing in *Drosophila* cells (5,9,11,12).

The interactions between GW182 proteins and deadenylase complexes are required for miRNA target deadenylation and degradation (8–10). Whether these interactions are also required for miRNA-mediated translational repression remains unclear. Three lines of evidence support a role for the CCR4–NOT deadenylase complex in translational repression of miRNA targets. First, the direct tethering of subunits of the CCR4–NOT complex to mRNA reporters lacking poly(A) tails represses translation in the absence of deadenylation (9,13). Second, depletion of subunits of the CCR4–NOT complex partially suppresses the silencing of mRNA reporters that lack a poly(A) tail; these reporters are silenced at the translational level without undergoing deadenylation (8,9). Third, mutations or deletions in GW182 proteins that disrupt the interactions with the CCR4–NOT complex suppress silencing, that is, translational repression and degradation of miRNA targets (8,9). However, other studies reported that although the depletion of CCR4–NOT complex subunits abolished the deadenylation and degradation of miRNA reporters, some reporters remained translationally repressed, suggesting that an additional mechanism could contribute to the repression (8,14,15). In addition, several studies have indicated that translational repression precedes deadenylation (3,15–19), although it remains unclear whether these two modes of regulation are linked or whether they represent independent mechanisms that are used by miRNAs to silence their mRNA targets.

In this study, we investigated whether the interactions of GW182 proteins with PABP and deadenylase complexes are also required for the translational repression of miRNA targets and thus, for target silencing, independently of the extent of target mRNA degradation. Accordingly, we first identified the regions in *D. melanogaster* GW182 that are required for deadenylase

complex binding. We subsequently generated mutants that are unable to interact with PABP and deadenylases and demonstrated that these mutants cannot rescue silencing in cells depleted of endogenous *D. melanogaster* GW182. These observations, when combined with the study of engineered minimal functional GW182 proteins, indicate that translational repression and target degradation are mechanistically linked and depend on the interaction of GW182 proteins with PABP and deadenylase complexes in both *D. melanogaster* and human cells.

MATERIALS AND METHODS

Plasmids

Luciferase reporters and plasmids for the expression of miRNAs, AGO1, GW182, PABP and subunits of the two deadenylase complexes studied in this article have been described previously (8,14,20).

Co-immunoprecipitation analyses and western blotting in S2 cells

S2 cells were transfected in six-well plates using Effectene transfection reagent (Qiagen). For co-immunoprecipitation assays, the transfection mixtures contained 1 μg of plasmid-expressing Green fluorescent Protein (GFP)-tagged GW182 or the corresponding mutants and 0.5 μg of human influenza hemagglutinin (HA)-tagged deadenylation subunits. Co-immunoprecipitations and western blots were performed as described by Braun *et al*. (8), except that cell lysates were supplemented with $CaCl_2$ and treated with micrococcal nuclease before immunoprecipitation. HA- and GFP-tagged proteins were detected using horseradish peroxidase–conjugated monoclonal anti-HA (Roche 3F10; 1:5000) and anti-GFP antibodies (Roche 11814460001; 1:2000), respectively. V5-tagged proteins were detected using anti-V5 antibodies (Invitrogen, 1:5000). Endogenous AGO1 and α-tubulin were detected using commercial antibodies at the following dilutions: *D. melanogaster* AGO1 (Abcam ab5070; 1:1000) and α-tubulin (Sigma T6199; 1:2000). Endogenous *D. melanogaster* GW182 was detected with a rat polyclonal antibody prepared in our laboratory (14). All western blots were developed using the ECL western blotting detection system (GE Healthcare) as recommended by the manufacturer.

Complementation assays in S2 cells

Complementation assays were performed as described previously (5). For miRNA-mediated silencing assays, the transfection mixtures contained 0.1 μg of firefly luciferase reporter plasmid, 0.4 μg of a *Renilla* transfection control and 0.1 μg of plasmids expressing miRNA primary transcripts or the corresponding vector without insert. Unless otherwise indicated, 20 ng (Figure 3) or 100 ng (all other Figures) of plasmids expressing recombinant proteins were cotransfected. Firefly and *Renilla* luciferase activities were measured 3 days after transfection using the Dual-Luciferase Reporter Assay System (Promega). Total RNA was isolated using TriFast (Peqlab Biotechnologies) and analyzed as described previously (21).

Immunoprecipitation analyses and luciferase assays in human cells

The R-Luc-3xlet-7 reporter and the corresponding R-Luc-Mut have been described previously (22). The R-Luc-Hmga2 wild-type and the R-Luc-Hmga2 m7 mutant described by Mayr *et al*. (23) were subcloned into the pCI-neo (Promega) expression vector. Immunoprecipitation assays were performed in human cells as described by Braun *et al*. (8). GFP- and HA-tagged proteins and endogenous α-tubulin were detected as described above. Endogenous PABP and TNRC6A were detected using commercial antibodies at the following dilutions: PABP (Abcam ab21060; 1:10 000) and human TNRC6A (Bethyl A302-329A; 1:2000).

For luciferase assays, human HeLa cells were seeded in six-well plates and transfected using Lipofectamine 2000 (Life technologies). The transfection mixtures contained 0.05 μg of R-Luc-3xlet-7 or 0.2 μg R-Luc-HMG2a reporter plasmids, or the corresponding reporters carrying mutations in the let-7 binding sites (R-Luc-Mut and R-Luc-Hmga2-mut7), and 0.3 μg of the pEGFP-N3-F-Luc transfection control. In the overexpression experiment described in Figure 9, the transfection mixtures contained in addition 1.5 μg of plasmids expressing GFP-CNOT1 fragments or the GFP-CNOT7 catalytically inactive mutant. The CNOT7 mutant carries alanine substitutions of the catalytic residues D40 and E42. A plasmid expressing GFP-tagged maltose binding protein (GFP-MBP) served as a negative control. R-Luc and F-Luc activities were measured 48 h after transfection using the Dual-Luciferase Reporter Assay System (Promega). Complementation assays were performed as described previously (5). The following siRNAs were used: TNRC6A 5′-GCCUAAUCUCCGUGCUCA ATT-3′; TNRC6B 5′-GGCCUUGUAUUGCCAGCA ATT-3′ and β-Gal 5′-CUACACAAAUCAGCGAUU UUU-3′ (Dharmacon).

Reverse transcription and quantitative real-time polymerase chain reaction were performed as described by Zekri *et al*. (4) using the following oligos: R-Luc forward (5′-ACTTCGAAAGTTTATGATCC-3′), R-Luc reverse (5′-TGTTCATTTTTGAGAACTCG-3′), F-Luc forward (5′-GGTGAGCAAGGGCGAGGAGC-3′) and F-Luc reverse (5′-CGCCGGACACGCTGAACTTG-3′).

GST pull-down assays

A cDNA encoding the SD of TNRC6A was cloned into the BamH1–Not1 restriction sites of plasmid pGEX6P (GE Healthcare) and expressed in *Escherichia coli* as an N-term GST-fusion. Mutations were introduced using the QuikChange mutagenesis kit (Stratagene) and the appropriate oligonucleotides. For the GST pull-down assays shown in Figure 8, lysates from *E. coli* cells expressing GST, GST-TNRC6A-SD or the indicated mutants were incubated with 40 μl of Protino Glutathione Agarose 4B beads (Macherey Nagel; 50% slurry) in lysis buffer

(10 mM Hepes [pH 7.5], 300 mM NaCl and 1 mM DTT) for 1 h at 4°C. The beads were washed three times using 1 ml of lysis buffer each time. The pre-coated beads were then incubated with lysates from HEK293T cells (ca. 2×10^6 cells/pull down) expressing CNOT1 in a total volume of 1 ml of NET buffer (10 mM Hepes [pH 7.5], 150 mM NaCl, 1 mM EDTA and 1% [v/v] Triton-X100) for 1 h at 4°C. The beads were washed three times using 1 ml of NET buffer each time. Proteins were eluted with 40 µl of sample buffer and separated on a 10% sodium dodecyl sulfate-polyacrylamide gel electrophoresis.

RESULTS

Drosophila melanogaster GW182 interacts with NOT1 through an extended silencing domain

The conserved core of the *D. melanogaster* CCR4–NOT complex consists of NOT1, NOT2, NOT3 and two catalytic subunits, CCR4 and POP2 (24). Of these, NOT1 and NOT2 are efficiently co-immunoprecipitate with *D. melanogaster* GW182 from Schneider cell (S2 cells) lysates (8,9). In addition, similar to human TNRC6 proteins, *D. melanogaster* GW182 interacts with PAN3 (8,9). In contrast to the human proteins, however, the deletion of the SD from *D. melanogaster* GW182 does not prevent interactions with deadenylation factors, indicating that sequences upstream of the SD also contribute to binding (8,9). In agreement with these observations, an N-term region of *D. melanogaster* GW182 (containing the N-term effector domain [NED]; Figure 1) has been shown to bind NOT1 and possess silencing activity (9,11,25).

To precisely define the regions of *D. melanogaster* GW182 involved in deadenylase binding, we performed co-immunoprecipitation experiments in S2 cells using a series of GW182 deletion mutants. First, we confirmed that deletion of the GW182 SD (ΔSD) reduced but did not abolish *D. melanogaster* GW182 binding to NOT1, whereas the binding to NOT2 and PAN3 was unaffected (Figure 2A–C, lanes 8). As expected, deletion of the SD did not prevent binding to AGO1 (which is mediated through the ABD); however, PABP binding was abrogated [Figure 2D and E, lanes 8 (4,5,12)].

Notably, although the SD is sufficient for PABP binding (Figure 2D, lane 9 (4,5)), in isolation, this domain interacted with NOT1 much less efficiently than full-length *D. melanogaster* GW182 and did not interact with NOT2 and PAN3 (Figures 2A–C, lanes 9). These results indicate that sequences upstream of the SD contribute to the interaction between GW182 and deadenylases. Furthermore, these results also indicate that deadenylases and PABP can independently interact with *D. melanogaster* GW182. The interactions with deadenylases are also independent of AGO1, because a *D. melanogaster* GW182 mutant that does not interact with AGO1, that is, in which all 12 N-term GW-repeats are mutated to alanines (12xGW mutant; Figure 2E, lane 10), interacted with NOT1, NOT2 and PAN3 as efficiently as wild-type *D. melanogaster* GW182 (Figure 2A–C, lanes 10).

To further delineate the regions of *D. melanogaster* GW182 required for NOT1 deadenylase binding, we extended the SD to include additional N-term sequences of increasing length (Figure 2F). We observed that full binding activity required fragment 713–1384 or the combination of the entire Q-rich region and the SD (Q+SD; i.e. 635–1384) (Figure 2F and G). Conversely, a *D. melanogaster* GW182 protein lacking both the Q-rich region and the SD (ΔQ+SD) did not interact with NOT1 (Figure 2G, lane 7). Surprisingly, PAN3 interacted with these two non-overlapping protein fragments, whereas NOT2 interacted primarily with the Q+SD region (Supplementary Figure S1A and B, lanes 7 and 8).

We conclude that the interaction of *D. melanogaster* GW182 with NOT1 is mediated by the Q-rich region together with the SD. Another important conclusion from these results is that PAN3 can interact with the *D. melanogaster* GW182 fragment 1–634 (i.e. ΔQ+SD) independently of NOT1, although the binding efficiency in this case is reduced relative to that observed with full-length *D. melanogaster* GW182. In addition, PAN3 and NOT2 also interact with the Q+SD region.

A complex network of interactions recruits deadenylases to *D. melanogaster* GW182

To identify the sequences sufficient for NOT2 and PAN3 binding, we performed co-immunoprecipitation assays using a series of *D. melanogaster* GW182 N-term fragments of increasing length (Supplementary Figure S1). These fragments were chosen based on the published activity of these fragments in tethering assays (11,25,26). Collectively, these experiments revealed the following observations.

First, GW182 residues 1–830 and 1–1115 are sufficient for NOT2 and PAN3 binding, respectively (Supplementary Figure S1C–E), whereas, as mentioned earlier, NOT1 binding requires residues 635–1384 (i.e. Q+SD).

Second, the GW182 ABD (residues 1–539) does not interact with deadenylase subunits (Supplementary Figure S1C–E, lanes 11) despite the fact that this fragment contains the NED. In accordance with these results, deletion of the NED from *D. melanogaster* GW182 did not affect NOT1, NOT2 or PAN3 binding (Supplementary Figure S1C–E, lanes 16). All fragments interacted with endogenous AGO1 as expected (Supplementary Figure S1C).

Third, the contribution of GW182 N-term sequences (residues 1–539) to deadenylase binding becomes apparent only when the C-term region is deleted (Supplementary Figure S1F and G; compare fragments 1–1115 versus 539–1115 for PAN3, and fragments 1–830 versus 539–830 for NOT2).

We conclude that *D. melanogaster* GW182 interacts with deadenylases through multiple binding sites that appear to contribute additively to the affinity of the interaction. Moreover, because deadenylase subunits interact with each other (24), these subunits could bind *D. melanogaster* GW182 either directly or indirectly. For example, although NOT2 interacts with GW182 N-term

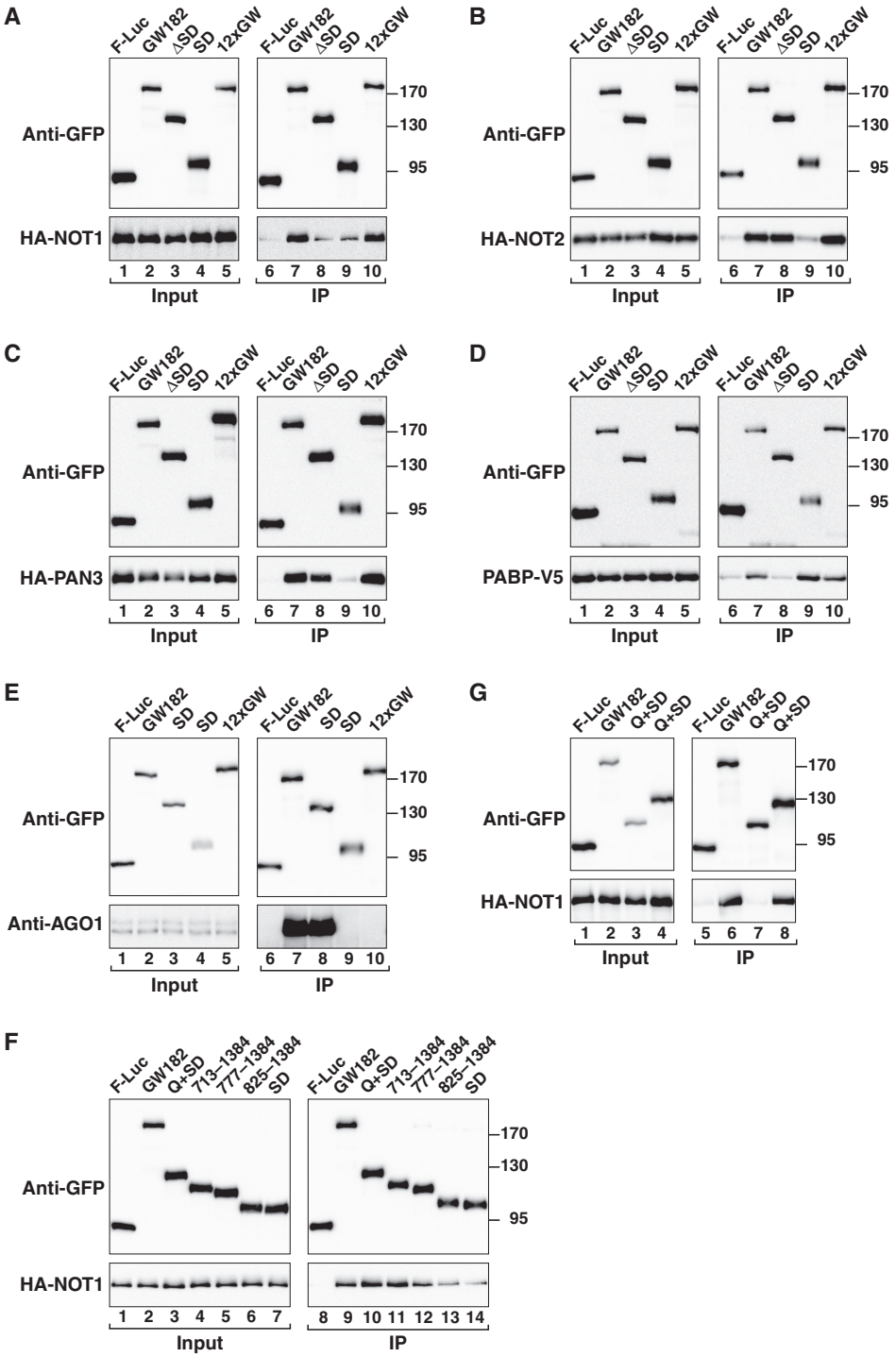

Figure 2. Interaction of *Drosophila melanogaster* GW182 with NOT1, NOT2 and PAN3. (**A–G**) S2 cells were cotransfected with plasmids expressing GFP-tagged *D. melanogaster* GW182 (wild-type or mutants) and HA-tagged deadenylase subunits or V5-tagged PABP as indicated. Cell lysates were immunoprecipitated using a polyclonal anti-GFP antibody. GFP-tagged firefly luciferase served as a negative control. Inputs (1%) and immunoprecipitates (5% for GFP-tagged proteins or 40% for HA- or V5-tagged proteins) were analyzed by western blotting using the corresponding antibodies. In all panels, cell lysates were treated with micrococcal nuclease before immunoprecipitation. The presence of endogenous AGO1 in the immunoprecipitates was determined using a specific anti-AGO1 antibody (E).

sequences, it also interacts with the Q+SD region (most likely via NOT1). This connectivity and redundancy of the GW182 interaction network helps to explain why the contribution of the NED to deadenylase binding becomes apparent only when SD regions are deleted.

GW182 generally requires the SD to silence miRNA targets

Our previous results demonstrated that deleting the SD from *D. melanogaster* GW182 abrogates its silencing activity in complementation assays, wherein GW182

protein mutants are tested for their ability to restore silencing in cells that are depleted of endogenous GW182 (5,8,12). In contrast, other studies have shown that N-term fragments of *D. melanogaster* GW182 (e.g. 1–605 and 1–830) can rescue the silencing of at least one miRNA reporter in S2 cells (11,25). Furthermore, *D. melanogaster* GW182 N-term fragments confer strong repression *in vivo* when artificially tethered to reporter mRNAs, independently of whether the reporter contains a poly(A) tail [Supplementary Figure S2A and B (11,25–27)]. Because *D. melanogaster* GW182 N-term fragments do not interact with PABP, it was important to determine whether these fragments complement silencing in cells that are depleted of endogenous *D. melanogaster* GW182.

For these complementation assays, we used two previously characterized firefly luciferase reporters: the F-Luc-Nerfin-1 and F-Luc-Par-6 reporters silenced by miR-279 and miR-1, respectively (20,21). At steady state, the F-Luc-Nerfin-1 reporter is predominantly repressed at the level of translation, with a small reduction in mRNA abundance (Figure 3A and B, lane 2 versus 1); however, the F-Luc-Par-6 mRNA is degraded in a miR-1-dependent manner (Figure 3E and F, lane 2 versus 1). The depletion of endogenous *D. melanogaster* GW182 suppressed the silencing of both reporters, leading to a 4- to 5-fold increase in firefly luciferase expression (Figure 3C and G). For the F-Luc-Par-6 reporter, a corresponding increase in mRNA levels was also observed (Figure 3F and H). These results confirm that *D. melanogaster* GW182 is required for both miRNA-mediated translational repression and mRNA degradation, as previously reported (14,28).

In depleted cells, a dsRNA-resistant version of *D. melanogaster* GW182 fully rescued the silencing of both reporters (Figure 3B–D and F–H). In contrast, *D. melanogaster* GW182 fragments lacking the SD (1–539, 1–605 and ΔSD) did not restore silencing, whereas a protein lacking the NED was fully active (Figure 3B–D and F–H). All proteins were expressed at comparable levels (Figure 3I). Notably, the inactive GW182 protein fragments and fragment 1–830 remained inactive, even when expressed at higher levels (Supplementary Figure S3A–C). Finally, a *D. melanogaster* GW182 mutant lacking the RRM and the C-term region (fragment 1–1115) complemented silencing, although less efficiently than full-length GW182 (Figure 3B–D and F–H and Supplementary Figure S3A and B). A western blot analysis indicated that the levels of *D. melanogaster* GW182 in the depleted cells were reduced below 10% of the control levels (Supplementary Figure S3D). We concluded that the ability of GW182 protein fragments to complement silencing is independent of whether silencing occurs at the level of translation (the F-Luc-Nerfin-1 reporter) or mRNA stability (the F-Luc-Par-6 reporter), suggesting that these two modes of regulation are not mediated through different GW182 protein domains; thus, these effects might be mechanistically linked.

Previous studies have reported that GW182 N-term fragments can rescue the silencing of the F-Luc-Nerfin-1 reporter when silenced by miR-9b (11,25). In line with those studies, we observed that GW182 protein fragments 1–605 and 1–830 (but not 1–539) restored the silencing of the F-Luc-Nerfin-1 reporter by miR-9b (Supplementary Figure S4A–C). Paradoxically, as shown above, these N-term protein fragments did not rescue the silencing of the F-Luc-Par-6 and F-Luc-Nerfin-1 reporters when silencing was mediated via miR-1 and miR-279, respectively.

To resolve this apparent discrepancy, we further examined the silencing of additional reporters, including the F-Luc-CG3548, F-Luc-CG5281 and F-Luc-CG7709 reporters silenced by miR-12; the F-Luc-Vha-68-1 reporter silenced by miR-9b and the F-Luc-CG11206 reporter silenced by both miR-9b and miR-12 (20,21). We observed that *D. melanogaster* GW182 N-term fragments (1–605, 1–830 and ΔSD) did not rescue the silencing of these reporters (Figure 4A–F). Furthermore, these N-term fragments inhibited silencing in a dominant-negative manner in control cells (Supplementary Figure S5A–G).

We conclude that although the N-term region of *D. melanogaster* GW182 is sufficient for the silencing of the F-Luc-Nerfin-1 reporter via miR-9b, this region was not sufficient to rescue the silencing of the additional miRNA reporters tested. Furthermore, in the context of the full-length protein, the SD is required for the silencing of a majority of the reporters tested, whereas the NED is dispensable. Finally, an N-term fragment containing the NED (1–539) was not sufficient to rescue silencing, although this fragment binds AGO1. On the basis of these results and our previous observations (12), we conclude that the SD is required for the silencing of most miRNA targets (5,8,12). Nevertheless, because one of nine reporters was silenced independently of the SD, it would be interesting to determine how many targets are SD independent (and thus independent of the GW182–PABP interaction) on a genome-wide level, and what features confer this independence.

Design of a minimal functional GW182 protein

Having established that the SD is generally required for silencing, we next examined whether this domain is also sufficient for silencing. Because the SD does not interact with AGO1, we therefore generated a chimeric protein containing a minimal AGO-binding domain fused to the *D. melanogaster* GW182 SD. We selected the AGO-binding domain (ABD) of the highly divergent *Caenorhabditis elegans* GW182 protein AIN-2, which binds to *D. melanogaster* AGO1 [Figure 5 (29)]. The AIN-2 ABD (herein referred to as ABD2) comprises 147 amino acids and contains only 3 GW repeats (Figure 1). Importantly, and in contrast to the *D. melanogaster* GW182 ABD, ABD2 does not interact with deadenylases and has no silencing activity in complementation assays (Figure 5).

We constructed a chimeric protein containing ABD2 fused to the isolated *D. melanogaster* GW182 SD or the SD plus additional N-term sequences. We also generated chimeric proteins containing the NED, the Q+SD fragment (635–1384) or the complementary N-term fragment (1–634, i.e. ΔQ+SD). Remarkably, in cells depleted of endogenous *D. melanogaster* GW182, the

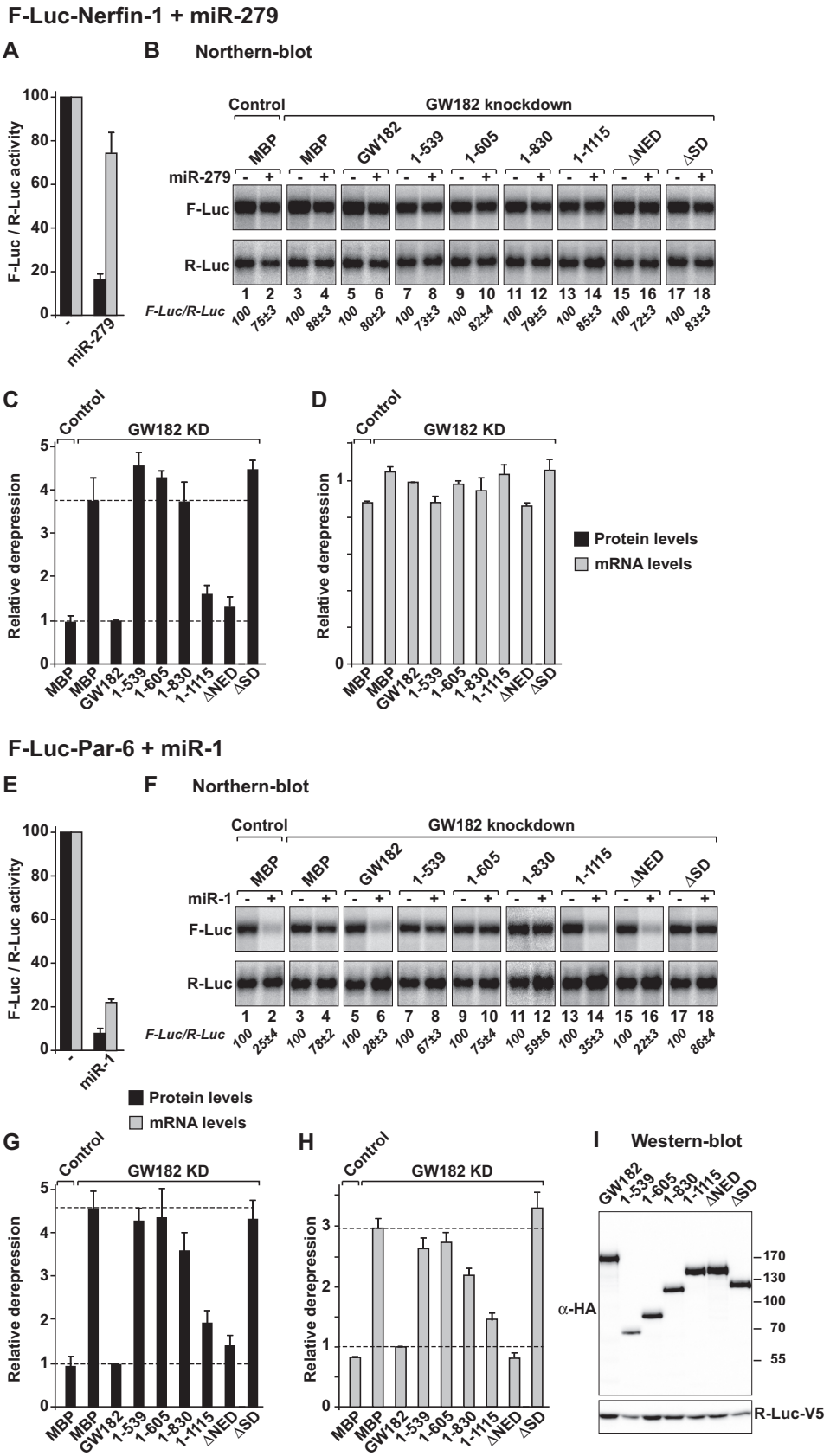

Figure 3. The *Drosophila melanogaster* GW182 SD is generally required for miRNA-mediated translational repression and target degradation. (**A–I**) Control S2 cells (treated with glutathion S-transferase (GST) dsRNA) or cells depleted of endogenous GW182 were transfected with a mixture of three plasmids: one expressing the indicated F-Luc reporters; a second expressing miRNA primary transcripts or the corresponding empty vector (−)

(continued)

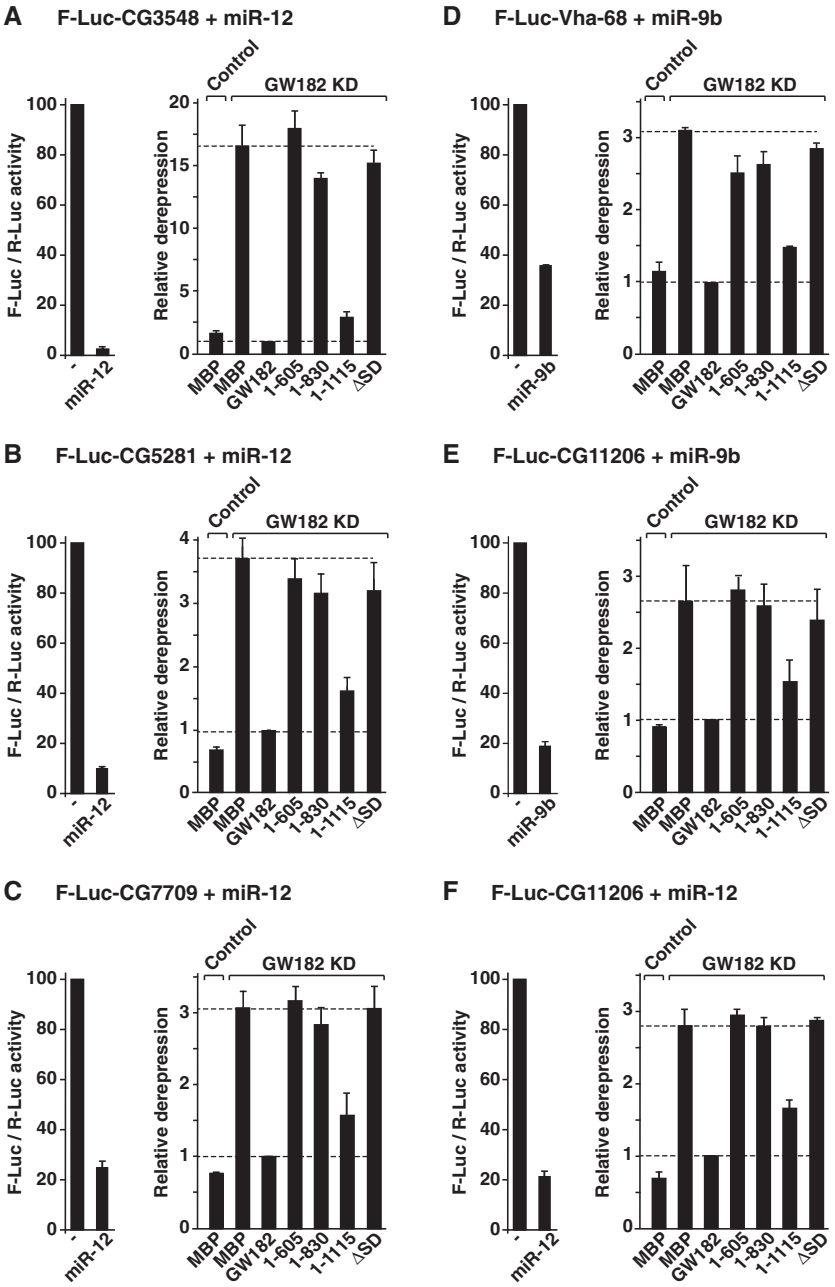

Figure 4. The *Drosophila melanogaster* GW182 SD is generally required for silencing. (**A–F**) Complementation assays using the indicated miRNA reporters were carried out as described in Figure 3. The graphs on the left of each panel show normalized firefly luciferase activities in the absence or presence of miRNAs in control cells (i.e. cells treated with *GFP* dsRNA and expressing MBP). The graphs on the right of each panel show the relative derepression of the F-Luc reporters for each condition. Mean values ± standard deviations from three independent experiments are shown. Labels are as described in Figure 3.

Figure 3. Continued
and a third expressing *Renilla* luciferase (R-Luc). Plasmids encoding HA-GW182 (wild-type or deletion mutants) or HA-MBP (negative control) were included in the transfection mixtures as indicated. For each condition, firefly luciferase activities and mRNA levels were normalized to those of the *Renilla* luciferase transfection control and set at 100% in cells transfected with the empty vector (i.e. in the absence of the miRNAs). (A and E) Normalized firefly luciferase activities and mRNA levels in the absence or presence of miRNAs in control cells (i.e. cells treated with *GFP* dsRNA and transfected with a plasmid expressing MBP). (B and F) Northern blot analysis of representative RNA samples. Numbers in italics below the panels indicate the levels of the F-Luc reporters normalized to that of R-Luc mRNA and set at 100 in the absence of the miRNAs. (C and G) Relative derepression of F-Luc activity for each condition. (D and H) Relative F-Luc mRNA levels. Throughout this study, error bars represent standard deviations from at least three independent experiments. Upper and lower dashed lines indicate maximal derepression and repression, respectively, observed in depleted cells. (I) A western blot showing that GW182 mutants were expressed at levels equivalent to that of the wild-type protein.

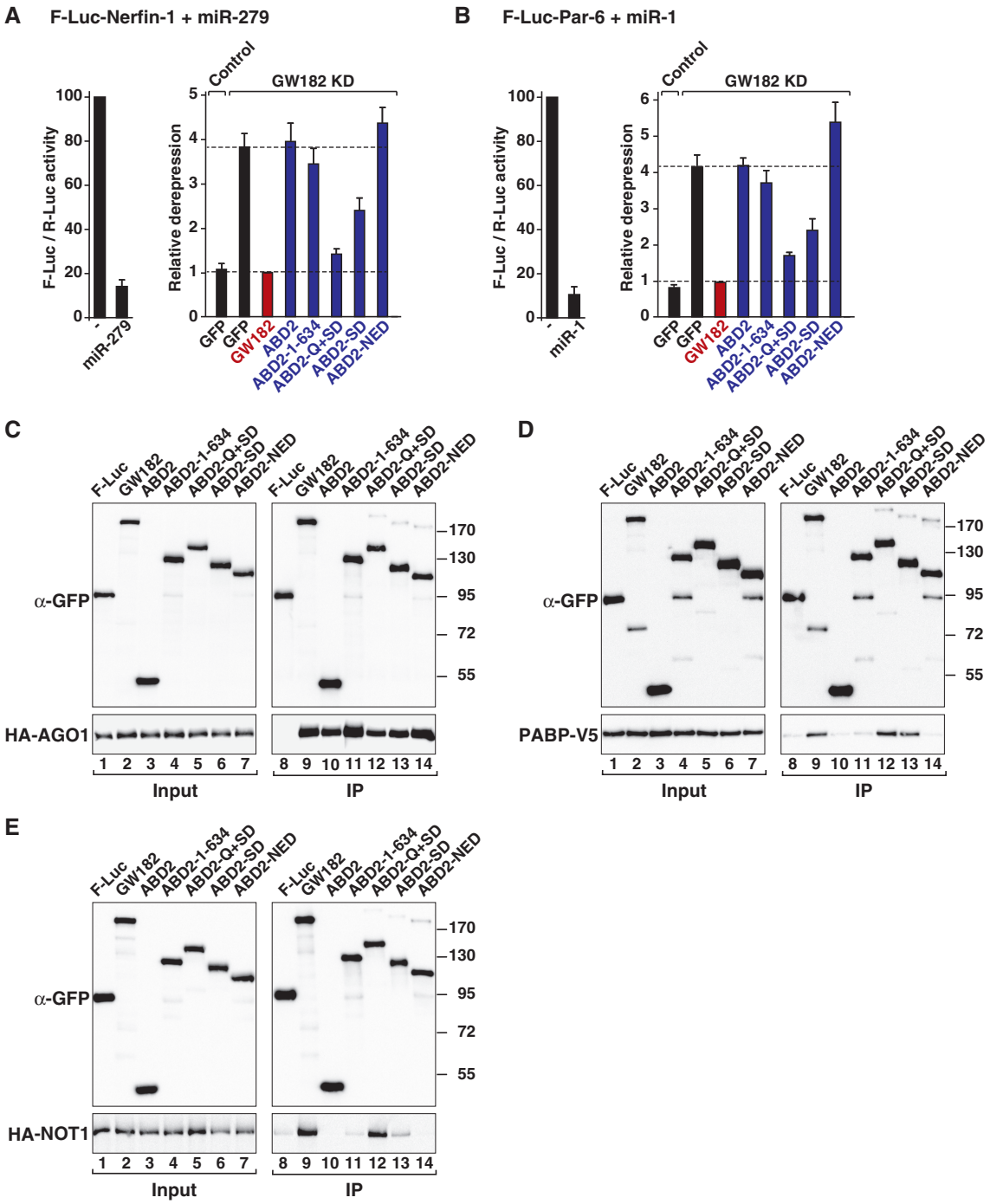

Figure 5. The *Drosophila melanogaster* GW182 Q+SD region is sufficient for silencing. (**A** and **B**) The silencing activity of chimeric proteins containing the *Caenorhabditis elegans* ABD2 fused to various GW182 fragments was tested in complementation assays as described in Figure 3 except that control cells were treated with GST dsRNA and transfected with a plasmid expressing GFP. (**C–E**) The interactions of the chimeric ABD2–GW182 proteins with AGO1, PABP and NOT1 were analyzed as described in Figure 2.

chimeric protein containing the Q+SD region rescued the silencing of the F-Luc-Nerfin-1 and F-Luc-Par6 reporters although not as efficiently as wild-type *D. melanogaster* GW182 (Figure 5A and B), suggesting that sequences upstream of the Q-rich region although not essential, contribute to silencing. The chimeric protein containing the isolated SD or the SD and additional N-term sequences partially rescued silencing (Figure 5A and B, and Supplementary Figure S5H and I). In contrast, the chimeric proteins containing the NED or residues 1–634 did not rescue silencing, even when expressed at higher levels (Figure 5A and B, and Supplementary Figure S6A–C). Notably, a chimeric protein containing only the Q-rich region was also inactive in complementation assays (Supplementary Figure S6A and B), although this region is active in tethering assays (11,25,26). All proteins were

expressed at comparable levels and interacted with *D. melanogaster* AGO1 (Figure 5C and Supplementary Figure S6C).

Consistent with the results shown in Figure 2, the chimeric protein containing the Q+SD region interacted with PABP and NOT1 as efficiently as the full-length *D. melanogaster* GW182 (Figure 5D and E, lanes 12) and also bound PAN3 and NOT2 (Supplementary Figure S7A and B). The chimera containing the SD interacted with PABP (Figure 5D, lane 13), whereas the chimera containing the NED did not exhibit any binding affinity towards PABP or NOT1 (Figure 5D and E, lanes 14). Finally, the chimeric protein that contained fragment 1–634 did not rescue silencing, despite the observation that this fragment interacts with PAN3 and NOT2 (Figure 5A and B and Supplementary Figure S1A and B). We concluded that the silencing activity of the chimeric GW182 protein correlates with binding to both PABP and deadenylases because only the Q + SD fragment efficiently rescues silencing.

A minimal GW182 protein reveals interactions that are required for silencing

Recent studies have identified W-containing motifs in the M1, M2 and C-term regions of human SDs that are required for the interaction with NOT1 and PAN3 and described mutations in these motifs that abolish binding and silencing (9,10). The motifs in the M1 and C-term regions were termed CIM-1 and CIM-2, respectively (10). The CIM-2 motif is absent in *D. melanogaster* GW182; however, *D. melanogaster* GW182 contains a CIM-1 motif and six tryptophan residues in the M2 region (9,10). The contribution of these motifs to deadenylase binding in the context of the full-length *D. melanogaster* GW182 protein has not been analyzed.

The finding that a minimal chimeric protein consisting of ABD2 and the *D. melanogaster* GW182 Q+SD region could complement silencing in S2 cells provided an opportunity to test how the specific disruption of PABP or deadenylase binding interferes with silencing in a cellular context in the absence of the contribution of the GW182 N-term sequences. Therefore, we introduced amino acid substitutions into the PAM2 and CIM-1 motifs and in the M2 region (individually or in combination) and assessed the interaction of the mutant proteins with PABP and deadenylases using immunoprecipitation assays; the silencing activity was also tested using complementation assays. We again used a reporter silenced at the translational level (F-Luc-Nerfin-1) and a reporter that is degraded under steady-state conditions (F-Luc-Par-6). These studies revealed the following observations.

First, a single amino acid substitution in the PAM2 motif (F961A) or mutations in the CIM-1 motif did not affect PABP or NOT1 binding (Figure 6A and B, lanes 10 and 11) and had no significant effect on silencing activity (Figure 6C and D). The alanine substitution of all six tryptophan residues in the M2 region (6xW) reduced both PABP and NOT1 binding and, consequently, silencing activity (Figure 6A and B, lanes 12 and Figure 6C and D), as previously reported (9). For all mutants tested, PAN3 and NOT2 binding mirrored NOT1 binding (Supplementary Figure S7A and B).

Second, when combined, mutations in the CIM-1 motif and the M2 region strongly reduced PABP and NOT1 binding and silencing activity (Figure 6A and B, lanes 13 and Figure 6C and D). The silencing activity of the chimeric protein was abolished when the PAM2 motif was mutated in combination with the CIM-1 and the 6xW mutations (Figure 6C and D). Importantly, similar results were obtained when F-Luc-Par-6 mRNA levels were analyzed (Figure 6E and F), indicating that the mutations affect translational repression and mRNA degradation in a similar way. Together, these results indicate that the silencing activity of GW182 proteins correlates with both PABP and deadenylase binding.

A recent study reported the identification of another conserved motif, the P-GL motif, in the M2 region of GW182 proteins [Figure 1 and Supplementary Figure S7F (30)]. This motif was shown to contribute to the translational repression and deadenylation of polyadenylated targets in zebrafish embryos (30). We observed that the corresponding mutations in the *D. melanogaster* GW182 P-GL motif did not affect the silencing activity of the chimeric ABD2-Q+SD protein and did not exacerbate the effect of mutations in the CIM-1 or PAM2 motifs (Supplementary Figure S8A and B). Furthermore, mutations in the P-GL motif did not affect binding to PABP and deadenylases [Supplementary Figure S8C–E (30)]. These results confirm that the P-GL motif does not contribute to silencing in S2 cells (9).

The human TNRC6C SD is sufficient for silencing

Because the mechanism of silencing is conserved and we have previously shown that human TNRC6 proteins complement silencing in *Drosophila* cells (5), we next determined whether a minimal protein consisting of ABD2 fused to the human TNRC6C SD could rescue silencing in S2 cells depleted of endogenous *D. melanogaster* GW182. This question was particularly interesting because, unlike the *D. melanogaster* GW182 SD, human SDs are sufficient for the interaction with PABP and deadenylases (3,5,8–10). Quite remarkably, we observed that a chimeric protein containing ABD2 fused to the TNRC6C SD complemented the silencing of the F-Luc-Nerfin-1 and F-Luc-Par-6 reporters in GW182-depleted cells (Figure 7A and B).

We next examined the contribution of the CIM-1, CIM-2 and PAM2 motifs to PABP and NOT1 binding and silencing activities. We observed that mutations in the CIM-1 or CIM-2 motifs reduced silencing activity, and the effect of mutations in CIM-2 was stronger (Figure 7A and B); these findings are in agreement with the observation that the CIM-1 and CIM-2 motifs are not functionally equivalent (10). The CIM-1 and CIM-2 mutations reduced NOT1 binding without affecting the interaction with PABP (Figure 7C and D, lanes 11 and 12). When combined, mutations in the CIM-1 and CIM-2 motifs strongly reduced NOT1 binding and silencing activity (Figure 7A–D). The

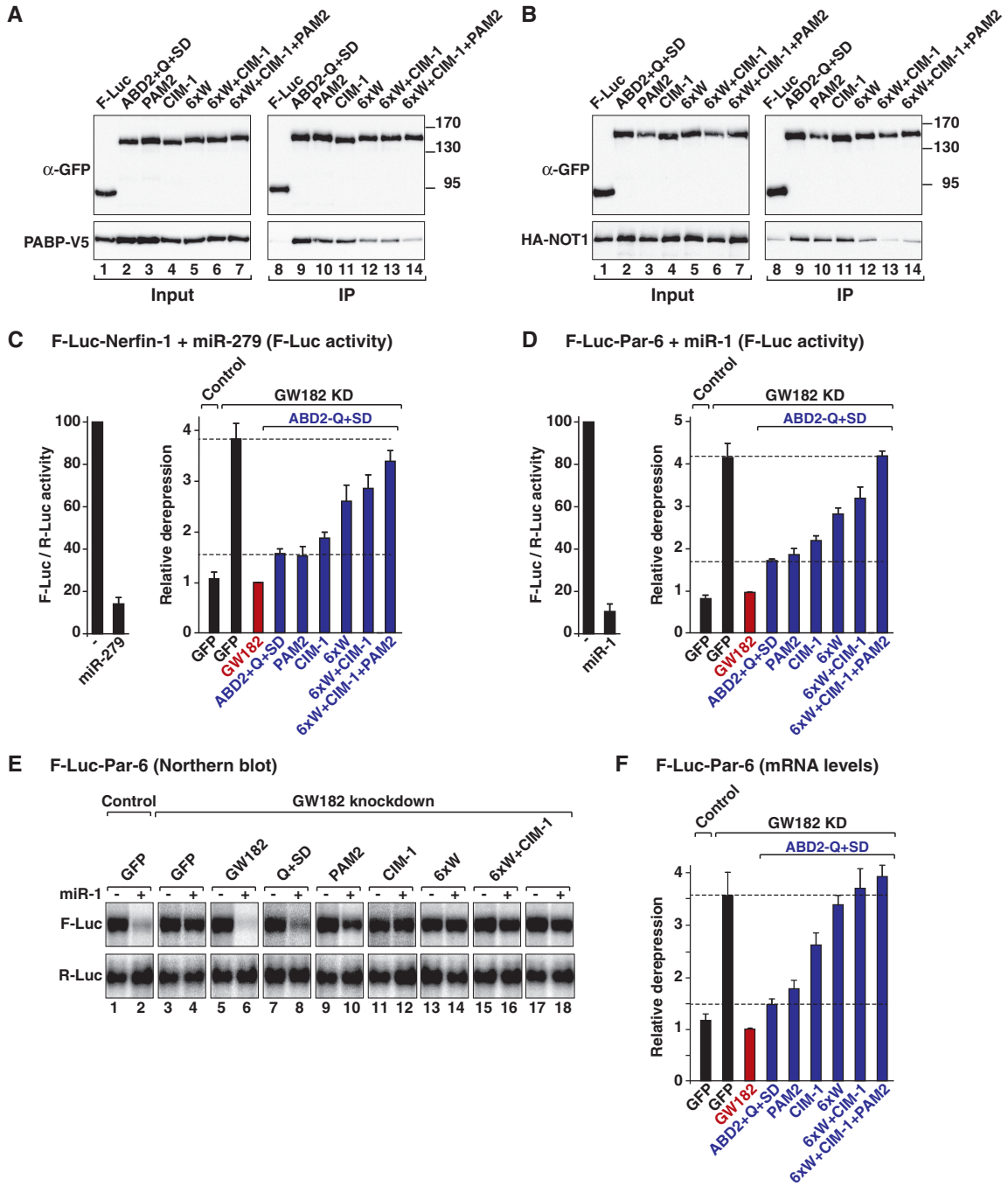

Figure 6. PABP and deadenylase binding are required for silencing. Mutations in the PAM2 and CIM-1 motifs and the M2 region were introduced in a minimal GW182 protein consisting of *Caenorhabditis elegans* ABD2 fused to the GW182 Q+SD region (ABD2-Q+SD). The PAM2 mutant carries a single amino acid substitution (F961A) in the PAM2 motif. Mutations in the CIM-1 motif are shown in Supplementary Figure S7. The 6xW mutant carries alanine substitutions of all six tryptophan residues in the M2 region of the SD. (**A** and **B**) The interactions of the ABD2-Q+SD protein (wild-type or mutant) with PABP and NOT1 were analyzed as described in Figure 2. (**C–F**) The silencing activity of the ABD2-Q+SD protein (wild-type or mutants) was tested in complementation assays as described in Figure 5.

double mutations also abrogated PABP binding (Figure 7C, lane 13), consistent with the observation that the GW182-PABP interaction in S2 cells is predominantly indirect. The effect of the CIM-1+2 double mutation was exacerbated when combined with the F1389A substitution in the PAM2 motif (Figure 7A–D). The F1389A mutation alone abolished PABP binding (Figure 7C, lane 10) and impaired silencing activity, particularly for the F-Luc-Nerfin-1 reporter [Figure 7A and B (5,8)], although NOT1 binding was only slightly reduced (Figure 7D, lane 10). Collectively, the results obtained with the chimeric proteins demonstrate that full silencing activity requires interactions between GW182 proteins and both PABP and deadenylases.

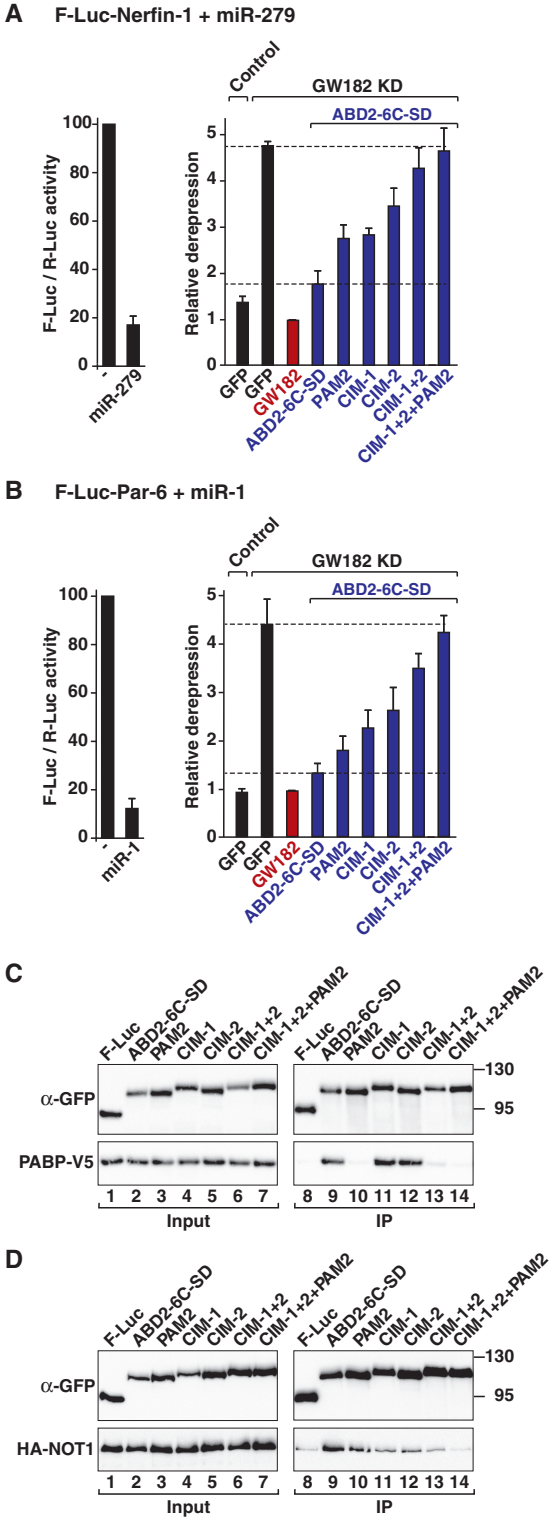

Figure 7. The TNRC6 SD is sufficient for silencing. Mutations in the PAM2, CIM-1 and CIM-2 motifs were introduced in a minimal GW182 protein consisting of *Caenorhabditis elegans* ABD2 fused to the human TNRC6C SD region (ABD2-6C-SD). The PAM2 mutant carries a single amino acid substitution (F1389A) in the PAM2 motif. Mutations in the CIM-1 and CIM-2 motifs are shown in Supplementary Figure S7. (**A** and **B**) The silencing activity of the chimeric ABD2-6C-SD protein (wild-type or mutant) was tested in complementation assays as described in Figure 5. (**C** and **D**) The interactions of the ABD2-6C-SD protein (wild-type or mutant) with PABP and NOT1 were analyzed as described in Figure 2.

The interaction of TNRC6s with PABP and deadenylases is required for silencing in human cells

Having established that the interaction with NOT1 and PABP is important for silencing in the context of the chimeric ABD2-TNRC6C SD, we subsequently investigated the contribution of these interactions to the silencing activity of TNRC6A protein in human cells. Accordingly, we used a previously characterized F-Luc reporter containing three Let-7 miRNA binding sites in the 3′ UTR, which is primarily regulated at the translational level [Figure 8A (22)]. The knockdown of TNRC6 proteins was achieved using siRNAs targeting TNRC6A and TNRC6B. This double depletion inhibited the silencing of the reporter, leading to a 2.8-fold increase in F-Luc activity (Figure 8A and B). A western blot analysis indicated that the levels of TNRC6A in the depleted cells were reduced to 10% of the control levels (Figure 8C). The silencing of F-Luc-3xlet-7 was rescued in cells expressing a siRNA-resistant form of wild-type TNRC6A (Figure 8B).

As shown above, mutations in either the CIM-1 or the CIM-2 motifs or alanine substitutions of the six tryptophan residues in the M2 region (6xW) reduced human NOT1 (CNOT1), but not PABP binding (Figure 8D). These mutations impaired silencing activity in complementation assays; a stronger effect was observed for the mutations in the M2 region and CIM-2 motif (Figure 8B). The CIM-1+2 double mutant was strongly impaired with respect to CNOT1 binding and silencing activity (Figure 8B and D). However, in contrast to the results observed in S2 cells, this mutant retained the ability to bind PABP in human cells (Figure 8D). Thus, the interaction of TNRC6A with PABP is not sufficient for silencing. Conversely, CNOT1 binding is also insufficient for full silencing activity because a TNRC6A mutant carrying a F1359A substitution in the PAM2 motif interacted with CNOT1, but not with PABP, and was impaired in complementation assays (Figure 8B and D). The silencing activity was reduced further when the mutation in the PAM2 motif was combined with the mutations in the CIM-1 and CIM-2 motifs or in the M2 region (Figure 8B). A protein carrying mutations in the M2 region and the CIM-1, CIM-2 and PAM2 motifs was inactive as observed using a protein lacking the entire SD (Figure 8B). All proteins were expressed at comparable levels (Figure 8E) and have no dominant negative effects in control cells (Supplementary Figure S9). These results demonstrated that the interactions of human TNRC6 proteins with PABP and CNOT1 are also required for full silencing activity in human cells.

Overexpression of the CNOT1 Mid domain suppresses silencing

The experiments described above suggest that silencing (i.e. translational repression and target degradation) requires an interaction between GW182 proteins and the CCR4–NOT complex. We next sought to further validate the contribution of this complex to silencing using an overexpression approach. These experiments were conducted in human cells, wherein the interaction of

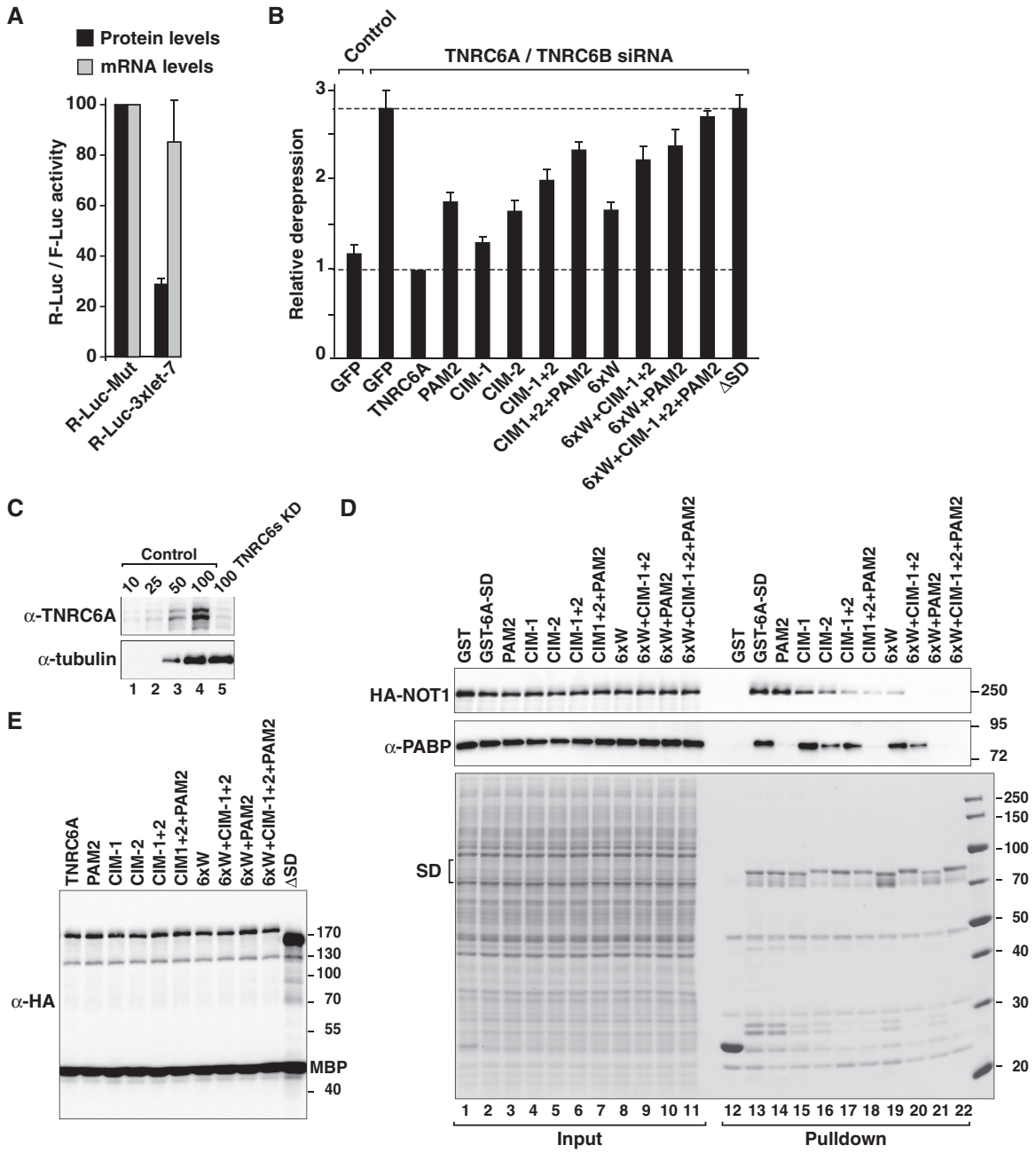

Figure 8. Complementation assay in human cells. (**A–C**) Control HeLa cells (transfected with β-Gal siRNA) or cells codepleted of TNRC6A and TNRC6B were transfected with a mixture of three plasmids: the R-Luc-3xlet-7 or the corresponding reporter carrying mutations in let-7–binding sites (R-Luc-Mut), a plasmid expressing F-Luc as a transfection control, and a plasmid expressing GFP or siRNA-resistant versions of HA-TNRC6A (wild-type or mutant). For each condition, *Renilla* luciferase activity was measured, normalized to that of the F-Luc transfection control and set at 100% in cells expressing R-Luc-Mut. (A) Normalized *Renilla* luciferase activities in control cells (i.e. cells treated with β-Gal siRNA and expressing GFP). (B) Relative fold derepression for each condition. Mean values ± standard deviations are shown. (C) Western blot showing the efficiency of the TNRC6A knockdown. Dilutions of control cell lysates were loaded in lanes 1–4 to estimate the efficacy of the depletion. α-tubulin served as a loading control. (**D**) Interaction of GST-tagged TNRC6A-SD (wild-type or mutants) with CNOT1 and endogenous PABP. Inputs (1%) and bound fractions (40%) were analyzed by western blotting. (**E**) Western blot analysis showing that all proteins were expressed at comparable levels.

TNRC6s with CNOT1 is direct and mediated through the SD, without any contribution from N-term sequences (8–10).

CNOT1 is a large protein containing 2376 amino acids and is predicted to be mainly α-helical. Sequence alignments and secondary structure predictions suggest that CNOT1 consists of N-term (CNOT1-N), Mid (CNOT1-M) and C-term (CNOT1-C) domains (Figure 9A). In immunoprecipitation assays, we observed that the CNOT1-M domain was sufficient for the interaction with the TNRC6A SD (Figure 9B, lane 9). CNOT1-N showed no detectable binding, whereas CNOT1-C exhibited some residual binding affinity (Figure 9B, lane 10). The CNOT1-M domain also interacts

with CNOT7 [also known as CAF1 (31)]. Therefore, we tested whether overexpression of the CNOT1-M domain, either alone or together with a catalytically inactive CNOT7 mutant, could inhibit silencing in a dominant negative manner.

Previous studies have demonstrated that the overexpression of a catalytically inactive CNOT7 mutant or the depletion of the subunits of the CCR4–NOT complex suppressed miRNA-mediated mRNA deadenylation and degradation, although translation of the reporters was not fully restored (14,15,21,31–33). Consistent with these studies, we observed that overexpression of the CNOT7 catalytically inactive mutant partially suppressed silencing of the R-Luc-3xlet-7 reporter (Figure 9C). Interestingly, overexpression of the CNOT1-M domain also partially suppressed the silencing of the R-Luc-3xlet-7 reporter (Figure 9C). Silencing was abrogated in cells coexpressing the NOT1-M domain together with the CNOT7 catalytically inactive mutant (Figure 9C).

To further confirm these results, we analyzed the effects of coexpressing the CNOT1-M domain together with the CNOT7 mutant on silencing of the R-Luc-Hmga2 reporter, which is also silenced by Let-7 (23). Silencing of this reporter was also suppressed in cells that coexpressed both proteins (Figure 9D). Taken together with results of recent reports showing that translational repression precedes target degradation and decay (15–17), these results further support the conclusion that the interaction of GW182 proteins with the CCR4–NOT complex is required for both miRNA-mediated translational repression and target degradation. Thus, the CCR4–NOT complex is a major effector complex of silencing.

DISCUSSION

Recent studies indicate that translational repression of miRNA targets precedes deadenylation and decay (3,15–19). Here, we show that these two functional outcomes of miRNA regulation are linked and both require the interaction of GW182 proteins with PABP and deadenylases.

The GW182–PABP interaction is required for maximal silencing activity

The interaction of GW182 proteins with PABP has been well documented using biochemical and structural studies, and the PAM2 motif is highly conserved among vertebrate and insect GW182 proteins (3–7). Despite conservation, the study of the role of PABP in silencing in different systems has led to conflicting conclusions. For example, several studies have reported that the PABP–GW182 interaction is important for silencing in *D. melanogaster* and human cells and in cell-free systems that recapitulate silencing (3,5,6,8,10,34,35). Furthermore, PABP depletion prevented miRNA-mediated deadenylation in cell-free extracts from mouse Krebs-2 ascites cells (3), and mutations in the PAM2 motif of TNRC6C reduced the rate of deadenylation in tethering assays (6). In addition, a study in *D. melanogaster* cell-free extracts wherein silencing is mediated through endogenous preloaded miRISCs indicated that PABP stimulates silencing by facilitating the association of miRISC complexes with mRNA targets (35). It was also shown that on miRISC binding, PABP progressively dissociated from the mRNA target, in the absence of deadenylation (35).

In contrast to the studies mentioned above, studies in zebrafish embryos and in a *D. melanogaster* cell-free assay wherein miRISCs are loaded with exogenously supplemented miRNA duplexes indicate that PABP is dispensable for miRNA-mediated silencing (26,30). Intriguingly, efficient silencing in zebrafish embryos required the GW182 PAM2 motif (30). Moreover, the observation that multiple and non-overlapping fragments of *D. melanogaster* GW182 (including N-term fragments that do not interact with PABP) silenced mRNA reporters in tethering assays was interpreted as evidence that the interaction of GW182 proteins with PABP is not required for silencing (26). In this study, we show that unlike in tethering assays, N-term fragments of GW182 fail to restore the silencing of a majority of the reporters tested in complementation assays. Thus, tethering assays bypass the requirement for PABP binding, and may not faithfully recapitulate silencing. Furthermore, the observation that PABP dissociates from the poly(A) tail of miRNA targets in the absence of deadenylation (35) provides one explanation for the occurrence of silencing in extracts in which PABP has been depleted or displaced from the poly(A) tail using an excess of Paip2 (26,30).

In summary, our results confirm and further extend previous observations that a single amino acid substitution in the PAM2 motif of human TNRC6 proteins abolishes PABP binding and impairs silencing activity, despite the interaction of this mutant with deadenylases (3–8). Furthermore, *D. melanogaster* GW182 N-term protein fragments that bind deadenylases, but not PABP, failed to complement the silencing of eight of the nine reporters tested, although they are active in tethering assays. These results provide evidence for a role of PABP in silencing in human and *Drosophila* cells. However, it is possible that PABP becomes dispensable for silencing depending on cellular conditions or the nature of the specific mRNA target, as shown, for example, for the F-Luc-Nerfin-1 reporter when silencing is mediated by miR-9b [this study (11,25,26,30)].

Drosophila melanogaster GW182 establishes an intricate network of interactions with deadenylases

The SDs of human TNRC6 proteins directly interact with CNOT1 through tryptophan-containing motifs in the M1, M2 and C-term regions of the SD (9,10). Here, we show that these motifs contribute additively to CNOT1 binding and silencing activity in human cells. Indeed, when at least two motifs are simultaneously mutated, CNOT1 binding is strongly reduced and silencing activity impaired.

The interaction between GW182 and deadenylases is conserved in *D. melanogaster*; however, in contrast to human SDs, the *D. melanogaster* SD is not sufficient for

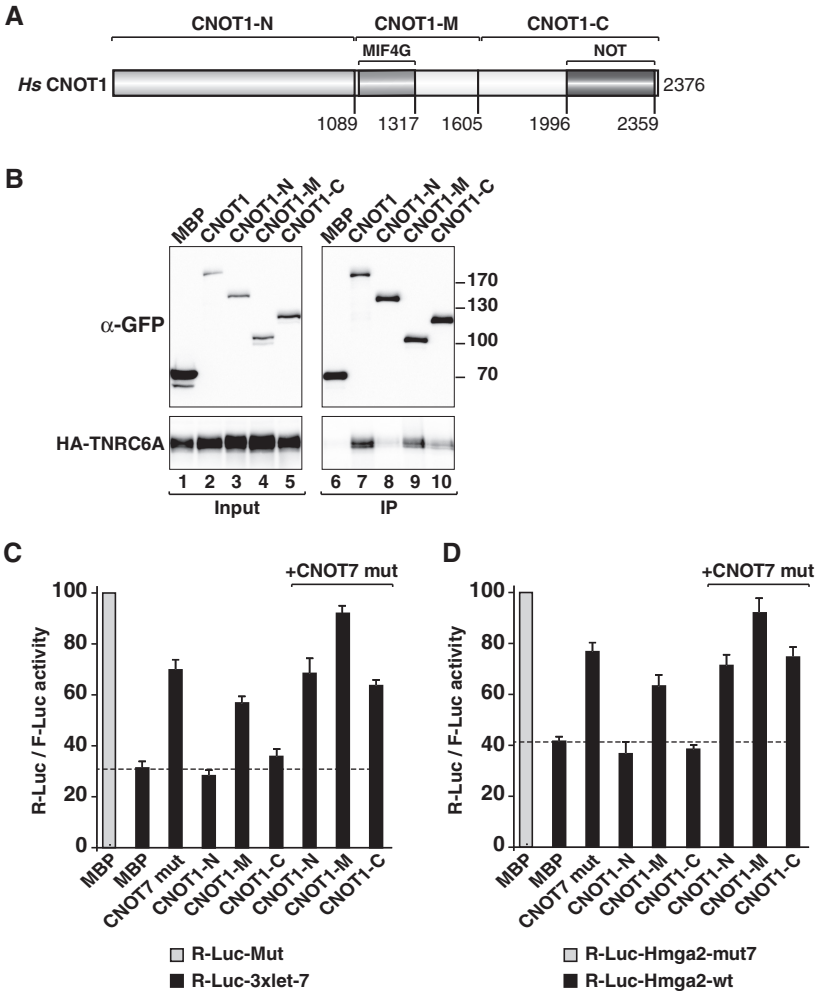

Figure 9. Overexpression of the CNOT1-M domain inhibits silencing in a dominant negative manner. (**A**) Domain organization of human CNOT1. CNOT1-N, N-terminal domain; CNOT1-M, middle domain containing the MIF4G domain (31); CNOT1-C, C-terminal domain containing the NOT homology domain. Amino acid positions at domain boundaries are indicated below the protein outlines and correspond to the NCBI protein sequence NP_057368.3. (**B**) Interaction of GFP-tagged human CNOT1 (wild-type or fragments) and human HA-TNRC6A. Inputs (1%) and immunoprecipitates (5% for CNOT1 or 10% for TNRC6A) were analyzed by western blotting. F-Luc-GFP served as a negative control. (**C** and **D**) Human cells were transfected with the indicated Let-7 reporters or the corresponding controls (Mut) as described in Figure 8. The transfection mixtures also contained plasmids encoding GFP-CNOT1-M and GFP-CNOT7 (catalytically inactive mutant, D40A+E42A), as indicated. A plasmid encoding GFP-MBP served as a negative control. For each condition, R-Luc activities were normalized to that of a F-Luc transfection control and set at 100% for the Mut reporters (gray bars, shown only for control cells). Error bars represent standard deviations from three independent experiments.

NOT1 binding. Here, we show that in addition to the SD, the Q-rich region is required for full NOT1 binding activity. Thus, although *D. melanogaster* GW182 has lost the CIM-2 motif, this protein has acquired additional motifs that can interact with NOT1. We also show that in contrast to the human proteins, *D. melanogaster* GW182 can interact with NOT2 and PAN3 via N-term sequences. Consequently, *D. melanogaster* GW182 can recruit deadenylases in multiple ways. Considering that (i) NOT1 interacts with NOT2 [reviewed in (36)], (b) the PAN2–PAN3 complex interacts with PABP (37) and (c) the CCR4–NOT and PAN2–PAN3 complexes form a larger multiprotein complex *in vivo* (38), our observations indicate a high degree of connectivity and redundancy within the GW182 interaction network, which could explain why mutations in individual motifs do not abolish partner binding or silencing activity, but a combination of two or more mutations is required to abrogate binding and silencing activity.

In addition, the ability of *D. melanogaster* GW182 N-term fragments to bind deadenylases also explains why these fragments are potent triggers of translational repression and mRNA degradation in tethering assays (9,11,25–27), whereas the corresponding fragments of the human proteins exhibit only residual activity (11,25,39,40). As discussed previously, despite their activity in tethering assays, *D. melanogaster* GW182 N-term fragments failed to complement the silencing of several of the reporters tested. The reason for the different activities of these fragments in tethering and complementation assays remains unknown.

Definition of a minimal protein interaction network required for silencing

In this study, we demonstrated that silencing (i.e. translational repression and target degradation) requires the interaction between GW182 proteins and both PABP and deadenylases. Several lines of evidence support this conclusion. First, the TNRC6C SD, which is sufficient for PABP and deadenylase binding, rescues silencing when fused to a minimal ABD. Similarly, the minimal fragment of *D. melanogaster* GW182 that rescues silencing comprises the Q+SD region, which also binds both deadenylases and PABP. Second, the *D. melanogaster* GW182 N-term fragments that bind deadenylases but not PABP are generally inactive in complementation assays. Third, mutations that specifically disrupt TNRC6 binding to PABP or deadenylase impair silencing, and mutations that disrupt deadenylase binding exhibit a stronger deleterious effect. Silencing activity is abolished when these mutations are combined. Finally, silencing is inhibited in human cells overexpressing the CNOT1 Mid domain together with a catalytically inactive CNOT7 mutant. In combination with the previously published data (1,2), our results indicate that silencing minimally requires an AGO, a GW182 protein, PABP and deadenylases, thus defining the minimal interaction network required for silencing. Our findings do not rule out that additional interactions are potentially required to achieve maximal repression, depending on the cellular context or the mRNA target. For example, the P-GL motif is highly conserved and important for silencing in zebrafish embryos (30). This motif may mediate interactions with additional partners.

The finding that deadenylase complexes, in particular, are required for miRNA-mediated translational repression has broad implications regarding post-transcriptional mRNA regulation. Indeed, in addition to the GW182 proteins, various sequence-specific mRNA-binding proteins, such as Nanos, Bicaudal-C and Pumilio, recruit the CCR4–NOT complex to their mRNA targets [reviewed in (36)]. Furthermore, the direct tethering of the subunits of the CCR4–NOT complex represses the translation of mRNA reporters lacking a poly(A) tail, suggesting that the CCR4–NOT complex promotes translational repression in the absence of deadenylation (9,13). Therefore, elucidating the mechanism by which the CCR4–NOT complex regulates the fates of mRNA targets promises to increase our understanding of the mechanism underlying repression by miRNAs and diverse sequence-specific RNA-binding proteins.

SUPPLEMENTARY DATA

Supplementary Data are available at NAR Online: Supplementary Figures 1–9.

ACKNOWLEDGEMENTS

We thank S. Heimstädt for providing the plasmid used for the expression of GW182 protein fragments and performing preliminary assays, and we also thank M. Fauser and S. Helms for excellent technical assistance.

FUNDING

Max Planck Society; the Deutsche Forschungsgemeinschaft (DFG, FOR855 and the Gottfried Wilhelm Leibniz Program awarded to E.I.). Funding for open access charge: Max Planck Society.

Conflict of interest statement. None declared.

REFERENCES

1. Huntzinger,E. and Izaurralde,E. (2011) Gene silencing by microRNAs: contributions of translational repression and mRNA decay. *Nat. Rev. Genet*., **12**, 99–110.
2. Fabian,M.R. and Sonenberg,N. (2012) The mechanics of miRNA-mediated gene silencing: a look under the hood of miRISC. *Nat. Struct. Mol. Biol*., **19**, 586–593.
3. Fabian,M.R., Mathonnet,G., Sundermeier,T., Mathys,H., Zipprich,J.T., Svitkin,Y.V., Rivas,F., Jinek,M., Wohlschlegel,J., Doudna,J.A. *et al.* (2009) Mammalian miRNA RISC recruits CAF1 and PABP to affect PABP-dependent deadenylation. *Mol. Cell*, **35**, 868–880.
4. Zekri,L., Huntzinger,E., Heimstädt,S. and Izaurralde,E. (2009) The silencing domain of GW182 interacts with PABP to promote translational repression and degradation of miRNA targets and is required for target release. *Mol. Cell. Biol*., **29**, 6220–6231.
5. Huntzinger,E., Braun,J.E., Heimstädt,S., Zekri,L. and Izaurralde,E. (2010) Two PABP-binding sites in GW182 proteins promote miRNA-mediated gene silencing. *EMBO J*., **29**, 4146–4160.
6. Jínek,M., Fabian,M.R., Coyle,S.M., Sonenberg,N. and Doudna,J.A. (2010) Structural insights into the human GW182-PABC interaction in microRNA-mediated deadenylation. *Nat. Struct. Mol. Biol*., **17**, 238–240.
7. Kozlov,G., Safaee,N., Rosenauer,A. and Gehrin,K. (2010) Structural basis of binding of P-body associated protein GW182 and Ataxin-2 by the MLLE domain of poly(A)-binding protein. *J. Biol. Chem*., **285**, 13599–13606.
8. Braun,J.E., Huntzinger,E., Fauser,M. and Izaurralde,E. (2011) GW182 proteins recruit cytoplasmic deadenylase complexes to miRNA targets. *Mol. Cell*, **44**, 120–133.
9. Chekulaeva,M., Mathys,H., Zipprich,J.T., Attig,J., Colic,M., Parker,R. and Filipowicz,W. (2011) miRNA repression involves GW182-mediated recruitment of CCR4-NOT through conserved W-containing motifs. *Nat. Struct. Mol. Biol*., **18**, 1218–1226.
10. Fabian,M.R., Cieplak,M.K., Frank,F., Morita,M., Green,J., Srikumar,T., Nagar,B., Yamamoto,T., Raught,B., Duchaine,T.F. *et al.* (2011) miRNA-mediated deadenylation is orchestrated by GW182 through two conserved motifs that interact with CCR4–NOT. *Nat. Struct. Mol. Biol*., **18**, 1211–1217.
11. Chekulaeva,M., Filipowicz,W. and Parker,R. (2009) Multiple independent domains of dGW182 function in miRNA-mediated repression in Drosophila. *RNA*, **15**, 794–803.
12. Eulalio,A., Helms,S., Fritzsch,C., Fauser,M. and Izaurralde,E. (2009) A C-terminal silencing domain in GW182 is essential for miRNA function. *RNA*, **15**, 1067–1077.
13. Cooke,A., Prigge,A. and Wickens,M. (2010) Translational repression by deadenylases. *J. Biol. Chem*., **285**, 28506–28513.
14. Behm-Ansmant,I., Rehwinkel,J., Doerks,T., Stark,A., Bork,P. and Izaurralde,E. (2006) mRNA degradation by miRNAs and GW182 requires both CCR4:NOT deadenylase and DCP1:DCP2 decapping complexes. *Genes Dev*., **20**, 1885–1898.
15. Béthune,J., Artus-Revel,C.G. and Filipowicz,W. (2012) Kinetic analysis reveals successive steps leading to miRNA-mediated silencing in mammalian cells. *EMBO Rep*., **13**, 716–723.
16. Bazzini,A.A., Lee,M.T. and Giraldez,A.J. (2012) Ribosome profiling shows that miR-430 reduces translation before causing mRNA decay in zebrafish. *Science*, **336**, 233–237.

17. Djuranovic,S., Nahvi,A. and Green,A. (2012) miRNA-mediated gene silencing by translational repression followed by mRNA deadenylation and decay. *Science*, **336**, 237–240.
18. Mathonnet,G., Fabian,M.R., Svitkin,Y.V., Parsyan,A., Huck,L., Murata,T., Biffo,S., Merrick,W.C., Darzynkiewicz,E., Pillai,R.S. *et al*. (2007) MicroRNA inhibition of translation initiation in vitro by targeting the cap-binding complex eIF4F. *Science*, **17**, 1764–1767.
19. Zdanowicz,A., Thermann,R., Kowalska,J., Jemielity,J., Duncan,K., Preiss,T., Darzynkiewicz,E. and Hentze,M.W. (2009) *Drosophila* miR2 primarily targets the m7GpppN cap structure for translational repression. *Mol. Cell*, **35**, 881–888.
20. Eulalio,A., Rehwinkel,J., Stricker,M., Huntzinger,E., Yang,S.F., Doerks,T., Dorner,S., Bork,P., Boutros,M. and Izaurralde,E. (2007) Target-specific requirements for enhancers of decapping in miRNA-mediated gene silencing. *Genes Dev.*, **21**, 2558–2570.
21. Eulalio,A., Huntzinger,E., Nishihara,T., Rehwinkel,J., Fauser,M. and Izaurralde,E. (2009) Deadenylation is a widespread effect of miRNA regulation. *RNA*, **15**, 21–32.
22. Pillai,R.S., Bhattacharyya,S.N., Artus,C.G., Zoller,T., Cougot,N., Basyuk,E., Bertrand,E. and Filipowicz,W. (2005) Inhibition of translational initiation by Let-7 MicroRNA in human cells. *Science*, **309**, 1573–1576.
23. Mayr,C., Hemann,M.T. and Bartel,D.P. (2007) Disrupting the pairing between let-7 and Hmga2 enhances oncogenic transformation. *Science*, **315**, 1576–1579.
24. Temme,C., Zaessinger,S., Meyer,S., Simonelig,M. and Wahle,E. (2004) A complex containing the CCR4 and CAF1 proteins is involved in mRNA deadenylation in *Drosophila*. *EMBO J.*, **23**, 2862–2871.
25. Chekulaeva,M., Parker,R. and Filipowicz,W. (2010) The GW/WG repeats of Drosophila GW182 function as effector motifs for miRNA-mediated repression. *Nucleic Acids Res.*, **38**, 6673–6683.
26. Fukaya,T. and Tomari,Y. (2011) PABP is not essential for microRNA-mediated translational repression and deadenylation in vitro. *EMBO J.*, **30**, 4998–5009.
27. Yao,B., Li,S., Jung,H.M., Lian,S.L., Abadal,G.X., Han,F., Fritzler,M.J. and Chan,E.K. (2011) Divergent GW182 functional domains in the regulation of translational silencing. *Nucleic Acids Res.*, **39**, 2534–2547.
28. Eulalio,A., Huntzinger,E. and Izaurralde,E. (2008) GW182 interaction with Argonaute is essential for miRNA-mediated translational repression and mRNA decay. *Nat. Struct. Mol. Biol.*, **15**, 346–353.
29. Kuzuoglu-Öztürk,D., Huntzinger,E., Schmidt,S. and Izaurralde,E. (2012) The *Caenorhabditis elegans* GW182 protein AIN-1 interacts with PAB-1 and subunits of the PAN2-PAN3 and CCR4-NOT deadenylase complexes. *Nucleic Acids Res.*, **40**, 5651–5665.
30. Mishima,Y., Fukao,A., Kishimoto,T., Sakamoto,H., Fujiwara,T. and Inoue,K. (2012) Translational inhibition by deadenylation-independent mechanisms is central to microRNA-mediated silencing in zebrafish. *Proc. Natl Acad. Sci. USA*, **109**, 1104–1109.
31. Petit,A.P., Wohlbold,L., Bawankar,P., Huntzinger,E., Schmidt,S., Izaurralde,E. and Weichenrieder,O. (2012) The structural basis for the interaction between the CAF1 nuclease and the NOT1 scaffold of the human CCR4-NOT deadenylase complex. *Nucleic Acids Res*, **40**, 11058–11072.
32. Chen,C.Y., Zheng,D., Xia,Z. and Shyu,A.B. (2009) Ago-TNRC6 triggers microRNA-mediated decay by promoting two deadenylation steps. *Nat. Struct. Mol. Biol.*, **16**, 1160–1166.
33. Piao,X., Zhang,X., Wu,L. and Belasco,J.G. (2010) CCR4-NOT deadenylates mRNA associated with RNA-induced silencing complexes in human cells. *Mol. Cell. Biol*, **30**, 1486–1494.
34. Walters,R.W., Bradrick,S.S. and Gromeier,M. (2010) Poly(A)-binding protein modulates mRNA susceptibility to cap-dependent miRNA-mediated repression. *RNA*, **16**, 239–250.
35. Moretti,F., Kaiser,C., Zdanowicz-Specht,A. and Hentze,M.W. (2012) PABP and the poly(A) tail augment microRNA repression by facilitated miRISC binding. *Nat. Struct. Mol. Biol.*, **19**, 603–608.
36. Collart,M.A. and Panasenko,O.O. (2012) The Ccr4–not complex. *Gene*, **492**, 42–53.
37. Siddiqui,N., Mangus,D.A., Chang,T.C., Palermino,J.M., Shyu,A.B. and Gehring,K. (2007) Poly(A) nuclease interacts with the C-terminal domain of polyadenylate-binding protein domain from poly(A)-binding protein. *J. Biol. Chem.*, **282**, 25067–25075.
38. Zheng,D., Ezzeddine,N., Chen,C.Y., Zhu,W., He,X. and Shyu,A.B. (2008) Deadenylation is prerequisite for P-body formation and mRNA decay in mammalian cells. *J. Cell. Biol.*, **182**, 89–101.
39. Zipprich,J.T., Bhattacharyya,S., Mathys,H. and Filipowicz,W. (2009) Importance of the C-terminal domain of the human GW182 protein TNRC6C for translational repression. *RNA*, **15**, 781–793.
40. Lazzaretti,D., Tournier,I. and Izaurralde,E. (2009) The C-terminal domains of human TNRC6A, B and C silence bound transcripts independently of the Argonaute proteins. *RNA*, **15**, 1059–1066.

Figure S1

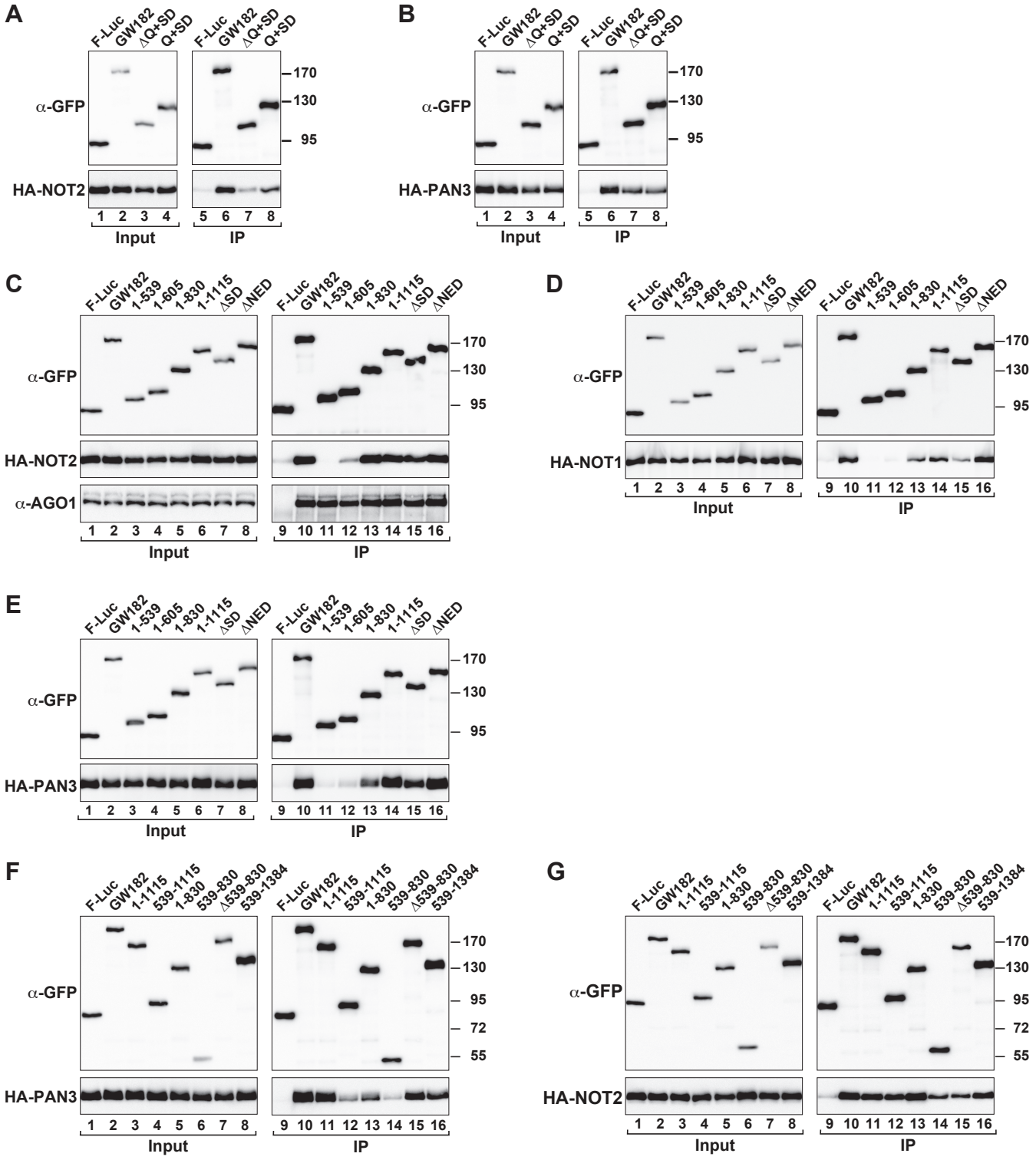

Figure S1. Interaction of *Dm* GW182 N-term fragments with NOT1, NOT2 and PAN3. (**A**–**G**) The interactions between GFP-tagged wild-type *Dm* GW182 or the indicated protein fragments and HA-tagged deadenylation factors were analyzed as described in Figure 2. In panel C, the presence of endogenous *Dm* AGO1 in the immunoprecipitates was analyzed using a specific anti-AGO1 antibody.

Figure S2

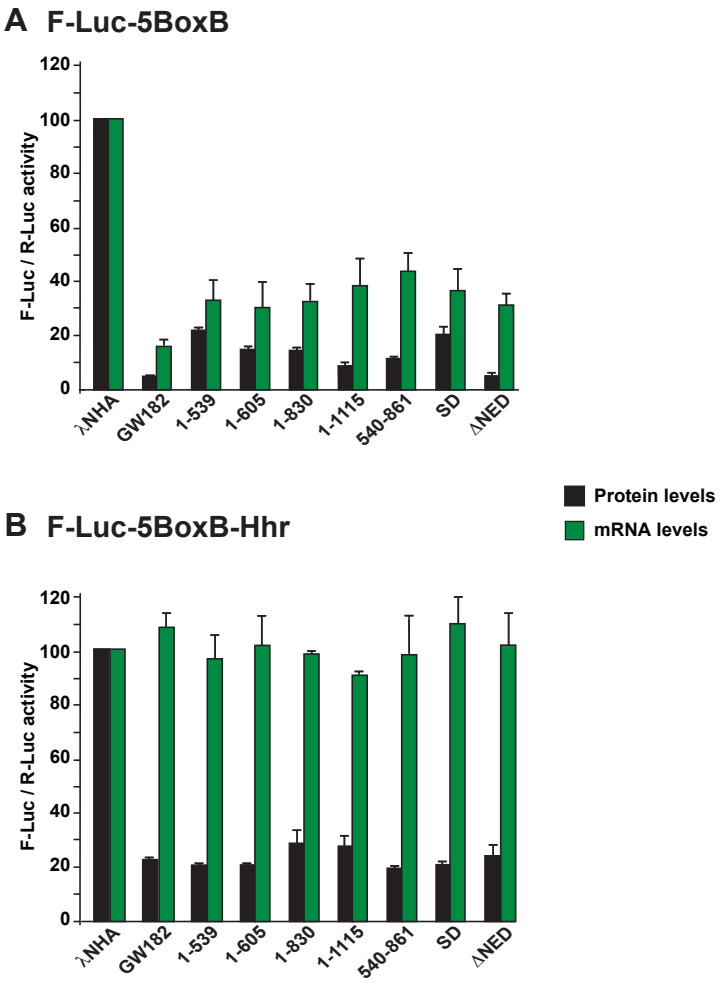

Figure S2. Activity of GW182 protein fragments in tethering assays. (**A**) S2 cells were transfected with a mixture of three plasmids: one expressing the F-Luc-5BoxB reporter; another expressing the λN-HA peptide or λN-HA-tagged *Dm* GW182 (full-length or fragments); and a third expressing *Renilla* luciferase (R-Luc). Firefly luciferase activity and mRNA levels were normalized to those of the *Renilla* luciferase control. For each condition, the normalized values of F-Luc activity and mRNA levels were set at 100% in cells expressing the λN-HA peptide. Mean values ± standard deviations from three independent experiments are shown. (**B**) The experiment shown in panel A was repeated using the F-Luc-5BoxB-Hhr reporter in which the polyadenylation signal was substituted by a self-cleavable hammerhead ribozyme (Hhr). A western blot showing equivalent expression levels for all protein fragments is shown in Figure 3I.

Figure S3

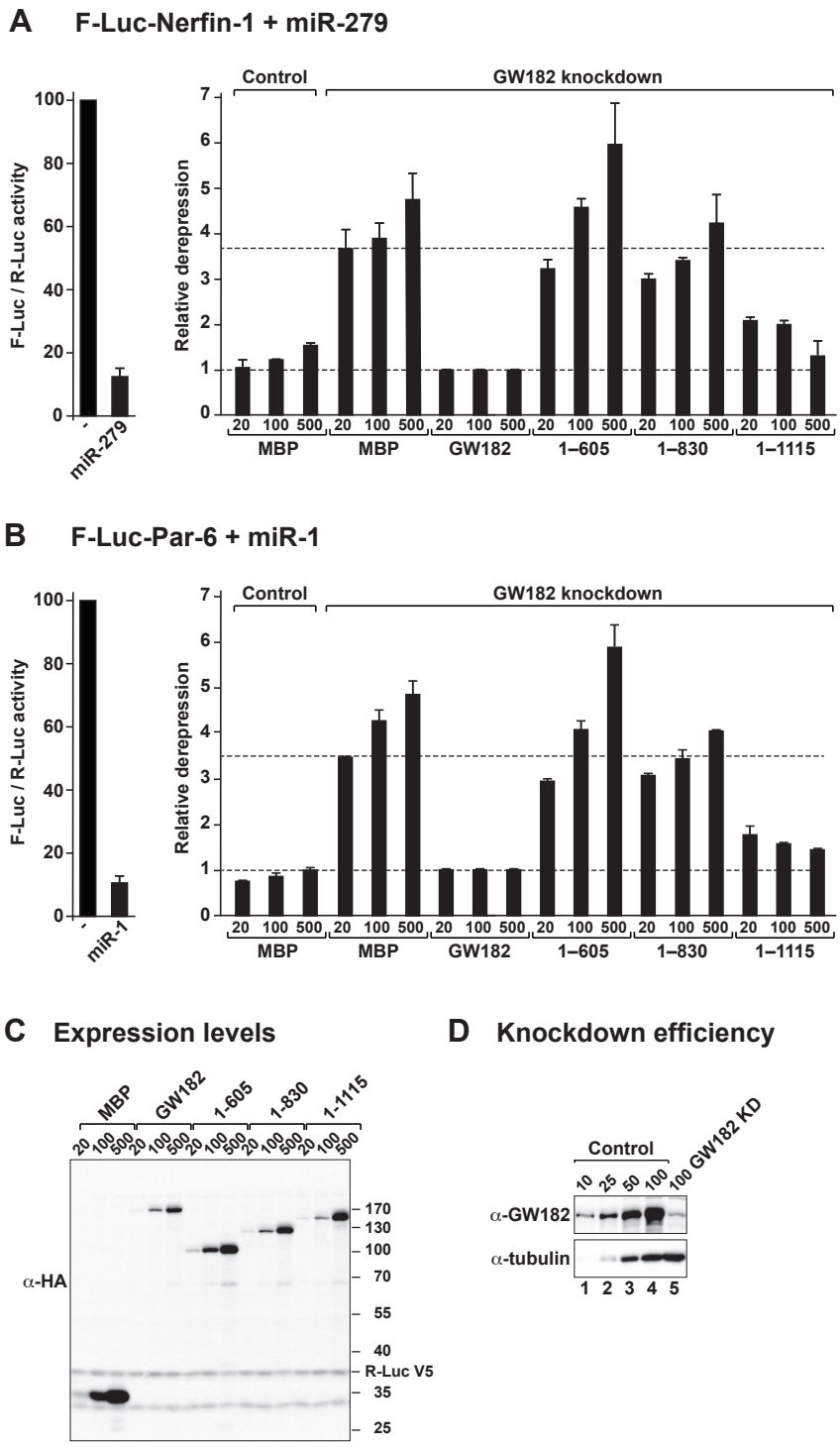

Figure S3. The *Dm* GW182 SD is generally required for silencing. Complementation assays using the indicated miRNA reporters were carried out as described in Figure 3. The graphs on the left of each panel show normalized firefly luciferase activities in the absence or presence of miRNAs in control cells (i.e., cells treated with GFP dsRNA and transfected with MBP). The graphs on the right show the relative derepression of the F-Luc reporters for each condition. Mean values ± standard deviations from three independent experiments are shown. (**A, B**) Complementation assays using the F-Luc-Nerfin-1 and F-Luc-Par-6 reporters and increasing amounts of the indicated GW182 N-term fragments. (**C**) A western blot showing the expression levels of full-length GW182 and N-term fragments. (**D**) Western blot showing the efficiency of the GW182 knockdown. Dilutions of control cell lysates were loaded in lanes 1–4 to estimate the efficacy of the depletion. α-tubulin served as a loading control.

Figure S4

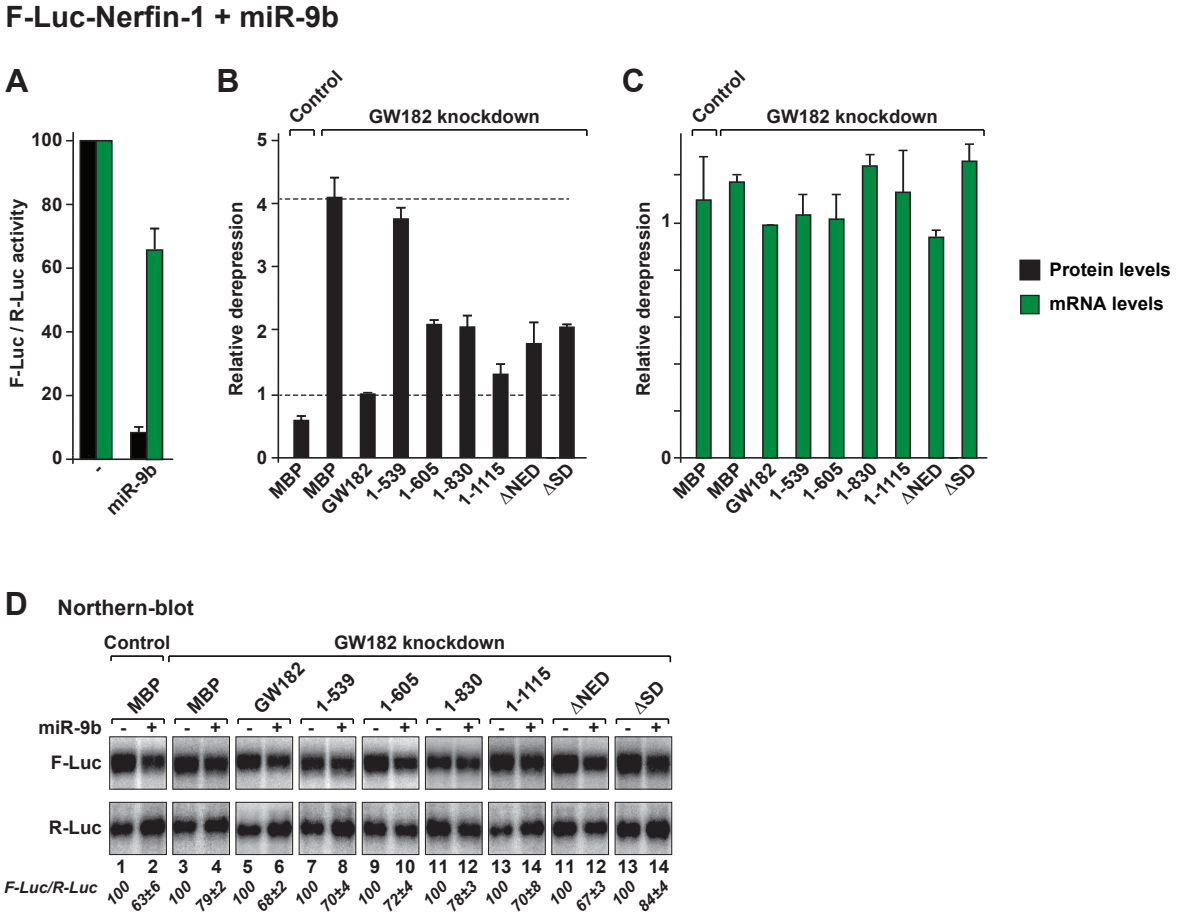

Figure S4. The *Dm* GW182 N-terminal fragments complement silencing of the F-Luc-Nerfin reporter silenced by miR-9b. (**A–D**) A complementation assay using the F-Luc-Nerfin reporter silenced by miR-9b was carried out as described in Figure 3. Numbers in italics below panel (D) indicate the levels of the F-Luc-Nerfin reporter normalized to that of R-Luc mRNA and set at 100 in the absence of miR-9b.

Figure S5

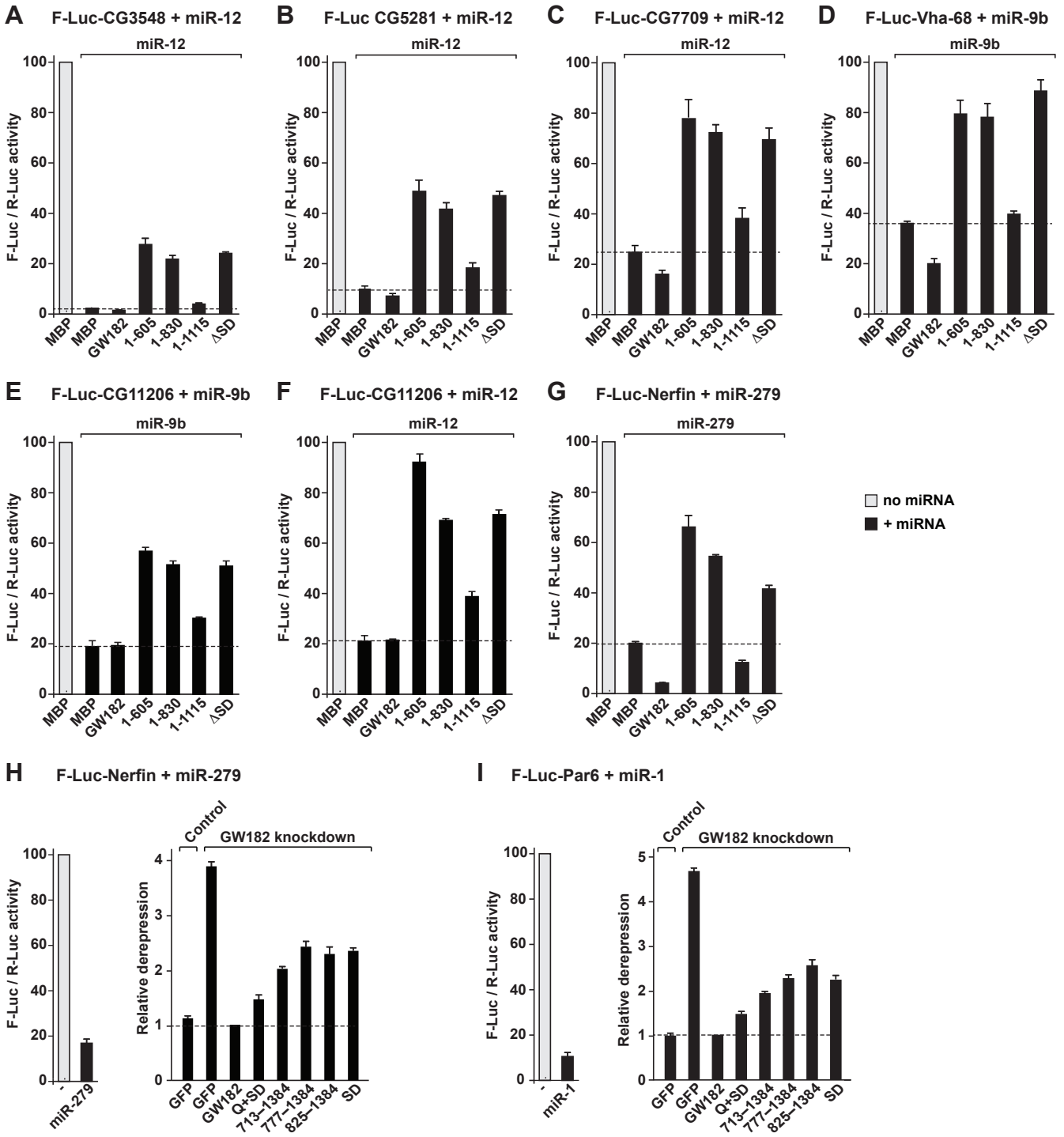

Figure S5. GW182 N-term fragments generally inhibit silencing in a dominant negative manner in control cells. The effects of expressing *Dm* GW182 N-term protein fragments on silencing of the indicated reporters were analyzed in control cells. The corresponding experiment, which was performed in parallel in depleted cells is shown in Figure 4. (**A–G**) Normalized F-Luc activities in cells in the absence or presence of miRNAs. Cells were co-transfected with plasmids expressing MBP or *Dm* GW182 (wild-type or mutant) as indicated. For some reporters, overexpression of wild-type GW182 enhances silencing (panels C, D and G). For all reporters, overexpression of *Dm* GW182 N-term fragments (1–605, 1–830 and ΔSD) inhibits silencing in a dominant negative manner. Mean values ± standard deviations from three independent experiments rare shown. (**H, I**) Complementation assays using the indicated miRNA reporters were carried out as described in Figure 5. The graphs on the left of each panel show normalized firefly luciferase activities in the absence or presence of miRNAs in control cells. The graphs on the right of each panel show the relative derepression of the F-Luc reporters for each condition.

Figure S6

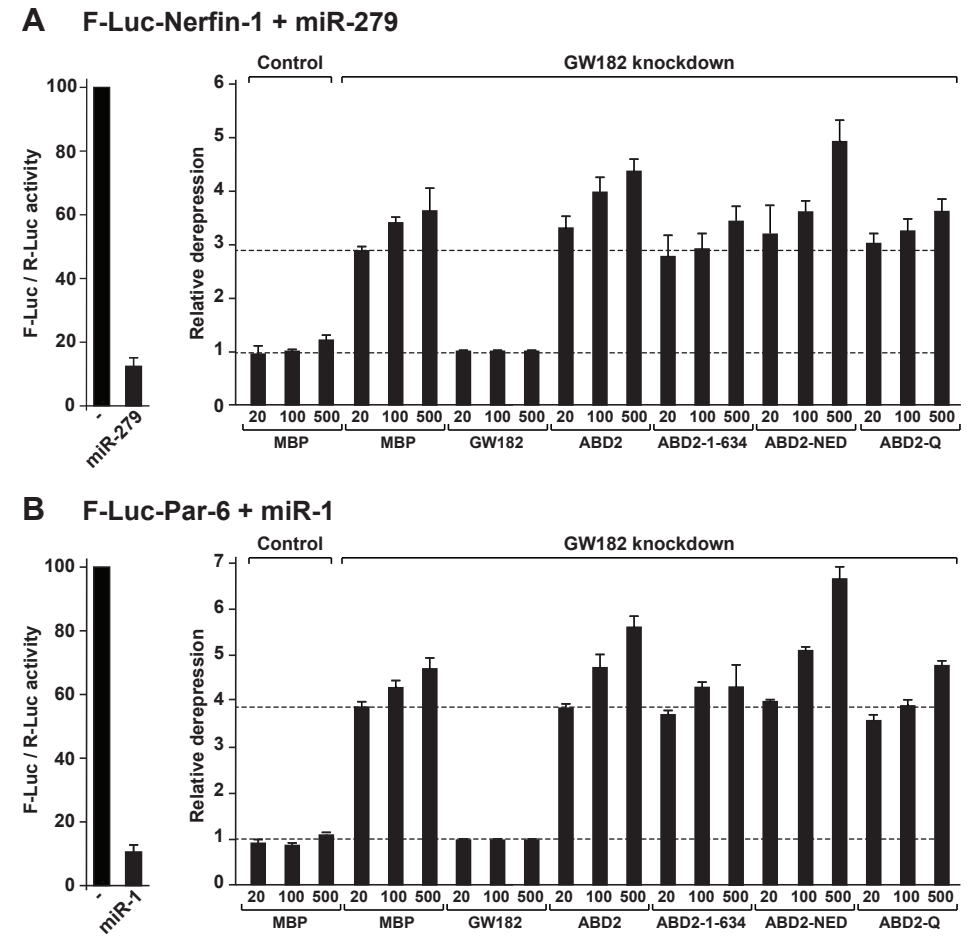

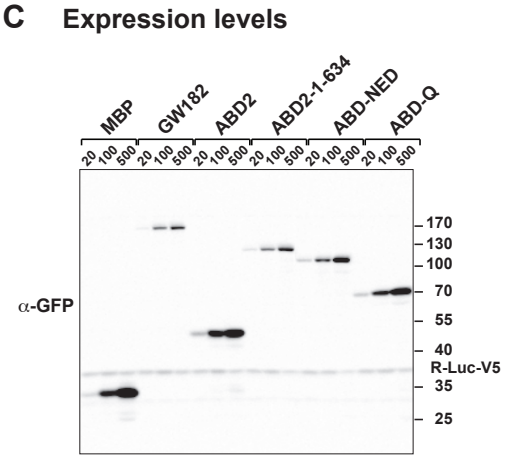

Figure S6. A chimeric GW182 protein containing the Q+SD region rescues silencing in cells depleted of *Dm* GW182. (**A, B**) Complementation assays using the F-Luc-Nerfin-1 and F-Luc-Par-6 reporters and increasing amounts of the indicated proteins were carried out as described in Figure 3. Mean values ± standard deviations from three independent experiments are shown. Labels are as described in Figure 3. (**C**) A western blot showing the expression levels of the proteins tested in panels A and B.

Figure S7

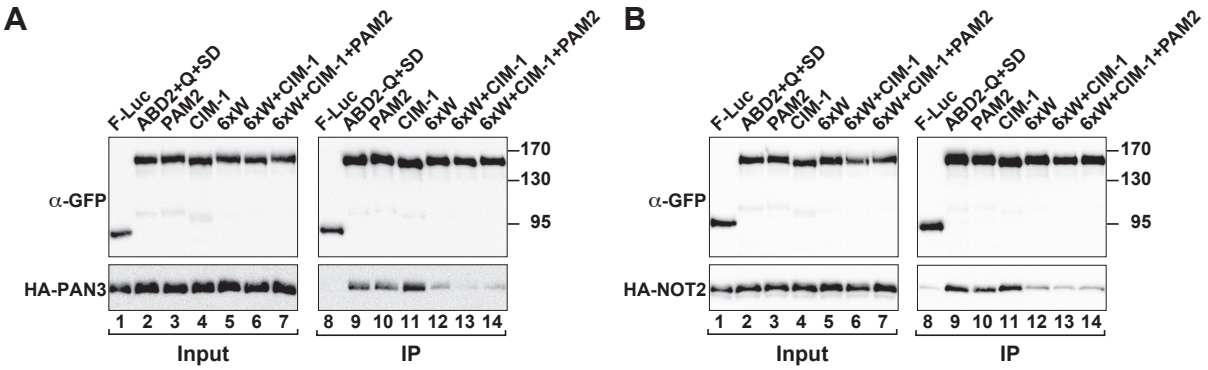

C PAM2 motif

Hs TNRC6A	1352	SVN--WPPEFRPGEPWKGYP	1369
Hs TNRC6B	1361	SSNASWPPEFQPGVPWKGIQ	1380
Hs TNRC6C	1382	SIN--WPPEFHPGVPWKGLQ	1399
Dr TNRC6A	1362	NVN--WPPEFRPGEPWKGYP	1379
Dm GW182	952	TAYTDLVQEFEPGKPWKGSQ	971

D CCR4-interacting motif 1 (CIM-1)

Hs TNRC6A	1276	KEP---QSRLRKWTTVDSIS	1292
Hs TNRC6B	1277	GKEAGTESRFKQWTSMMEGL	1296
Hs TNRC6C	1288	KDPSQSQSRLPQWTHPNSMD	1307
Dr TNRC6A	1286	KEP---QSRLKKWTAMDISV	1302
Dm GW182	863	QGASNQQSRLNQWKLPVLDK	882

E CCR4-interacting motif 2 (CIM-2)

Hs TNRC6A	1661	HGTSLWG-TPHYSTSLWGPP	1679
Hs TNRC6B	1678	AGASLWG-PPNYSSSLWGVP	1696
Hs TNRC6C	1643	SSELLWGGVPQYSSSLWGPP	1662
Dr TNRC6A	1659	HGSSLWG-VPNYSTSLWGSP	1677

F P-GL motif

Hs TNRC6A	1473	NITAPSR-PPPGLTGQKPPL	1491
Hs TNRC6B	1484	NTTPLPR-PPPGLTNPKPSS	1502
Hs TNRC6C	1467	NSTAPTR-PPPGLTNPKPSS	1485
Dr TNRC6A	1481	GISAPSR-PPPGLTGQKQPS	1499
Dm GW182	1055	LNKSSSRGPPPGLTANSNKS	1074

Figure S7. Conserved motifs in GW182 family proteins. (**A, B**) The interactions of the chimeric ABD2-Q+SD protein (wild-type or mutants) with PAN3 and NOT2 were analyzed as described in Figure 2. (**C–F**) Sequence alignment of the conserved PAM2 (C), CIM-1 (D), CIM-2 (E) and PG-L (F) motifs from *H. sapiens* (*Hs*) TNRC6A–C, *Danio rerio* (*Dr*) TNRC6A and *D. melanogaster* (*Dm*) GW182. Conserved residues are shown in red. Residues substituted with alanines in this study are indicated by asterisks. CIM-2 is absent in *Dm* GW182.

Figure S8

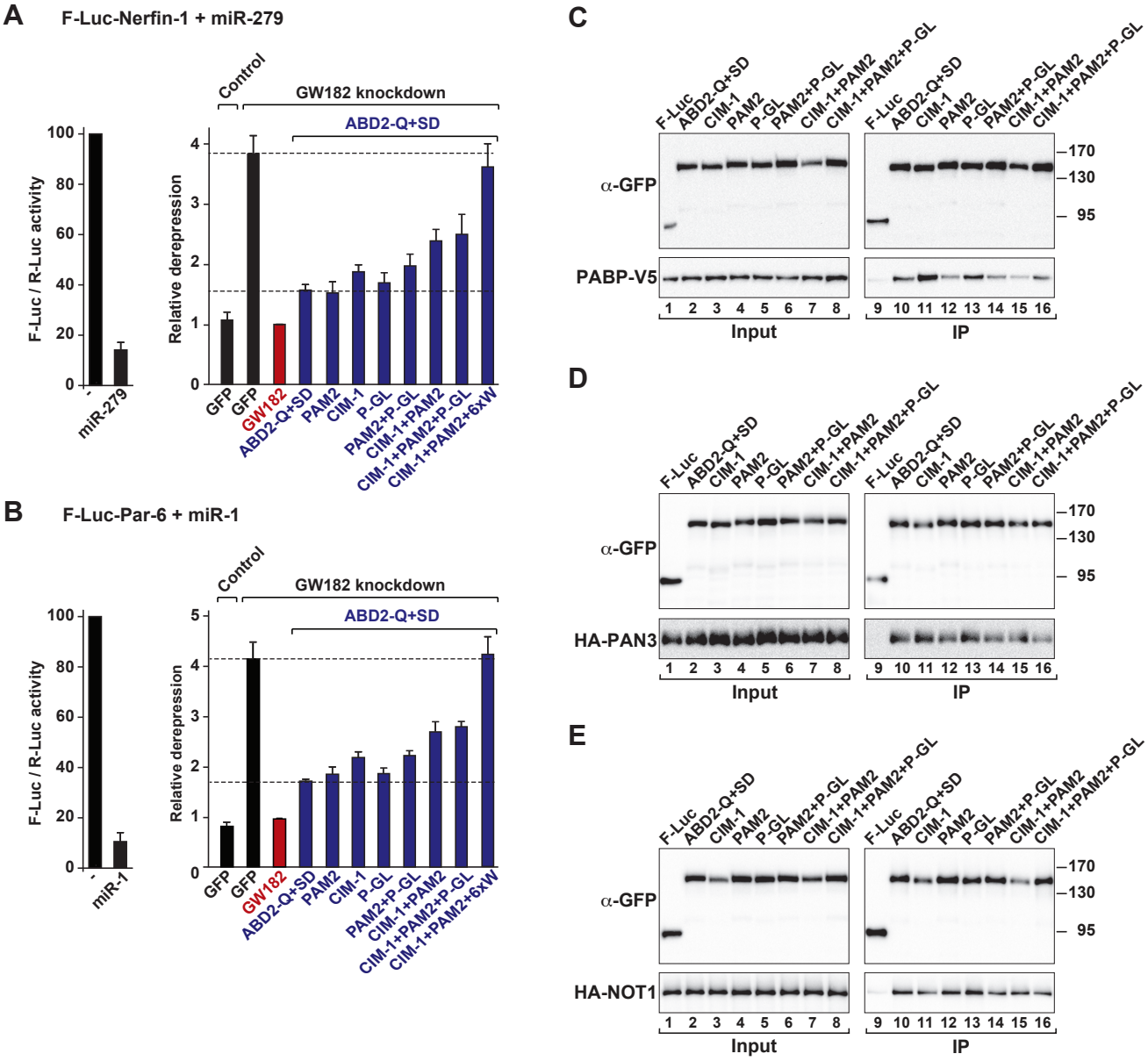

Figure S8. The PG-L motif of *Dm* GW182 does not contribute to silencing in S2 cells. Mutations in the PG-L motif were introduced in a minimal GW182 protein consisting of *Ce* AIN-2 ABD (ABD2) fused to the GW182 Q+SD region (ABD2-Q+SD). The mutations are shown in Supplementary Figure S7F. (**A, B**) The silencing activity of the ABD2-Q+SD protein (wild-type or mutants) was tested in complementation assays as described in Figure 3. (**C–F**) The interactions of ABD2-Q+SD protein (wild-type or mutants) with PABP, PAN3 and NOT1 were analyzed as described in Figure 2.

Figure S9

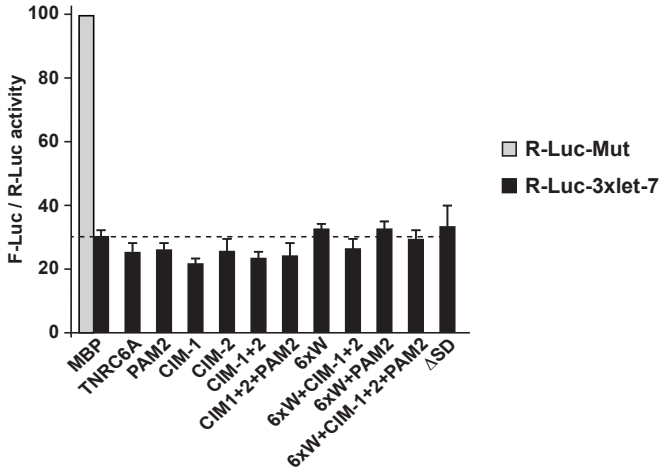

Figure S9. TNRC6A mutants do not inhibit silencing in a dominant negative manner in control cells. The effect of expressing TNRC6A mutants on silencing of the R-Luc-3xlet-7 reporter was analyzed in control cells. The corresponding experiment, which was performed in parallel in depleted cells is shown in Figure 8. HeLa cells were transfected with a mixture of three plasmids: the R-Luc-3xlet-7 or the corresponding reporter carrying mutations in let-7-binding sites (R-Luc-Mut), a plasmid expressing F-Luc as a transfection control, and a plasmid expressing GFP or siRNA-resistant versions of GFP-TNRC6A (wild-type or mutant). For each condition, *Renilla* luciferase activity was measured, normalized to that of the F-Luc transfection control and set at 100% in cells expressing R-Luc-Mut. Normalized *Renilla* luciferase activities are shown. The expression levels of the proteins tested is shown in Figure 8E.

Structure and assembly of the NOT module of the human CCR4–NOT complex

Andreas Boland[1,2], Ying Chen[1,2], Tobias Raisch[1,2], Stefanie Jonas[1,2], Duygu Kuzuoğlu-Öztürk[1], Lara Wohlbold[1], Oliver Weichenrieder[1] & Elisa Izaurralde[1]

The CCR4–NOT deadenylase complex is a master regulator of translation and mRNA stability. Its NOT module orchestrates recruitment of the catalytic subunits to target mRNAs. We report the crystal structure of the human NOT module formed by the CNOT1, CNOT2 and CNOT3 C-terminal (-C) regions. CNOT1-C provides a rigid scaffold consisting of two perpendicular stacks of HEAT-like repeats. CNOT2-C and CNOT3-C heterodimerize through their SH3-like NOT-box domains. The heterodimer is stabilized and tightly anchored to the surface of CNOT1 through an unexpected intertwined arrangement of peptide regions lacking defined secondary structure. These assembly peptides mold onto their respective binding surfaces and form extensive interfaces. Mutagenesis of individual interfaces and perturbation of endogenous protein ratios cause defects in complex assembly and mRNA decay. Our studies provide a structural framework for understanding the recruitment of the CCR4–NOT complex to mRNA targets.

The CCR4–NOT deadenylase complex has a crucial role in post-transcriptional mRNA regulation. It catalyzes the removal of mRNA poly(A) tails and consequently represses translation and promotes mRNA degradation[1,2]. Remarkably, the CCR4–NOT complex can also repress translation independently of deadenylation, and it facilitates dissociation of the cytoplasmic poly(A)-binding protein (PABP) from mRNA poly(A) tails[3–6].

In addition to its central role in bulk and specific mRNA degradation, the CCR4–NOT complex has been implicated in transcription initiation and elongation, in DNA repair and in ubiquitination and protein modification[1,2]. Given the diverse activities associated with the CCR4–NOT complex, it is not surprising that it has a role in a wide range of biological processes, including cell proliferation, apoptosis, oogenesis and embryogenesis, spermatogenesis, heart function, bone formation and energy metabolism[1,2].

The conserved core of the CCR4–NOT complex consists of two major modules: a catalytic module comprising two deadenylases (CAF1 or its paralog POP2, and CCR4a or its paralog CCR4b) and the NOT module, which minimally consists of NOT1, NOT2 and NOT3. Additional subunits within the complex have been described, including NOT4, CAF40 and the species-specific subunits CAF130, NOT10 and NOT11 (refs. 1,2). NOT1 functions as a modular scaffold to provide binding sites for the NOT10–NOT11 module at its N terminus, the CAF1–CCR4 catalytic module and CAF40 in its middle region and the NOT2 and NOT3 subunits at the C terminus. Thus, NOT1 is essential for the assembly of the complete CCR4–NOT complex[3,7–16].

The precise molecular function of the NOT module remains unclear. Current evidence indicates that it regulates the stability and activity of the catalytic module. Another crucial role for the NOT module is the recruitment of the CCR4–NOT complex to a plethora of specific mRNAs[2,17]. These include microRNA targets and mRNAs containing AU-rich elements, to which the CCR4–NOT complex is recruited through interactions of NOT1 with GW182 proteins and tristetraprolin, respectively[4,18–21]. Furthermore, a multitude of translational regulators, which include Nanos, Bicaudal-C, CUP and Smaug, recruit the CCR4–NOT complex to their targets through interactions with NOT-module subunits[17].

The mechanistic understanding of the assembly, regulation and function of the NOT module requires elucidation of its three-dimensional structure, specifically of the C-terminal regions of NOT1, NOT2 and NOT3, which mediate NOT-module assembly[1–3,12,22,23]. These regions comprise a highly conserved NOT1 superfamily homology (SH) domain in NOT1 and a conserved NOT-box domain[22,23] in NOT2 and NOT3. Currently there are no structural models available for these regions, owing to the lack of sequence homology to known structural folds.

To provide the missing structural framework for understanding the assembly and functions of the NOT module, we determined the crystal structure of a ternary complex formed by the human CNOT1-C, CNOT2-C and CNOT3-C regions. This was achieved by a stepwise approach wherein we first determined the boundaries and crystal structures of the isolated human CNOT2 and CNOT3 NOT-box domains and of the *Chaetomium thermophilum* (*Ct*) NOT1 SH domain. We then used this information for the assembly and structure determination of the ternary CNOT1–CNOT2–CNOT3 complex. The structures reveal a rigid scaffold for the NOT1 SH domain,

[1]Department of Biochemistry, Max Planck Institute for Developmental Biology, Tübingen, Germany. [2]These authors contributed equally to this work. Correspondence should be addressed to E.I. (elisa.izaurralde@tuebingen.mpg.de) or O.W. (oliver.weichenrieder@tuebingen.mpg.de).

Received 30 May; accepted 20 August; published online 13 October 2013; doi:10.1038/nsmb.2681

consisting of two perpendicularly arranged stacks of α-helices, and an SH3-like fold for the CNOT2 and CNOT3 NOT boxes, which mediate heterodimerization. Perhaps the most remarkable structural features are the intertwined N-terminal extensions of CNOT2 and CNOT3 that wrap around their partners in the heterodimer and also form an extended interface with CNOT1. Functional studies reveal the relevance of the interaction interfaces for complex assembly and mRNA degradation.

RESULTS

Mutual interactions between CNOT1, CNOT2 and CNOT3

Our previous studies indicated that the interactions between *Drosophila melanogaster* (*Dm*) NOT1, NOT2 and NOT3 are mediated by their C-terminal regions[3]. Coimmunoprecipitations in human cells demonstrated that this mode of interaction is conserved in the human orthologs (**Supplementary Fig. 1a–e**). Moreover, although CNOT1 interacted with both CNOT2 and CNOT3, the interaction with CNOT3 was enhanced in cells coexpressing CNOT2 (**Supplementary Fig. 1f**).

To determine whether the observed interactions are direct and to further define the domain boundaries, we performed pulldown assays with isolated C-terminal protein fragments expressed in *Escherichia coli*. We observed direct interactions for all possible binary domain combinations (**Supplementary Fig. 1g–j**). Further analysis indicated that the CNOT2-C fragment (residues 344–540) interacts with both CNOT1 and CNOT3, whereas a shorter fragment (residues 429–540) binds CNOT3 but is not sufficient for CNOT1 binding (**Fig. 1a** and **Supplementary Fig. 1g**,**h**). The smallest CNOT3 fragment that maintained CNOT2 binding comprised residues 656–753 (**Supplementary Fig. 1i**). On the basis of these results and our structural analysis, we will refer to residues 429–525 of CNOT2 and residues 656–747 of CNOT3 as the NOT-box domains (**Fig. 1a**). We conclude that the NOT-box domains mediate the CNOT2-CNOT3 interaction, whereas additional N-terminal sequences are required for CNOT1 binding.

The NOT1 SH domain features two perpendicular HEAT stacks

To determine the structure of the CNOT1-C domain, we initially identified a proteolytically stable fragment in CNOT1 (residues 1842–2371; **Fig. 1a**) that was expressed in a soluble form but failed to crystallize. We then expressed an equivalent fragment of *Ct* NOT1 (residues 1676–2193; **Supplementary Fig. 2**), which yielded crystals that diffracted X-rays to 3.2-Å resolution (**Table 1**).

The overall architecture of *Ct* NOT1-C is L-shaped and consists of two tightly interacting subdomains connected by a surface-attached and well-structured linker loop (loop L11; **Fig. 1b–d**). The two subdomains correspond to two perpendicularly arranged stacks of α-helices: an N-terminal subdomain (N-SD, helices α1–α14) that runs left to right and a C-terminal subdomain (C-SD, helices α15–α23) that runs bottom to top (**Fig. 1b–d**). The helices are packed as antiparallel HEAT-like pairs, with six hairpins in the N-SD and four hairpins in the C-SD. The arrangement of HEAT-like repeats in perpendicular stacks is different from the usually continuous arrangement[24], and it occurs more than once in the context of NOT1 (ref. 10).

Our structural analysis redefines the boundaries of the NOT1 SH domain and reveals that most of the highly conserved residues map to the extensive interface (1,151 Å^2) between the N- and C-SDs (**Supplementary Fig. 2**), indicating that the mutual arrangement

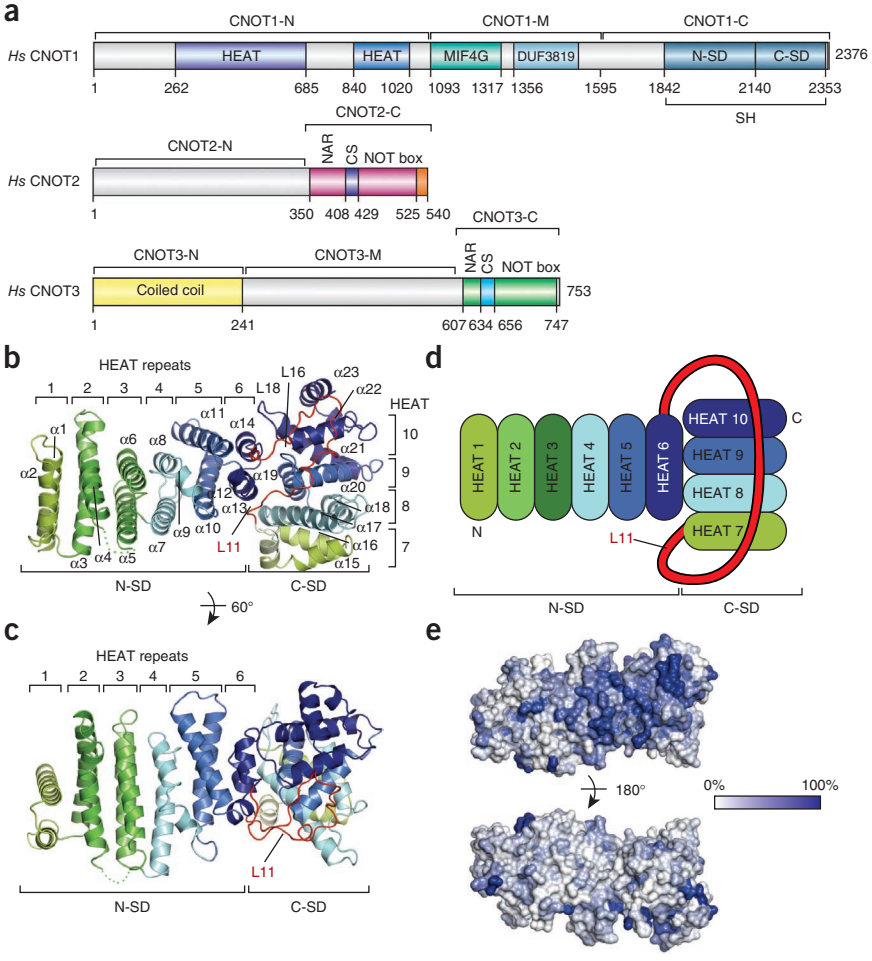

Figure 1 Domain organization of *Homo sapiens* (*Hs*) CNOT1–CNOT3 and the structure of the *Ct* NOT1 superfamily homology domain. (**a**) Diagrams of CNOT1 with N-terminal, middle and C-terminal regions (CNOT1-N, CNOT1-M and CNOT1-C, respectively). The CNOT1-N consists of two HEAT-repeat domains. CNOT1-M contains a MIF4G domain and a domain of unknown function (DUF3819). CNOT1-C contains the NOT1 superfamily homology (SH) domain. The C-terminal regions of both CNOT2 and CNOT3 contain a NOT1 anchor region (NAR), a connector sequence (CS) and a NOT-box domain (38% sequence identity for the CNOT2 and CNOT3 NOT boxes)[22,23]. CNOT3 displays an N-terminal coiled coil domain (CNOT3-N) and a linker region (CNOT3-M). The numbers below the protein outline represent amino acid positions at the domain boundaries as defined in this study. (**b**,**c**) Cartoon representations of the *Ct* SH domain. Two views, related by 60° rotation, are shown in **b** and **c**. The N- and C-terminal subdomains (N-SD and C-SD, respectively) are each colored in a gradient from green to dark blue from the N to C terminus. HEAT repeats are indicated. Loop L11 linking the two lobes is highlighted in red. (**d**) Schematic drawing of the *Ct* NOT1 structure with the same colors as in **b**. (**e**) Surface conservation of NOT1 SH domain colored in a gradient from white to blue. The orientation of the top structure corresponds to that shown in **c**.

Table 1 Data collection and refinement statistics

	Ct NOT1 (Se)	*Ct* NOT1	*Hs* CNOT2 (Se)	*Hs* CNOT2	*Hs* CNOT3 (Se)	*Hs* CNOT3	*Hs* CNOT1–2–3
Data collection[a]							
Space group	$P2_12_12_1$	$P2_1$	$P4_1$	$P6_522$	$P2_12_12_1$	$P2_12_12_1$	$P2_12_12$
Cell dimensions							
a, *b*, *c* (Å)	126.6, 129.6, 154.1	77.8, 127.2, 130.2	76.4, 76.4, 86.3	64.8, 64.8, 412.3	52.2, 97.3, 142.3	52.3, 97.6, 141.5	91.6, 165.9, 78.8
α, β, γ (°)	90, 90, 90	90, 93.1, 90	90, 90, 90	90, 90, 120	90, 90, 90	90, 90, 90	90, 90, 90
Resolution (Å)	90.9–3.6 (3.69–3.6)	90.9–3.2 (3.28–3.2)	76.4–3.4 (3.49–3.4)	49.3–2.4 (2.46–2.4)	80.3–2.5 (2.57–2.5)	49.1–2.4 (2.46–2.4)	48.5–3.2 (3.28–3.2)
R_{sym} (%)	17.2 (73.1)	10.6 (54.5)	16.2 (68.4)	9.6 (80.2)	8.6 (73.5)	5.4 (70.4)	11.9 (55.9)
$I / \sigma I$	16.4 (5.1)	11.3 (2.9)	17.5 (4.9)	13.2 (2.4)	17.7 (3.7)	18.1 (3.2)	10.1 (2.2)
Completeness (%)	100.0 (100.0)	99.9 (99.9)	99.7 (96.0)	99.2 (99.1)	99.9 (99.1)	99.5 (99.8)	98.9 (98.9)
Redundancy	26.8 (27.9)	5.4 (5.2)	20.1 (18.1)	6.7 (6.7)	12.9 (12.9)	5.9 (6.2)	3.3 (3.4)
Refinement							
Resolution (Å)		63.6–3.2		49.3–2.4		49.1–2.4	48.5–3.2
No. reflections		41,820		21,287		28,937	20,241
R_{work} / R_{free} (%)		21.7 / 25.9		21.7 / 26.3		22.1 / 25.7	22.4 / 27.3
No. atoms							
Protein		15,737		3,483		4,984	6,864
Water		–		102		76	–
B factors (Å^2)							
Protein		88		51		69	71
Water		–		48		52	–
r.m.s. deviations							
Bond lengths (Å)		0.002		0.002		0.002	0.002
Bond angles (°)		0.53		0.64		0.62	0.52

[a]One crystal was used per data set. Values in parentheses are for highest-resolution shell.

between the two subdomains is evolutionarily conserved. Additional conserved surface residues map to only one of the two helical surfaces of the domain (**Fig. 1e**).

The NOT-box domain adopts an SH3-related fold

The CNOT3 NOT-box domain crystallized as a homodimer (2.4-Å resolution; **Table 1** and **Fig. 2a**), consistent with the results from multiangle static laser light scattering and size-exclusion chromatography, which also indicated that the protein was dimeric in solution (**Supplementary Fig. 3a**).

The structure of the NOT-box domain consists of three N-terminal α-helices (α1–α3) followed by a C-terminal SH3-like five-stranded open β-barrel (β1–β5), with β-strands β4 and β5 strongly bent (**Fig. 2a**,**b**). The N-terminal helices form an antiparallel bundle that packs against one side of the β-barrel. Notably, the inner core of the β-barrel and the interface with the N-terminal helices consist almost exclusively of aromatic side chains (**Supplementary Fig. 3b**,**c**).

The N-terminal helices also provide the interface for the dimerization of the NOT-box domain (**Fig. 2a**). The dimer has a two-fold symmetry with a parallel arrangement of the α2 helices, which provide

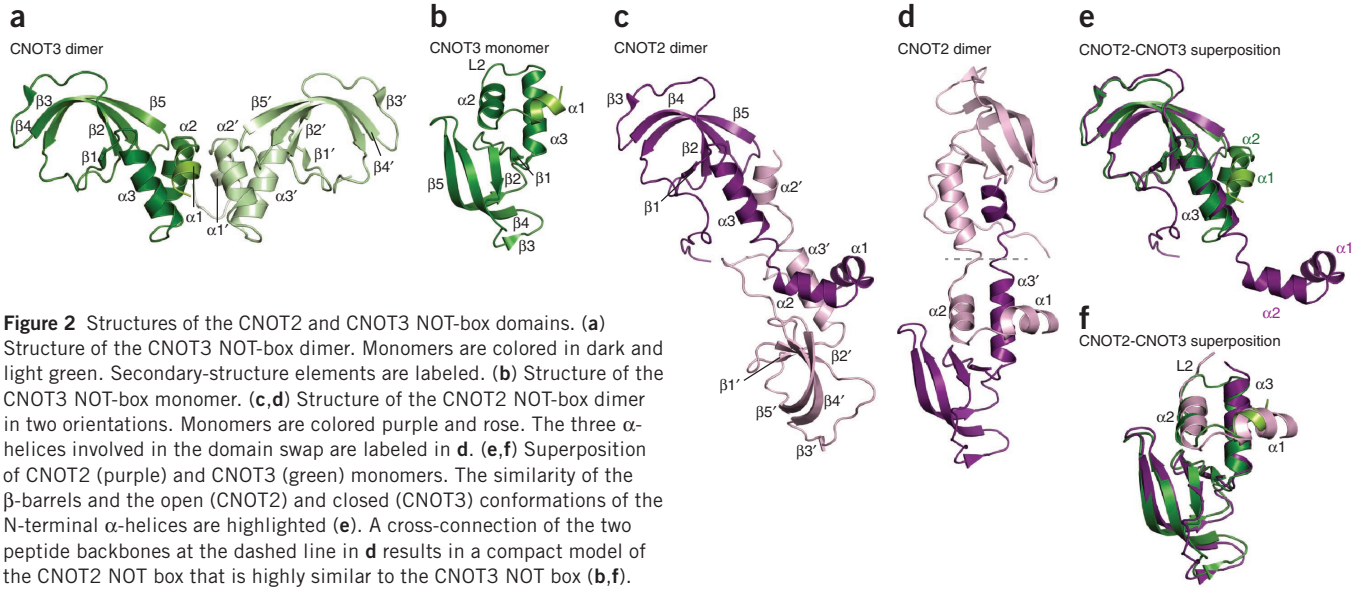

Figure 2 Structures of the CNOT2 and CNOT3 NOT-box domains. (**a**) Structure of the CNOT3 NOT-box dimer. Monomers are colored in dark and light green. Secondary-structure elements are labeled. (**b**) Structure of the CNOT3 NOT-box monomer. (**c**,**d**) Structure of the CNOT2 NOT-box dimer in two orientations. Monomers are colored purple and rose. The three α-helices involved in the domain swap are labeled in **d**. (**e**,**f**) Superposition of CNOT2 (purple) and CNOT3 (green) monomers. The similarity of the β-barrels and the open (CNOT2) and closed (CNOT3) conformations of the N-terminal α-helices are highlighted (**e**). A cross-connection of the two peptide backbones at the dashed line in **d** results in a compact model of the CNOT2 NOT box that is highly similar to the CNOT3 NOT box (**b**,**f**).

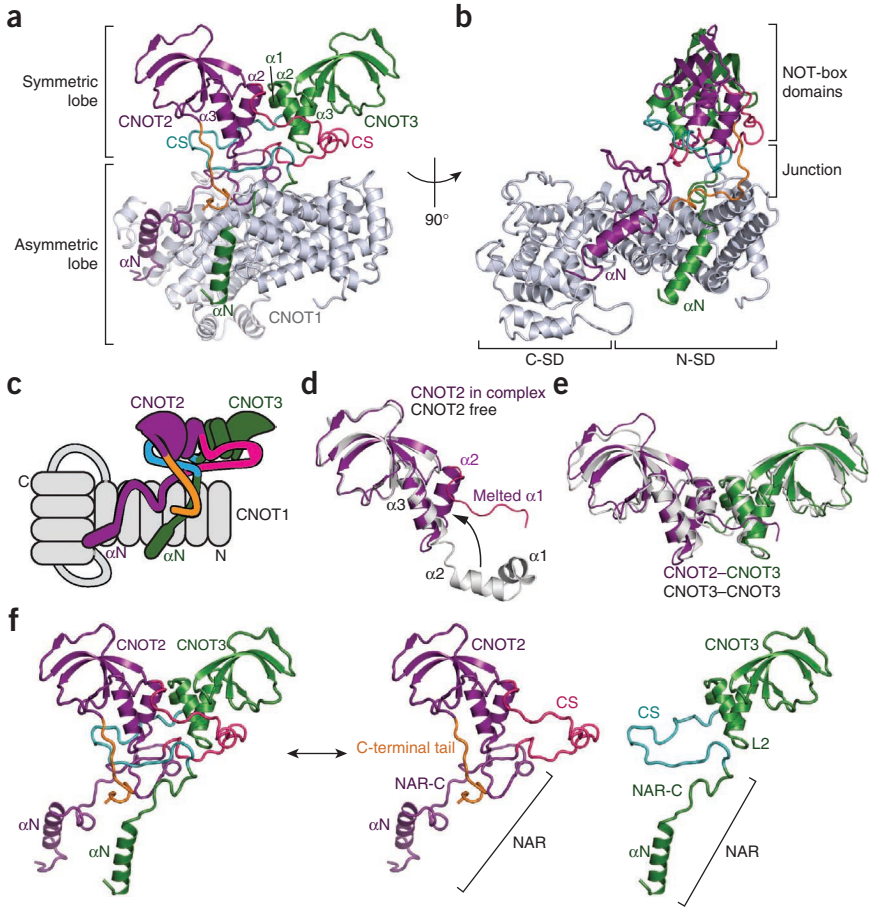

Figure 3 Structure of the CNOT1–CNOT2–CNOT3 ternary complex. (**a**,**b**) Structural overview. CNOT2 (purple) and CNOT3 (green) form a heterodimer through their NOT-box domains and preceding connector sequences (CS; magenta and cyan, respectively). The NOT1 anchor regions (NAR) tether the heterodimer onto the surface of CNOT1 (gray). They consist of an N-terminal α-helix (αN) and a NAR C-terminal region (NAR-C). The CNOT2 C-terminal tail is shown in orange. (**c**) Schematic drawing of the CNOT1–CNOT2–CNOT3 structure with colors as in **a**. (**d**) Superposition of the CNOT2 NOT-box domain in the complex (purple) with the isolated domain (gray). (**e**) Superposition of the CNOT2–CNOT3 heterodimer (purple and green) with the CNOT3 NOT-box homodimer (gray). (**f**) Structures of CNOT2 and CNOT3 from the ternary complex. The heterodimer (left) is taken apart (right) to show the extended conformation of the NAR and CS regions.

most of the contacts with additional contributions from helices α1 and loops L1. The contacts are mainly hydrophobic and lead to an interface of 560 Å^2.

The CNOT2 NOT-box domain forms a domain-swapped dimer

The CNOT2 NOT-box domain packs as a dimer of dimers (2.4-Å resolution, **Fig. 2c**,**d** and **Table 1**), consistent with its behavior in solution (**Supplementary Fig. 3d**,**e**). As expected on the basis of sequence homology (**Supplementary Fig. 3f**), the CNOT2 and CNOT3 NOT boxes adopt a similar fold (**Fig. 2c–f**). However, in the CNOT2 crystals the N-terminal helices adopt an extended (open) conformation (**Fig. 2c–e**), in which helices α1 and α2 of one monomer interact with helix α3 and the open β-barrel of the other monomer (**Fig. 2d**). Consequently, the dimers that result from this domain swap are structurally distinct from the CNOT3 homodimers, burying a large interface of 1,900 Å^2.

The ability of the NOT-box domains to homodimerize in two different ways and to adopt an open (CNOT2) or a closed (CNOT3) conformation is intriguing. With regard to the assembly of the NOT module, CNOT2 and CNOT3 may form heterodimers that correspond to one of the two crystallized arrangements. To discriminate between these two potential interaction modes, we determined the structure of the ternary complex, which also includes CNOT1.

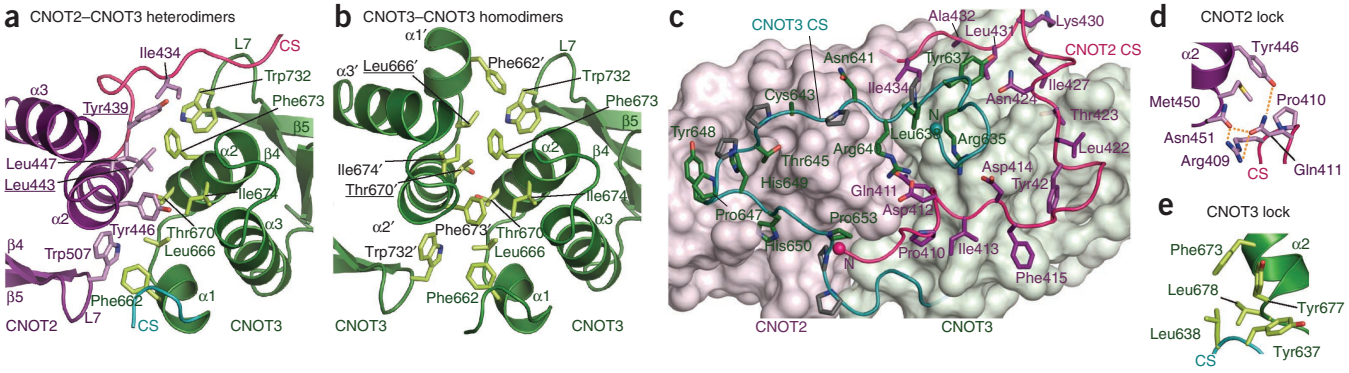

Figure 4 The CNOT2–CNOT3 heterodimerization interface. (**a**) Close-up of the interface between the NOT-box domains of CNOT2 and CNOT3, with interface residues shown as sticks. (**b**) The corresponding interface of the CNOT3 homodimer. Underlined residues indicate marked differences between the interfaces of the CNOT2–CNOT3 heterodimer and the CNOT3 homodimer. (**c**) Packing of the CNOT2 CSs (magenta) against the CNOT3 NOT-box domain (green surface) and of the CNOT3 CS (cyan) against the CNOT2 NOT-box domain (purple surface). Interacting residues are shown as sticks in purple (CNOT2) and green (CNOT3). Proline residues in CNOT3 CS are shown in gray. (**d**,**e**) Circular locks for CNOT2 (**d**) and CNOT3 (**e**). Residues locking back the N-terminus of the CS to its own NOT-box domain are drawn as sticks. For CNOT2, contacts are mediated by hydrogen bonds (orange). For CNOT3, contacts are hydrophobic.

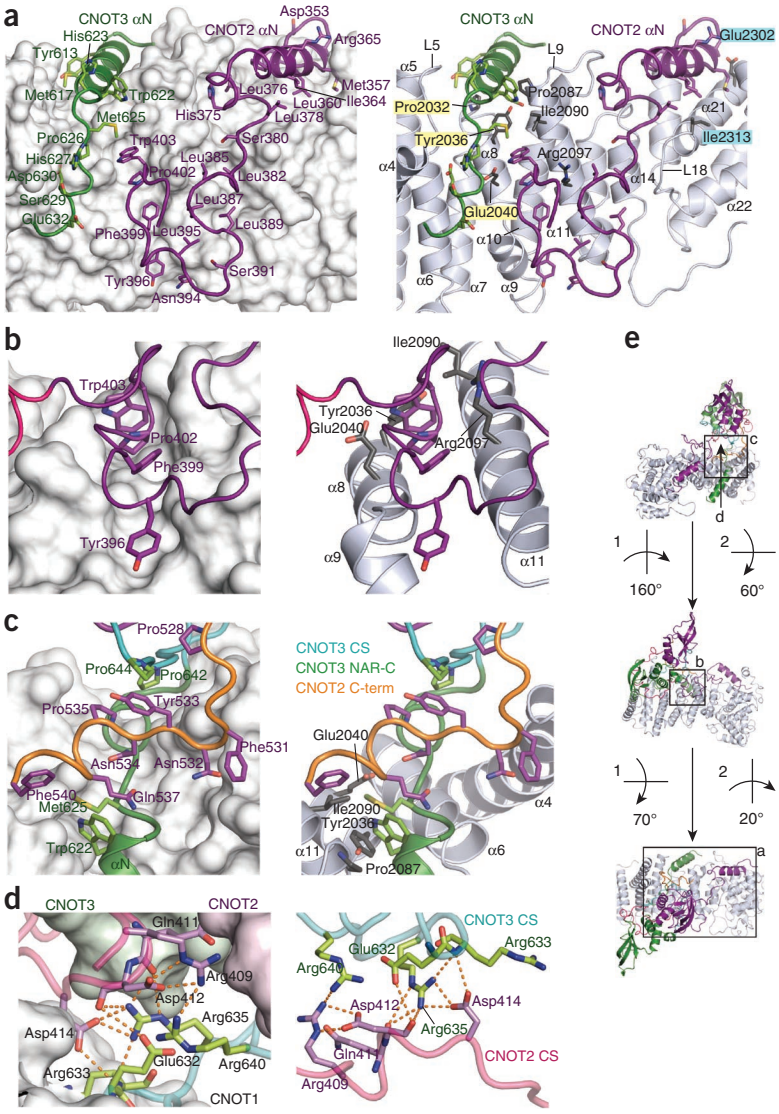

Figure 5 The interface between CNOT1 and the CNOT2–CNOT3 heterodimer. (**a**) Packing of the NARs (purple, CNOT2; green, CNOT3) against the surface of CNOT1 (gray, cartoon representation on the right). Interacting residues are shown as sticks and are labeled on the left for CNOT2 and CNOT3 and on the right for CNOT1. Highlighted labels correspond to CNOT1 mutants M1 (yellow) and M5 (cyan). (**b**) Close-up view of a hydrophobic canyon on the surface of CNOT1 filled with side chains of CNOT2. (**c**) Interactions of the CNOT2 C-terminal tail (C-term, orange) with CNOT3 and CNOT1. Labeling of interacting residues is as in **a**. (**d**) Close-up views of the junction between the symmetric and asymmetric lobes of the ternary NOT-module complex. (**e**) Overview of the trimeric complex for orientation. The rectangles indicate the views shown in **a**–**d**.

Crystal structure of the assembled NOT-module core

The core of the human NOT module comprising CNOT1 (residues 1565–2371), CNOT2 (residues 344–540) and CNOT3 (residues 607–753) was coexpressed in *E. coli* cells and co-purified. Limited proteolysis by thermolysin removed the N-terminal part of CNOT1, resulting in a stable fragment corresponding to the NOT1 SH domain (**Supplementary Fig. 4a**). Surprisingly, limited proteolysis did not affect the N-terminal extensions of the CNOT2-C and CNOT3-C fragments, although they are predicted to lack secondary structure. In the absence of CNOT1, thermolysin rapidly degraded CNOT2-C and CNOT3-C, a result suggesting that large portions of the two proteins are flexible and unfolded in isolation (**Supplementary Fig. 4a**,**b**).

The 3.2-Å-resolution structure of the heterotrimeric complex (**Fig. 3**, **Supplementary Fig. 4c**–**f** and **Table 1**) contains CNOT1 (1842–2353), CNOT2 (350–540) and CNOT3 (607–748) in a stoichiometry of 1:1:1. The complex is organized into two lobes: an asymmetric lobe containing CNOT1 is fixed by an unusual junction to a roughly two-fold-symmetric lobe containing the NOT boxes of CNOT2 and CNOT3 (**Fig. 3a**–**c**).

The structure of human CNOT1 in the complex is similar to the structure of the isolated *Ct* NOT1-C (r.m.s. deviation of 1.99 Å over 397 equivalent Cα positions; **Supplementary Fig. 4g**), thus indicating that CNOT1 does not undergo major structural rearrangements upon binding the CNOT2–CNOT3 heterodimer. Similarly, the CNOT3 NOT-box domain in the complex adopts an almost identical conformation as does its isolated counterpart (r.m.s. deviation of 0.55 Å over 90 equivalent Cα atoms; **Supplementary Fig. 4h**). In contrast to the isolated structure, the CNOT2 NOT-box domain adopts the closed conformation in the ternary complex, and its helix α1 is partially melted (**Fig. 3d** and **Supplementary Fig. 4i**).

The symmetric lobe

CNOT2 and CNOT3 interact with each other through their NOT-box domains in the same arrangement that was observed for the CNOT3 homodimer (**Fig. 3e**,**f**), thereby leading to a highly symmetric heterodimer. Heterodimerization is mediated by hydrophobic interactions between helices α1 and α2 and loop L7 of both proteins. Importantly, the interface of the CNOT2–CNOT3 heterodimer exhibits a higher degree of complementarity than does the interface in the CNOT3 homodimer (**Fig. 4a**,**b**). This is especially apparent for CNOT2 residues Y439 and L443, which form knobs that fit neatly into the holes on the CNOT3 surface, whereas the corresponding CNOT3 residues L666 and T670 fill these holes less efficiently.

The heterodimer interface is extended by N-terminal sequences that we named connector sequences (CSs) and that wrap like clamps around the NOT-box domains of their partners (**Figs. 3f** and **4c** and **Supplementary Fig. 5a**,**b**). The CSs describe a full circle starting from their C termini and wrap around the L2 loops of their respective partners (**Fig. 3f**), inserting into the cleft formed between the β-barrel and the N-terminal α-helices (**Fig. 4c**). In the vicinity of their N termini, the CSs lock themselves back through side chain interactions with helix α2 of their own NOT-box domain (**Fig. 4c**–**e**). The side chain interactions at the locks are different for the two proteins. In CNOT2, polar residues are involved for the most part (interaction of CS residues R409, P410 and Q411 with Y446, M450 and N451 in helix α2; **Fig. 4d**), whereas in CNOT3, the interactions are mainly hydrophobic (interaction of CS residues Y637 and L638 with residues F673, Y677 and L678 in helix α2; **Fig. 4e**). Most remarkably,

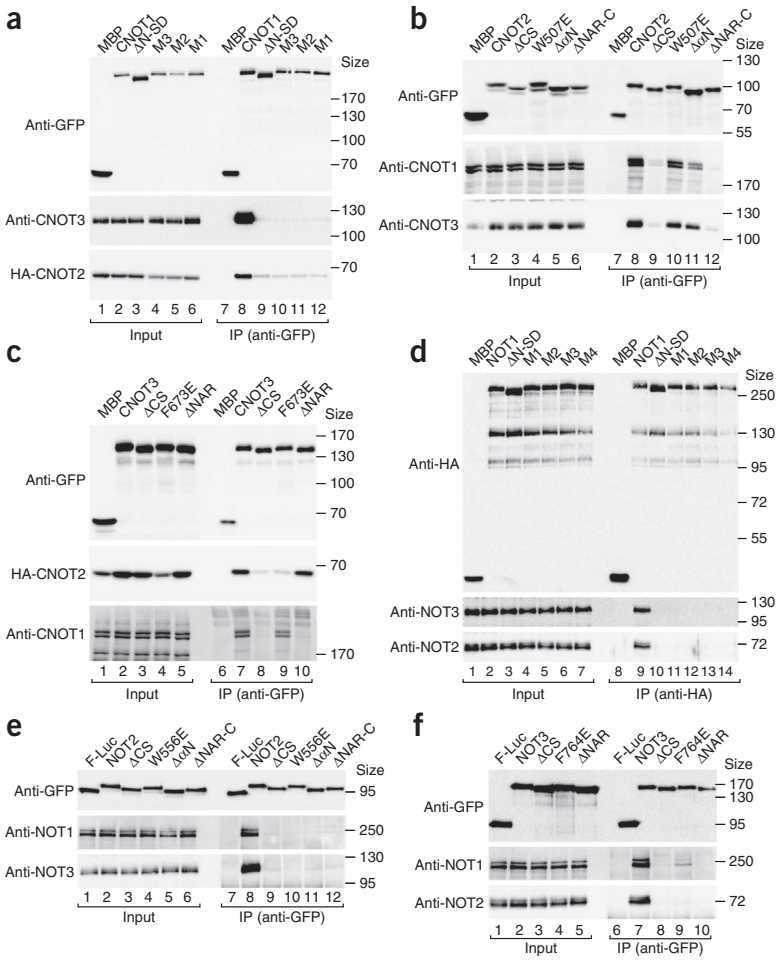

Figure 6 Mutagenesis of the NOT1-NOT2-NOT3 interfaces in human and *Dm* S2 cells. (**a**–**c**) Interaction of GFP-tagged CNOT1, CNOT2 or CNOT3 (either wild-type or the indicated mutants) with the indicated proteins (either endogenous CNOT3 and CNOT1 or CNOT2 tagged with human influenza hemagglutinin (HA)). GFP-tagged maltose binding protein (MBP) served as a negative control. (**d**) Interaction of HA-tagged *Dm* NOT1 (either wild-type or mutants) with the indicated endogenous proteins in S2 cells. HA-MBP served as a negative control. (**e**,**f**) Interaction of GFP-tagged *Dm* NOT2 or NOT3 (either wild-type or mutants) with the indicated endogenous proteins in S2 cells. GFP-tagged firefly luciferase (GFP-F-Luc) served as a negative control. In all panels, cell lysates were treated with RNase A before immunoprecipitation. IP, immunoprecipitated fraction. Size markers (kDa) are shown on the right of each panel. Original western blots shown in this figure can be found in **Supplementary Figure 8**.

the CSs are interlocked, thereby providing a topological constraint for the dissociation of the two proteins and suggesting a hierarchical assembly.

The CSs probably favor heterodimerization over homodimerization because they differ substantially in sequence and in length (**Figs. 3f** and **4c**). Notably, the CNOT3 CS is shorter and highly enriched in prolines (38%; **Fig. 4c** and **Supplementary Fig. 5a**,**b**). Thus, the interactions mediated by the CSs in the heterodimer are unlikely to occur in the context of the homodimers. This view is supported by the observation that the CNOT2 and CNOT3 fragments (containing the CSs in addition to the NOT boxes) aggregate and precipitate in isolation, thus indicating that the CSs do not participate favorably in the formation of homodimers. Upon coexpression, however, CNOT2-C and CNOT3-C remain soluble and form exclusively heterodimers (**Supplementary Fig. 3g**).

The asymmetric lobe

The CNOT2–CNOT3 heterodimer interacts predominantly with the conserved helical surface of the CNOT1 N-SD (**Fig. 3a**,**b**). The interaction does not use the NOT-box domains and involves only the NOT1 anchor regions (NARs) of both proteins, which consist of an N-terminal α-helix (αN) and a C-terminal region (NAR-C) entirely devoid of secondary structure (**Fig. 3f** and **Fig. 5a**–**d**). The αN helices insert into grooves on the lateral surface of CNOT1 (**Fig. 5a**). The extreme N-terminal residues of CNOT2 enter a cleft formed by loops L15 and L19 and helix α21 in the CNOT1 C-SD (**Fig. 5a**).

The NAR-Cs mold into the conserved helical surface of the CNOT1 N-SD (**Fig. 5a**). The short CNOT3 NAR-C crosses over the surface of helices α4, α6 and α8 of CNOT1, with which it interacts through hydrophobic and polar residues (**Fig. 5a**) before entering the junction. The long CNOT2 NAR-C zigzags across the CNOT1 surface and contains a series of aromatic residues (Y396, F399 and W403) that stick into the hydrophobic cleft between CNOT1 helices α8, α9 and α11 (**Fig. 5a**,**b**). Furthermore, residues 382–395 extensively interact with helix α11 of CNOT1 and exhibit several well-defined contacts (**Fig. 5a**).

The junction and the orientation of the two lobes

The NAR-Cs link to the CSs at the junction of the two lobes in the structure (**Fig. 3a**). The core of this junction is stabilized by hydrophilic interactions between the N-terminal ends of the CSs, which include residues from CNOT2 (R409, Q411, D412 and D414) and CNOT3 (E632, R633, R635 and R640; **Fig. 5d**). Furthermore, the relative orientation of the two lobes is stabilized by the C-terminal tail of CNOT2, which clamps the CNOT3 CS into a tunnel and hooks back onto CNOT1 (helix α11) while crossing over the CNOT3 NAR-C (**Fig. 5c**). Clearly, the interactions of the CNOT2 C-terminal tail must occur late in the assembly of the NOT module and impose additional topological constraints, thereby preventing the dissociation of CNOT3 in the presence of CNOT2. Surface conservation analysis indicated that the interfaces in the trimeric complex are conserved (**Supplementary Fig. 6a**–**e**), suggesting a similar assembly mode across multiple species.

In vivo assembly and mutagenesis of the NOT module

To determine the structural requirements for the assembly of the NOT module *in vivo*, we tested whether overexpressed protein variants are incorporated into endogenous CCR4–NOT complexes in human cells. To this end, we performed coimmunoprecipitation assays and used available anti-CNOT1 and anti-CNOT3 antibodies (**Fig. 6**). We included hemagglutinin (HA)-tagged CNOT2 in the transfection mixtures because of the lack of specific antibodies. Collectively, these experiments revealed the following observations.

First, GFP-CNOT1 interacted with HA-CNOT2 and endogenous CNOT3 (**Fig. 6a**, lane 8). As expected, a deletion of the CNOT1 N-SD (ΔN-SD) prevented these interactions (**Fig. 6a**, lane 9). Remarkably,

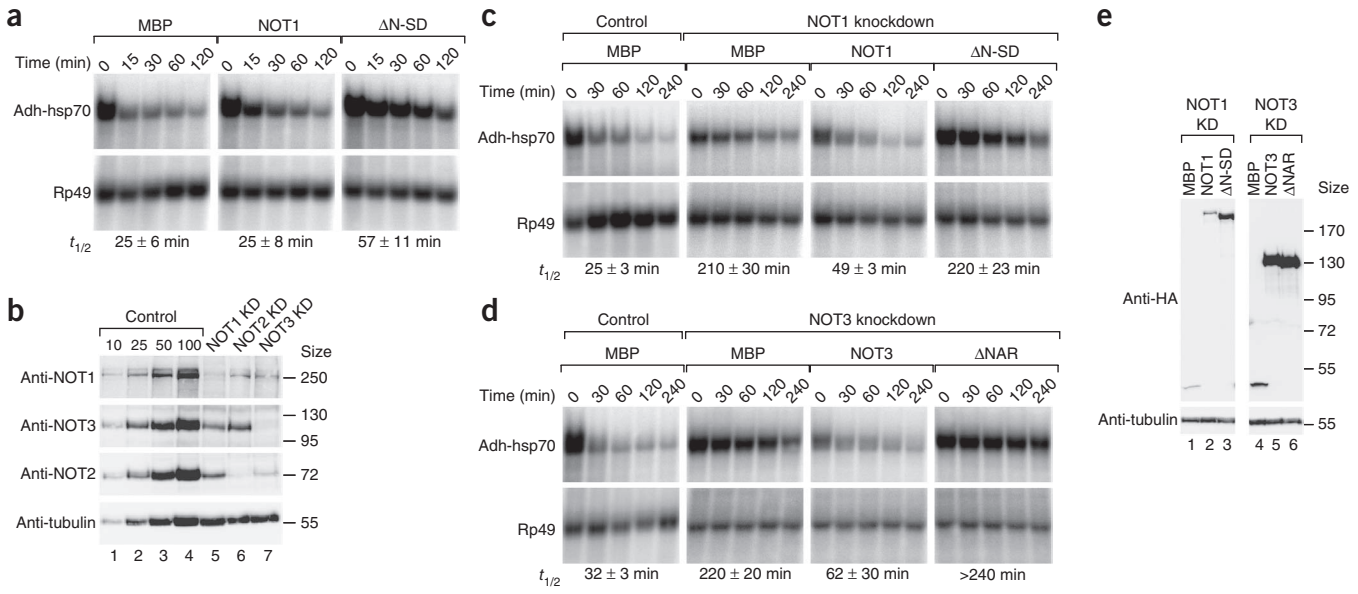

Figure 7 Effects on mRNA degradation. (**a**) Northern blot analysis showing the decay of the adh-hsp70 mRNA in control cells (expressing MBP) and in cells expressing NOT1 (either wild-type or mutant). The mRNA half-lives ($t_{1/2}$) ± s.d. calculated from the decay curves obtained from three independent experiments (**Supplementary Fig. 7d**) are indicated at bottom. Rp49 served as a loading control. (**b**) Western blot analysis of S2 cells depleted of NOT1, NOT2 or NOT3. Dilutions of control cell lysates were loaded in lanes 1–4 to estimate the efficacy of the depletion. Tubulin served as a loading control. KD, knockdown. Size markers (kDa) are indicated on the right. (**c**,**d**) Northern blots showing the decay of the adh-hsp70 mRNA in control cells (treated with GFP dsRNA and expressing MBP) or in cells depleted of NOT1 (**c**) or NOT3 (**d**) expressing MBP or the indicated proteins. The mRNA half-lives ($t_{1/2}$) ± s.d. calculated from the decay curves of three independent experiments (**Supplementary Fig. 7f,g**) are indicated at bottom. (**e**) Western blot showing the expression levels of the dsRNA-resistant, HA-tagged NOT1 and NOT3 proteins used in the complementation assays. Size markers (kDa) are indicated on the right. Original images of western and northern blots shown in this figure can be found in **Supplementary Figure 8**.

it was sufficient to substitute only two or three surface residues on CNOT1 that make direct contact with CNOT2 (mutants M5 and M6) or CNOT3 (mutant M1; **Fig. 5a** and **Supplementary Fig. 2**) to achieve a similar effect (**Fig. 6a**, **Supplementary Fig. 7a** and **Supplementary Table 1**). These CNOT1 mutants still interacted with CNOT7 (**Supplementary Fig. 7b**,**c**), a result suggesting that the mutations do not affect the CNOT1 fold. Consequently, subtle alterations of the CNOT1 binding surface are sufficient to prevent its interaction with CNOT2 and CNOT3 *in vivo*, a result consistent with a specific but rather weak, entropically costly interaction.

Second, GFP-CNOT2 interacted with endogenous CNOT1 and CNOT3 (**Fig. 6b**, lane 8). A deletion of the NAR-C region strongly reduced binding to endogenous CNOT1 (**Fig. 6b**, lane 12). This deletion also abolished binding to endogenous CNOT3 (**Fig. 6b**, lane 12), although a CNOT2 mutant lacking the entire NAR still interacted with CNOT3 *in vitro* (**Supplementary Fig. 1h**). This observation confirms that our assay detects the incorporation of CNOT2 into endogenous CCR4–NOT complexes, rather than detecting binary interactions alone. The results also suggest that there is no excess of free CNOT3 in the cell to interact with CNOT2. Conversely, a deletion of the CNOT2 CS also prevented the interaction with both CNOT1 and CNOT3 (**Fig. 6b**, lane 9). In contrast, a point mutation at the NOT-box interface (W507E) or the deletion of αN were ineffectual (**Fig. 6b**, lanes 10,11). These results highlight the importance of the CNOT2 CS and the NAR-C for NOT-module assembly.

Third, GFP-CNOT3 interacted with endogenous CNOT1 and with HA-CNOT2 (**Fig. 6c**, lane 7). As observed for CNOT2, the deletion of the CS prevents interaction not only with HA-CNOT2 but also with endogenous CNOT1 (**Fig. 6c**, lane 8), thus indicating that mutated GFP-CNOT3 is not incorporated into endogenous NOT modules. In contrast, a single amino acid substitution in CNOT3 helix α2 (F673E) disrupted HA-CNOT2 binding, but this mutant maintained interaction with endogenous CNOT1 (**Fig. 6c**, lane 9), a result suggesting that the CNOT3 NAR could be sufficient for incorporation into NOT modules even when the interaction with CNOT2 is disrupted. Consistent with this, the deletion of the NAR abrogated binding to endogenous CNOT1 (**Fig. 6c**, lane 10).

Finally, analogous experiments in *Dm* Schneider cells (S2 cells), demonstrated that all of the aforementioned mutations and deletions abolished the interaction of *Dm* NOT1, NOT2 and NOT3 with the other two endogenous partners (**Fig. 6d–f**). These results confirm the conclusion that endogenous NOT1, NOT2 and NOT3 are fully assembled into NOT modules and indicate that each subunit requires interaction with both of its partners to be incorporated into the NOT modules in *Dm* S2 cells. Together with the topological constraints seen in the structure, the results also suggest a highly coordinated and hierarchical assembly with built-in quality controls.

The integrity of the NOT module and mRNA degradation

To test whether a disturbed assembly of the NOT module has consequences on mRNA degradation, we used a heat-shock mRNA reporter containing the coding region of the *Dm* alcohol dehydrogenase gene (*Adh*) fused to the *hsp70* (official symbol *Hsp70Ab*) 3′ untranslated region (construct denoted adh-hsp70), which is sufficient to recapitulate *hsp70* mRNA decay[25] and results in a half-life of 25 ± 6 min (**Fig. 7a**).

In the first round of experiments, we overexpressed the NOT1 protein in S2 cells. We found that wild-type NOT1 had no effect on mRNA half-life (**Fig. 7a** and **Supplementary Fig. 7d**), whereas the expression of the NOT1 ΔN-SD mutant resulted in a two-fold increase of the mRNA half-life (57 ± 11 min; **Fig. 7a** and **Supplementary Fig. 7d**). Because this mutant still interacts with CAF1 (**Supplementary Fig. 7e**),

it probably sequesters the catalytic module into inactive complexes or it is assembled into defective complexes that are no longer recruited to the mRNA reporter.

In the second round of experiments, we depleted the individual subunits. Western blot analysis indicated that the depletion of single subunits of the ternary NOT1–NOT2–NOT3 complex co-depleted the other two subunits (**Fig. 7b**), in agreement with previous studies[11,13,15,25,26] (**Fig. 7b**). These observations demonstrate that the respective protein ratios are strictly controlled in the cell.

Because the depletions of NOT1 and NOT3 efficiently co-depleted the other two partners, we expected that such depletions would affect adh-hsp70 mRNA degradation in a similar manner. Consistent with this expectation and a previous study[25], the half-life of the hsp70 mRNA reporter in NOT1- and NOT3-depleted cells increased almost ten-fold relative to control cells (210 ± 30 and 220 ± 20 min, respectively; **Fig. 7c**,**d** and **Supplementary Fig. 7f**,**g**).

Next, we performed complementation assays, wherein NOT1 or NOT3 mutants were tested for their ability to restore mRNA degradation in cells that were depleted of the corresponding endogenous protein. Reintroduction of a double-stranded RNA (dsRNA)-resistant version of wild-type NOT1 partially restored the degradation of the reporter and reduced the mRNA half-life to 49 ± 3 min in NOT1-depleted cells (**Fig. 7c** and **Supplementary Fig. 7f**). In contrast, the NOT1 ΔN-SD mutant did not restore degradation, and the adh-hsp70 mRNA half-life (220 ± 23 min) was similar to that observed in NOT1-depleted cells (**Fig. 7c** and **Supplementary Fig. 7f**), even though expression was higher for the NOT1 mutant than for the wild-type (**Fig. 7e**).

Similarly, the reintroduction of a dsRNA-resistant version of wild-type NOT3 restored the degradation of the reporter and reduced the mRNA half-life to 62 ± 30 min in NOT3-depleted cells (**Fig. 7d** and **Supplementary Fig. 7g**). In contrast, the NOT3 ΔNAR mutant did not restore degradation (half-life > 240 min; **Fig. 7d**), even though the mutant was expressed at similar levels to wild-type NOT3 (**Fig. 7e**).

In summary, these experiments demonstrate a strict requirement for the cell to balance the levels of the NOT-module protein components. They also show that a properly assembled NOT module, as observed in the crystal structure, is essential for the activity and/or recruitment of the CCR4–NOT complex and hence is crucial for mRNA degradation.

DISCUSSION

Unusual assembly principles for the NOT module

A remarkable and unexpected structural feature of the NOT module is the role that the NAR and CS regions of CNOT2 and CNOT3 have in the assembly of the trimer. Particularly striking is that these regions not only hook up onto their prefolded molecular partners, as observed in assemblies such as the ribosome[27,28], but also stabilize each other and exclusively orchestrate the three-dimensional assembly of the entire NOT module. This mode of assembly is rather unusual and is clearly distinct from the classical principle of mutual recognition by complementary tertiary structures such as observed for the interaction of CAF1 with the NOT1 MIF4G domain[10,14]. In particular, the embracement of the NOT-box domains by the CSs, the formation of the junction and the adaptation of the NAR-Cs to the CNOT1 surface could not happen without disorder-to-order transition and cofolding[29].

According to the most general definition, the NAR and CS regions could be classified as intrinsically disordered, i.e., as protein sequences that are largely unstructured in the absence of their specific binding partners and that adopt their three-dimensional shape only upon binding[30,31]. This classification is based primarily on the lack of secondary-structure elements and of intramolecular contacts, which means that the relative orientation of the amino acids as observed in the complex will not be fixed in the absence of the binding partner. Consequently, the sequences are presumably disordered in isolation, as reflected by the susceptibility to proteolytic degradation (**Supplementary Fig. 4a**,**b**). However, sequence analysis does not identify the NAR and CS regions as typical intrinsically disordered regions[30,31].

In summary, we report the following new observations: first, even upon binding, the NAR and CS regions remain largely devoid of α-helices and β-strands, thus demonstrating that specific surface recognition and the formation of the structured core in the junction are possible without such elements. Second, rather than only threading along surface grooves, peptide regions of sufficient length, such as the CNOT2 NAR-C, can read out entire molecular surfaces by zig-zagging back and forth. Third, synergistic cofolding[29] of the CNOT2 and CNOT3 assembly peptides leads to a mutual stabilization and a specific hydrophilic core at the junction between the two lobes of the complex. Fourth, the interaction with these peptides is the sole determinant for NOT-module assembly and for the relative orientation of the two structured lobes, thus demonstrating that assembly peptides without secondary structure can guide and determine the shape of multimolecular complexes. Finally, topological constraints such as the described interlocks between the CSs increase the structural complexity and additionally stabilize the assembly.

Control of protein ratios and NOT-module assembly

The unexpected topological complexity of the NOT module suggests a requirement for a hierarchical and coordinated assembly of the individual subunits with the CNOT3 NAR binding the CNOT1 surface before CNOT2. Additional complexity arises from both CNOT2 and CNOT3 being able to form homodimers in the absence of their preferred binding partner, and these homodimers might compromise CCR4–NOT complex assembly or interfere with its function. Consequently, it is not surprising that the relative protein ratios of the NOT-module components are tightly controlled in the cell. In this context, the NAR and CS regions could have additional functions. They could interact with general chaperones or even specialized assembly factors that prevent nonspecific aggregation and/or promote the ordered incorporation into the CCR4–NOT complex. Alternatively, the NAR and CS regions could trigger an accelerated degradation of the proteins in the absence of their binding partners[32], owing to their susceptibility to cellular proteases, thus providing a simple mechanism to coordinate the expression of the subunits of the complex.

Recruitment of the CCR4–NOT complex to mRNA targets

The CCR4–NOT complex is assembled through the interaction of a catalytic module with the NOT module. Although the catalytic subunits catalyze deadenylation, the NOT module orchestrates the recruitment of these subunits to mRNA targets. This is achieved through interactions with RNA-associated proteins[2,17] (including GW182, Bicaudal-C, Nanos, CUP and Roquin), which have been shown to interact with NOT-module components[4,18–20,33–37]. The molecular details of these interactions remain unknown. In this context, our structural analysis reveals a highly conserved solvent-exposed surface on the NOT module that extends from the CNOT1 C-SD over the CNOT2 NAR to the CNOT3 NOT box (**Supplementary Fig. 6a**), and this surface probably provides a binding platform for conserved binding partners.

Remarkably, for the binding partners that have been characterized in more detail (GW182, Nanos and CUP)[4,18–20,35,36], the regions that

mediate binding to the NOT module are predicted to be unstructured. Thus their interactions with the NOT module may follow a similar structural principle as observed for the NAR and CS regions of CNOT2 and CNOT3. For example, the GW182 proteins interact with the CCR4–NOT complex through tryptophan-containing motifs[4,18–20] that probably bind in hydrophobic pockets along the CNOT1 scaffold and that may function similarly to the aromatic residues in the CNOT2 NAR-C. Understanding such interactions in molecular terms remains an important challenge for future studies.

METHODS

Methods and any associated references are available in the online version of the paper.

Accession codes. Coordinates for the structures have been deposited in the Protein Data Bank under accession codes 4C0D (ternary complex of CNOT1–CNOT2–CNOT3), 4C0E (SH domain of *Ct* NOT1), 4C0F (NOT-box domain of CNOT2) and 4C0G (NOT-box domain of CNOT3).

Note: Any Supplementary Information and Source Data files are available in the online version of the paper.

ACKNOWLEDGMENTS

We are grateful to J. Su (Max Planck Institute for Developmental Biology) for providing the cDNA for the CNOT1 fragment (residues 1565–2371) and to E. Wahle (Martin Luther University Halle-Wittenberg) for the kind gift of anti–*Dm* NOT1–NOT3 antibodies. This work was supported by the Max Planck Society, by grants from the Deutsche Forschungsgemeinschaft (DFG, FOR855 and the Gottfried Wilhelm Leibniz Program awarded to E.I.) and the European Union Seventh Framework Program through a Marie Curie Fellowship to S.J. (FP7, 275343).

AUTHOR CONTRIBUTIONS

A.B., Y.C., T.R. and S.J. contributed equally to this work. A.B. and Y.C. purified, crystallized and solved the structures of CNOT3 and CNOT2 oligomers and of *Ct* NOT1. A.B. and Y.C. cloned, expressed and established the purification protocol for the ternary complex. T.R. purified and crystallized the ternary complex. T.R. and S.J. solved the structure of the ternary complex. A.B., Y.C., T.R., S.J. and O.W. collected and analyzed diffraction data. L.W. performed pulldowns and coimmunoprecipitations in human cells. D.K.-Ö. performed coimmunoprecipitations and functional assays in S2 cells. E.I. conceived of the project. E.I. and O.W. supervised the project. All authors contributed to the writing of the manuscript.

COMPETING FINANCIAL INTERESTS

The authors declare no competing financial interests.

1. Collart, M.A. & Panasenko, O.O. The Ccr4-Not complex. *Gene* **492**, 42–53 (2012).
2. Wahle, E. & Winkler, G.S. RNA decay machines: deadenylation by the Ccr4-Not and Pan2-Pan3 complexes. *Biochim. Biophys. Acta* **1829**, 561–570 (2013).
3. Bawankar, P., Loh, B., Wohlbold, L., Schmidt, S. & Izaurralde, E. NOT10 and C2orf29/NOT11 form a conserved module of the CCR4-NOT complex that docks onto the NOT1 N-terminal domain. *RNA Biol.* **10**, 228–244 (2013).
4. Chekulaeva, M. *et al.* miRNA repression involves GW182-mediated recruitment of CCR4–NOT through conserved W-containing motifs. *Nat. Struct. Mol. Biol.* **18**, 1218–1226 (2011).
5. Cooke, A., Prigge, A. & Wickens, M. Translational repression by deadenylases. *J. Biol. Chem.* **285**, 28506–28513 (2010).
6. Zekri, L., Kuzuoğlu-Öztürk, D. & Izaurralde, E. GW182 proteins cause PABP dissociation from silenced miRNA targets in the absence of deadenylation. *EMBO J.* **32**, 1052–1065 (2013).
7. Bai, Y. *et al.* The CCR4 and CAF1 proteins of the CCR4-NOT complex are physically and functionally separated from NOT2, NOT4, and NOT5. *Mol. Cell. Biol.* **19**, 6642–6651 (1999).
8. Lau, N.C. *et al.* Human Ccr4-Not complexes contain variable deadenylase subunits. *Biochem. J.* **422**, 443–453 (2009).
9. Liu, H.Y. *et al.* The NOT proteins are part of the CCR4 transcriptional complex and affect gene expression both positively and negatively. *EMBO J.* **17**, 1096–1106 (1998).
10. Basquin, J. *et al.* Architecture of the nuclease module of the yeast Ccr4-Not complex: the Not1-Caf1-Ccr4 interaction. *Mol. Cell* **48**, 207–218 (2012).
11. Ito, K., Takahashi, A., Morita, M., Suzuki, T. & Yamamoto, T. The role of the CNOT1 subunit of the CCR4–NOT complex in mRNA deadenylation and cell viability. *Protein Cell* **2**, 755–763 (2011).
12. Maillet, L., Tu, C., Hong, Y.K., Shuster, E.O. & Collart, M.A. The essential function of Not1 lies within the Ccr4-Not complex. *J. Mol. Biol.* **303**, 131–143 (2000).
13. Mauxion, F., Prève, B. & Séraphin, B. C2ORF29/CNOT11 and CNOT10 form a new module of the CCR4-NOT complex. *RNA Biol.* **10**, 267–276 (2013).
14. Petit, A.P. *et al.* The structural basis for the interaction between CAF1 nuclease and the NOT1 scaffold of the human CCR4-NOT deadenylase complex. *Nucleic Acids Res.* **40**, 11058–11072 (2012).
15. Russell, P., Benson, J.D. & Denis, C.L. Characterization of mutations in NOT2 indicates that it plays an important role in maintaining the integrity of the CCR4-NOT complex. *J. Mol. Biol.* **322**, 27–39 (2002).
16. Winkler, G.S., Mulder, K.W., Bardwell, V.G., Kalkhoven, E. & Timmers, H.T. Human Ccr4-Not complex is a ligand-dependent repressor of nuclear receptor-mediated transcription. *EMBO J.* **25**, 3089–3099 (2006).
17. Barckmann, B. & Simonelig, M. Control of maternal mRNA stability in germ cells and early embryos. *Biochim. Biophys. Acta* **1829**, 714–724 (2013).
18. Braun, J.E., Huntzinger, E., Fauser, M. & Izaurralde, E. GW182 proteins recruit cytoplasmic deadenylase complexes to miRNA targets. *Mol. Cell* **44**, 120–133 (2011).
19. Fabian, M.R. *et al.* miRNA-mediated deadenylation is orchestrated by GW182 through two conserved motifs that interact with CCR4–NOT. *Nat. Struct. Mol. Biol.* **18**, 1211–1217 (2011).
20. Huntzinger, E. *et al.* The interactions of GW182 proteins with PABP and deadenylases are required for both translational repression and degradation of miRNA targets. *Nucleic Acids Res.* **41**, 978–994 (2013).
21. Fabian, M.R. *et al.* Structural basis for the recruitment of the human CCR4–NOT deadenylase complex by tristetraprolin. *Nat. Struct. Mol. Biol.* **20**, 735–739 (2013).
22. Albert, T.K. *et al.* Isolation and characterization of human orthologs of yeast CCR4-NOT complex subunits. *Nucleic Acids Res.* **28**, 809–817 (2000).
23. Zwartjes, C.G., Jayne, S., van den Berg, D.L. & Timmers, H.T. Repression of promoter activity by CNOT2, a subunit of the transcription regulatory Ccr4-Not complex. *J. Biol. Chem.* **279**, 10848–10854 (2004).
24. Andrade, M.A., Petosa, C., O'Donoghue, S.I., Müller, C.W. & Bork, P. Comparison of ARM and HEAT protein repeats. *J. Mol. Biol.* **309**, 1–18 (2001).
25. Temme, C. *et al.* Subunits of the *Drosophila* CCR4-NOT complex and their roles in mRNA deadenylation. *RNA* **16**, 1356–1370 (2010).
26. Ito, K. *et al.* CNOT2 depletion disrupts and inhibits the CCR4–NOT deadenylase complex and induces apoptotic cell death. *Genes Cells* **16**, 368–379 (2011).
27. Brodersen, D.E. & Nissen, P. The social life of ribosomal proteins. *FEBS J.* **272**, 2098–2108 (2005).
28. Klein, D.J., Moore, P.B. & Steitz, T.A. The roles of ribosomal proteins in the structure assembly, and evolution of the large ribosomal subunit. *J. Mol. Biol.* **340**, 141–177 (2004).
29. Demarest, S.J. *et al.* Mutual synergistic folding in recruitment of CBP/p300 by p160 nuclear receptor coactivators. *Nature* **415**, 549–553 (2002).
30. Tompa, P. Intrinsically disordered proteins: a 10-year recap. *Trends Biochem. Sci.* **37**, 509–516 (2012).
31. Dyson, H.J. & Wright, P.E. Intrinsically unstructured proteins and their functions. *Nat. Rev. Mol. Cell Biol.* **6**, 197–208 (2005).
32. Prakash, S., Tian, L., Ratliff, K.S., Lehotzky, R.E. & Matouschek, A. An unstructured initiation site is required for efficient proteasome-mediated degradation. *Nat. Struct. Mol. Biol.* **11**, 830–837 (2004).
33. Temme, C., Zaessinger, S., Meyer, S., Simonelig, M. & Wahle, E. A complex containing the CCR4 and CAF1 proteins is involved in mRNA deadenylation in *Drosophila*. *EMBO J.* **23**, 2862–2871 (2004).
34. Chicoine, J. *et al.* Bicaudal-C recruits CCR4-NOT deadenylase to target mRNAs and regulates oogenesis, cytoskeletal organization, and its own expression. *Dev. Cell* **13**, 691–704 (2007).
35. Suzuki, A., Igarashi, K., Aisaki, K., Kanno, J. & Saga, Y. NANOS2 interacts with the CCR4-NOT deadenylation complex and leads to suppression of specific RNAs. *Proc. Natl. Acad. Sci. USA* **107**, 3594–3599 (2010).
36. Igreja, C. & Izaurralde, E. CUP promotes deadenylation and inhibits decapping of mRNA targets. *Genes Dev.* **25**, 1955–1967 (2011).
37. Leppek, K. *et al.* Roquin promotes constitutive mRNA decay via a conserved class of stem-loop recognition motifs. *Cell* **153**, 869–881 (2013).

ONLINE METHODS

Coimmunoprecipitation assays and western blotting. Plasmids expressing CCR4–NOT deadenylase subunits and coimmunoprecipitation assays in human and *Dm* S2 cells have been previously described[18]. HA- and GFP-tagged proteins were detected with horseradish peroxidase–conjugated anti-HA[18] (Roche 3F10; 1:3,000) and anti-GFP antibodies[18] (Roche 11814460001; 1:2,000), respectively. Endogenous human CNOT1 was detected with a polyclonal anti-CNOT1 antibody generated by immunization of rabbits with the purified untagged MIF4G domain of human NOT1 expressed in *E. coli*[14] (1:2,000). Endogenous CNOT3 was detected with a commercially available anti-CNOT3 antibody (Abcam ab55681; 1:1,000). The specificity of this antibody is shown in **Figure 6**. Endogenous *Dm* NOT1, NOT2 and NOT3 were detected with antibodies kindly provided by E. Wahle[25,33]. All western blots were developed with the ECL western blotting detection system (GE Healthcare).

***In vitro* pulldown assays.** The indicated GST- or MBP-tagged CNOT1, CNOT2 and CNOT3 fragments were expressed separately in BL21 (DE3) Star cells (Invitrogen) at 20 °C overnight. Cells were lysed in 10 mM HEPES, pH 7.6, 300 mM NaCl and 1 mM DTT supplemented with lysozyme (1 μg/ml), DNaseI (5 μg/ml) and protease inhibitors. Cell lysates were sonicated and cleared by centrifugation. The cleared supernatants containing the respective binding partners were mixed to obtain an approximately 1:1 ratio of the protein partners and incubated in binding buffer (10 mM HEPES, pH 7.6, 150 mM NaCl, 0.4% Triton X-100, 1 mM DTT, and protease inhibitors) for 20 min at 4 °C. After this, 50 μl (50% slurry) of Protino Glutathione agarose 4B beads (Macherey Nagel) or 50 μl (50% slurry) of amylose resin (New England BioLabs) was added to each sample, and incubation was continued for another hour at 4 °C with gentle rotation. Beads were washed three times with binding buffer. Bound proteins were eluted with 2× sample buffer and analyzed by SDS-PAGE.

His_6-tagged CNOT1 (residues 1565–2371) was expressed in *E. coli* BL21 (DE3) Star cells in LB medium at 20 °C overnight and purified through nickel-affinity chromatography followed by anion-exchange chromatography and finally size-exclusion chromatography, with a running buffer containing 50 mM HEPES, pH 8.0, 400 mM NaCl, 10% glycerol and 2 mM DTT. The purified protein (20 μg) was added to 200 μl of lysate expressing the respective MBP-tagged CNOT2 or CNOT3 and incubated in binding buffer (10 mM HEPES, pH 7.6, 300 mM NaCl, 1 mM DTT and protease inhibitors) for 20 min at 4 °C. After this, 50 μl (50% slurry) of amylose resin was added to each sample, and incubation was continued for another hour at 4 °C with gentle rotation. Beads were washed three times with binding buffer. Bound proteins were eluted with 2× sample buffer and analyzed by SDS-PAGE.

In the experiment shown in **Supplementary Figure 3g**, MBP-tagged CNOT2 and His_6-tagged CNOT3 were coexpressed in *E. coli*. The heterodimers were co-purified with MBP pulldown and subsequent Ni-affinity purification (lanes 1 and 2) or Ni-affinity purification and subsequent MBP pulldown (lanes 3 and 4). The stoichiometry of the complex was similar in all cases, thus indicating that the proteins heterodimerize in solution and that there was no excess of MBP-NOT2 or His_6-NOT3 homodimers.

Protein expression and purification. The DNA encoding *Ct* NOT1-C (residues 1676–2193) was amplified by PCR from a synthetic template (Gene Art, codon-optimized for *E. coli*) and inserted into *XhoI and BamHI* restriction sites of the pnYC vector, which provides an N-terminal His_6-tag followed by a TEV protease site[38]. His_6-tagged *Ct* NOT1-C was expressed in *E. coli* BL21 Star (DE3) cells at 20 °C overnight. After an initial Ni-affinity purification step (Hi-Trap chelating HP Nickel column; GE Healthcare), the protein was purified by gel filtration (HiLoad Superdex 200 26/60; GE Healthcare), in a buffer containing 10 mM HEPES, 200 mM NaCl and 2 mM DTT, and concentrated to 7 mg/ml.

The DNA encoding the CNOT2 NOT-box domain (residues 429–540) was amplified from total human cDNA and inserted into the *Nde*I and *BamH*I restriction sites of a pnYC vector downstream of a His_6-MBP tag. The fusion protein was expressed in *E. coli* BL21 Star cells at 37 °C for 5 h and purified over a Ni-NTA column. After cleavage by HRV3C protease at 4 °C overnight, the His_6-MBP tag was removed from the solution by binding to amylose resin and subsequent size-exclusion chromatography (HiLoad 16/60 Superdex 75; GE Healthcare). Finally, the protein was purified with a MonoQ GL 15/50 column, dialyzed overnight into 10 mM CHES, pH 9.0, 100 mM NaCl and 1 mM DTT and concentrated to 3.5 mg/ml.

The DNA encoding the CNOT3 NOT-box domain (residues 656–753) was amplified by PCR using total human cDNA as template and inserted into the *Nco*I and *KpnI* sites of the pETM60 vector, which provides an N-terminal His_6-NusA tag (Novagen). The fusion protein was expressed in *E. coli* BL21 Star cells at 20 °C overnight. After initial purification with Ni-NTA affinity chromatography, the His_6-NusA tag was cleaved by TEV protease at 4 °C overnight. CNOT3 was separated from the tag by size-exclusion chromatography (HiLoad 16/60 Superdex 75, GE Healthcare) and concentrated to 4.5 mg/ml in 10 mM CHES, pH 9.0, 150 mM NaCl and 1 mM DTT.

To obtain selenomethionine-substituted proteins, the CNOT2 NOT-box, CNOT3 NOT-box and *Ct* NOT1-C proteins were expressed in minimal medium supplemented with selenomethionine[39] and purified as described for the respective native proteins.

The trimeric complex consisting of CNOT1 (residues 1565–2371), CNOT2 (residues 344–540) and CNOT3 (residues 607–753) was coexpressed in *E. coli* BL21 (DE3) Star cells in LB medium at 20 °C overnight. CNOT1 was expressed with an N-terminal His_6-tag cleavable with TEV protease. CNOT2 and CNOT3 were expressed from a bicistronic plasmid, wherein CNOT2 contained an N-terminal MBP tag cleavable by HRV3C protease, and CNOT3 contained a noncleavable His_6 tag.

CNOT1, CNOT2 and CNOT3 were co-purified from crude lysates in lysis buffer (50 mM sodium phosphate, pH 7.5, 300 mM NaCl and 2 mM β-mercaptoethanol, supplemented with protease inhibitors, lysozyme and DNaseI) with amylose resin and eluted with lysis buffer supplemented with 25 mM maltose. The purified complex was digested overnight with HRV3C and TEV proteases during dialysis into imidazole buffer (10 mM Tris-HCl, pH 8.6, 200 mM NaCl, 2 mM β-mercaptoethanol, 10% glycerol and 20 mM imidazole). The complex was further purified by Ni-affinity chromatography and finally by size-exclusion chromatography (HiLoad Superdex 75 16/60 column; GE Healthcare) in gel-filtration buffer (10 mM Tris-HCl, pH 8.6, 200 mM NaCl and 2 mM DTT). The ternary complex was subjected to limited proteolysis for 4.5 h in proteolysis buffer (20 mM HEPES, pH 7.5, 100 mM NaCl, 50 μM $CaCl_2$ and 2 mM DTT) supplemented with 21 μg/ml thermolysin (Sigma-Aldrich) and separated from the protease and smaller CNOT1 fragments by gel filtration.

For the experiment shown in **Supplementary Figure 4b**, the ternary complex was assembled in 30 μl of proteolysis buffer with CNOT2 (residues 344–540) and CNOT3 (residues 607–753) at a concentration of 0.3 mg/ml and 0.63 mg/ml CNOT1 (residues 1833–2361). The binary complex of CNOT2 (residues 344–540) and CNOT3 (residues 607–753) was diluted in 30 μl of proteolysis buffer to a concentration of 0.3 mg/ml. After addition of 8 μl thermolysin (0.3 mg/ml) and incubation on ice, the reaction was stopped at different time points with 10 μl 5× SDS gel loading buffer and analyzed on a 15% SDS-PAGE gel.

Crystallization. Crystals of the native and selenomethionine-substituted *Ct* NOT1-C constructs were obtained by hanging-drop and sitting-drop vapor diffusion, respectively, at 18 °C and 22 °C. The best crystals for data collection and phase determination were obtained with selenomethionine-substituted protein, from a condition containing 0.1 M MES, pH 6.0, 0.18 M $MgCl_2$, 5% PEG 20000 and 10 mM proline with a 1:1 protein/reservoir ratio. Crystals were cryoprotected by addition of a final concentration of 25% glycerol to the reservoir solution and then flash-frozen in liquid nitrogen before data collection.

Crystals of the native CNOT2 NOT-box domain were grown by hanging-drop vapor diffusion at 18 °C. The protein solution was mixed in a 1:1 ratio with a reservoir solution containing 100 mM trisodium citrate, pH 5.6, 10% PEG 4000 and 10% isopropanol. Crystals were optimized by hair seeding. Before being flash frozen in liquid nitrogen, the crystals were cryoprotected in the reservoir solution supplemented with 15% or 20% glycerol (final concentration). Crystals of the selenomethionine-substituted CNOT2 construct were obtained by sitting-drop vapor diffusion at 22 °C over a reservoir of 100 mM HEPES, pH 7.5, 10% PEG 4000 and 10% isopropanol.

Crystals of the native and selenomethionine-substituted CNOT3 NOT-box domain were grown by hanging-drop vapor diffusion in a 1:1 protein/reservoir ratio, with the reservoir buffer containing 100 mM HEPES, pH 7.8, 13% PEG 4000, 2% glycerol and 12% isopropanol at 18 °C. Crystals were optimized by hair

doi:10.1038/nsmb.2681

seeding and were flash frozen in liquid nitrogen. Glycerol (supplemented to 20% in the reservoir solution) was used as a cryoprotectant.

Crystals of the CNOT1–CNOT2–CNOT3 complex were obtained once in a single condition. They grew after one day by sitting-drop vapor diffusion at 22 °C in a drop consisting of 0.2 µl of the protein complex solution (5 mg/ml) and 0.2 µl of the reservoir solution containing 0.1 M MES, pH 6.5 and 12% PEG 20000. The crystals were cryoprotected with the reservoir solution supplemented with glycerol (15% final concentration) and flash frozen in liquid nitrogen.

Data collection, structure solution and refinement. All diffraction data sets were recorded on a PILATUS 6M detector at the PXII beamline of the Swiss Light Source (SLS) at a temperature of 100 K. Data sets for different crystal forms of *Ct* NOT1-C were collected at a wavelength of 0.97925 Å with high redundancy and processed with XDS[40]. Selenium sites were identified with data sets from crystal form I (space group $P2_12_12_1$, 3.6 Å) with SHELX[41]. These sites were used to obtain phases, and an initial backbone model was built with PHENIX AutoSol[42]. This model was fed into Buccaneer[43] from the CCP4 package[44] for assigning and autobuilding side chains. The sequence register was confirmed by inspection of the anomalous difference Fourier maps from the selenomethionine data set, with peaks corresponding to the methionine positions. After several rounds of refinement in PHENIX[45] and manual model improvement in Coot[46], the model was used for molecular replacement (Phaser)[47] with a data set of crystal form II (space group $P12_11$, 3.2 Å). The structure was finalized by several cycles of manual building in Coot and refinement in PHENIX against this high-resolution data set. For *Ct* NOT1, 98.3% of all residues lie in the favored regions of the Ramachandran plot, with outliers totaling 0.2%.

Data for the native CNOT2 NOT-box domain were collected at a wavelength of 1.0 Å, whereas data from selenomethionine-labeled crystals were recorded at a wavelength of 0.97925 Å (peak). The best native crystal of CNOT2 led to a data set of 2.4-Å resolution with space group $P6_522$, whereas the best data set of selenomethionine-substituted protein reached a resolution of 3.4 Å with a space group of $P4_1$. Data sets were processed in XDS[40]. Initial selenium sites were identified by SAD with SHELX and refined with SHARP[48]. Additional sites were identified upon inspection of the anomalous difference density map and refined with SHARP. The resulting electron density map was used for initial model building with Buccaneer. The model was subsequently improved manually in Coot and refined with PHENIX. The high-resolution structure of the native protein was solved by molecular replacement (Phaser) with the structure of the selenomethionine-substituted protein as the search model. The structure of the native protein was finalized by iterative refinement cycles with PHENIX and model building in Coot.

The data sets for the CNOT3 NOT-box domain were collected at wavelengths of 0.9795 Å (peak) and 1.0000 Å (low-energy remote) and processed with XDS. Selenium sites were identified by SAD with SHELX. The heavy-atom model was further improved with SHARP as described for CNOT2. The model was initially built with Buccaneer and manually completed in Coot. Refinement was done in PHENIX against the low-energy remote data set, which had the highest resolution (2.4 Å). For the NOT-box domains of CNOT2 and CNOT3, there are 98.3% and 97.4% of all residues in the favored regions of the Ramachandran plot, respectively, and no outliers.

Diffraction data for the complex of CNOT1–CNOT2–CNOT3 were recorded at a wavelength of 0.99999 Å. The best data set was processed and scaled with XDS/XSCALE. Initial phase information was obtained by molecular replacement with Phaser, with the structure of *Ct* CNOT1-C as a search model. The initial electron density was improved by solvent flattening with PARROT[49] from the CCP4 package, and the previously determined models of the CNOT2 and CNOT3 NOT-box domains were manually placed into the density map with Coot. The CNOT1 model was subsequently rebuilt with the sequence of the human protein. Additional parts of the structure, which primarily consisted of the N-terminal extensions of the CNOT2 and CNOT3 NOT-box domains, were manually built in Coot. The model was subsequently improved by iterative cycles of refinement and building with PHENIX and Coot. For the ternary complex, 96.7% of all residues were in the favored regions of the Ramachandran plot, and there were no outliers. The correct stereochemical properties of all the structures were verified with MolProbity[50], and structure figures were generated in PyMOL (http://www.pymol.org/). The data collection and refinement statistics are summarized in **Table 1**.

Multiangle static laser light scattering (MALLS). The purified CNOT2 NOT-box and CNOT3 NOT-box proteins were diluted to a final concentration of 20 µM in their respective storage buffers. For both proteins, a volume of 100 µl was loaded onto an analytical gel-filtration column (Superdex 200 10/300, GE Healthcare) connected to the miniDAWN TREOS and Optilab rEX instruments (Wyatt Technologies). Samples were analyzed by static light scattering, and the absolute molecular weight of each protein was calculated from the MALLS data with ASTRA (Wyatt Technologies).

Functional assays in S2 cells. The adh-hsp70 reporter was described previously[51]. Cells were transfected with 300 ng of plasmid DNA for expression of the adh-hsp70 reporter per well in six-well plates. Knockdowns with dsRNA were performed as described previously[18]. For the measurement of the mRNA half-life, transfected cells were treated with actinomycin D (final concentration 5 µg/ml) 3 d after transfection and harvested at the indicated time points. Total RNA was isolated with TriFast (PeqLab Biotechnologies) and analyzed as described previously[51]. Adh-hsp70 mRNA levels were normalized to the levels of long-lived rp49 mRNA and were plotted against time.

Original images of gels and western and northern blots used in this study can be found in **Supplementary Figure 8**.

38. Diebold, M.-L., Fribourg, S., Koch, M., Metzger, T. & Romier, C. Deciphering correct strategies for multiprotein complex assembly by co-expression: application to complexes as large as the histone octamer. *J. Struct. Biol.* **175**, 178–188 (2011).
39. Doublié, S. Preparation of selenomethionyl proteins for phase determination. *Methods Enzymol.* **276**, 523–530 (1997).
40. Kabsch, W. XDS. *Acta Crystallogr. D Biol. Crystallogr.* **66**, 125–132 (2010).
41. Sheldrick, G.M. Experimental phasing with SHELXC/D/E: combining chaintracing with density modification. *Acta Crystallogr. D Biol. Crystallogr.* **66**, 479–485 (2010).
42. Terwilliger, T.C. *et al.* Decision-making in structure solution using Bayesian estimates of map quality: the PHENIX AutoSol wizard. *Acta Crystallogr. D Biol. Crystallogr.* **65**, 582–601 (2009).
43. Cowtan, K. The Buccaneer software for automated model building. *Acta Crystallogr. D Biol. Crystallogr.* **62**, 1002–1011 (2006).
44. Winn, M.D. *et al.* Overview of the CCP4 suite and current developments. *Acta Crystallogr. D Biol. Crystallogr.* **67**, 235–242 (2011).
45. Adams, P.D. *et al.* PHENIX: a comprehensive Python-based system for macromolecular structure solution. *Acta Crystallogr. D Biol. Crystallogr.* **66**, 213–221 (2010).
46. Emsley, P. & Cowtan, K. Coot: model-building tools for molecular graphics. *Acta Crystallogr. D Biol. Crystallogr.* **60**, 2126–2132 (2004).
47. McCoy, A.J. *et al.* Phaser crystallographic software. *J. Appl. Crystallogr.* **40**, 658–674 (2007).
48. Vonrhein, C., Blanc, E., Roversi, P. & Bricogne, G. Automated structure solution with autoSHARP. *Methods Mol. Biol.* **364**, 215–230 (2007).
49. Zhang, K.Y.J., Cowtan, K. & Main, P. Combining constraints for electron-density modification. *Methods Enzymol.* **277**, 53–64 (1997).
50. Chen, V.B. *et al.* MolProbity: all-atom structure validation for macromolecular crystallography. *Acta Crystallogr. D Biol. Crystallogr.* **66**, 12–21 (2010).
51. Behm-Ansmant, I., Gatfield, D., Rehwinkel, J., Hilgers, V. & Izaurralde, E. A conserved role for cytoplasmic poly(A)-binding protein 1 (PABPC1) in nonsense-mediated mRNA decay. *EMBO J.* **26**, 1591–1601 (2007).

Supplementary Information

Structure and assembly of the NOT module of the human CCR4-NOT complex

Andreas Boland, Ying Chen, Tobias Raisch, Stefanie Jonas, Duygu Kuzuoğlu-Öztürk, Lara Wohlbold, Oliver Weichenrieder and Elisa Izaurralde

Nature Structural and Molecular Biology: doi:10.1038/nsmb.2681

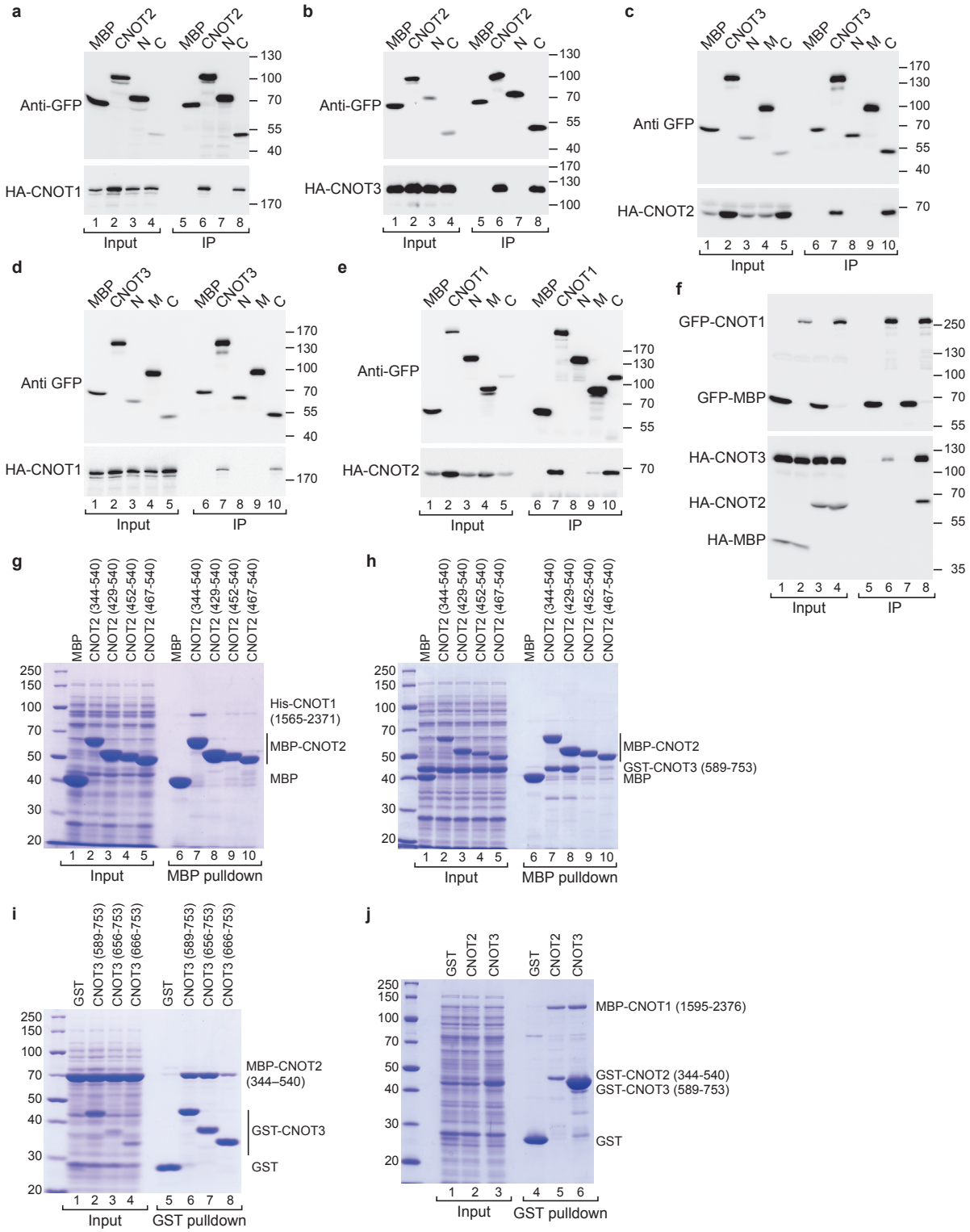

Supplementary Figure 1 CNOT1, CNOT2 and CNOT3 interact via their C-termini. (**a**,**b**) Interaction between GFP-tagged CNOT2 (full-length or fragments) and HA-tagged CNOT1 (a) and CNOT3 (b). GFP-tagged MBP served as a negative control. In all panels, cell lysates were treated with RNase A. (**c**,**d**) Interaction between GFP-tagged CNOT3 (full-length or fragments) and HA-tagged CNOT2 (c) and CNOT1 (d). (**e**,**f**) Interaction between GFP-tagged CNOT1 (full-length or fragments) and HA-tagged CNOT2 (e) and CNOT3 (f). In panel (f), the interaction with CNOT3 was analyzed in the absence (lanes 2 and 6) or presence (lanes 4 and 8) of CNOT2. (**g**) Interaction between MBP-CNOT2 fragments and His_6-tagged CNOT1 (residues 1565–2371). (**h**) Interaction between MBP-CNOT2 fragments and GST-CNOT3 (residues 589–753). (**i**) Interaction between MBP-CNOT2 (residues 344–540) and GST-CNOT3 fragments. (**j**) Interaction between MBP-CNOT1 (residues 1595–2376) and GST-CNOT2 (residues 344–540) or GST-CNOT3 (residues 589–753).

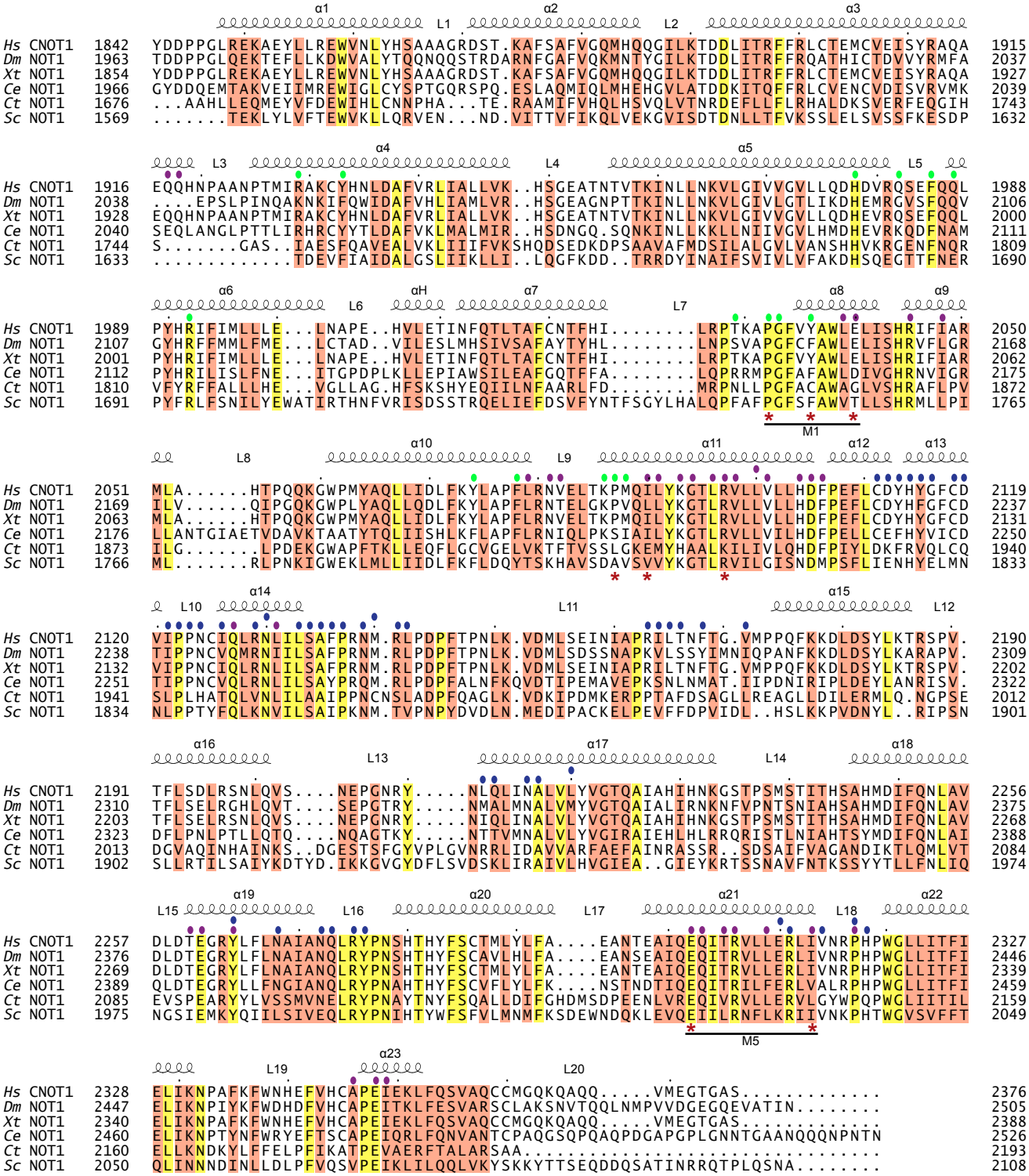

Supplementary Figure 2 Structure-based sequence alignment of the NOT1 superfamily homology (SH) domain. Secondary structure elements as determined from the Hs CNOT1 structure are shown above the alignment. Residues conserved in all aligned sequences are shown with a yellow background and residues with >70% similarity are highlighted in orange. Residues interacting with CNOT2 and CNOT3 are indicated by purple and green dots, respectively. Residues involved in CNOT1 subdomain interactions are indicated by blue dots. Residues mutated in this study are marked by red asterisks. Residues substituted in mutant M1 and M5 are indicated. The species abbreviations are as follows: *Hs* (*Homo sapiens*), *Dm* (*Drosophila melanogaster*), *Xt* (*Xenopus tropicalis*), *Ce* (*Caenorhabditis elegans*), *Ct* (*Chaetomium thermophilum*) and *Sc* (*Saccharomyces cerevisiae*).

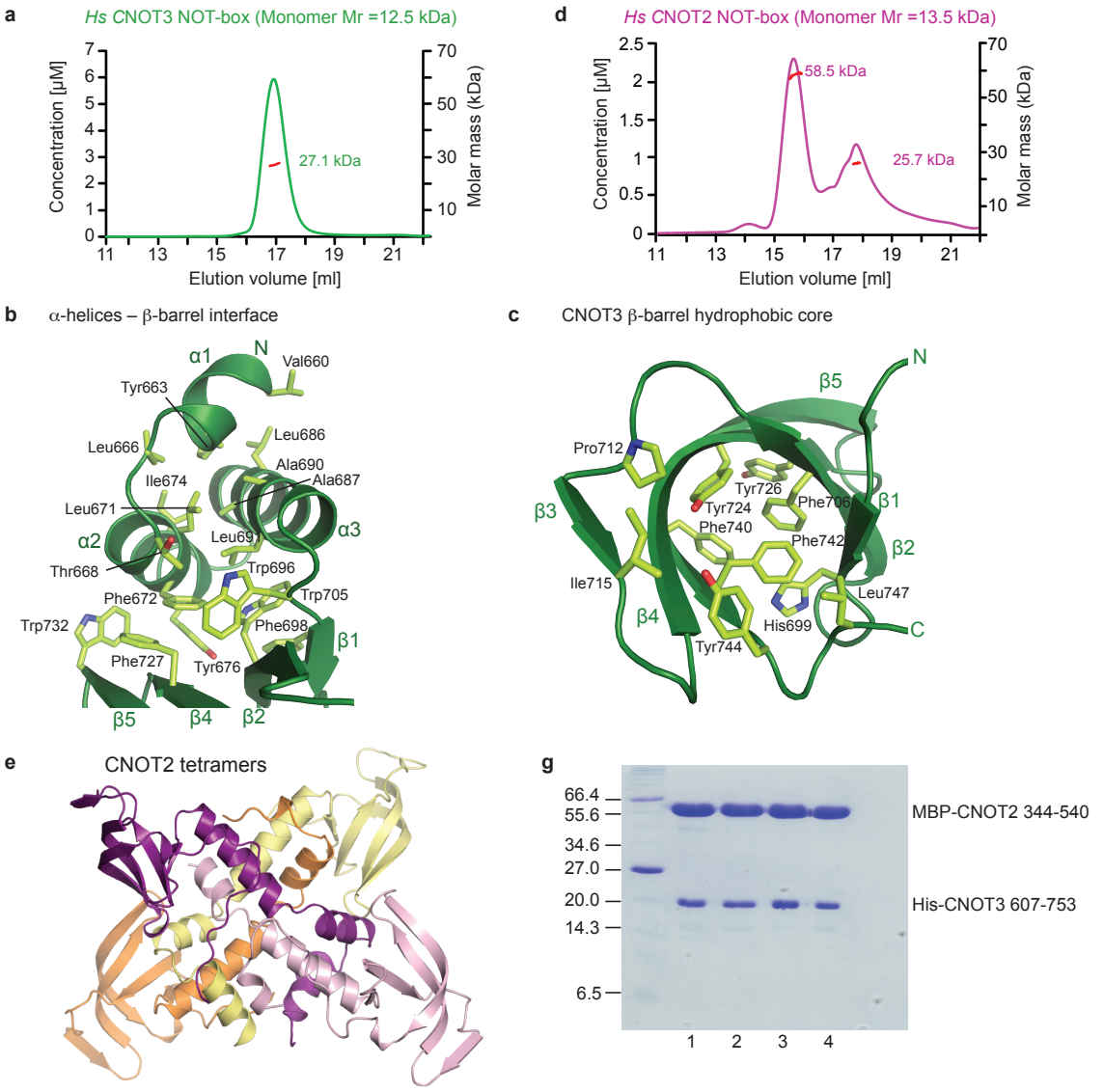

f

```
                    α1          α2                α3          β1    β2    β3    β4
                  L1    L2          L3    L4    L5    L6
Hs CNOT3  656  HSDTVEFYQRLSTETLFFIFYYLEGTKAQYLAAKALKKQSWRFHTKYMMWFQRH..EEPKTI.TDEFEQGTYIYFD  728
Dm NOT3   747  IYDTVEFYQRLSTETLFFVFYYMEGSKAQYLAAKALKKQSWRFHTKYMMWFQRH..EEPKII.NDDYEQGTYIYFD  819
Ct NOT3   529  IFDDPRLYSRIDSDTLFYVFYYKQGTYQQYLAARALKDQSWRFHKQYQTWFQRH..EEPKQI.TEEFEKGTYRFFD  601
Sc NOT3   693  YAKILENFRTLEMFSLFYNYYFAITPLEREIAYKILNERDWKVSKDGTMWFLRQ..GEVKFF.NEICEVGDYKIFK  765

Hs CNOT2  429  DKLAAIKLGRYGEDLLFYLYYMNGGDVLQLLAAVELFNRDWRYHKEERVWITRAPGMEPTMK.TNTYERGTYYFFD  503
Dm NOT2   478  DKLTAPVLKKLQEDLLFFLFYTNIGDMMQLMAAAELHSREWRYHVEEKIWITRIPGIDQYEK.NGTKERGTFYYFD  552
Ct NOT2   262  VQPIEAKISSFNEETLMWIFYSCPRDIKQQMAAIELNNRNWRWHKKLQLWLTKDDLMAPQVL.GPNHERGYYVVWD  336
Sc NOT2    97  IQNDQQRVALFQDETLFFLFYKHPGTVIQELTYLELRKRNWRYHKTLKAWLTKDPMMEPIVSADGLSERGSYVFFD  172

                      L7      β5
Hs CNOT3  729  YEK.WGQRKKEGFTFEYRYLEDRDLQ.....................................................  753
Dm NOT3   820  YEK.WSQRKKEGFTFEYKYLEDKELN.....................................................  844
Ct NOT3   602  LDD.WTVIDKINFRLDYSFLQPPVDTASEVRDVSVDNNN(33).....................................  694
Sc NOT3   766  YESTWMNRRKADFEFHYKYLEDELVHLNTGQSVMALRYR(54).....................................  836

Hs CNOT2  504  CLN.WRKVAKE.FHLEYDKLEERPHLPSTFNYNPAQQAF.....................................  540
Dm NOT2   553  AQS.WKRLSKV.FQIDPEKLDKCPNISAFMNGQSV...........................................  585
Ct NOT2   337  TVN.WRKERRE.LTLHYADLDTNPGTPLQSIAA.............................................  367
Sc NOT2   173  PQR.WEKCQRD.FLLFYNAIM.........................................................  191
```

Supplementary Figure 3 CNOT2 and CNOT3 multimerize in solution. (**a**,**d**) MALLS analysis of the CNOT3 and CNOT2 NOT-box domains, respectively. The molecular weight of the protein in solution is indicated in the elution profile. (**b**) Interfaces between the CNOT3 NOT-box α-helices and the β-barrel. Residues along the interfaces are shown as sticks. (**c**) Hydrophobic core of the CNOT3 NOT-box β-barrel. (**e**) Structure of the CNOT2 tetramer as observed in the crystal. The tetramer consists of two pairs of dimers (orange-yellow vs. purple-rose) with a perpendicular orientation to each other. (**f**) Structure-based sequence alignments of the NOT2 and NOT3 NOT-box domains. Secondary structure elements as determined from the CNOT2 and CNOT3 structures are shown above the alignment. Residues conserved in all aligned sequences are shown with a yellow background, and residues with >70% similarity are highlighted in orange. A NOT2-specific insertion is boxed in purple. Black squares mark residues that form the interface between the NOT-Box N-terminal α-helices and the β-barrel. Gray squares mark residues that form the hydrophobic core of the β-barrel. The species abbreviations are the same as those in **Supplementary Fig. 2**. (**g**) Pulldowns showing that CNOT2-C and CNOT3-C exclusively form heterodimers in solution. MBP-tagged CNOT2 and His6-tagged CNOT3 were coexpressed in E. coli. The heterodimers were copurified using MBP pulldown followed by Ni-affinity purification (lanes 1 and 2) or Ni-affinity purification followed by MBP pulldown (lanes 3 and 4).

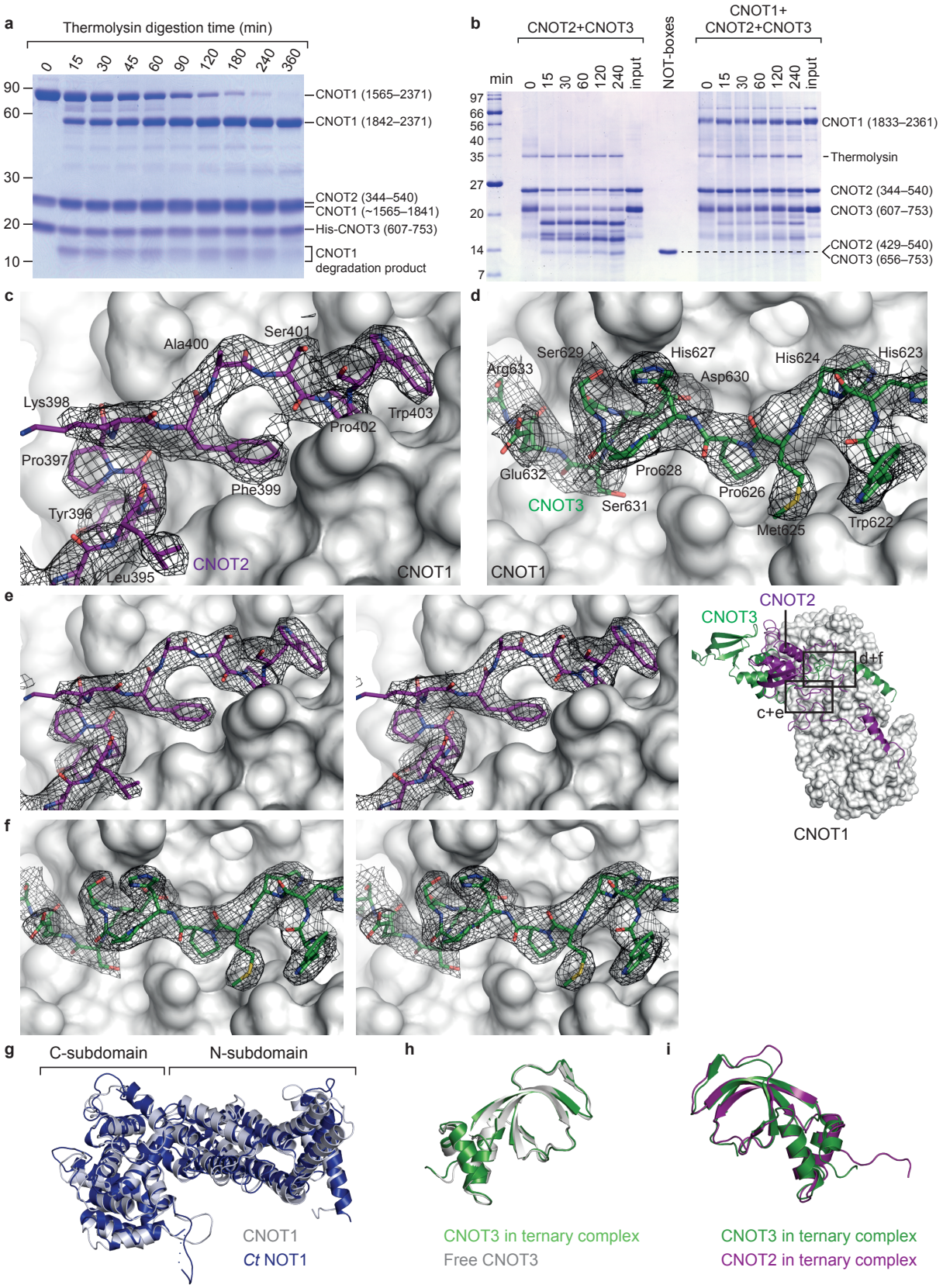

Supplementary Figure 4 Structure of the NOT module. (**a**) Time course of a limited proteolysis of the ternary complex between CNOT1 (residues 1565–2371), CNOT2 (residues 344–540) and CNOT3 (residues 607–753) by thermolysin. CNOT1 is digested into a stable C-terminal fragment corresponding to the SH and an N-terminal fragment (which comigrates with CNOT2), while CNOT2 and CNOT3 remain uncleaved. (**b**) Time course of a limited proteolysis of CNOT2 (residues 344–540) and CNOT3 (residues 607–753) by thermolysin in the absence or presence of CNOT1 SH (1833–2361). In the absence of CNOT1, CNOT2 and CNOT3 are digested into stable C-terminal fragments corresponding approximately to the NOT-boxes and the CSs, but they remain largely uncleaved in the presence of CNOT1 (**c**,**d**) Omit electron density map of the CNOT2 (c) and CNOT3 (d) NAR-Cs folded onto the CNOT1 surface. The electron density (black mesh, 2F0-FC of a composite omit map, calculated with Phenix.AutoBuild) is contoured at 1.0 σ. (**e**,**f**) Refined electron density of the CNOT2 (e) and CNOT3 (f) NAR-C regions in stereo view. The views correspond to panels (c) and (d), respectively. The electron density (black mesh, 2F0-FC map) is contoured at 1.0 σ. (**g**) Superposition of Ct NOT1 (blue) and Hs CNOT1 (gray) showing strong structure conservation. (**h**) Superposition of the CNOT3 NOT-box domain in isolation (gray) and in the complex (green). (**i**) Superposition of the NOT-box domains of CNOT2 (purple) and CNOT3 (green) as observed in the ternary complex.

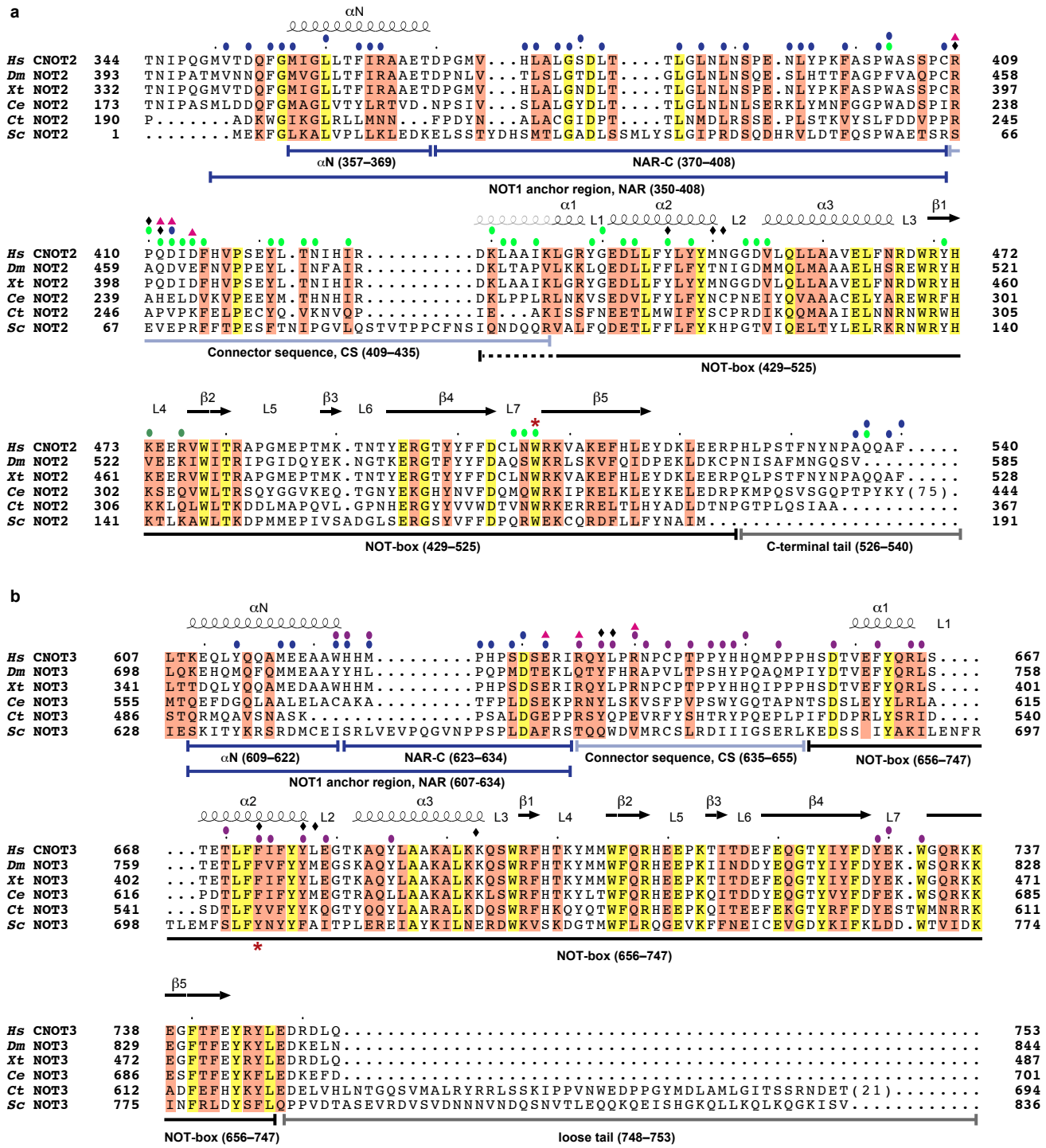

Supplementary Figure 5 Structure-based sequence alignment of the CNOT2 and CNOT3. Secondary structure elements as determined from the CNOT2 and CNOT3 structure are shown above the alignment. Symbols are as described in **Supplementary Fig. 2**. Residues interacting with the respective partner proteins are indicated by dots above the alignments and are colored blue for CNOT1, purple for CNOT2 and green for CNOT3. Residues forming the lock are marked with black diamonds, and residues at the junction between the symmetric and asymmetric lobes of the ternary complex are marked with pink triangles. The species abbreviations are the same as those in **Supplementary Fig. 2**.

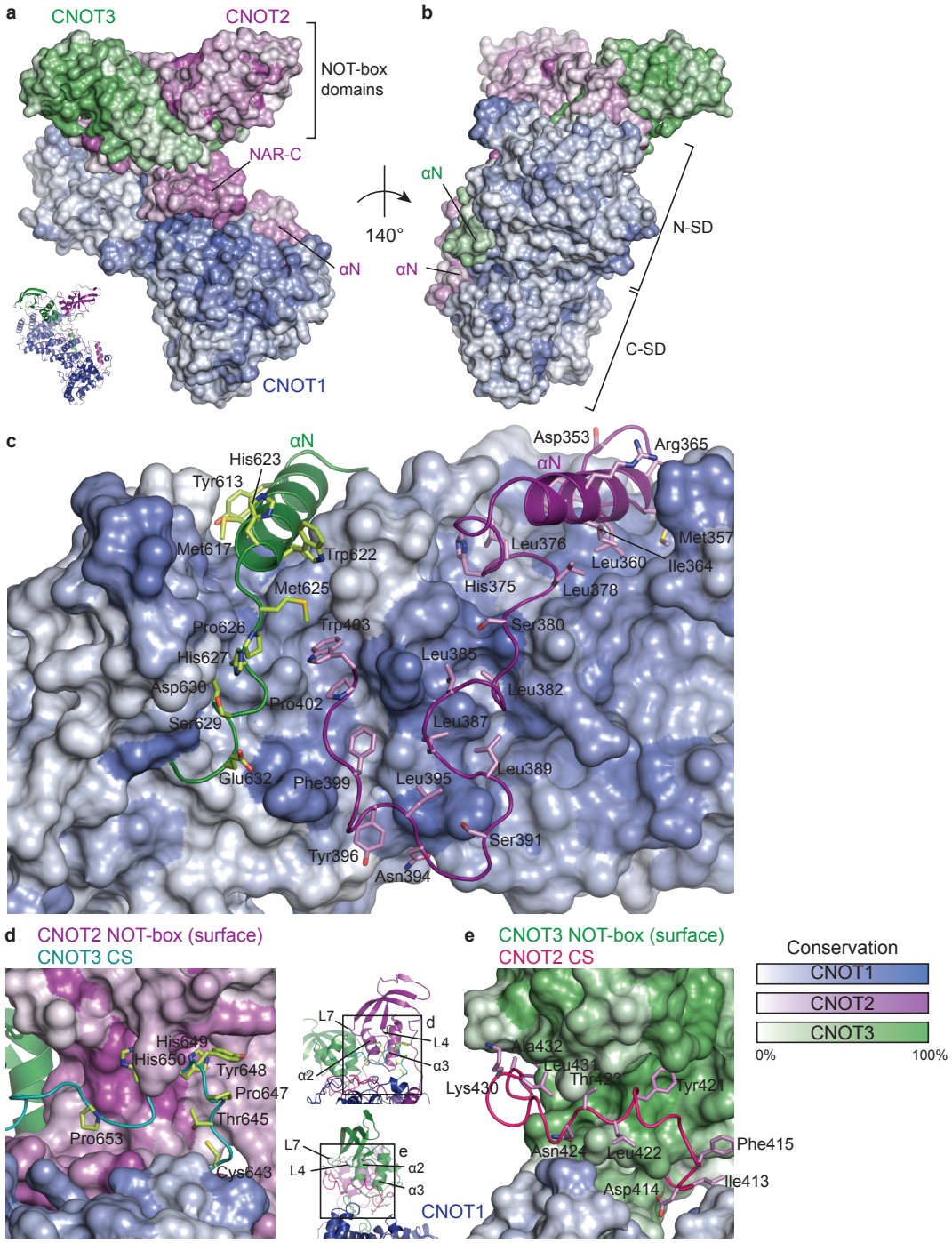

Supplementary Figure 6 Surface conservation of the trimeric complex. (**a**–**e**) The conservation scores of the individual residues are represented on the surface by color gradients from light (no conservation) to dark colors (100% conservation) for CNOT1 (blue), CNOT2 (purple) and CNOT3 (green). Conservation scores were calculated based on well-balanced multiple alignments covering all eukaryotic strata. (a) View from the CNOT1 surface that binds CNOT2 and CNOT3 (a) or the opposite surface (b). Conservation of the CNOT1 surface contacting CNOT2 and CNOT3 (c). The view is the same as that shown in **Fig. 5a**. (d) Conservation of CNOT2 surface residues contacting the CNOT3 connector sequence (CS). The CNOT3 residues involved in the interaction with CNOT2 are shown as sticks. (e) Conservation of CNOT3 surface contacting the CNOT2 connector sequence (CS). The CNOT2 residues involved in CNOT3 binding are shown as sticks.

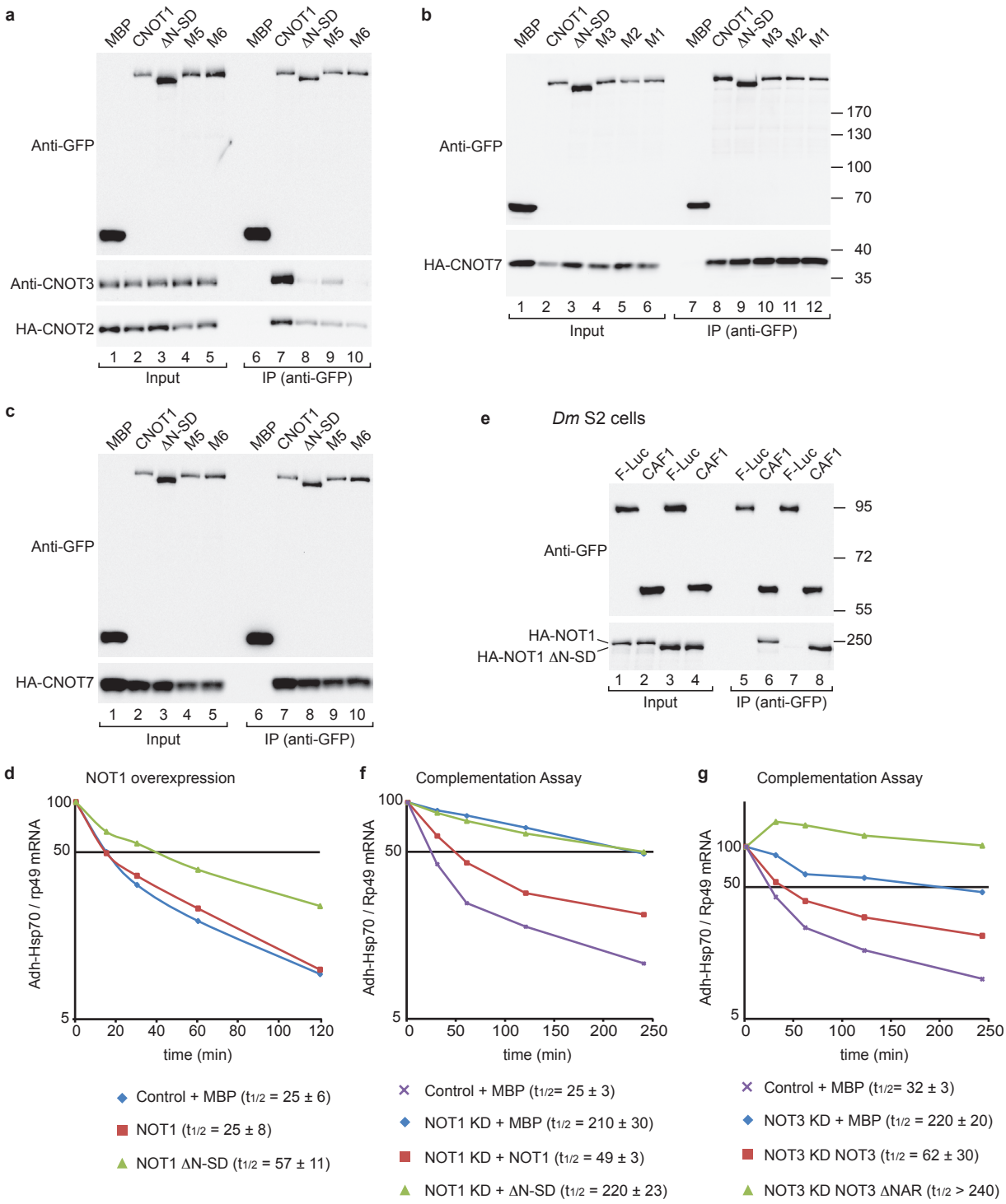

Supplementary Figure 7 Mutagenesis of the NOT1-NOT2-NOT3 interfaces in human and Dm S2 cells. (**a**) Interaction of GFP-CNOT1 (either wild-type or the indicated mutants) with endogenous CNOT3 and HA-CNOT2. (**b**,**c**) Interaction of GFP-CNOT1 (either wild-type or the indicated mutants) with HA-CNOT7 in human cells. (**d**) The decay of the adh-hsp70 mRNA was monitored in control cells (expressing MBP) and in cells expressing NOT1 (either wild-type or mutant). Adh-hsp70 mRNA levels were normalized to the levels of long-lived rp49 mRNA and plotted against time. A representative Northern blot is shown in Fig. 7a. The mRNA half-lives (t1/2) ± standard deviations calculated from the decay curves obtained from three independent experiments are indicated. (**e**) Interaction of GFP-tagged Dm CAF1 with wild-type NOT1 or NOT1ΔN-SD in S2 cells. F-Luc-GFP served as a negative control. (**f**,**g**) The decay of adh-hsp70 mRNA was analyzed in control cells (treated with GFP dsRNA and expressing MBP) or in cells depleted of NOT1 or NOT3 and expressing MBP or the indicated proteins. Northern blots corresponding to the decay curves are shown in **Fig. 7c** and **7d**, respectively. Adh-hsp70 mRNA levels were normalized to the levels of rp49 mRNA and plotted against time. The mRNA half-lives (t1/2) ± standard deviations obtained from three independent experiments are indicated.

Fig 6a

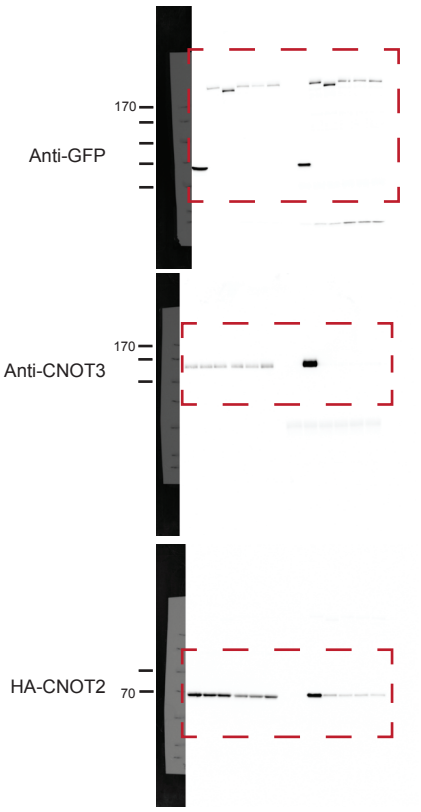

Fig 6b

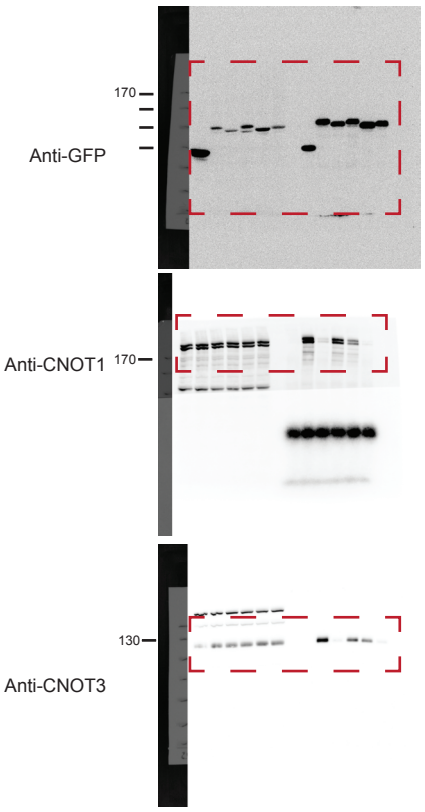

Fig 6c

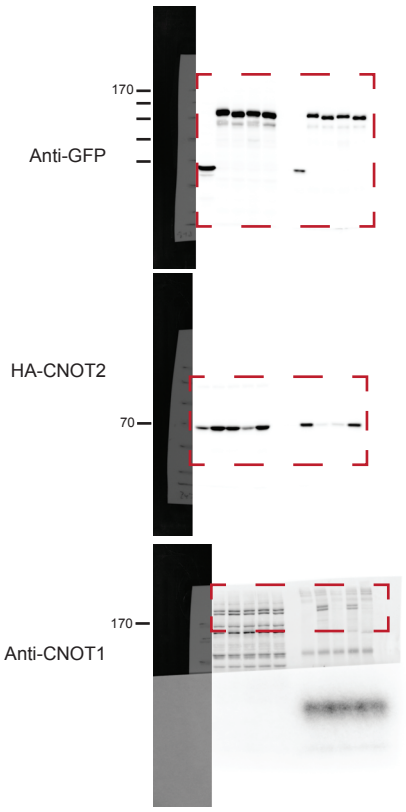

Fig 6d

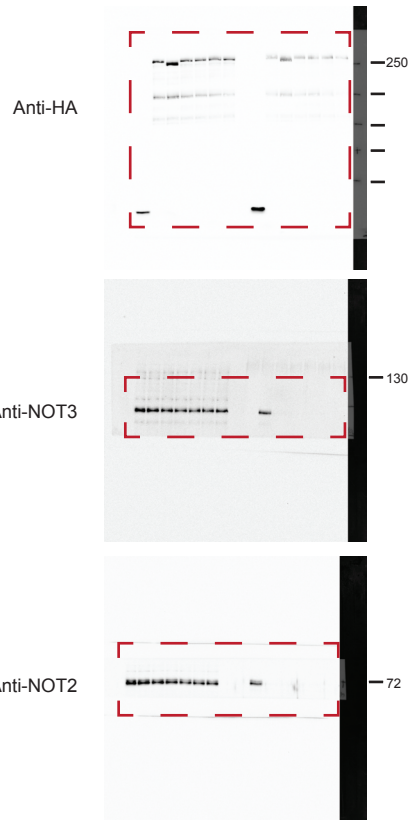

Fig 6e

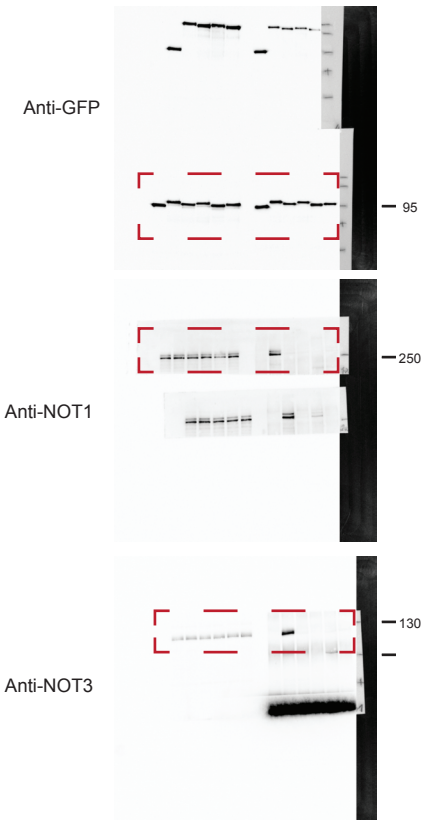

Fig 6f

Nature Structural and Molecular Biology: doi:10.1038/nsmb.2681

Fig 7a

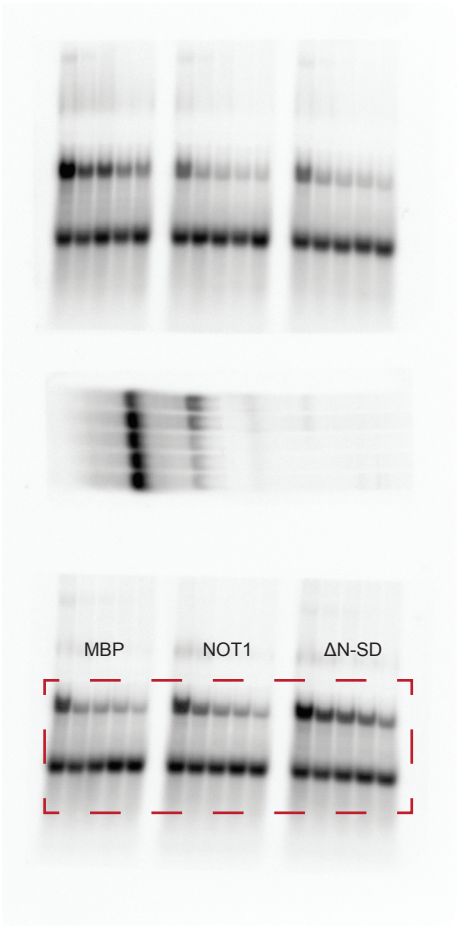

Fig 7d

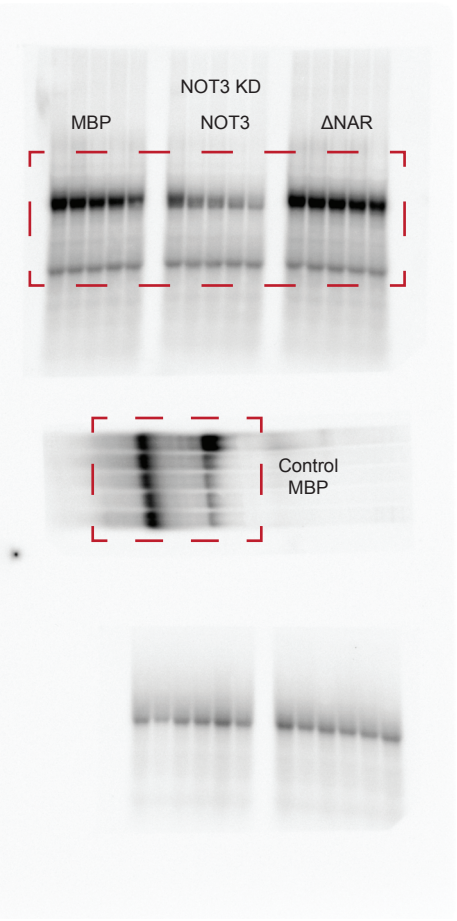

Fig 7c

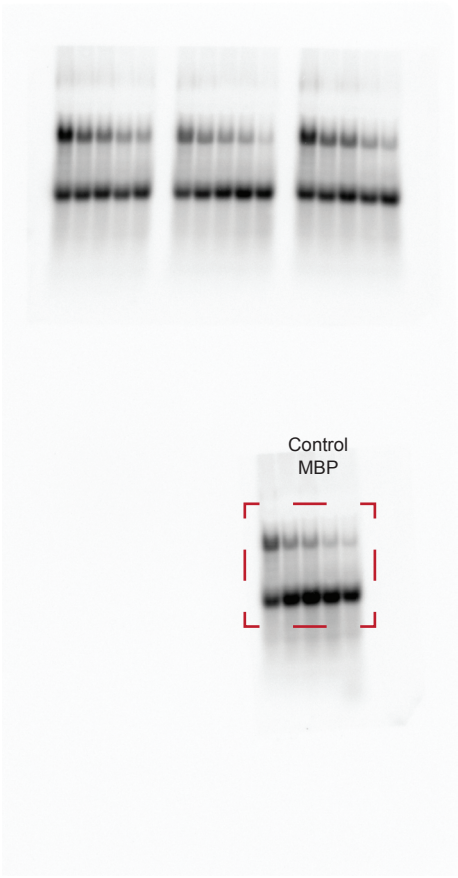

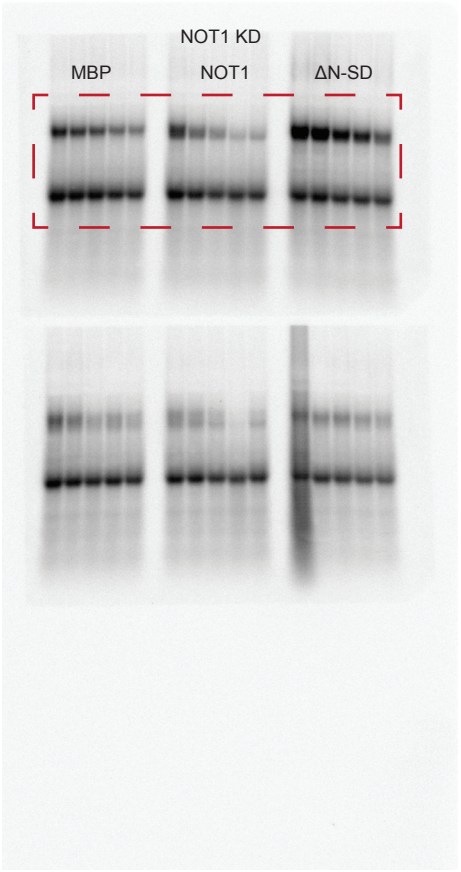

Fig 7b

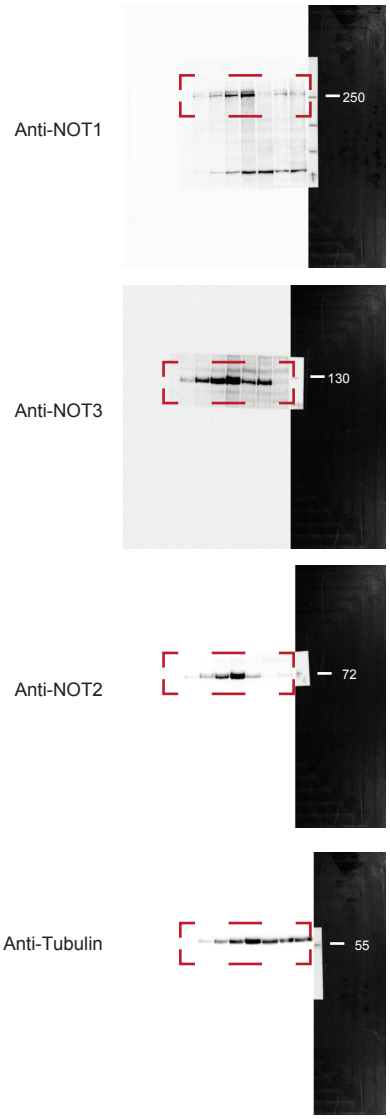

Fig 7e

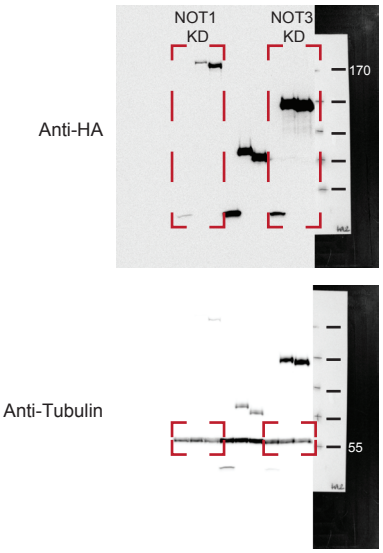

Supplementary Figure 8 Original images of gels, western and northern blots used in this study.

Supplementary Table 1. Mutants used in this study

Name	***Dm* NOT1**	***Hs* CNOT1**
ΔN-SD	Δ1967-2251	Δ1844-2133
M1	P2150Y, F2152C, E2158A, P2205Q, L2208E	P2032Y, Y2036C, E2040A
M2	P2150Y, F2152C, E2158A, P2205Q, L2208E, E2421A	P2032Y, Y2036C, E2040A, P2087Q, I2090E, E2302A
M3	P2150Y, F2152C, E2158A, P2205Q, E2421A, L2208E, R2215D	P2032Y, Y2036C, E2040A, P2087Q, I2090E, R2097D, E2302A, I2313R
M4	P2150Y, F2152C, E2158A, P2205Q, E2421A, L2208E, R2215D, I2432R	
M5		E2302A+I2313R
M6		R2097D+I2313R
CNOT1-N		1–1089
CNOT1-M		1085–1605
CNOT1-C		1595–2376

Name	***Dm* NOT2**	***Hs* CNOT2**
ΔN-CS	Δ 458–482	Δ 409–432
ΔαN	Δ 393–429	Δ 344–380
ΔN-NAR-C	Δ 429–453	Δ 380–404
L7	W556E	W507E
CNOT2-N		1–352
CNOT2-C		344–540

Name	***Dm* NOT3**	***Hs* CNOT3**
ΔN-CS	Δ 723–745	Δ 632–654
ΔNAR	Δ 698–725	Δ 607–634
α2	F764E	F673E
CNOT3-N		1–241
CNOT3-M		239–590
CNOT3-C		589–753

Molecular Cell
Article

A DDX6-CNOT1 Complex and W-Binding Pockets in CNOT9 Reveal Direct Links between miRNA Target Recognition and Silencing

Ying Chen,[1,2] Andreas Boland,[1,2] Duygu Kuzuoğlu-Öztürk,[1,2] Praveen Bawankar,[1] Belinda Loh,[1] Chung-Te Chang,[1] Oliver Weichenrieder,[1,*] and Elisa Izaurralde[1,*]
[1]Department of Biochemistry, Max Planck Institute for Developmental Biology, Spemannstrasse 35, 72076 Tübingen, Germany
[2]Co-first authors
*Correspondence: oliver.weichenrieder@tuebingen.mpg.de (O.W.), elisa.izaurralde@tuebingen.mpg.de (E.I.)
http://dx.doi.org/10.1016/j.molcel.2014.03.034

SUMMARY

CCR4-NOT is a major effector complex in miRNA-mediated gene silencing. It is recruited to miRNA targets through interactions with tryptophan (W)-containing motifs in TNRC6/GW182 proteins and is required for both translational repression and degradation of miRNA targets. Here, we elucidate the structural basis for the repressive activity of CCR4-NOT and its interaction with TNRC6/GW182s. We show that the conserved CNOT9 subunit attaches to a domain of unknown function (DUF3819) in the CNOT1 scaffold. The resulting complex provides binding sites for TNRC6/GW182, and its crystal structure reveals tandem W-binding pockets located in CNOT9. We further show that the CNOT1 MIF4G domain interacts with the C-terminal RecA domain of DDX6, a translational repressor and decapping activator. The crystal structure of this complex demonstrates striking similarity to the eIF4G-eIF4A complex. Together, our data provide the missing physical links in a molecular pathway that connects miRNA target recognition with translational repression, deadenylation, and decapping.

INTRODUCTION

miRNAs are endogenous noncoding RNAs that associate with Argonaute proteins (AGOs) into miRNA-induced silencing complexes (miRISCs) and posttranscriptionally silence the expression of mRNAs containing complementary sequences (Ameres and Zamore, 2013). In animals, most mRNA targets are only partially complementary to the miRNA. As a result, even catalytically active AGOs cannot cleave the mRNA target and recruit additional proteins to mediate silencing (Fabian and Sonenberg, 2012; Braun et al., 2013).

GW182 proteins are the best-characterized AGO-binding partners required for miRNA-mediated silencing in animal cells (Fabian and Sonenberg, 2012; Braun et al., 2013). There are three GW182 paralogs (termed TNRC6A, TNRC6B, and TNRC6C) in vertebrates and only one family member in *Drosophila melanogaster* (*Dm* GW182; Braun et al., 2013). These proteins bind directly to AGOs via multiple GW (glycine and tryptophan) repeats present in the N-terminal AGO-binding domain and then recruit effector complexes, such as the CCR4-NOT and PAN2-PAN3 deadenylase complexes (Braun et al., 2013).

Similar to the interaction with AGOs, GW182 proteins interact with the deadenylase complexes through W-containing motifs, which in this case are located in their C-terminal silencing domains (SDs) (Figure 1A; Braun et al., 2011; Chekulaeva et al., 2011; Christie et al., 2013; Fabian et al., 2011; Huntzinger et al., 2013). The crystal structures of human AGO2 and *Dm* PAN3 homodimers have revealed the molecular basis for their interaction with the W-containing motifs in GW182 proteins (Schirle and MacRae, 2012; Christie et al., 2013). However, it is not known how the W motifs interact with the CCR4-NOT complex.

The CCR4-NOT complex consists of several independent modules that dock with the NOT1 subunit, which serves as a scaffold for complex assembly (Wahle and Winkler, 2013). NOT1 consists of an N-terminal (NOT1-N), middle (NOT1-M), and C-terminal (NOT1-C) region (Figures 1A and S1A available online). The NOT1-M region comprises two domains: a MIF4G domain that is structurally related to the middle domain of eIF4G and a domain of unknown function (DUF3819). The MIF4G domain interacts with the catalytic module of the CCR4-NOT complex, comprising the two deadenylases CAF1 (or its paralog POP2) and CCR4a (or its paralog CCR4b) (Wahle and Winkler, 2013). The DUF3819 domain interacts with the highly conserved Armadillo (ARM) repeat domain of the CNOT9 subunit (Figure 1A; also known as CAF40, RQCD1, or RCD1) (Bawankar et al., 2013). Importantly, the CNOT1-M region has been shown to mediate the interaction of CCR4-NOT with the silencing domain of TNRC6C (6C-SD) (Huntzinger et al., 2013). Furthermore, the RNA helicase DDX6 (also known as Dhh1, RCK/p54, or Me31B) also interacts with CNOT1 (Coller et al., 2001; Hata et al., 1998; Maillet and Collart, 2002). DDX6 functions as a translational repressor and decapping activator (Presnyak and Coller, 2013) and has previously been implicated in the miRNA pathway (Chu and Rana, 2006; Eulalio et al., 2007; Nishihara et al., 2013).

The CCR4-NOT complex not only mediates mRNA deadenylation, but it is also required both for the translational

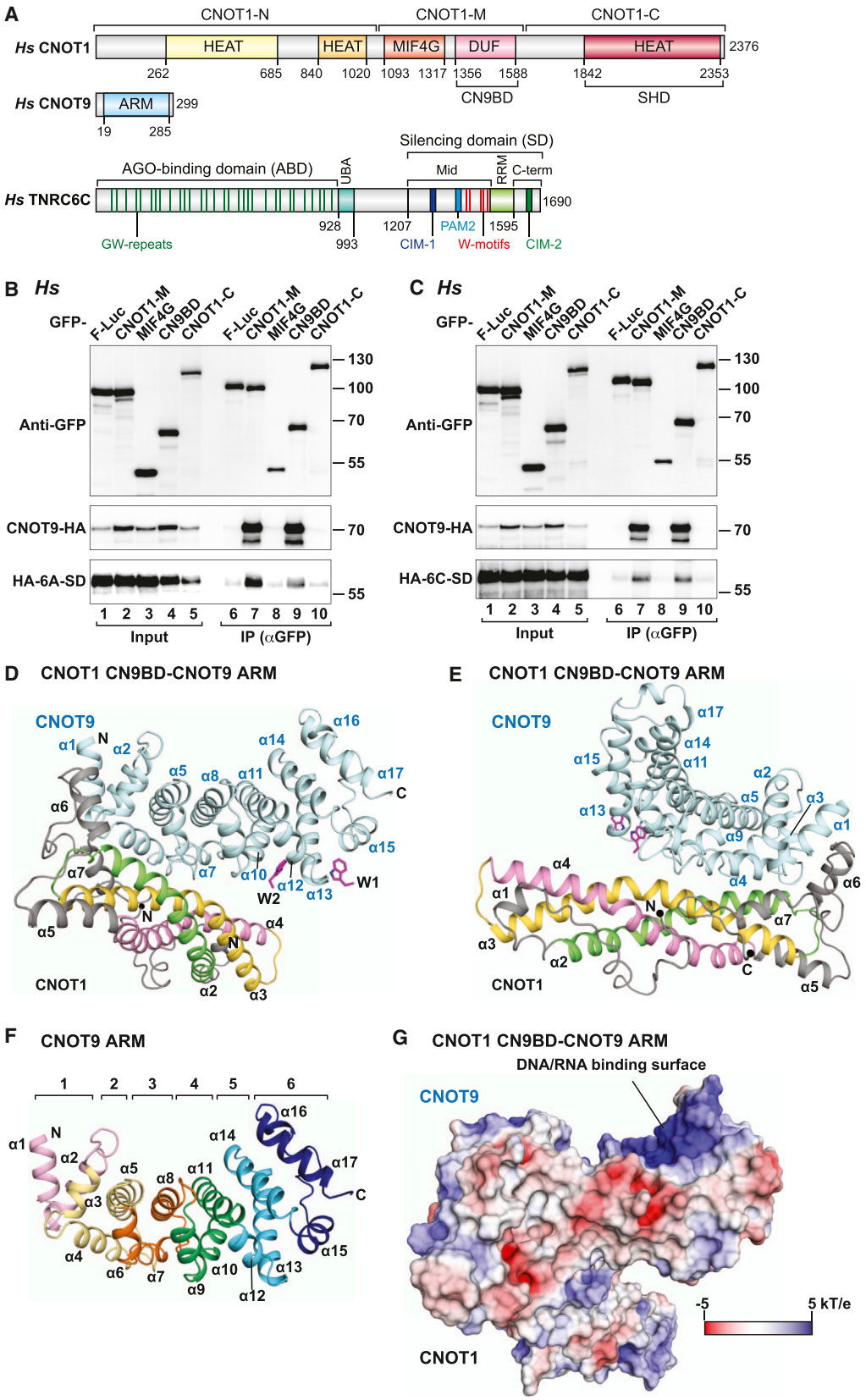

(legend on next page)

repression and degradation of miRNA targets (Braun et al., 2011; Chekulaeva et al., 2011; Fabian et al., 2011; Huntzinger et al., 2013; Zekri et al., 2013). miRNA target degradation is catalyzed by the enzymes of the 5′-to-3′ mRNA decay pathway (Huntzinger and Izaurralde, 2011). In this pathway, mRNAs are first deadenylated by the CCR4-NOT complex, decapped by the decapping enzyme DCP2 and additional coactivators, and finally degraded from the 5′ end by the exonuclease XRN1. However, it has remained unclear whether and how decay factors, including the decapping enzyme DCP2 and the 5′ exonuclease XRN1, would be recruited directly by the CCR4-NOT complex. Similarly, the mechanism of translational repression by CCR4-NOT has remained elusive, although it has recently been proposed that the DEAD-box protein eIF4A2 may play a role (Meijer et al., 2013). In particular, it was suggested that the CNOT1 MIF4G domain could recruit eIF4A2 via an interaction similar to the one observed in the eIF4G-eIF4A complex (Meijer et al., 2013). eIF4A2 could then prevent ribosome scanning by clamping onto the 5′ UTR of the mRNA (Meijer et al., 2013).

In this study, we investigated the molecular basis for the interactions mediated by the human CNOT1-M region and its role in silencing. We show that the CNOT1 DUF3819 domain forms a binary complex with the ARM repeat domain of the CNOT9 subunit and was hence termed the CN9BD (*CAF40/CNOT9 b*inding *d*omain). We pinpoint the CN9BD-CNOT9 complex as a primary binding site for the TNRC6 silencing domains (TNRC6-SDs) in the CNOT1-M region. The crystal structure of the CN9BD-CNOT9 complex shows that the CN9BD adopts a defined fold that is recognized and stabilized by CNOT9 binding. This structure also reveals tandem W-binding pockets in CNOT9, suggesting a mechanism for the recruitment of the CCR4-NOT complex by W-rich GW182/TNRC6 proteins. Furthermore, we identified the CNOT1 MIF4G domain as a specific binding partner for DDX6 rather than eIF4A2. The crystal structure of the MIF4G-DDX6 complex reveals an eIF4G-eIF4A-like interaction, which is compatible with the simultaneous binding of CAF1 to the MIF4G domain and the recruitment of decapping factors (EDC3, LSm14A, or Pat) by DDX6. Together, our data now allow us to trace the direct molecular interactions that ultimately lead from miRNA target recognition to the translational repression, deadenylation, and decapping of the mRNA target.

RESULTS

Dual Functions of the CNOT1 DUF3819 Domain in TNRC6 and CNOT9 Binding

To pinpoint the TNRC6-SD binding site within the CNOT1-M region (Figures 1A and S1A), we performed coimmunoprecipitation assays in human embryonic kidney 293T (HEK293T) cells. We found that TNRC6A-SD and TNRC6C-SD interacted primarily with the DUF3819 domain rather than with the MIF4G domain (Figures 1B and 1C, lane 9), overlapping with the sequences required to bind the ARM repeat domain of CAF40/CNOT9 in human cells (Figures 1B and 1C, lane 9, and S1B) and in *Dm* Schneider (S2) cells (Figure S1C; Bawankar et al., 2013). The DUF3819 domain was therefore termed the CAF40/CNOT9 binding domain or CN9BD.

To elucidate the molecular basis for the observed interactions, we expressed suitable protein constructs in *Escherichia coli* (Table S1) and used specific tags for pull-down assays (Figure S1B) and protein purification. The ARM repeat domain of CNOT9 (residues 19–285) formed homodimers in solution, as observed previously (Garces et al., 2007) and as confirmed by size-exclusion chromatography and multiangle static laser light scattering (MALLS; Figure S1D). Protein constructs corresponding to the CN9BD precipitated upon removal of the solubility tag, indicating instability or improper folding in the absence of CNOT9. However, several CN9BD constructs (residues 1,356–1,581, 1,356–1,607, and 1,356–1,628) could be coexpressed and copurified with the ARM repeat domain of CNOT9 (Figure S1B). Under these conditions, size-exclusion chromatography and MALLS indicate the formation of a binary CN9BD-CNOT9 complex that appears to be mutually exclusive with CNOT9 homodimerization (Figures S1D and S1E).

We obtained crystals of the CN9BD-CNOT9 complex that diffracted X-rays to a 1.65 Å resolution (Table 1). Crystals were exclusively obtained using the CN9BD 1,356–1,607 construct, although a shorter construct (CN9BD 1,356–1,581) was also soluble and formed a binary complex with CNOT9 (Figure S1B). In a bid to identify putative TNRC6 binding sites, we also crystallized the complex in the presence of L-tryptophan (W). These crystals diffracted X-rays to a 2.05 Å resolution (Table 1).

Figure 1. Structure of the CNOT1 CN9BD Bound to the CNOT9 ARM Repeat Domain

(A) Diagram of CNOT1 with N-terminal, middle, and C-terminal regions (CNOT1-N, CNOT1-M, and CNOT1-C, respectively). CNOT1-N consists of two HEAT-like repeat domains. CNOT1-M contains an MIF4G domain and the CN9BD (previously DUF3819). CNOT1-C contains the NOT1 superfamily homology domain (SHD). CNOT9 contains an armadillo (ARM) repeat domain. TNRC6C contains and N-terminal AGO-binding domain (ABD), a ubiquitin-associated-like domain (UBA), and a C-terminal silencing domain (SD). The SD comprises a Mid region, an RNA recognition motif (RRM), and a C-terminal (C-term) region. The positions of the CCR4-NOT interacting motifs 1 and 2 (CIM-1 and CIM-2) and the PAM2 motif (PABP-interacting motif 2) are indicated. Vertical green and red lines indicate the positions of W-containing motifs binding to AGOs and deadenylases, respectively. Amino acid positions at domain boundaries are indicated below the protein outlines. See also Figure S1A.

(B and C) Western blot showing the interaction between GFP-CNOT1 fragments and HA-MBP-tagged CNOT9 and HA-tagged TNRC6A-SD (6A-SD) or TNRC6C-SD (6C-SD) in HEK293T cells. GFP-F-Luc served as a negative control. See also Figures S1B–S1H.

(D and E) Overall structure of the CN9BD-CNOT9 binary complex in two orientations. CNOT9 is shown in cyan; the three long α helices in the CNOT1 CN9BD are shown in pink, yellow, and green. Bound W residues are shown as magenta sticks. Secondary structure elements are labeled in blue for CNOT9 and in black for CNOT1.

(F) Cartoon representation of the ARM repeat domain of CNOT9. The ARM repeats are colored in a gradient from pink to dark blue from the N to C terminus.

(G) Surface representation of the CN9BD-CNOT9 binary complex in the same orientation as that in (D) and colored according to surface potential contoured from −5 kT/e (red) to +5 kT/e (blue). The position of the DNA/RNA binding surface is indicated. See also Figures S1F and S1G.

Table 1. Data Collection and Refinement Statistics

Data Set	CNOT1-CNOT9 Complex	CNOT1-CNOT9-W Complex	CNOT1-DDX6 Complex
Space group	C2	C2	$P2_1\,2_1\,2_1$
Unit Cell			
Dimensions (a / b / c) (Å)	154.8 / 67.2 / 72.3	154.1 / 66.8 / 72.0	43.9 / 90.8 / 95.8
Angles (α / β / γ) (°)	90 / 99.6 / 90	90 / 100.3 / 90	90 / 90 / 90
Data Collection			
Wavelength (Å)	1.000	1.000	1.000
Resolution range (Å)	76.3–1.65 (1.69–1.65)	61.1–2.05 (2.10–2.05)	65.9–1.75 (1.80–1.75)
R_{sym} (%)	2.9 (63.6)	6.0 (78.6)	5.3 (78.9)
Completeness (%)	99.5 (99.0)	99.5 (99.0)	99.2 (99.5)
Mean $I/\sigma(I)$	19.8 (1.8)	14.9 (1.8)	17.1 (2.3)
No. of unique reflections	87,658 (6,377)	45,149 (3,317)	39,120 (2,837)
Multiplicity	3.4 (3.4)	6.8 (6.4)	5.0 (5.0)
Refinement			
Data range (Å)	76.3–1.65	61.1–2.05	47.9–1.75
R_{work} (%)	16.0	17.6	16.2
R_{free} (%)	17.9	21.5	20.3
No. of Atoms per Asymmetric Unit			
All atoms (no H)	4,590	4,178	3,386
Nonsolvent	4,116	4,030	3,193
Water	474	148	193
Average B Factor (Å^2)			
All atoms	38.5	64.3	31.3
Nonsolvent	37.9	64.5	30.7
Water	43.6	58.7	41.3
Ramachandran Plot			
Favored regions (%)	99.0	98.8	99
Disallowed regions (%)	0	0	0
Root-Mean-Square Deviation from Ideal Geometry			
Bond lengths (Å)	0.011	0.006	0.011
Bond angles (°)	1.27	0.88	1.31

Values in parentheses are for highest-resolution shell.

Crystal Structures of the CN9BD-CNOT9 Complex

The structures were solved by molecular replacement using the CNOT9 structure (Protein Data Bank ID code [PDB] 2FV2; Garces et al., 2007) as a search model and refined to final R_{free} values of 17.9% in the absence and 21.5% in the presence of L-tryptophan (Table 1 and Figures 1D and 1E). Overall, the two structures are highly similar and superpose with a root-mean-square deviation (rmsd) of 0.16 Å over 431 Cα atoms. The CN9BD-CNOT9 complex adopts a V-shaped architecture resulting from the rod-shaped CN9BD bound to the N-terminal, convex surface of the crescent-shaped CNOT9 (Figure 1E).

CNOT9 consists of 17 α helices arranged into 6 imperfect ARM repeats (Figures 1F and S2). The structure of CNOT9 in the complex is virtually identical to the structure of the isolated CNOT9 ARM repeat domain (rmsd of 0.51 Å over 246 equivalent Cα positions; Figure S1F; Garces et al., 2007), indicating that CNOT9 does not undergo major structural rearrangements upon binding to CNOT1. The CN9BD-CNOT9 interface partially overlaps with the CNOT9 homodimerization interface, as determined from the structure of the isolated CNOT9 (Figure 1D versus S1G and Figures S3A–S3D; Garces et al., 2007). This observation explains why CNOT1 binding is mutually exclusive with CNOT9 homodimerization. In both of these alternative complexes, a positively charged cleft located on the opposite, concave face of the CNOT9 crescent remains exposed and fully accessible to interact with potential RNA or DNA ligands (Figure 1G; Garces et al., 2007).

Intriguingly, the C-terminal tail of the CN9BD (residues 1,589–1,607) is largely disordered but required for crystallization. It makes a crystal contact with a neighboring CNOT9 molecule, inserting W1603 into a specific W-binding pocket (pocket 1). Consequently, W1603 is clearly defined in both structures (Figures 1D and 1E; W1); at 1.65 Å resolution, the backbone of the flanking residues 1,601–1,604 is also visible (see below). A second W-binding pocket (pocket 2) on CNOT9 becomes apparent and occupied in the presence of additional L-tryptophan in the crystallization solution (Figures 1D and 1E; W2).

CN9BD Folds into a Defined Domain Arranged as a Three-Helix Bundle

In contrast to all CNOT1 subdomains structurally determined so far, the CN9BD is not organized into HEAT-like repeats. Instead, it is composed of seven α helices, with helices α2–α4 arranged as an antiparallel, rod-shaped bundle of three kinked α helices (Figures 1D and 1E). These helices comprise 42–44 residues and are kinked once (α3) or twice (α2 and α4). The side of the bundle that binds CNOT9 is flanked by three additional short helices (helices α5–α7; Figures 1E and S4). Two of these helices (α6 and α7), together with the connecting loop L6, are part of the interaction interface and are likely adaptable. In the crystal, their position might also be influenced by packing interactions because loop L6 and helix α6 contact the equivalent structural elements of a neighboring symmetry mate (Figure S4B). However, a CNOT1 fragment lacking helix α7 (1,356–1,561) did not interact with CNOT9 in solution (Figure S1B), indicating that these helices and the spatial arrangement observed in the crystal are indeed relevant for complex formation.

One remarkable structural feature of the CN9BD is that both the N- and C-terminal peptides fold back on the three-helix bundle, forming multiple hydrophobic interactions (Figures 2A, 2B, and S4C). As a result, the N and C termini of the domain enter close proximity and form a main-chain contact between Y1357 and F1582 (Figures 2A and 2B). Furthermore, the C-terminal peptide (around P1580-G1581) becomes locked into its conformation by interactions with CNOT9 residues V71 and P75 (Figure 2C), consistent with the observation that a deletion of the C-terminal peptide destabilizes the interaction between the *Dm* proteins (Figure S1C). Overall, the CN9BD adopts a rather unique protein fold that has no close structural homologs in the PDB.

CNOT9 Recognizes and Stabilizes the Fold of the CN9BD

The interface between CNOT1 and CNOT9 is larger than the interface for CNOT9 homodimerization (3,170 Å^2 versus 2,005 Å^2; Figures S3B–S3D) and thus likely favored in vivo. It is predominantly hydrophobic and centered on the first three N-terminal ARM repeats (ARM1–ARM3) of CNOT9, which engage a surface composed of helices α2, α3, α6, α7, loop L6, and the very C-terminal end (C-term) of the CNOT1 CN9BD (Figures 1D, 1E, 2A, 2C, and 2D).

ARM1 includes an important serine (S30) and fixes loop L6 and helix α7, whereas ARM3, which includes an important phenylalanine (F118), contacts helices α2 and α3 (Figure S2). ARM2 makes numerous contacts, including each of the CNOT1 interface elements. In particular, the central F60 in the elbow loop L3, between ARM2 helices α3 and α4, and the following helix α4 insert into a hydrophobic groove of the CN9BD that is flanked by CNOT1 helices α2, α3, and α7 (Figures 2A–2D, S2, and S4). The respective interface residues include F60 (L3), G61 (L3), A64 (α4), L67 (α4), V71 (α4), Y74 (L4), P75 (L4), and P79 (L4) on the side of CNOT9. On the side of CNOT1, there are T1419 (α2), I1423 (α2), K1426 (α2), D1427 (α2), F1428 (α2), M1444 (α3), L1448 (α3), G1451 (α3), I1455 (α3), M1452 (α3), R1458 (α3), L1559 (L6), V1564 (L6), Q1568 (L6), L1569 (L6), V1571 (α7), Y1572 (α7), F1575 (α7), P1580 (C-term), and G1581 (C-term). These complex hydrophobic contacts allow CNOT9 to recognize and stabilize the CN9BD as a folded domain.

Additional polar flanking interactions provide further specificity and, in particular, allow helix α6 of the CN9BD to adapt to the surface of CNOT9. Here, CNOT9 H58 plays an important role. It is read out by water-mediated hydrogen bonds from Q1549 (α6) and from the invariant lysine K1426 (α2) of the CN9BD and additionally stacks on Y1548 (α6; Figure 2D).

To validate the interface, we initially generated single point mutations, but these only reduced the interaction (e.g., F60A) or had no effect (A64Y; Figure S4D). To disrupt the interface, it was necessary to introduce four mutations in CNOT9 (Mut1; H58A, F60A, A64Y, V71Y) or in the CNOT1 CN9BD (4×M; K1426S, G1451Y, R1458A, Q1549A; Figures S4D and S4E). Importantly, the CNOT9 Mut1 retained the ability to homodimerize (Figure S1H), indicating that the mutations do not disrupt protein folding.

For in vivo coimmunoprecipitation assays in HEK293T cells, it was also necessary to use the quadruple CNOT9 mutation (Mut1) to disrupt the interaction with full-length CNOT1 or with the CNOT1-M region (Figures 2E and S4F). In CNOT1, it was even necessary to generate a quintuple mutation (5×M; I1423D plus 4×M) because the quadruple mutation still showed residual binding (Figures 2F and S4G). These results are consistent with a rather extensive and high-affinity interaction.

Finally, to demonstrate the conservation of the interface, we repeated the coimmunoprecipitation experiments in *Dm* S2 cells. Notably, double mutations in CNOT9 and single G1562E or K1537S mutations in CNOT1 (corresponding to human G1451 and K1426) were sufficient to disrupt the interaction in this case (Figures 2G, 2H, and S4H). These results suggest that the interface is indeed conserved, but that affinities may vary among orthologs.

CNOT9 Harbors Tandem Tryptophan-Binding Pockets

Perhaps one of the most striking features of the CNOT1-CNOT9 structure is the presence of tryptophan residues bound to tandem hydrophobic pockets in CNOT9. These pockets are located on ARM5, on either side of the kink between helices α12 and α13, on the convex surface of the crescent (Figures 3 and S2).

Pocket 1 is flanked by helix α15 of ARM6 and lined by residues C200, Q201, T202, Y203, F206, R244, A245, and A248 (Figures 3A–3C). It accommodates W1603 (W1) from a symmetry-related CNOT1 molecule in both crystal structures. W1603 stacks between Y203 and R244 and is specifically recognized on its N7 nitrogen by the carbonyl group of C200 (Figures 3A–3C). Pocket 2 is flanked by helix α10 of ARM4 and lined by residues I164, P165, L168, Y198, I199, R205, H208, and V209. It accommodates a free L-tryptophan (W2) that is absent in the high-resolution structure obtained in the absence of L-tryptophan in the crystallization condition. W2 stacks between P165 and R205 and is also recognized specifically on its N7 nitrogen by a hydrogen bond to H208 (Figures 3B, 3D, and S2).

Similar to the situation in the AGO2 structure, the distance between the two bound tryptophan residues is 20–25 Å. This is a typical intervening distance between tryptophan residues in TNRC6 proteins and can be spanned by approximately 8–10 residues in an extended conformation (Schirle and MacRae, 2012).

The CNOT9 W-Binding Pockets Are Binding Sites for GW182/TNRC6 Proteins

To test whether the W-binding pockets in CNOT9 represent bona fide binding sites for TNRC6 proteins, we substituted residues lining the pockets and performed pull-down assays in vitro. In pocket 1, we substituted A248 with phenylalanine to fill the cavity with a bulky side chain. We also substituted Y203 and R244 with alanine to prevent stacking interactions. In pocket 2, we substituted P165 with glycine and R205 with alanine to prevent stacking interactions and H208 with alanine to prevent specific recognition of the W ligand via hydrogen bonding (Table S1).

We observed that the TNRC6A-SD (6A-SD), which was expressed in *E. coli* with a maltose-binding protein (MBP) tag, pulled down CNOT9 in the absence of CNOT1, indicating that the interaction is direct (Figures 4A, lane 7, and 4B). Furthermore, efficiently disrupting this interaction required mutating both W-binding pockets simultaneously, demonstrating that they are indeed responsible for binding TNRC6 SDs (Figure 4A, lanes 10–12 as compared to lanes 8 and 9). Similar results were obtained for the TNRC6C-SD (Figure S5A). Importantly, the mutations in the W-binding pockets did not affect CNOT9 homodimerization (as shown by MALLS; Figures S5B–S5G) or binding to the CNOT1 CN9BD (Figure S5H), indicating that the mutations do not disrupt the CNOT9 fold.

Finally, a complex containing the CN9BD bound to the CNOT9 P1+P2a mutant did not interact with the 6A-SD (Figure S5I), indicating that the W-binding pockets in CNOT9 represent the primary binding sites for TNRC6 proteins in the CN9BD-CNOT9 complex and that the CN9BD is not sufficient to recruit TNRC6 proteins.

Next, we investigated the contribution of the CNOT9 W-binding pockets to TNRC6 binding in a cellular context. To this end, the mutations described above were introduced into full-length

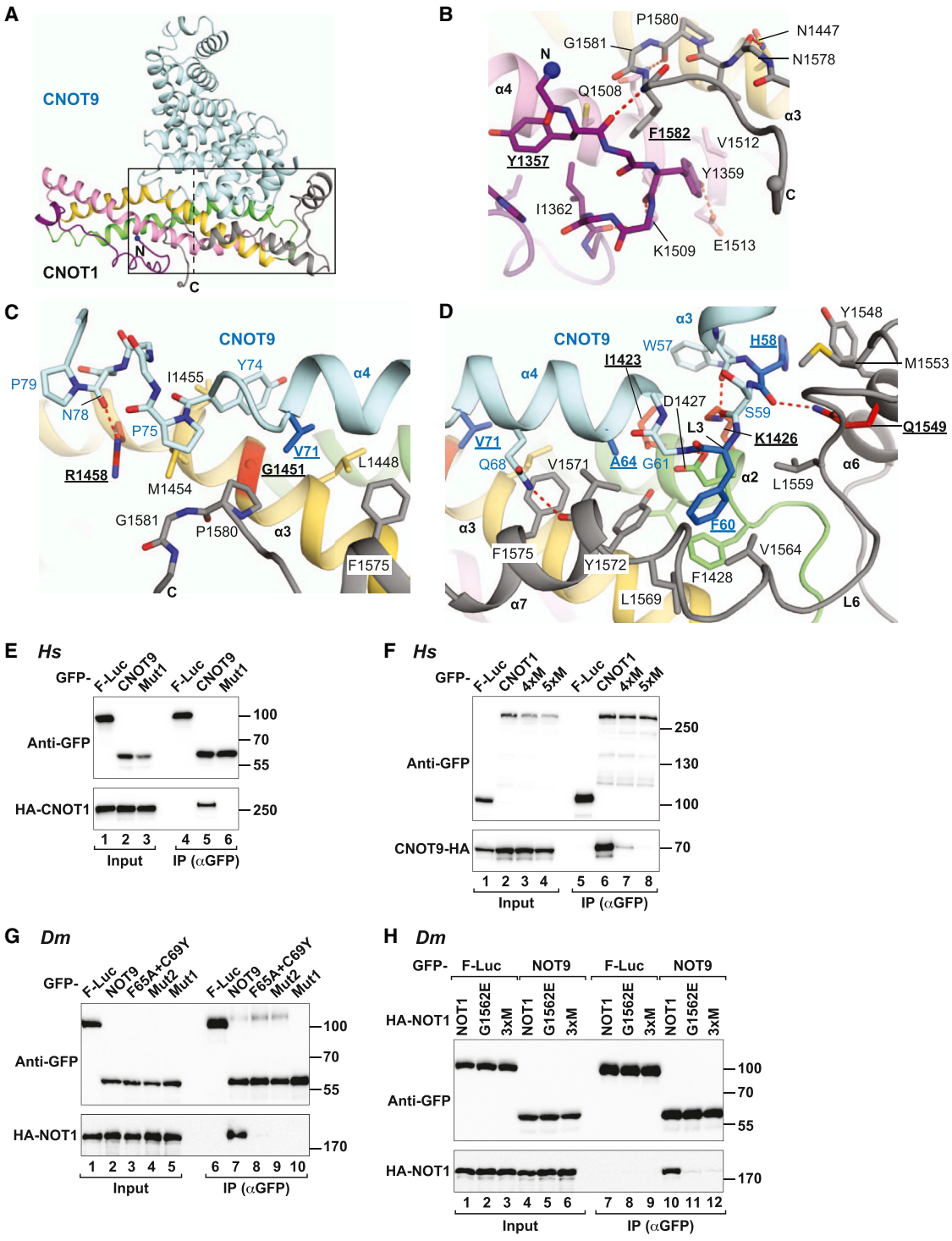

Figure 2. The CN9BD-CNOT9 Binding Interface

(A–D) Overview and close-up views of the interface between the CNOT1 CN9BD and the CNOT9 ARM domain, with selected interface residues shown as sticks. Residues mutated in this study are underlined and shown as red sticks (CNOT1) or dark blue sticks (CNOT9). The small and large rectangles in (A) indicate the views shown in (C) and (D), respectively. Residues and secondary structure elements are labeled in black for CNOT1 and in blue for CNOT9. Hydrogen bonds are shown as red dashed lines. See also Figures S2–S4.

(E) Interaction of GFP-CNOT9 (full-length wild-type or quadruple mutant, Mut1) with HA-CNOT1 (full length) in human cells. See also Figure S4.

(legend continued on next page)

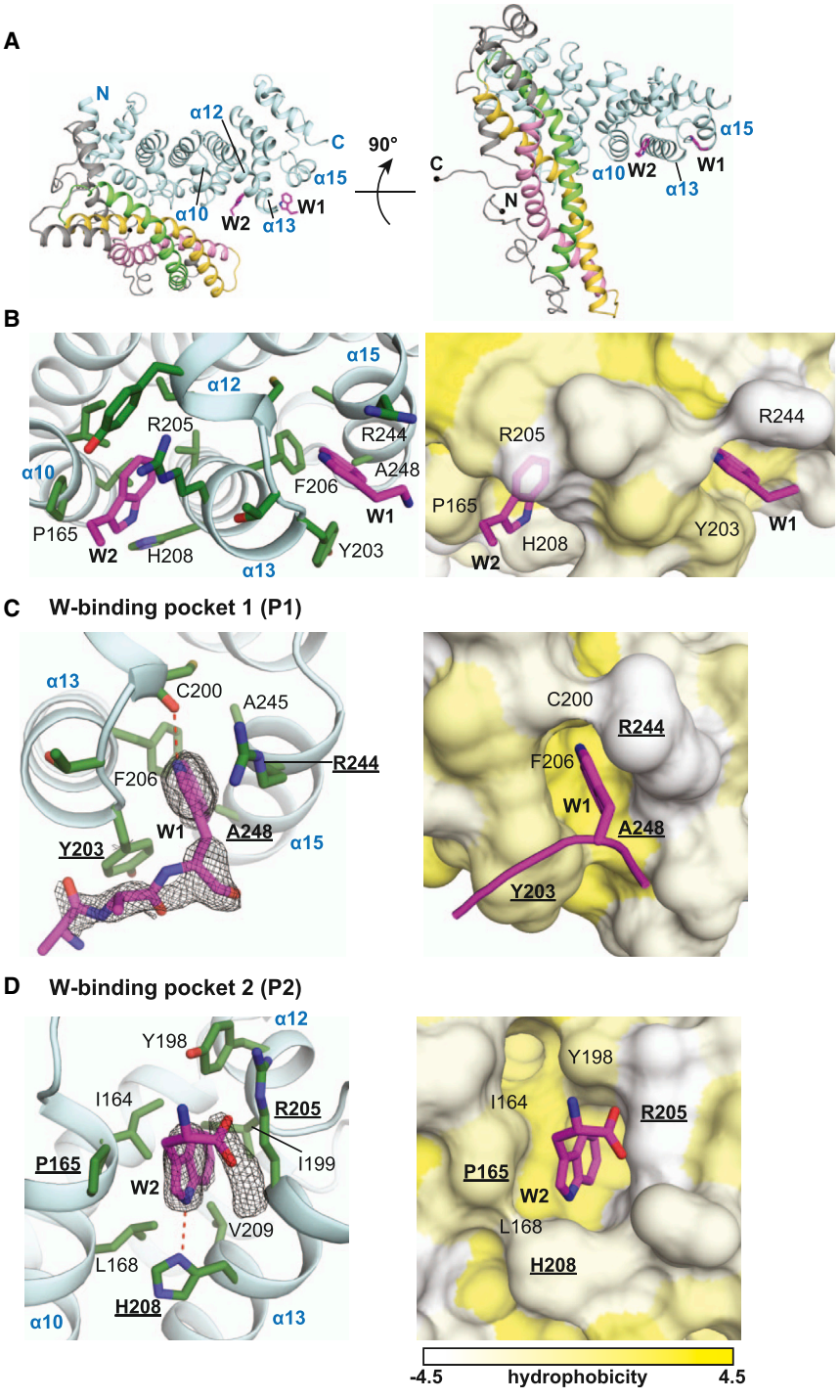

Figure 3. CNOT9 Harbors Tandem W-Binding Pockets

(A) Overview of the CN9BD-CNOT9 complex is shown for orientation. The W residues (W1 and W2 corresponding to CNOT1 W1603 and free W, respectively) bound to CNOT9 are shown as sticks. (B) Close-up views of the W-binding pockets. The right panel shows a surface representation of the view in the left panel, with the CNOT9 surface colored white to yellow with increasing hydrophobicity (scores according to Kawashima et al., 2008). (C and D) Close-up views of W-binding pocket 1 (C) (high-resolution structure) and W-binding pocket 2 (D) (low-resolution structure). The electron difference densities (Fo-Fc, contoured at 2.5 σ) for the W-containing peptide and the free W residue are shown as a gray mesh, and the corresponding structural models are displayed as magenta sticks. Residues mutated in this study are underlined. Hydrogen bonds are shown as red dashed lines. See also Figures S2 and S4 and Table S1.

CNOT9 and tested for interaction with TNRC6s. The CN9BD-CNOT9 complex interacts with the 6A-SD and 6C-SD (Figures 4C and S5J, lane 8). These interactions were abolished by mutations in the CNOT9 W-binding pockets (Figures 4C and S5J, lanes 9–11). As expected, the pocket mutations did not interfere with CNOT1 binding (Figures 4C, 4D, and S5J). Surprisingly, CNOT9 Mut1, which cannot interact with CNOT1, also failed to interact with the TNRC6 proteins (Figures 4C and S5J, lane 12), although this mutant interacts with the 6A-SD in vitro (Figure 4B, lane 12). These observations suggest that, in vivo, CNOT9 only binds TNRC6s when it is assembled into the CCR4-NOT complex.

Importantly, CNOT1 (or the CCR4-NOT complex) provides binding sites for TNRC6s independently of CNOT9 because full-length CNOT1 mutants (4×M and 5×M) that are defective in binding CNOT9 (Figure 2F) still interact with 6C-SD and 6A-SD (Figures 4E and S5K).

To investigate whether the role of the W-pockets in NOT9 is conserved, we performed similar coimmunoprecipitation assays with the *Dm* NOT9 and GW182 proteins in *Dm* S2 cells. In agreement with the results in human cells, we made the following observations. First, the NOT9 W-binding pockets are the major GW182-binding sites in the CN9BD-NOT9 complex because mutations in these pockets abrogate the interaction with GW182 without affecting complex formation (Figure 4F, lanes 8–11). Second, NOT9 interacts with GW182

(F) Interaction of GFP-CNOT1 (full-length wild-type or mutants) with CNOT9-HA-MBP in HEK293T cells.
(G) Interaction of GFP-tagged *Dm* NOT9 (wild-type or mutants) with HA-NOT1 in *Dm* S2 cells.
(H) Interaction of GFP-tagged *Dm* NOT9 with HA-NOT1 (wild-type or mutants) in *Dm* S2 cells. In all panels, cell lysates were treated with RNase A prior to immunoprecipitation. See also Figure S4 and Table S1.

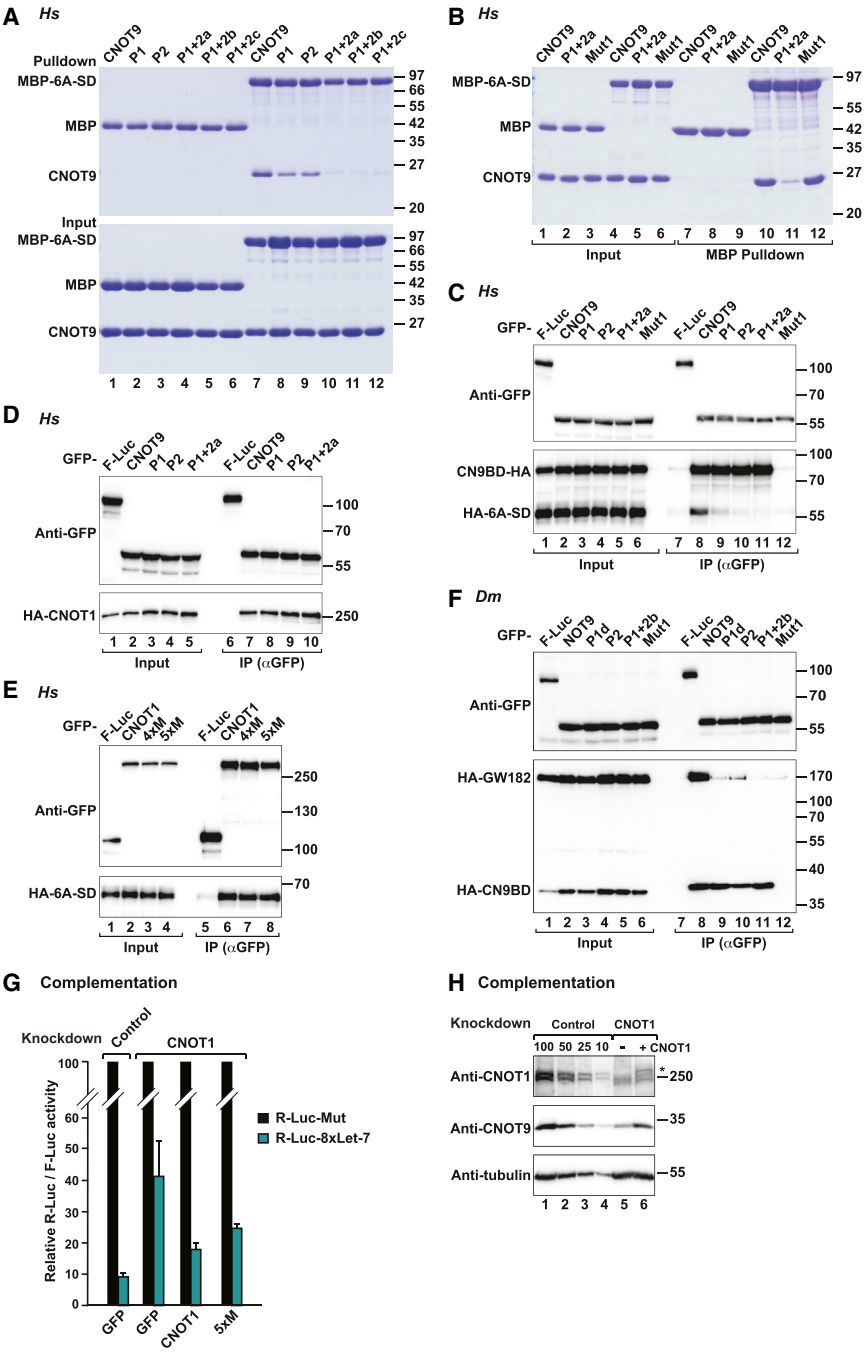

Figure 4. The CNOT9 W-Binding Pockets Mediate Binding to the TNRC6s

(A) MBP pull-downs using recombinant MBP-tagged 6A-SD and His-tagged CNOT9 ARM domain (wild-type or the indicated mutants). MBP served as a negative control. See also Figure S5.

(B) MBP pull-downs using recombinant MBP-tagged 6A-SD and His-tagged CNOT9 ARM domain (wild-type or the indicated mutants).

(C) Interaction between GFP-CNOT9 (wild-type or the indicated mutants) and HA-6A-SD in the presence of HA-MBP-tagged CN9BD in HEK293T cells.

(D) Interaction between GFP-CNOT9 (wild-type or the indicated mutants) and full-length HA-CNOT1 in HEK293T cells.

(E) Interaction between GFP-CNOT1 (wild-type or the 4×M and 5×M mutants that do not bind CNOT9) and HA-6A-SD in HEK293T cells.

(F) Interaction between GFP-CNOT9 (wild-type or the indicated mutants) and HA-GW182 in the presence of HA-tagged CN9BD in *Dm* S2 cells. See also Figure S5 and Table S1.

(G) HeLa cells (transfected with a control shRNA) or cells depleted of CNOT1 were transfected with a mixture of three plasmids: the psiCHECK-8×Let-7 or the corresponding reporter carrying mutations in Let-7-binding sites (R-Luc-Mut), a plasmid expressing F-Luc as a transfection control, and a plasmid expressing shRNA-resistant versions of GFP-CNOT1 (wild-type or 5×M mutant) or GFP. For each condition, *Renilla* luciferase activity was measured, normalized to that of the F-Luc transfection control, and set at 100% in cells expressing R-Luc-Mut (black bars). Mean values ± SD from five independent experiments are shown.

(H) Western blots showing the efficiency of the CNOT1 knockdown and the expression levels of endogenous CNOT9. Dilutions of control cell lysates were loaded in lanes 1–4 to estimate the efficacy of the depletion. α-tubulin served as a loading control. The asterisk indicates the position of the GFP-CNOT1 used in the complementation assay. See also Figures S5N and S5O.

only when bound to NOT1 in cell lysates (Figure 4F, lane 12). Third, an extended M region of NOT1 is sufficient for binding to GW182 proteins, independent of CNOT9 (Figures S5L and S5M, lane 6 versus 5).

Collectively, our results indicate that CNOT1 (or the CCR4-NOT1 complex) provides multiple binding sites for GW182/TNRC6 proteins, with two sites located in the CN9BD-CNOT9 module. The presence of multiple binding sites in CNOT1 is consistent with the observation that the GW182/TNRC6 proteins contact CNOT1 through multiple W-containing motifs that contribute additively to the interaction (Braun et al., 2011; Chekulaeva et al., 2011; Fabian et al., 2011; Huntzinger et al., 2013).

In agreement with the redundancy of binding sites, we observed that the CN9BD-CNOT9 interaction contributes to, but is not essential for, silencing. Indeed, the CNOT1 5×M mutant that does not interact with CNOT9 was still able to rescue silencing of a Let-7 reporter (psiCHECK-8×Let-7; Iwasaki et al., 2009) in cells depleted of endogenous CNOT1, although not as efficiently as wild-type CNOT1 (Figure 4G). Western blot analysis indicated that the levels of CNOT1 in the depleted cells were reduced to 10% of the control levels (Figure 4H). Interestingly, CNOT9 levels were also strongly reduced, suggesting that CNOT9 is destabilized in the absence of CNOT1 (Figure 4H, lane 5). In contrast, the levels of endogenous AGO2 and TNRC6A

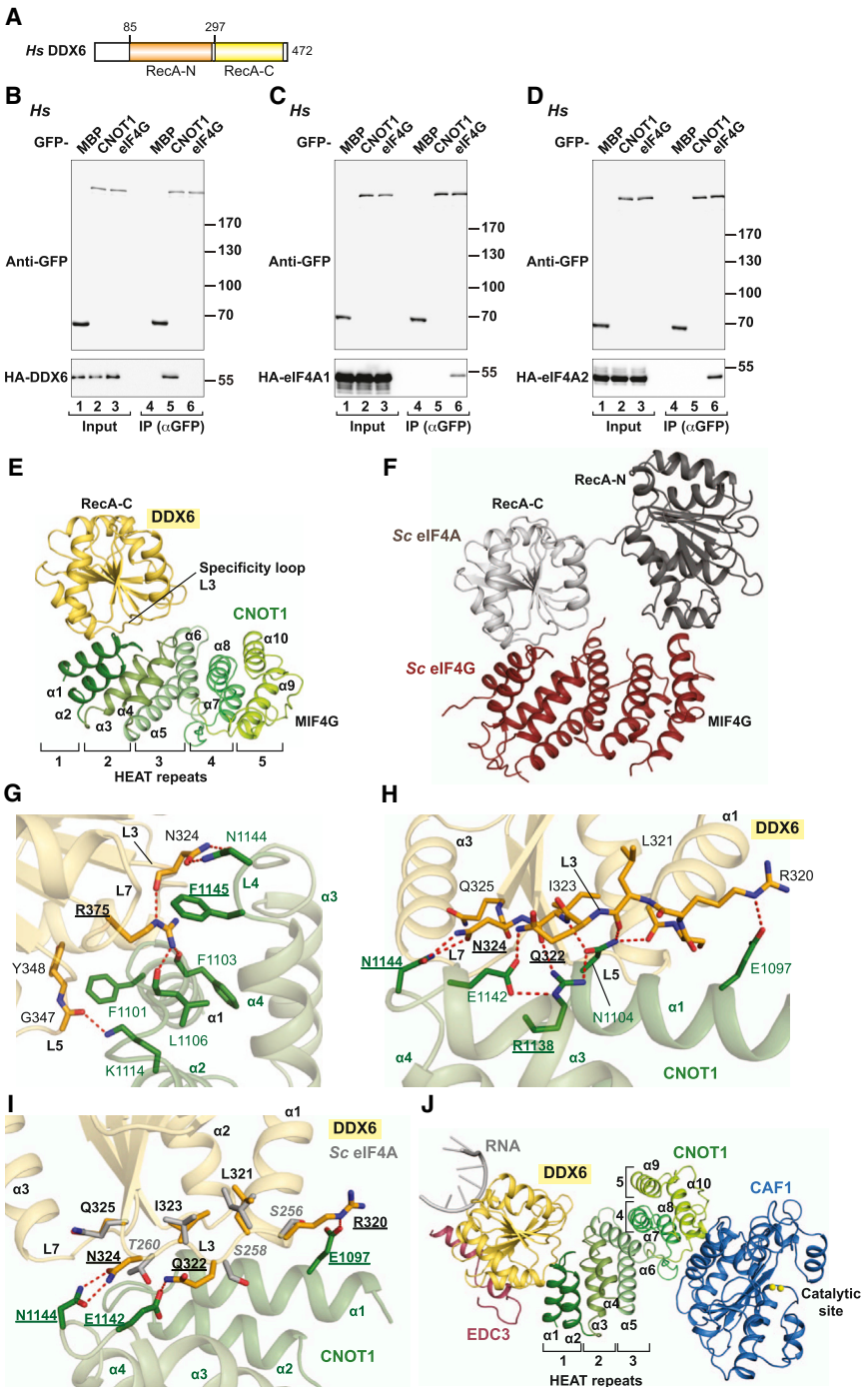

Figure 5. Structure of the CNOT1 MIF4G Domain Bound to the DDX6 RecA-C Domain

(A) DDX6 consists of two RecA-like domains, termed RecA-N and RecA-C, connected by a flexible linker.

(B–D) Interaction of GFP-CNOT1 or GFP-eIF4G with HA-tagged DDX6 (B), eIF4A1 (C), or eIF4A2 (D) in HEK293T cells. See also Figure S6.

(E and F) Overall structure of the CNOT1 MIF4G-DDX6 RecA-C complex (this study) (E) and the *Saccharomyces cerevisiae* eIF4G MIF4G-eIF4A complex (2VSO; Schütz et al., 2008) (F). Selected secondary structure elements are indicated.

(G and H) Close-up views of the interface between the CNOT1 MIF4G domain and the DDX6 RecA-C domain showing the DDX6 arginine anchor residue R375 (G) and loop L3 (H). Selected interface residues are shown as sticks and colored green (CNOT1) or orange (DDX6). Residues and secondary structural elements are labeled in green for CNOT1 and in black for DDX6. Residues mutated in this study are underlined.

(I) Superposition of *Sc* eIF4A loop L3 (residues 255–262) onto *Hs* DDX6 L3 (329–336). Selected interface residues in loop L3 of the DDX6 and eIF4A RecA-C domains are shown as sticks and colored in orange (DDX6) and gray (eIF4A). The CNOT1 MIF4G residues that specifically form hydrogen bonds with DDX6 residues are shown in green. The residues that contribute to the specificity of the interaction are underlined and shown in bold. eIF4A residues are labeled in italics. Backbone cartoons of *Sc* eIF4G and eIF4A are omitted for clarity.

(J) A structural model built by superposition of DDX6 bound to the EDC3 FDF peptide (PDB 2WAX), DDX6 bound to the CNOT1 MIF4G domain (this study), and the CNOT1 MIF4G bound to CAF1 (PDB 4GMJ). The RNA is modeled based on the structure of Vasa bound to RNA (PDB 2DB3). See also Figure S6J.

were not affected (Figure S5N). The CNOT1 proteins were expressed at comparable levels (Figure S5O). We conclude that the W-binding pockets in CNOT9 assist in the recruitment of the CCR4-NOT complex to miRNA targets.

The MIF4G Domain of CNOT1 Interacts with DDX6

To investigate the hypothesis that the CNOT1 MIF4G domain could directly recruit eIF4A2, we performed coimmunoprecipitation assays using HEK293T cell lysates treated with ribonuclease A (RNase A). We included eIF4A1 as well as DDX6 (Figure 5A) because this helicase has previously been shown to interact with the CCR4-NOT complex in yeast and *Dm* cells (Coller et al., 2001; Hata et al., 1998; Maillet and Collart, 2002; Temme et al., 2010).

We could not observe an interaction between the CNOT1 MIF4G domain and either eIF4A2 or eIF4A1, but we obtained a clear signal with DDX6 (Figures 5B–5D, lane 5). Conversely, eIF4G interacted with both eIF4A1 and eIF4A2 as expected (Yoder-Hill et al., 1993) but exhibited no affinity for DDX6 (Figures 5B–5D, lane 6), indicating that the respective interactions are specific. Further studies indicated that the C-terminal RecA (RecA-C) domain of DDX6 interacted with the CNOT1 MIF4G domain and that this interaction was direct (Figures S6A–S6D).

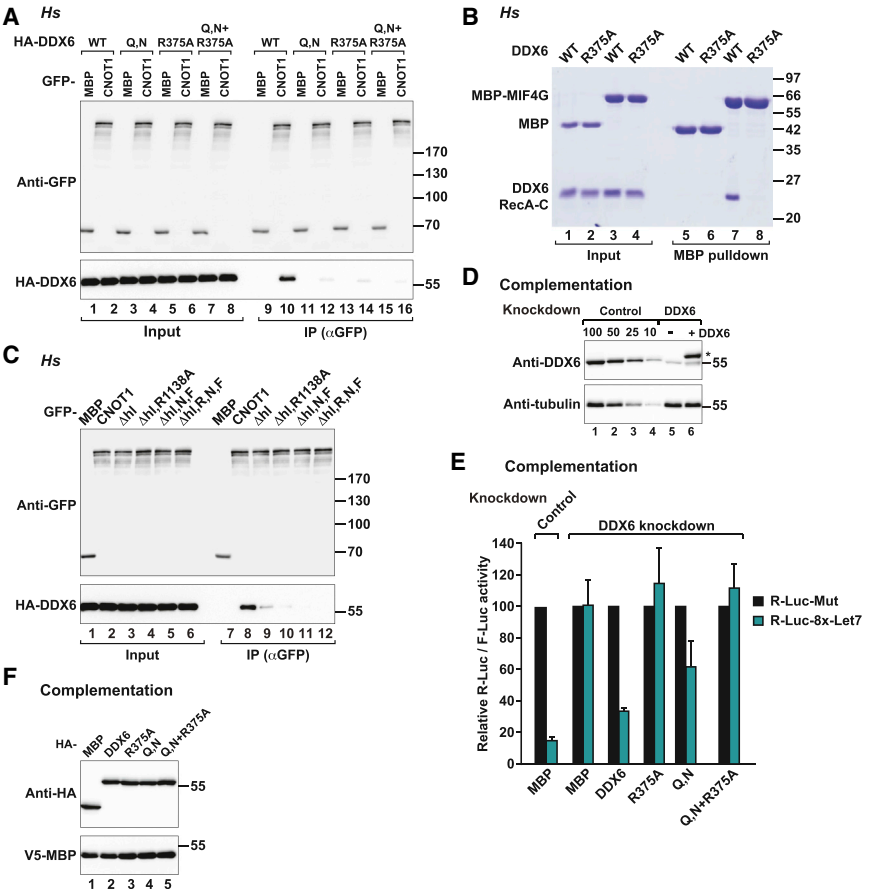

Figure 6. Validation of the CNOT1 MIF4G-DDX6 Binding Interface

(A) Interaction between HA-DDX6 (wild-type or the indicated mutants) and GFP-CNOT1 in HEK293T cells. GFP-MBP served as negative control.

(B) MBP pull-downs using recombinant MBP-tagged CNOT1 MIF4G domain and His-tagged DDX6 RecA-C (wild-type or the R375A mutant). MBP served as a negative control.

(C) Interaction between GFP-CNOT1 (wild-type or the indicated mutants) and HA-DDX6 in HEK293T cells. See also Figure S6 and Table S1.

(D) Western blots showing the efficiency of the DDX6 knockdown. Dilutions of control cell lysates were loaded in lanes 1–4 to estimate the efficacy of the depletion. α-tubulin served as a loading control. The asterisk indicates the position of the HA-DDX6 used in the complementation assay shown in (E).

(E) A complementation assay was performed as described in Figure 4G in cells depleted of DDX6. Mean values ± SD from three independent experiments are shown. See also Figures S5N, S6E, and S6H.

(F) Western blot analysis showing the equivalent expression of the DDX6 proteins used in the complementation assay.

Crystal Structure of CNOT1 MIF4G-DDX6 RecA-C Complex

To understand the molecular basis for the CNOT1-DDX6 interaction, we cocrystallized the CNOT1 MIF4G domain with the DDX6 RecA-C domain and determined the structure of the complex at a 1.75 Å resolution with a final R_{free} of 20.3% (Table 1). The model contains all residues of the CNOT1 MIF4G domain, as well as all residues from the DDX6 RecA-C domain, with the exception of the DDX6 C-terminal residues (454–472). The structures of the two domains from the complex superpose very well with the previously reported structures of the MIF4G domain in isolation (rmsd 0.34 Å; Petit et al., 2012) and the DDX6 RecA-C domain bound to EDC3 (rmsd 0.37 Å; Tritschler et al., 2009), indicating that the domains do not undergo major structural rearrangements upon binding.

Most importantly, the arrangement of the CNOT1 MIF4G and DDX6 RecA-C domains is highly similar to the arrangement of the complex of the eIF4G MIF4G domain bound to eIF4A RecA-C (Figures 5E and 5F; Schütz et al., 2008), adding to a growing number of structurally similar, yet specific, MIF4G-RecA-C complexes (Buchwald et al., 2013). Similar to the eIF4G-eIF4A interaction, the RecA-C domain binds the concave surface of the MIF4G domain, and the interface is formed by equivalent secondary structural elements. In particular, helix α1 and the loops L3, L5, and L7 of the RecA-C domains interact with the first two N-terminal HEAT repeats of the MIF4G domain, including mainly residues from helix α1 and α3 plus their adjacent interrepeat loops L2 and L4 (Figures 5G and 5H).

The interface area in the CNOT1-DDX6 complex is relatively small (640 $Å^2$) and dominated by polar interactions. Of particular interest is R375 in loop L7 of DDX6 (Figure 5G), which inserts deeply into a highly conserved patch in CNOT1 and makes hydrogen bonds with the main-chain oxygens of CNOT1 residues F1103 (helix α1) and L1106 (loop L2) while stacking onto F1145 (loop L4). This arginine is remarkably conserved in eIF4A1, eIF4A2, eIF4A3, and other DEAD-box proteins (Figure S6I) and plays an equivalent role in mediating interactions with MIF4G domains (Buchwald et al., 2013; Schütz et al., 2008). Consequently, this "arginine anchor" likely contributes significantly to the affinity of MIF4G-RecA-C interactions, but does not explain the specificity of individual pairs. This situation is different for residues R320, Q322, and N324 in loop L3 of DDX6 (Figures 5H and 5I). Although the length of this specificity loop is identical in eIF4A1-3 and other DEAD-box helicases, the sequence is not, thereby allowing the formation of unique polar contacts to residues E1097, R1138, E1142, and N1144 of CNOT1 and explaining the preference of CNOT1 for DDX6 (Figures 5H, 5I, and S6I).

To validate the interface experimentally, we mutated specific interface residues to alanine and performed pull-downs and coimmunoprecipitation assays. In DDX6, we substituted the anchor arginine (R375) or both Q322 and N324 (Q,N) from the specificity loop. These mutations abolished or strongly reduced binding of DDX6 to CNOT1 full length, the CNOT1-M fragment, or the MIF4G domain (Figures 6A, 6B, and S6E–S6G). In CNOT1, the deletion of helix α1 and loop L2 (CNOT1 ΔhI) led

to a reduced interaction with DDX6, which was disrupted completely when we additionally substituted R1138 (in α3) and N1144 and F1145 in loop L4 with alanine (Figure 6C, lanes 9–12, and S6H). Importantly, the mutations did not destroy the fold of the MIF4G domain because CAF1 binding was not affected (Figure S6H).

A Role for the CNOT1-DDX6 Interface in Silencing

To test the functional relevance of the CNOT1-DDX6 interaction in silencing, we used the complementation assay described above with the exception that DDX6 was depleted. Western blot analysis indicated that the levels of DDX6 in the depleted cells were reduced to 10% of the control levels (Figure 6D), without affecting endogenous AGO2 and TNRC6A expression (Figure S5N). In DDX6-depleted cells, silencing of the psiCHECK-8×Let-7 reporter was suppressed, leading to a 7-fold increase in F-Luc activity (Figure 6E), in agreement with previous studies (Chu and Rana, 2006; Eulalio et al., 2007). Silencing was rescued by expression of an shRNA-resistant version of wild-type DDX6, but not by the DDX6 R375A mutant, whereas the Q322A N324A double mutant was partially active (Figure 6E), in agreement with its residual binding to CNOT1 (Figure S6E, lane 12). The DDX6 proteins were expressed at similar levels (Figure 6F). These levels were comparable to the levels of endogenous DDX6 in control cells (Figure 6D, lane 6 versus lane 1). Our data support a role for the DDX6-CNOT1 interaction in silencing.

The CNOT1 MIF4G Domain Is a Central Node for CCR4-NOT Function

Structural superposition of the human CNOT1 MIF4G-DDX6 and CNOT1 MIF4G-CAF1 complexes demonstrates that CNOT1 can bind DDX6 and the CAF1 deadenylase simultaneously (Figures 5J and S6J). Similar superpositions show that the interaction of the DDX6 RecA-C domain with the isolated CNOT1 MIF4G domain does not interfere structurally with the recruitment of either EDC3, LSm14A, or Pat to their common binding surface on DDX6 RecA-C (reviewed by Jonas and Izaurralde, 2013). Together, these interactions provide a missing direct physical link between the major deadenylation complex (CCR4-NOT) and the decapping network where EDC3 and Pat act as decapping activators. In other words, the interaction of DDX6 with the CNOT1 MIF4G domain provides a plausible molecular explanation for the coupling of deadenylation to decapping and for the ability of the CCR4-NOT complex to repress translation in the absence of deadenylation. TNRC6-binding to the adjacent CN9BD-CNOT9 complex illustrates how the CCR4-NOT complex is recruited to miRNA targets.

DISCUSSION

The mechanisms by which the CCR4-NOT complex is recruited to miRNA targets and represses translation have remained elusive. Here, we show that the middle region of CNOT1 assists in the recruitment of the complex to miRNA targets via W-binding pockets in the CN9BD-CNOT9 module and orchestrates deadenylation, translational repression, and decapping via the MIF4G domain, which can bind to the CAF1 and CCR4 deadenylases and to the translational repressor and decapping activator DDX6. Notably, similar findings are reported by Mathys et al. (2014) in this issue.

The Functional Repertoire of CNOT9

In this study, we reveal an unexpected role for the highly conserved CNOT9 subunit of the CCR4-NOT complex in miRNA-mediated gene silencing. CNOT9 is required for retinoic acid-induced cell differentiation in mammals and is overexpressed in breast cancer cells (Hiroi et al., 2002; Ajiro et al., 2009). However, it remains unclear whether the role of CNOT9 in cell differentiation and proliferation is linked to or independent of its role as subunit of the CCR4-NOT complex. Through our structural analysis, we have generated CNOT9 mutants that retain the ability to homodimerize but are not incorporated in the CCR4-NOT complex, which provides an important tool to study CNOT9 function in vivo.

CNOT9 interacts with several protein partners in different cellular contexts. These interacting partners include Grb10 interacting proteins GIGYF1 and GIGYF2 that are involved in epidermal growth factor receptor (EGFR) signaling (Ajiro et al., 2009). Notably, GIGYF2 (also known as TNRC15) is a W-rich protein, which raises the possibility that some CNOT9 partners may compete with TNRC6s for binding to the W pockets. Clearly, the identification of the W-binding pockets increases the functional repertoire of CNOT9 that needs to be considered when studying CNOT9 function.

Interaction of GW182 Proteins with Their Binding Partners

GW182 proteins interact with AGOs and the PAN2-PAN3 and CCR4-NOT deadenylase complexes through W-containing motifs (Fabian and Sonenberg, 2012; Braun et al., 2013). Previous studies on the interaction of these motifs with AGOs and PAN3 indicate that molecular recognition is predominantly restricted to the W residues, which insert into hydrophobic pockets on the respective protein partners (Schirle and MacRae, 2012; Christie et al., 2013; Pfaff et al., 2013).

Here, we show that this mode of molecular recognition is also observed for the interaction of GW182 proteins with the CN9BD-CNOT9 complex. This raises the question of how binding specificity and affinity are achieved. One possibility is that the flanking sequences and the spatial arrangement of the Ws contribute to the affinity of the interaction (Schirle and MacRae, 2012; Pfaff et al., 2013). For example, a common feature of the W-binding pockets in AGO2 and CNOT9 is that the spatial arrangement of the pockets is similar, and both proteins can accommodate consecutive W residues provided that they are at least 8–10 residues apart (this study; Schirle and MacRae, 2012; Pfaff et al., 2013). Concerted binding of adjacent W residues may contribute to the affinity of the interaction via additive or avidity effects.

A remarkable aspect of the interaction of GW182 proteins with the CCR4-NOT complex is that it involves multiple binding sites (in addition to the ones identified on CNOT9), presumably leading to higher affinity and specificity. The precise location of these additional sites remains unclear because the isolated CNOT1-N, MIF4G, and CNOT1-C regions do not detectably interact with TNRC6s in coimmunoprecipitation assays. However, these

regions seem to synergize in the context of full-length CNOT1 because a CNOT1 mutant that does not bind CNOT9 retains full TNRC6-binding capacity (Figures 4E and S5M). A key direction for future work will be to identify these multiple and redundant binding sites and determine how they contribute to the recruitment of the CCR4-NOT complex to miRNA targets.

CNOT1-M Coordinates Deadenylation, Translational Repression, and Decapping

MIF4G domains are present in a wide variety of proteins and have been shown to interact with and regulate the activity of DEAD-box proteins (Buchwald et al., 2013). The MIF4G domain of eIF4G specifically binds to eIF4A1 (Schütz et al., 2008). Remarkably, other MIF4G domain-containing proteins, such as DAP5, CWC22, and Gle1, interact with the RecA-C domains of eIF4A1, eIF4A3, and Dbp5, respectively, using a recognition mode similar to that observed in the eIF4G-eIF4A complex (reviewed by Buchwald et al., 2013). Based on these observations, it has been proposed that the CNOT1 MIF4G domain interacts with eIF4A2 (Meijer et al., 2013). Here, we show that the CNOT1 MIF4G domain interacts preferentially with DDX6. The binding specificity is imparted by a few amino acid substitutions, in particular in loop L3 of the RecA-C domains, which establish specific hydrogen bonds (Figure 5I).

DDX6 plays a role in repressing translation by slowing translation elongation (Presnyak and Coller, 2013). Its role as an activator of decapping has been proposed to be an indirect consequence of the inhibition of translation (Presnyak and Coller, 2013). However, DDX6 interacts directly with the decapping factors EDC3 and Pat and indirectly with the catalytic core of the decapping complex formed by the decapping enzyme DCP2 and its coactivator DCP1 (Jonas and Izaurralde, 2013). Thus, DDX6 could play a direct role in decapping by promoting recruitment of decapping complexes to the mRNA target. These observations, together with our studies, indicate that the CNOT1-DDX6 complex provides a missing direct physical link between deadenylation and decapping.

The structure of the NOT1-DDX6 complex together with available structures of DDX6 bound to EDC3, EDC3 bound to metazoan DCP1, and the Dcp1-Dcp2 complex (reviewed by Jonas and Izaurralde, 2013) present snapshots of consecutive steps in the 5′-to-3′ mRNA decay pathway. Along with the structure of the CN9BD-CNOT9 complex, these structures establish a chain of physical interactions to describe in molecular terms how the CCR4-NOT complex is recruited to miRNA targets and enrolls a translational repressor, which in turn engages the decapping machinery (Figures 5J and S6J).

EXPERIMENTAL PROCEDURES

DNA constructs are described in detail in the Supplemental Information. Mutations used in this study are listed in Table S1.

Pulldowns, Coimmunoprecipitation Assays, and Western Blotting

Coimmunoprecipitation assays in human and *Dm* S2 cells were performed as previously described (Bawankar et al., 2013; Braun et al., 2011). Antibodies used in this study are listed in Table S1. All western blots were developed using the ECL Western Blotting Detection System (GE Healthcare). A detailed protocol for the pull-down assays using recombinant proteins can be found in the Supplemental Experimental Procedures.

Protein Expression and Purification

The CNOT1 CN9BD and the CNOT9 ARM domain were coexpressed in *E. coli* BL21 Star (DE3) cells (Invitrogen) and induced at an optical density 600 (OD_{600}) of 0.6 with 1 mM Isopropyl β-D-1-thiogalactopyranoside (IPTG). Following induction, the proteins were expressed overnight at 20°C. The complex was purified using amylose resin, a heparin column, and finally by size-exclusion chromatography as described in the Supplemental Experimental Procedures. The CNOT1 MIF4G domain and the DDX6 RecA-C domain were expressed separately in *E. coli* Rosetta 2 cells (Novagen). The proteins were purified as described previously (Petit et al., 2012; Tritschler et al., 2009), mixed at a ratio of 1:1.2 (CNOT1:DDX6), and concentrated to 10 mg/ml in 10 mM HEPES (pH 7.0), 300 mM NaCl, and 5 mM dithiothreitol (DTT).

Crystallization, Data Collection, and Structure Determination

Crystals of the CNOT1 CN9BD-CNOT9 ARM complex were obtained using the hanging-drop and sitting-drop vapor diffusion methods over a 500 μl reservoir at 18°C. The protein solution was mixed in a 1:1 ratio (0.8 μl + 0.8 μl) with a reservoir solution containing 100 mM MES (pH 6.0), 8% polyethylene glycol (PEG) 6,000, and 80 mM $MgCl_2$. Alternatively, crystals were obtained by mixing the protein solution in a 1:1 ratio (0.8 μl + 0.8 μl) with the reservoir solution containing 100 mM MES (pH 6.0), 11% PEG 6,000, and 50 mM $MgCl_2$ supplemented with 40 mM L-tryptophan. Crystals of the CNOT1 MIF4G-DDX6 RecA-C complex were obtained using the hanging-drop vapor diffusion method over a 500 μl reservoir (100 mM Tris (pH 8.0) and 16% PEG 6,000) at 20°C by mixing 1.5 μl of the protein solution with 1.5 μl of the reservoir solution. All crystals were cryoprotected using the corresponding reservoir solution supplemented with 25% glycerol and subsequently flash frozen in liquid nitrogen.

All diffraction data sets were recorded on a PILATUS 6 M detector at the PXII beamline of the Swiss Light Source (SLS) at a temperature of 100 K. A detailed description of the structure determination process can be found in the Supplemental Experimental Procedures. The refinement statistics are summarized in Table 1.

Complementation Assays in Human Cells

Knockdowns and complementation assays were performed as described in the Supplemental Experimental Procedures.

ACCESSION NUMBERS

The atomic coordinates of CNOT1-CN9BD bound to the CNOT9 ARM repeat in the absence or presence of tryptophan and of CNOT1 MIF4G bound to the DDX6 RecA-C domain were deposited in the Protein Data Bank (PDB) under ID codes 4CRU, 4CRV, and 4CRW, respectively.

SUPPLEMENTAL INFORMATION

Supplemental Information includes Supplemental Experimental Procedures, six figures, and one table and can be found with this article online at http://dx.doi.org/10.1016/j.molcel.2014.03.034.

AUTHOR CONTRIBUTIONS

Y.C., A.B., and D.K.-Ö. contributed equally to this work. Y.C. and A.B. purified, crystallized, and solved the structures of CNOT1-CN9BD bound to the CNOT9 ARM repeat and of the CNOT1 MIF4G bound to DDX6 RecA-C domain. Y.C., A.B., and O.W. collected and analyzed diffraction data. Y.C. and A.B. performed pull-downs in vitro. D.K.-Ö. performed coimmunoprecipitations and functional assays in human cells. P.B. performed coimmunoprecipitation assays in S2 cells. B.L. performed the DDX6 complementation assays. C.-T.C. performed DDX6 coimmunoprecipitation assays in human cells. E.I. conceived and supervised the project. A.B., E.I., and O.W. wrote the manuscript. All authors corrected the manuscript.

ACKNOWLEDGMENTS

We thank M. Fauser and S. Helms for excellent technical assistance. We are grateful to M. Christie, H. Budde, E. Huntzinger, and L. Wohlbold for generating some of the constructs used in this study; E. Huntzinger for performing initial experiments; R. Büttner for the setup of crystallization screens; Y. Tomari for providing the psiCHECK-8×Let-7 miRNA reporter; and the staff at the PX beamlines of the Swiss Light Source for assistance with data collection. This work was supported by the Max Planck Society and by grants from the Deutsche Forschungsgemeinschaft (DFG, FOR855, and the Gottfried Wilhelm Leibniz Program awarded to E.I.).

Received: January 24, 2014
Revised: February 13, 2014
Accepted: March 18, 2014
Published: April 24, 2014

REFERENCES

Ajiro, M., Katagiri, T., Ueda, K., Nakagawa, H., Fukukawa, C., Lin, M.L., Park, J.H., Nishidate, T., Daigo, Y., and Nakamura, Y. (2009). Involvement of RQCD1 overexpression, a novel cancer-testis antigen, in the Akt pathway in breast cancer cells. Int. J. Oncol. *35*, 673–681.

Ameres, S.L., and Zamore, P.D. (2013). Diversifying microRNA sequence and function. Nat. Rev. Mol. Cell Biol. *14*, 475–488.

Bawankar, P., Loh, B., Wohlbold, L., Schmidt, S., and Izaurralde, E. (2013). NOT10 and C2orf29/NOT11 form a conserved module of the CCR4-NOT complex that docks onto the NOT1 N-terminal domain. RNA Biol. *10*, 228–244.

Braun, J.E., Huntzinger, E., Fauser, M., and Izaurralde, E. (2011). GW182 proteins directly recruit cytoplasmic deadenylase complexes to miRNA targets. Mol. Cell *44*, 120–133.

Braun, J.E., Huntzinger, E., and Izaurralde, E. (2013). The role of GW182 proteins in miRNA-mediated gene silencing. Adv. Exp. Med. Biol. *768*, 147–163.

Buchwald, G., Schüssler, S., Basquin, C., Le Hir, H., and Conti, E. (2013). Crystal structure of the human eIF4AIII-CWC22 complex shows how a DEAD-box protein is inhibited by a MIF4G domain. Proc. Natl. Acad. Sci. USA *110*, E4611–E4618.

Chekulaeva, M., Mathys, H., Zipprich, J.T., Attig, J., Colic, M., Parker, R., and Filipowicz, W. (2011). miRNA repression involves GW182-mediated recruitment of CCR4-NOT through conserved W-containing motifs. Nat. Struct. Mol. Biol. *18*, 1218–1226.

Christie, M., Boland, A., Huntzinger, E., Weichenrieder, O., and Izaurralde, E. (2013). Structure of the PAN3 pseudokinase reveals the basis for interactions with the PAN2 deadenylase and the GW182 proteins. Mol. Cell *51*, 360–373.

Chu, C.Y., and Rana, T.M. (2006). Translation repression in human cells by microRNA-induced gene silencing requires RCK/p54. PLoS Biol. *4*, e210.

Coller, J.M., Tucker, M., Sheth, U., Valencia-Sanchez, M.A., and Parker, R. (2001). The DEAD box helicase, Dhh1p, functions in mRNA decapping and interacts with both the decapping and deadenylase complexes. RNA *7*, 1717–1727.

Eulalio, A., Rehwinkel, J., Stricker, M., Huntzinger, E., Yang, S.F., Doerks, T., Dorner, S., Bork, P., Boutros, M., and Izaurralde, E. (2007). Target-specific requirements for enhancers of decapping in miRNA-mediated gene silencing. Genes Dev. *21*, 2558–2570.

Fabian, M.R., and Sonenberg, N. (2012). The mechanics of miRNA-mediated gene silencing: a look under the hood of miRISC. Nat. Struct. Mol. Biol. *19*, 586–593.

Fabian, M.R., Cieplak, M.K., Frank, F., Morita, M., Green, J., Srikumar, T., Nagar, B., Yamamoto, T., Raught, B., Duchaine, T.F., and Sonenberg, N. (2011). miRNA-mediated deadenylation is orchestrated by GW182 through two conserved motifs that interact with CCR4-NOT. Nat. Struct. Mol. Biol. *18*, 1211–1217.

Garces, R.G., Gillon, W., and Pai, E.F. (2007). Atomic model of human Rcd-1 reveals an armadillo-like-repeat protein with in vitro nucleic acid binding properties. Protein Sci. *16*, 176–188.

Hata, H., Mitsui, H., Liu, H., Bai, Y.L., Denis, C.L., Shimizu, Y., and Sakai, A. (1998). Dhh1p, a putative RNA helicase, associates with the general transcription factors Pop2p and Ccr4p from Saccharomyces cerevisiae. Genetics *148*, 571–579.

Hiroi, N., Ito, T., Yamamoto, H., Ochiya, T., Jinno, S., and Okayama, H. (2002). Mammalian Rcd1 is a novel transcriptional cofactor that mediates retinoic acid-induced cell differentiation. EMBO J. *21*, 5235–5244.

Huntzinger, E., and Izaurralde, E. (2011). Gene silencing by microRNAs: contributions of translational repression and mRNA decay. Nat. Rev. Genet. *12*, 99–110.

Huntzinger, E., Kuzuoglu-Öztürk, D., Braun, J.E., Eulalio, A., Wohlbold, L., and Izaurralde, E. (2013). The interactions of GW182 proteins with PABP and deadenylases are required for both translational repression and degradation of miRNA targets. Nucleic Acids Res. *41*, 978–994.

Iwasaki, S., Kawamata, T., and Tomari, Y. (2009). Drosophila argonaute1 and argonaute2 employ distinct mechanisms for translational repression. Mol. Cell *34*, 58–67.

Jonas, S., and Izaurralde, E. (2013). The role of disordered protein regions in the assembly of decapping complexes and RNP granules. Genes Dev. *27*, 2628–2641.

Kawashima, S., Pokarowski, P., Pokarowska, M., Kolinski, A., Katayama, T., and Kanehisa, M. (2008). AAindex: amino acid index database, progress report 2008. Nucleic Acids Res. *36* (Database issue), D202–D205.

Maillet, L., and Collart, M.A. (2002). Interaction between Not1p, a component of the Ccr4-not complex, a global regulator of transcription, and Dhh1p, a putative RNA helicase. J. Biol. Chem. *277*, 2835–2842.

Mathys, H., Basquin, J., Ozgur, S., Czarnocki-Cieciura, M., Bonneau, F., Aartse, A., Dziembowski, A., Nowotny, M., Conti, E., and Filipowicz, W. (2014). Structural and Biochemical Insights to the Role of the CCR4-NOT Complex and DDX6 ATPase in MicroRNA Repression. Mol. Cell *54*. Published online April 24, 2014. http://dx.doi.org/10.1016/j.molcel.2014.03.036.

Meijer, H.A., Kong, Y.W., Lu, W.T., Wilczynska, A., Spriggs, R.V., Robinson, S.W., Godfrey, J.D., Willis, A.E., and Bushell, M. (2013). Translational repression and eIF4A2 activity are critical for microRNA-mediated gene regulation. Science *340*, 82–85.

Nishihara, T., Zekri, L., Braun, J.E., and Izaurralde, E. (2013). miRISC recruits decapping factors to miRNA targets to enhance their degradation. Nucleic Acids Res. *41*, 8692–8705.

Petit, A.P., Wohlbold, L., Bawankar, P., Huntzinger, E., Schmidt, S., Izaurralde, E., and Weichenrieder, O. (2012). The structural basis for the interaction between the CAF1 nuclease and the NOT1 scaffold of the human CCR4-NOT deadenylase complex. Nucleic Acids Res. *40*, 11058–11072.

Pfaff, J., Hennig, J., Herzog, F., Aebersold, R., Sattler, M., Niessing, D., and Meister, G. (2013). Structural features of Argonaute-GW182 protein interactions. Proc. Natl. Acad. Sci. USA *110*, E3770–E3779.

Presnyak, V., and Coller, J. (2013). The DHH1/RCKp54 family of helicases: an ancient family of proteins that promote translational silencing. Biochim. Biophys. Acta *1829*, 817–823.

Schirle, N.T., and MacRae, I.J. (2012). The crystal structure of human Argonaute2. Science *336*, 1037–1040.

Schütz, P., Bumann, M., Oberholzer, A.E., Bieniossek, C., Trachsel, H., Altmann, M., and Baumann, U. (2008). Crystal structure of the yeast eIF4A-eIF4G complex: an RNA-helicase controlled by protein-protein interactions. Proc. Natl. Acad. Sci. USA *105*, 9564–9569.

Temme, C., Zhang, L.B., Kremmer, E., Ihling, C., Chartier, A., Sinz, A., Simonelig, M., and Wahle, E. (2010). Subunits of the Drosophila CCR4-NOT complex and their roles in mRNA deadenylation. RNA *16*, 1356–1370.

Tritschler, F., Braun, J.E., Eulalio, A., Truffault, V., Izaurralde, E., and Weichenrieder, O. (2009). Structural basis for the mutually exclusive anchoring of P body components EDC3 and Tral to the DEAD box protein DDX6/Me31B. Mol. Cell *33*, 661–668.

Wahle, E., and Winkler, G.S. (2013). RNA decay machines: deadenylation by the Ccr4-not and Pan2-Pan3 complexes. Biochim. Biophys. Acta *1829*, 561–570.

Yoder-Hill, J., Pause, A., Sonenberg, N., and Merrick, W.C. (1993). The p46 subunit of eukaryotic initiation factor (eIF)-4F exchanges with eIF-4A. J. Biol. Chem. *268*, 5566–5573.

Zekri, L., Kuzuoğlu-Öztürk, D., and Izaurralde, E. (2013). GW182 proteins cause PABP dissociation from silenced miRNA targets in the absence of deadenylation. EMBO J. *32*, 1052–1065.

Molecular Cell, Volume *54*

Supplemental Information

A DDX6-CNOT1 Complex and W-Binding Pockets in CNOT9 Reveal Direct Links between miRNA Target Recognition and Silencing

Ying Chen, Andreas Boland, Duygu Kuzuoğlu-Öztürk, Praveen Bawankar, Belinda Loh, Chung-Te Chang, Oliver Weichenrieder, and Elisa Izaurralde

SUPPLEMENTAL FIGURES

Figure S1

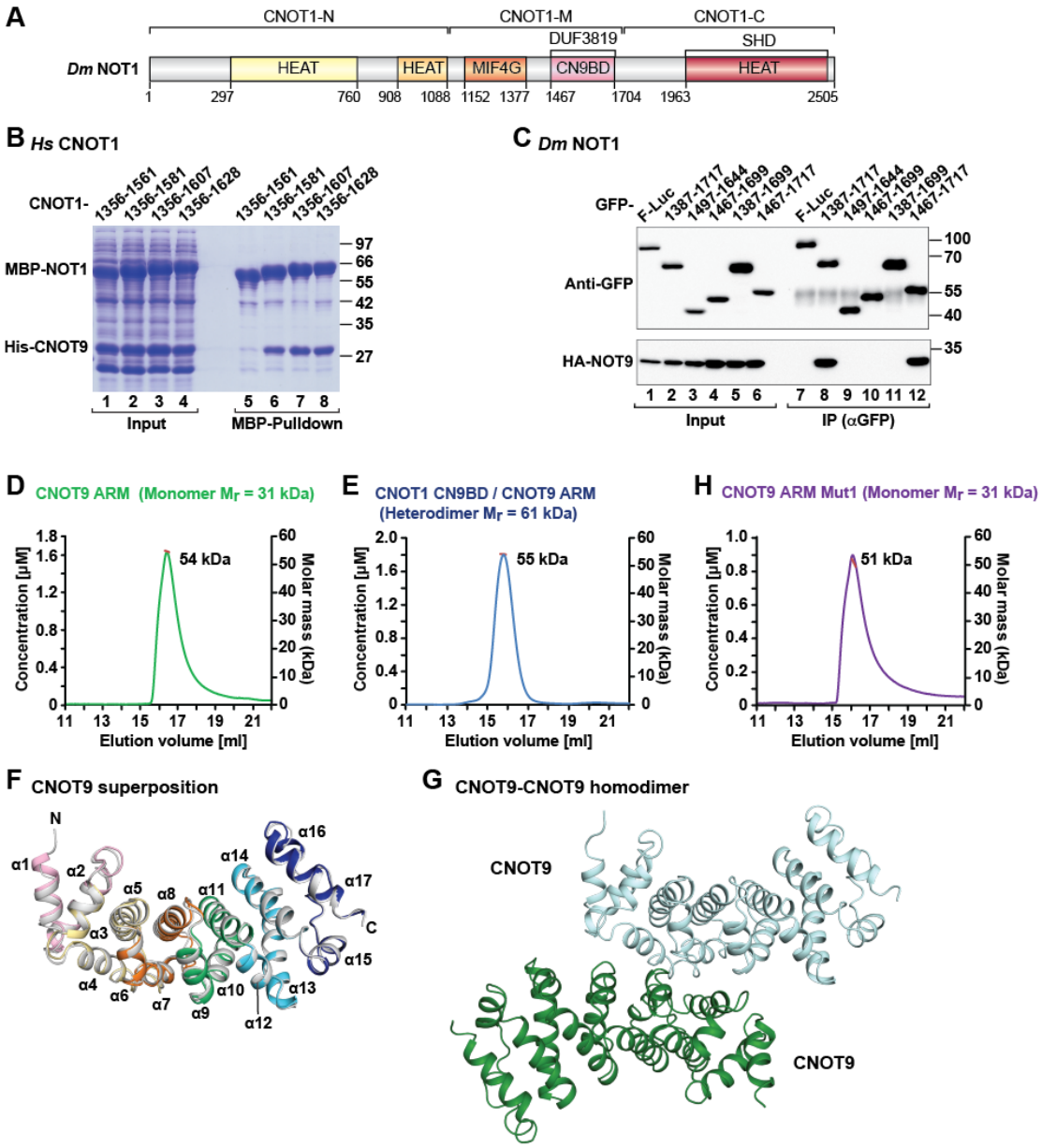

Figure S1, related to Figure 1. Interaction of NOT1 with NOT9 and MALLS analysis

(A) Domain organization of *Dm* NOT1. Abbreviations are as in Figure 1A.

(B) MBP pulldown showing the direct interaction between recombinant MBP-CNOT1 fragments and the His-tagged CNOT9 ARM-repeat domain (residues 19–285). See also Figure 1B,C.

(C) Western blot showing the interaction between GFP-NOT1 fragments and HA-

tagged NOT9 ARM-repeat domain in *Dm* S2 cells.

(D,E,H) Analytical size exclusion chromatography and multi-angle laser light scattering (MALLS). Isolated CNOT9 (D) or its CNOT9 Mut1 (H) form homodimers, which are incompatible with the CN9BD-CNOT9 binary complex (E). The expected molecular weights of the proteins (M_r) and the values measured in solution are indicated.

(F) Superposition of the CNOT9 ARM domain from the CNOT1-CNOT9 complex with CNOT1 (colored as in Figure 1F) with isolated CNOT9 (gray; PDB code 2FV2). See also Figure 1D–G.

(G) Cartoon representation of the CNOT9 ARM-repeat homodimer (PDB code 2FV2; Garces et al., 2007). The CNOT9 molecule in cyan is shown in the same orientation as in Figure 1D.

Figure S2

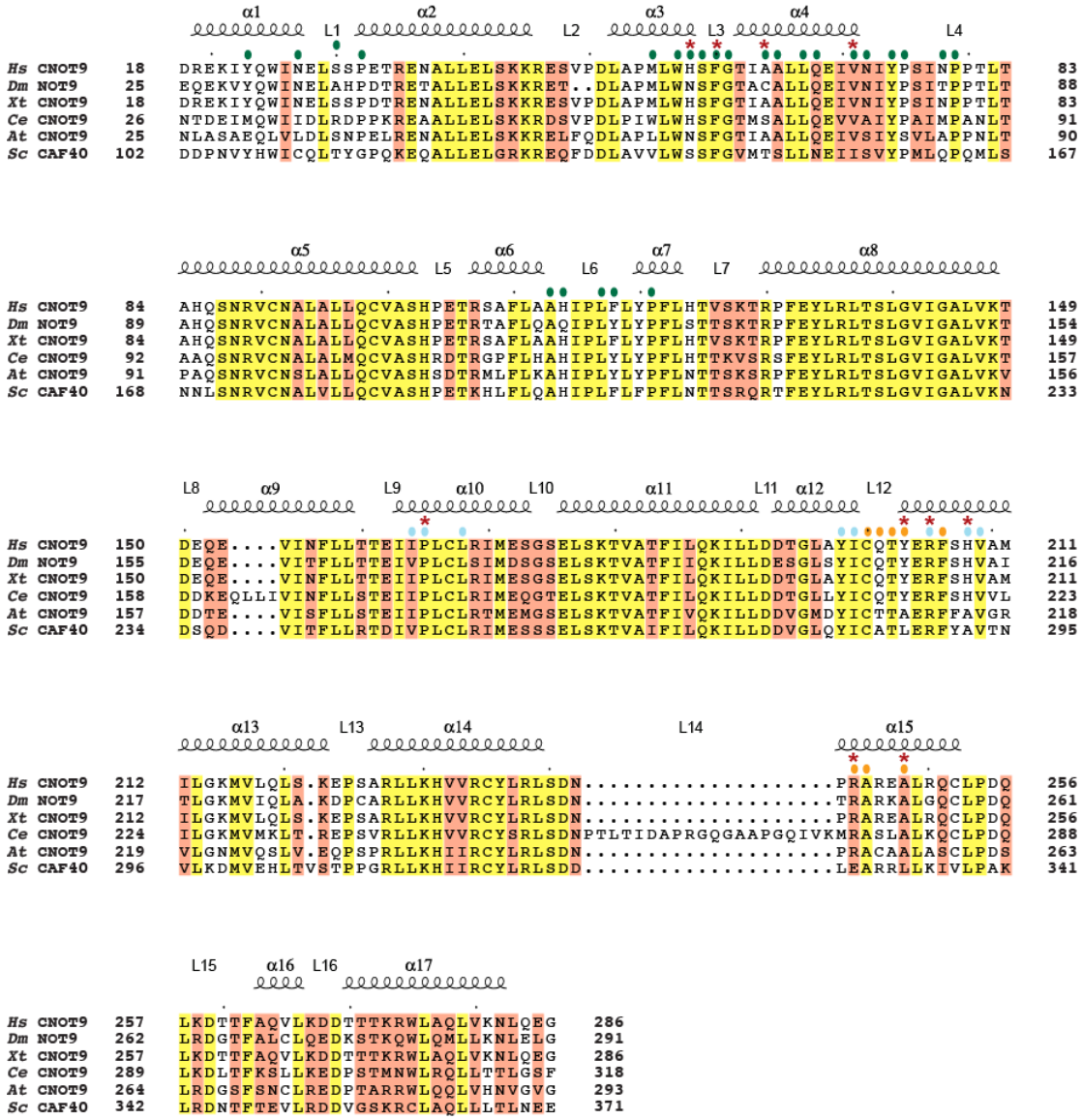

Figure S2, related to Figure 2. Structure-based multiple sequence alignment of the CNOT9 ARM-repeat domain

Secondary structure elements as determined from the structure are shown above the alignment. Residues conserved in all aligned sequences are shown with a yellow background, and residues with >70% similarity are highlighted in orange. Residues that form the interface with CNOT1 are indicated by green dots. Residues in pocket 1 and 2 are indicated by cyan and orange dots, respectively. Residues mutated in this study are marked by red asterisks. The species abbreviations are as follows: *Hs* (*Homo sapiens*), *Dm* (*Drosophila melanogaster*), *Xt* (*Xenopus tropicalis*), *Ce*

(*Caenorhabditis elegans*), *At* (*Arabodopsis thaliana*) and *Sc* (*Saccharomyces cerevisiae*). See also Figures 1–3. The alignments were carried out using ESPript (Gouet et al., 2003).

Figure S3

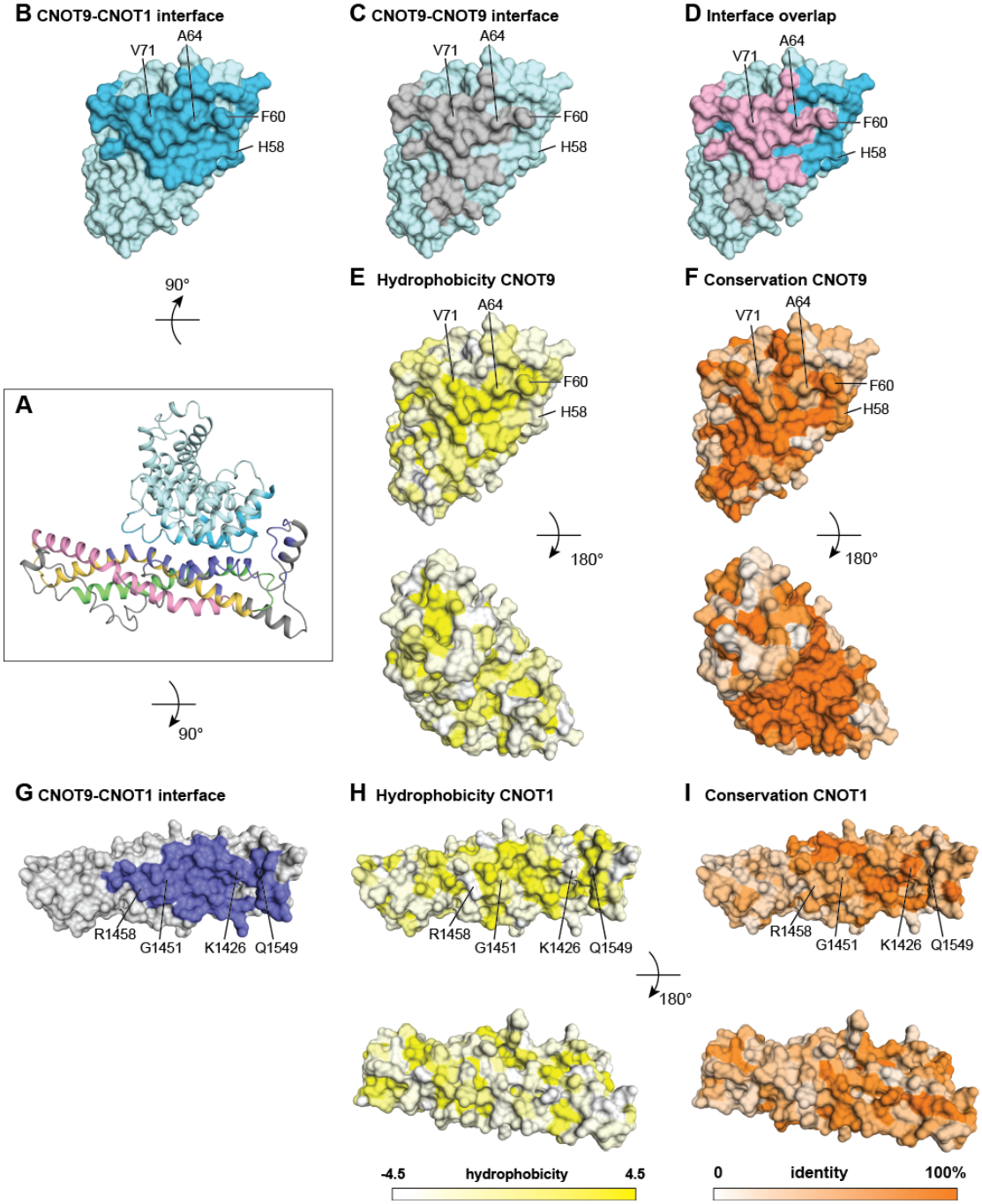

Figure S3, related to Figures 2 and 3. Conservation and hydrophobicity of the CN9BD-CNOT9 interface

(A) Cartoon representation of the CN9BD-CNOT9 complex (oriebtation as in Figure 1E). To visualize the interacting surfaces, the binding partners seen in (A) were rotated around the horizontal axis by 90º; upwards for the surface of CNOT9 (B–F), and downwards for the surface of the CN9BD (G–I). Selected interface residues are labeled for orientation.

(B–D) View of the CNOT9 surface that binds either CNOT9 in the homodimer or CNOT1 in the binary complex. The residues involved in CNOT1 binding and CNOT9 homodimerization are shown in dark cyan (B) and gray (C), respectively. Panel D shows a superposition of the views in panels B and C. The overlap between the two binding interfaces is shown in salmon. See also Figure 2.

(E and F) Surface representation of CNOT9 colored according to hydrophobicity (E) and conservation (F). The upper panels show a view of the CNOT1-binding interface in the same orientation as in panel (B). The lower panels show the opposite surface.

(G) View of the CN9BD surface that binds CNOT9 in the binary complex. The residues involved in CNOT9 binding are shown in purple.

(H and I) Surface representation of the CN9BD colored according to hydrophobicity (H) and conservation (I). The upper panels show a view in the same orientation as in panel (G). The lower panels show the opposite surface. The conservation scores of the individual residues are represented on the surface by color gradients from light (no conservation) to dark orange. Surfaces are colored white to yellow with increasing hydrophobicity as described in Figure 3.

Figure S4

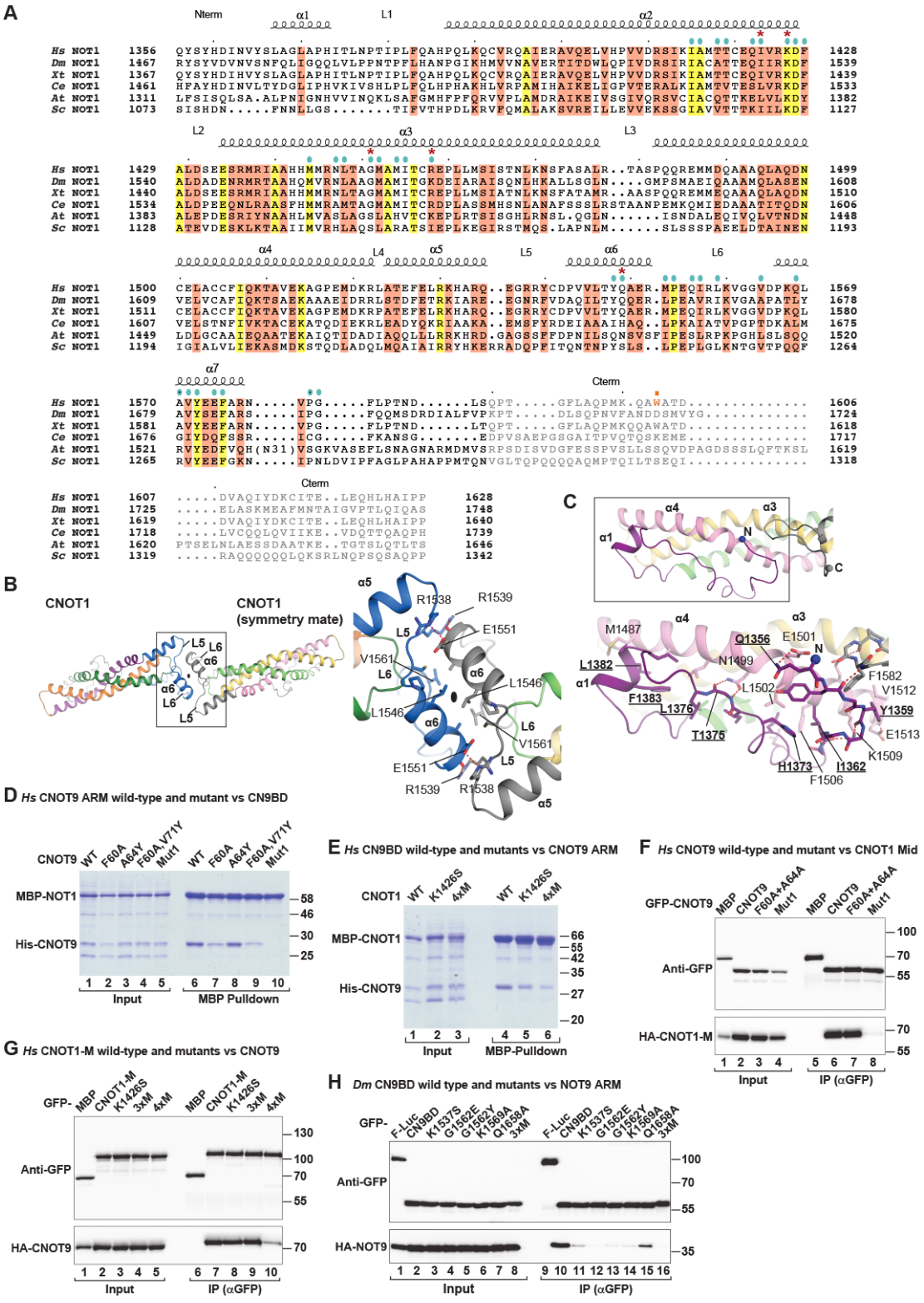

Figure S4, related to Figure 4. Structure-based sequence alignment of the CNOT1 CN9BD and interaction with CNOT9

(A) Secondary structure elements as determined from the CN9BD structure are shown above the alignment. Residues interacting with CNOT9 are indicated by cyan dots.

Residues that are not visible in the structure are shown in gray. Residue W1603, which inserts into the W-binding pocket in CNOT9, is shown in orange. Colors and species abbreviations are as described in Figure S2. See also Figures 1–4.

(B) Cartoon representation showing the crystal packing (left panel) and close-up view on the interactions between symmetry mates in the crystal lattice around a two-fold axis (right panel).

(C) Cartoon representation of the CN9BD (top panel) and close-up view (lower panel) showing how the N-terminal extension folds back and interacts with helix α4. N-terminal residues are shown in bold and are underlined. See also Figure 2.

(D and E) MBP pulldown using recombinant MBP-CNOT1 CN9BD (wild-type or the indicated mutants) and His-tagged CNOT9 ARM-repeat domain (wild-type or the indicated mutants).

(F) Western blot showing the interaction between GFP-CNOT9 (wild-type or the indicated mutants) and HA-CNOT1-M region in HEK293T cells. See also Figure S2.

(G) Western blot showing the interaction between GFP-CNOT1-M (wild-type or the indicated mutants) and HA-MBP-CNOT9 in HEK293T cells.

(H) Interaction between GFP-NOT1 CN9BD (wild-type or the indicated mutants) and HA-NOT9-ARM repeat domain in *Dm* S2 cells.

Figure S5

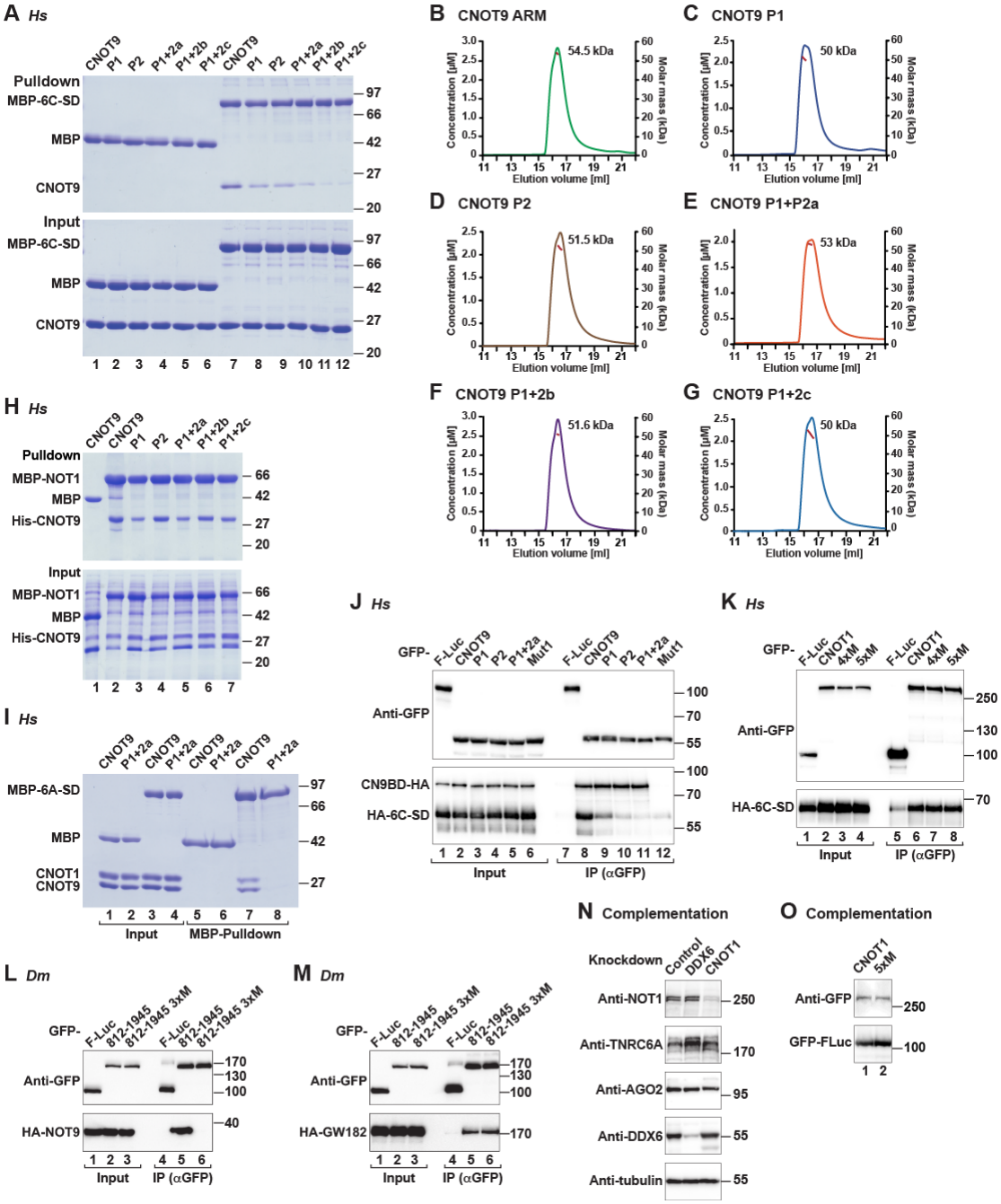

Figure S5, related to Figures 4 and 6. NOT9 W-binding pockets interact with GW182/TNRC6 proteins

(A) MBP pulldowns using recombinant MBP-tagged 6C-SD and His-tagged CNOT9 ARM-repeat domain (wild-type or the indicated pocket mutants). MBP served as a negative control. See also Figure 4 and Table S1.

(B-G) Analytical size exclusion chromatography and MALLS analysis of the wild-type CNOT9 homodimers or the indicated pocket mutants. The molecular weight of

the proteins measured in solution is indicated. The expected molecular weight for a dimer is 62 kDa.

(H) MBP pulldown showing the interaction of MBP-CNOT1 CN9BD with His-tagged CNOT9 ARM-repeat domain (wild-type or the indicated W-binding pocket mutants).

(I) MBP pulldown using recombinant MBP-tagged 6A-SD and pre-assembled CNOT1 CN9BD-CNOT9 ARM complexes containing CNOT9 wild-type or the P1+2a mutant. MBP served as a negative control.

(J) Interaction between GFP-CNOT9 (wild-type or the indicated mutants) and HA-6C-SD in the presence of HA-MBP tagged CN9BD in HEK293T cells.

(K) Interaction between GFP-CNOT1 (wild-type or the 4xM and 5xM mutants that do not bind CNOT9) and HA-6C-SD in HEK293T cells. The mutations are described in Table S1.

(L and M) Interaction of GFP-*Dm* NOT1 (residues 812-1945, either wild-type or the 3xM mutant) with CNOT9 (L) and *Dm* GW182 (M).

(N) Western blot analysis showing that the expression of endogenous AGO2 and TNRC6A is not affected in cells depleted of either CNOT1 or DDX6. The samples correspond to the depletions shown in Figures 4G and 6E.

(O) Western blot analysis showing the equivalent expression of the CNOT1 proteins used in the complementation assay shown in Figure 4G.

Figure S6

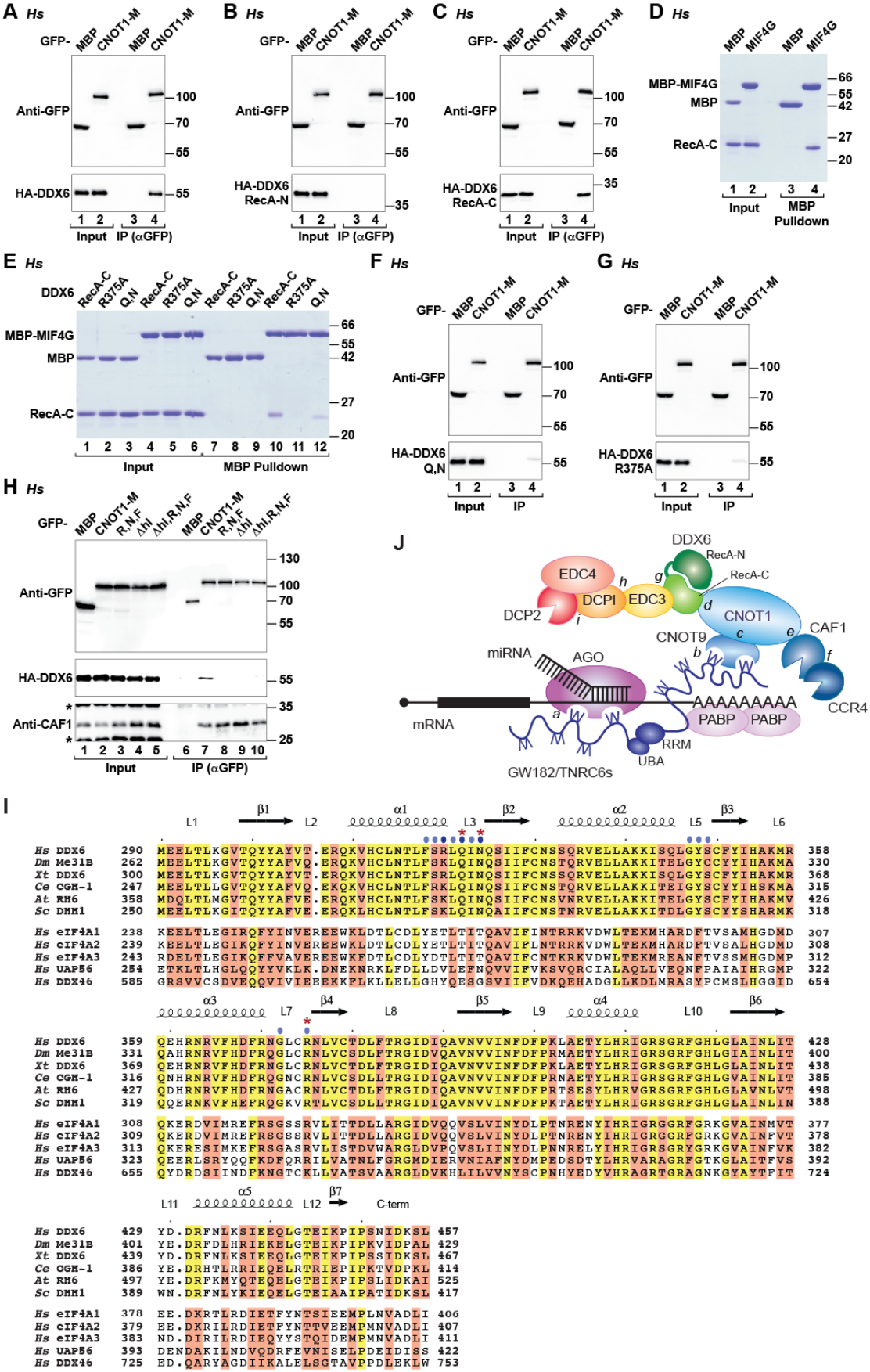

Figure S6, related to Figures 5 and 6. The CNOT1 MIF4G-DDX6 RecA-C

interaction

(A-C) Interaction between GFP-CNOT1-M and either full-length HA-tagged DDX6 (A), the RecA-N (B) or RecA-C (C) domains in HEK293T cells. See also Figure 5.

(D and E) MBP pulldowns using recombinant MBP-tagged CNOT1 MIF4G domain and His-tagged DDX6 RecA-C domain (wild-type or mutants). MBP served as a negative control.

(F and G) Interaction between GFP-CNOT1-M and HA-tagged wild-type DDX6 or the indicated DDX6 mutants in HEK293T cells. The coimmunoprecipitation shown in panel (A) was performed in parallel and served as positive control.

(H) Interaction between GFP-CNOT1-M (wild-type or the indicated mutants) and HA-tagged DDX6 in HEK293T cells. The presence of endogenous CAF1 in the immunoprecipitates was confirmed using specific anti-CAF1 antibodies. The asterisk indicates crossreactivity of the antibody with an endogenous protein in the input lysate. See also Figures 5 and 6, Figure S8 and Table S1.

(I) Structure-based multiple sequence alignment of DDX6 RecA-C domains with members of the eIF4A family and the DEAD box helicases UAP56 and DDX46. Secondary structure elements as determined from the structure are shown above the alignment. Residues that form the interface with the CNOT1 MIF4G domain are indicated by blue dots. Residues providing specificity are highlighted by dark blue dots. Residues mutated in this study are marked by red asterisks. Colors and species abbreviations are as described in Figure S2. See also Figures 5, 6, S7 and Table S1.

(J) The structure of the CNOT1-DDX6 complex described in this study together with the available structures of CNOT1 bound to deadenylases and of DDX6 in complex with decapping factors, present snapshots of consecutive steps of the 5'-to-3' mRNA decay pathway. Together with the structure of the CN9BD-CNOT9 complex, these structures establish a chain of physical interactions to describe how the CCR4-NOT

complex is recruited to miRNA targets and enrolls DDX6, which in turn represses translation and recruits the decapping machinery. See also Figure 5J. The letters in italics indicate the interactions supported by crystal or NMR structures. (a) Structure of human AGO2 bound to tryptophan (Schirle and MacRae, 2012); (b,c,d) Structures described in the present study. (e,f) Structure of the human CNOT1 MIF4G domain bound to CAF1 (Petit et al., 2012) and of *S. cerevisiae* Not1 bound to the Caf1-Ccr4 complex (Basquin et al., 2012). (g) Structure of DDX6 bound to EDC3 (Sharif et al., 2013; Tritschler et al., 2009). (h) Structure of EDC3 bound to an helical leucine rich motif (HLM) present in DCP1 in metazoans (Fromm et al., 2012). (i) Structure of the *S. pombe* Dcp1-Dcp2 complex (She et al., 2008).

Table S1. Mutants and antibodies used in this study

Name	*Hs* CNOT1 (1-2376)	*Dm* NOT1 (1-2505)	Location
CNOT1-N	1–1089	1–1148	
CNOT1-M	1085–1605	1147–1717	
CNOT1-C	1595–2376	1710–2505	
CNOT1 MIF4G	1093–1317	1152–1377	
CNOT1 SHD	1842-2353	1963–2478	
	1318–1605		
	1386–1535		
CBD/DUF3819	1356–1588	1467–1704	
	1356–1561		
	1356–1607		
	1356–1628		
	K1426S	K1537S	Interface with CNOT9
	G1451Y	G1562E, G1562Y	Interface with CNOT9
	R1458A	K1569A	Interface with CNOT9
	Q1549A	Q1658A	Interface with CNOT9
3xM	K1426S, G1451Y, R1458A	K1537S,G1562E,Q1658A	Interface with CNOT9
4xM	K1426S, G1451Y, R1458A, Q1549A		Interface with CNOT9
5xM	I1423D, K1426S, G1451Y, R1458A, Q1549A		Interface with CNOT9
Δhl	Δ1097–1110		Interface with DDX6
Δhl,N,F	Δhl,N1144A,F1145A		Interface with DDX6
Δhl,R1138A	Δhl,R1138A		Interface with DDX6
Δhl,R,N,F	Δhl,R1138A,N1144A,F1145A		Interface with DDX6

Name	*Hs* CNOT9 (1-299)	*Dm* NOT9 (1-304)	Location
ARM	19–285	25-291	
H58A	H58A	N63A	Interface with CNOT1
F60A	F60A	F65A	Interface with CNOT1
A64Y	A64Y	C69Y	Interface with CNOT1
V71Y	V71Y	V67Y	Interface with CNOT1
Quadruple Mut1	H58A,F60A,A64Y,V71Y	N63A,F65A,C69Y,V67Y	Interface with CNOT1
Mut2		N63A,F65A,C69Y	
P1a	Y203A	Y208A	Pocket 1
P1b	R244A	R249A	Pocket 1
P1c	A248F	A235F	Pocket 1
P1	Y203A,R244A	Y208A,R249A	Pocket 1
P1d	Y203A,A248F	Y208A,A253F	Pocket 1

P2a	P165G		Pocket 2
P2b	R205A		Pocket 2
P2c	H208A		Pocket 2
P2	R205A,H208A	R210A,H213A	Pocket 2
P1+2a	Y203A,R205A,H208A,R244A		Pocket 1+2
P1+2b	Y203A,R205A,H208A,A248F	Y208A,R210A,H253F,A253F	Pocket 1+2
P1+2c	P165G,Y203A,R205A, R244A		Pocket 1+2

Name	***Hs* DDX6 (1-472)** NCBI: NM_004397.3	**Location**
RecA-N	85–295	
RecA-C	296–463	
R375A	R375A	Interface with CNOT1
Q322A	Q322A	Interface with CNOT1
N324A	N324A	Interface with CNOT1
Q,N	Q322A,N324A	Interface with CNOT1

Antibody	**Source**	**Catalog Number**	**Dilution**	**Monoclonal/ Polyclonal**
Anti-HA-HRP	Roche	12 013 819 001	1:5,000	Monoclonal
Anti-GFP (for western blotting)	Roche	11 814 460 001	1:2,000	Monoclonal
Anti-GFP (for immunoprecipitations)	In house			Rabbit polyclonal
Anti-tubulin	Sigma *Aldrich*	T6199	1:5,000	Monoclonal
Anti-mouse-HRP	GE Healthcare	NA931V	1:10,000	Polyclonal
Anti-rabbit-HRP	GE Healthcare	NA934V	1:10,000	Polyclonal
Anti-DDX6	Bethyl Laboratories	A300-461A	1:3,000	Rabbit polyclonal
Anti-*Hs* CAF1	In house		1:2,000	Rabbit polyclonal
Anti-*Hs* CNOT1	In house		1:1,000	Rabbit polyclonal
Anti-*Hs* CNOT9	Proteintech	22503-1-AP	1:1,000	Rabbit polyclonal
Anti-*Hs* AGO2	Sigma *Aldrich*	SAB4200085	1:2,000	Monoclonal
Anti-*Hs* GW182 (TNRC6A)	Bethyl Laboratories	A302-329A	1:1,000	Rabbit polyclonal
Anti-V5	AbD Serotec	MCA1360GA	1:5,000	Monoclonal

SUPPLEMENTAL EXPERIMENTAL PROCEDURES

Plasmids

Plasmids expressing epitope-tagged proteins in human and *Dm* S2 cells have been previously described (Bawankar et al., 2013; Braun et al., 2011; Tritschler et al., 2009). For expression in *E. coli*, the DNAs coding for the human CNOT1 CN9BD domain (residues 1356–1607) and the ARM-repeat domain of CNOT9 (residues 19–285) were amplified by PCR using total human cDNA as the template and inserted between the XhoI and BamHI restriction sites of the pnYC-NpM (which provides an N-terminal MBP tag followed by a HRV3C protease cleavage site; Diebold et al., 2011) and pnEA-NpH (which provides an N-terminal 6xHis tag, followed by a HRV3C protease cleavage site; Diebold et al., 2011) vectors, respectively. Plasmids for expression of the CNOT1 MIF4G domain (residues 1093–1317) and the DDX6 RecA-C domain (residues 296–472) were described previously (Petit et al., 2013; Tritschler et al., 2009). DNA fragments encoding the TNRC6 silencing domains (TNRC6A residues 1462–1962 and TNRC6C residues 1261–1690) were amplified by PCR and inserted between the XhoI and AvrII restriction sites of the pnYC-NpM vector. A non-cleavable C-terminal 6x-His tag was introduced by PCR. Mutations were introduced using the QuikChange mutagenesis kit (Stratagene) with the appropriate oligonucleotides and confirmed by sequencing. The mutations used in this study are described in Table S1.

Protein Expression and Purification

The CNOT1 CN9BD domain and the CNOT9 ARM domain were co-expressed in *E. coli* BL21 Star (DE3) cells (Invitrogen) and induced at an OD_{600} of 0.6 with 1 mM Isopropyl β-D-1-thiogalactopyranoside (IPTG). Following induction the proteins were expressed overnight at 20^{o}C. The CN9BD-CNOT9 ARM complex was purified in

lysis buffer (50 mM potassium phosphate (pH 7.5), 300 mM NaCl, 2 mM ß-mercaptoethanol) supplemented with protease inhibitors (Roche complete EDTA-free, 1 tablet per 50 ml of lysis buffer), lysozyme (SIGMA, 1 mg/ml) and DNase I (10 µg/ml), using amylose resin (New England Biolabs Inc.) to capture MBP tagged CNOT1 CN9BD as an initial purification step. The complex was digested with HRV3C protease while dialyzing into 20 mM HEPES buffer (pH 7.5), 150 mM NaCl and 1 mM DTT. The complex was further purified on a heparin column (HiTrap Heparin HP 5 ml, GE Healthcare) and a final size exclusion chromatography step (HiLoad Superdex 200 26/60 column, GE Healthcare) equilibrated in storage buffer (10 mM HEPES (pH 7.5), 150 mM NaCl and 1 mM DTT). The protein complex was concentrated to 5 mg/ml prior to use for crystallization.

Structure Solution and Refinement

Diffraction data were collected at a wavelength of 1.000 Å and processed with XDS (Kabsch, 2010). The structures were solved by molecular replacement in PHASER (McCoy et al., 2007) using the CNOT9 monomer (PDB ID code 2FV2; Garces et al., 2007) as a search model for the CN9BD-CNOT9 complex (1.65 Å resolution). For the MIF4G-DDX6 complex (1.75 Å resolution), previously determined structures of the isolated domains were used as search models (PDB ID code 4GML; Petit et al., 2012; PDB ID code 2WAX; Tritschler et al., 2009). The structures were then built automatically using the PHENIX AutoSol wizard (Terwilliger et al., 2009) and BUCCANEER (Cowtan, 2006) from the CCP4 package (Winn et al., 2011). The models were subsequently improved manually in COOT (Emsley et al., 2010) and refined using PHENIX (Afonine et al., 2012). Final refinement rounds were carried out in PHENIX, refining TLS parameters in addition to individual B-factors and including hydrogens in the riding positions. The final model of the CN9BD-CNOT9

complex was then used as a molecular replacement model for the complex at 2.05 Å resolution using PHASER. This structure contains additional free tryptophan as a ligand and was refined without the use of hydrogens. All models were subsequently improved by iterative cycles of refinement and building using PHENIX and COOT. The correct stereochemical properties of the structures were verified with MOLPROBITY (Chen et al., 2010). Figures were generated in PyMOL (http://www.pymol.org). The data collection and refinement statistics are summarized in Table 1.

***In vitro* Pulldown Assays**

The TNRC6 silencing domains were expressed overnight in *E. coli* BL21 (DE3) Star cells (Invitrogen) at 20^{o}C. All purification steps were performed on ice in lysis buffer (50 mM potassium phosphate (pH 7.5), 300 mM NaCl, 2 mM ß-mercaptoethanol), supplemented with protease inhibitors (Roche complete EDTA-free, 2 tablets per 50 ml of lysis buffer), lysozyme (1 mg/ml) and DNAse I (5 µg/ml). The bacterial lysates were incubated with amylose resin for 1 hour and eluted in lysis buffer supplemented with 30 mM maltose. The silencing domain was subsequently loaded onto a Ni-column (HiTrap IMAC HP; GE Healthcare) to separate C-terminally truncated fragments from the full-length protein. The fusion protein was dialyzed into HEPES buffer (20 mM HEPES pH (7.5), 150 mM NaCl, 1 mM DTT) and further purified by size-exclusion chromatography (HiLoad Superdex 200 26/60 column, GE Healthcare). CNOT9 mutants were purified as described for the wild-type protein.

MBP pulldown assays were performed in a final volume of 100 µl of PBS buffer using 6.25 µM of purified silencing domain and CNOT9 (wild-type and mutants). The purified proteins were incubated for 30 min at room temperature before adding 50 µl (50% slurry) of amylose resin followed by another 30 min incubation. The beads were

washed four times with PBS buffer and eluted in elution buffer (PBS supplemented with 30 mM maltose). The eluted proteins were precipitated with TCA (trichloroacetic acid) and analyzed on a 14% SDS-PAGE.

For the CNOT9-CNOT1 pulls downs shown in Figures S1B and S5C,D, His-tagged *Hs* CNOT9 (residues 19–285, wild-type or mutants) and MBP-tagged *Hs* CNOT1 (wild-type, fragments or mutants) were co-expressed in *E. coli* BL21 (DE3) star cells. The cells were lysed in suspension buffer containing 50 mM Tris (pH 7.5), 150 mM NaCl, 0.1% Triton X-100 supplemented with protease inhibitors, lysozyme, DNAse I and 10% glycerol. Cell lysates were sonicated four times for 30 s and cleared by centrifugation at 20,000 ×*g*. The cleared supernatants were incubated with 50 µl (50% slurry) of amylose resin for 45 min at 25^{o}C. The beads were washed four times with suspension buffer, bound proteins were eluted using 2x protein sample buffer and analyzed on a 14% SDS-PAGE.

The DDX6-MIF4G pulldowns were performed at room temperature with purified proteins in binding buffer containing 25 mM HEPES (pH 7.0), 20 mM NaCl and 2mM DTT. The proteins were incubated for 30 min before adding 50 µl (50% slurry) of amylose resin at room temperature, followed by another 30 min incubation. Proteins were eluted and analyzed as described above.

Complementation Assays

Plasmids expressing short-hairpin RNAs (shRNAs) for knockdowns are derived from the pSUPER plasmid containing the puromycin-resistance gene for selection. The vector backbone was a kind gift from O. Mühlemann (University of Bern). The 19 nt target sequences are as follows: control ATTCTCCGAACGTGTCACG, CNOT1 ATTCAACATTCCCTTATA, and DDX6 GCAGAAACCCTATGAGATT. HeLa cells were grown in DMEM supplemented with 10% heat inactivated fetal calf serum,

2 mM L-Glutamine, 100 U/ml penicillin and 100 mg/ml streptomycin. Cells were transfected in 6-well plates using Lipofectamine 2000 (Invitrogen) according to the manufacturers protocol. Transfection mixtures contained 4 μg of plasmids expressing the relevant shRNA. Twenty-four hours after transfection, cells were selected in medium supplemented with 1.5 μg/ml puromycin. After 1 day of selection, cells were counted and seeded in 12-well plates in medium without puromycin for recovery. Twenty-four hours after reseeding, cells were re-transfected using Lipofectamine 2000. The transfection mixtures contained 0.36 μg of plasmids expressing the relevant shRNA, 0.12 μg of the reporter pSiCHECK-8xLet7 plasmid or the corresponding reporter carrying mutations in the Let-7 binding sites and 0.12 μg of the pEGFP-N3-F-Luc transfection control. For the CNOT1 complementation assays, the transfection mixtures contained either 1 μg pT7-EGFP-CNOT1 (wild-type or mutants) or pT7-EGFP as a control. For the DDX6 complementation, the transfection mixtures contained either 0.4 μg pCIneo-λN-HA-MBP or pCIneo-λN-HA-DDX6 (wild-type or mutants). Cell were harvested 72 hours after the second transfection. R-Luc and F-Luc activities were measured using the Dual-Luciferase Reporter Assay System (Promega).

Supplemental references

Afonine, P.V., Grosse-Kunstleve, R.W., Echols, N., Headd, J.J., Moriarty, N.W., Mustyakimov, M., Terwilliger, T.C., Urzhumtsev, A., Zwart, P.H. and Adams, P.D. (2012). Towards automated crystallographic structure refinement with phenix.refine. Acta Crystallogr. D Biol. Crystallogr. *68*, 352–367.

Basquin, J., Roudko, V.V., Rode, M., Basquin, C., Séraphin, B., and Conti, E. (2012). Architecture of the nuclease module of the yeast Ccr4-not complex: the Not1-Caf1-Ccr4 interaction. Mol. Cell *48*, 207–218.

Chen, V.B., Arendall, W.B., Headd, J.J., Keedy, D.A., Immormino, R.M., Kapral, G.J., Murray, L.W., Richardson, J.S., and Richardson, D.C. (2010). MolProbity: all-atom structure validation for macromolecular crystallography. Acta Crystallogr. D Biol. Crystallogr. *66*, 12–21.

Cowtan, K. (2006). The Buccaneer software for automated model building. 1. Tracing protein chains. Acta Crystallogr. D Biol. Crystallogr. *62*, 1002–1011.

Diebold, M.L., Fribourg, S., Koch, M., Metzger, T., and Romier, C. (2011). Deciphering correct strategies for multiprotein complex assembly by co-expression: application to complexes as large as the histone octamer. J. Struct. Biol. *175*, 178–188.

Emsley, P., Lohkamp, B., Scott, W.G. and Cowtan, K. (2010). Features and development of Coot. Acta Crystallogr. D Biol. Crystallogr. *66*, 486–501.

Fromm, S.A., Truffault, V., Kamenz, J., Braun, J.E., Hoffmann, N.A., Izaurralde, E., and Sprangers, R. (2012). The structural basis of Edc3- and Scd6-mediated activation of the Dcp1:Dcp2 mRNA decapping complex. EMBO J. *31*, 279–290.

Gouet, P., Robert, X., and Courcelle E. (2003). ESPript/ENDscript: extracting and rendering sequence and 3D information from atomic structures of proteins. Nucleic Acids Res. *31*, 3320–3323.

Kabsch, W. (2010). XDS. Acta Crystallogr. D Biol. Crystallogr. *66*, 125–132.

McCoy, A.J., Grosse-Kunstleve, R.W., Adams, P.D., Winn, M.D., Storoni, L.C., and Read, R.J. (2007). Phaser crystallographic software. J. Appl. Crystallogr. *40*, 658–674.

Sharif, H., Ozgur, S., Sharma, K., Basquin, C., Urlaub, H., and Conti, E. (2013). Structural analysis of the yeast Dhh1-Pat1 complex reveals how Dhh1 engages Pat1, Edc3 and RNA in mutually exclusive interactions. Nucleic Acids Res. *41*, 8377–8390.

She, M., Decker, C.J., Svergun, D.I., Round, A., Chen, N., Muhlrad, D., Parker, R., and Song, H. (2008). Structural basis of Dcp2 recognition and activation by Dcp1. Mol. Cell *29*, 337–349.

Terwilliger, T.C., Adams, P.D., Read, R.J., Mccoy, A.J., Moriarty, N.W., Grosse-Kunstleve, R.W., Afonine, P.V., Zwart, P.H., and Hung, L.W. (2009). Decision-making in structure solution using Bayesian estimates of map quality: the PHENIX AutoSol wizard. Acta Crystallogr. D Biol. Crystallogr. *65*, 582–601.

Winn, M.D., Ballard, C.C., Cowtan, K.D., Dodson, E.J., Emsley, P., Evans, P.R., Keegan, R.M., Krissinel, E.B., Leslie, A.G.W., McCoy, A.*, et al.* (2011). Overview of the CCP4 suite and current developments. Acta Crystallogr. D Biol. Crystallogr. *67*, 235–242.

miRISC and the CCR4-NOT complex repress and degrade mRNA targets independently of 43S ribosomal scanning

Duygu Kuzuoğlu-Öztürk, Dipankar Bhandari, Eric Huntzinger, Maria Fauser, Sigrun Helms and Elisa Izaurralde*

Department of Biochemistry, Max Planck Institute for Developmental Biology, Spemannstrasse 35, D-72076 Tübingen, Germany

*Correspondence should be addressed to:

Elisa Izaurralde

Phone: +49-7071-601-1350

Fax: +49-7071-601-1353

elisa.izaurralde@tuebingen.mpg.de

Running title: 43S ribosomal scanning is not required for silencing

Key words: Argonaute / Deadenylation / DDX6 / eIF4A / GW182 / mRNA decay / miRNA / TNRC6

ABSTRACT

miRNAs associate with Argonaute (AGO) proteins to silence the expression of mRNA targets by inhibiting translation and eliciting deadenylation, decapping and mRNA degradation. A current model for silencing indicates that AGOs mediate these effects through the sequential recruitment of GW182 proteins, the CCR4-NOT deadenylase complex and the translational repressor and decapping activator DDX6. An alternative model posits that AGOs repress translation by interfering with eIF4A function during 43S ribosomal scanning and that this mechanism is independent of GW182 and the CCR4-NOT complex in *Drosophila melanogaster.* Here we show that miRNAs, AGO, GW182 and NOT1 do not require 43S ribosomal scanning or eIF4A activity to repress translation but require DDX6 in human cells. We further show that the repressive activity of AGOs depends on their interaction with GW182, which in turn recruits the CCR4-NOT complex to mediate silencing in both human and *D. melanogaster* cells. Collectively, our data indicate that CCR4-NOT is a major downstream effector complex in the miRNA pathway.

Introduction

miRNAs are a class of small noncoding RNAs that assemble with Argonaute proteins into miRNA-induced silencing complexes (miRISCs) to mediate post-transcriptional repression of complementary mRNA targets (Ameres and Zamore 2013). In animal cells, silencing is effected by a combination of translational repression and mRNA destabilization, with the latter accounting for most of the miRNA-mediated repression observed in mammalian cell cultures (Hendrickson et al. 2009; Guo et al., 2010; Eichhorn et al. 2014).

miRNA target degradation is catalyzed by the enzymes of the 5'-to-3' mRNA decay pathway (Rehwinkel et al. 2005; Behm-Ansmant et al. 2006, Eulalio et al. 2007; Chen et al. 2009; Eulalio et al. 2009; Piao et al. 2010). In this pathway, mRNAs are first deadenylated by the PAN2-PAN3 and the CCR4-NOT complexes, then decapped by the decapping enzyme DCP2 and finally degraded from the 5'-end by the XRN1 exonuclease (Huntzinger and Izaurralde 2011). The GW182/TNRC6 proteins play a central role in this process by interacting with AGOs and recruiting the PAN2-PAN3 and the CCR4-NOT deadenylase complexes to miRNA targets, thereby accelerating their degradation (Fabian and Sonenberg 2012; Braun et al. 2013).

In addition to accelerating mRNA degradation, miRNAs also trigger translational repression, but the precise repressive mechanism remains poorly understood, and several models have been proposed (Fabian and Sonenberg 2012). One possible model is that the recruitment of the CCR4-NOT complex is sufficient to mediate silencing (Braun et al. 2013). This model is based on the following observations. First, the interaction of GW182 proteins with the CCR4-NOT complex is not only required for degradation but also for translational repression of miRNA targets (Braun et al. 2011; Chekulaeva et al. 2011; Fabian et al. 2011; Huntzinger et al. 2013; Zekri et al. 2013; Chen et al. 2014; Mathys et al. 2014). Second, like

miRISC, the CCR4-NOT complex represses translation in the absence of deadenylation (Cooke et al. 2010; Braun et al. 2011; Chekulaeva et al. 2011; Bawankar et al. 2013; Zekri et al. 2013). Translational repression by the CCR4-NOT complex can, at least in part, be explained by a direct interaction between the NOT1 subunit and the DEAD box RNA helicase DDX6 (also known as RCK). Human DDX6 and its *Dm* ortholog Me31B repress translation, activate decapping and play a role in silencing (Chu and Rana 2006; Eulalio et al. 2007; Nishihara et al. 2013; Presnyak and Coller 2013; Chen et al. 2014; Mathys et al. 2014, Rouya et al. 2014).

An alternative model of silencing involves the translation initiation factor eIF4A. eIF4A proteins are DEAD-box RNA helicases that unwind secondary structures within mRNA 5' UTRs, allowing the 43S preinitiation complex (PIC) to scan the 5'-UTR toward the start codon (Jackson et al. 2010). Several studies have indicated that miRISCs inhibit 43S scanning by interfering with eIF4A function (Meijer et al. 2013, Ricci et al. 2013; Fukao et al. 2014; Fukaya et al. 2014). How this interference is achieved remains unclear. One study reported that NOT1 interacts with eIF4A2, but not with its paralog eIF4A1 in human cells (Meijer et al. 2013). It was suggested that this interaction locks eIF4A2 onto the mRNA 5'-UTR and represses translation by blocking 43S scanning (Meijer et al. 2013). However, the interaction between NOT1 and eIF4A2 was not confirmed in subsequent studies (Chen et al. 2014; Mathys et al. 2014; Rouya et al. 2014).

Furthermore, in contrast to the model proposed by Meijer et al., two recent studies indicated that miRNAs repress translation by releasing rather than recruiting eIF4A2 and that both eIF4A1 and eIF4A2 are dislodged from silenced mRNAs (Fukao et al. 2014; Fukaya et al. 2014). Remarkably, *Dm* AGO1 promotes eIF4A displacement independently of GW182, and *Dm* GW182 caused eIF4A and eIF4E displacement independently of AGO1 (Fukaya et al. 2014). These and additional

observations suggested that *Dm* AGO1 exhibits silencing activity independently of GW182 proteins in *D. melanogaster* (Fukaya and Tomari 2012; Wu et al. 2013; Fukaya et al. 2014). Whether this is also the case for human AGOs has not been investigated.

In sum, the mechanism by which miRNAs repress translation is still not fully understood, and it is not known whether the recruitment of the CCR4-NOT complex fully explains silencing or whether parallel and potentially species-specific repressive mechanisms exist. To clarify these open questions, we adopted a comparative approach and investigated the silencing mechanisms in human and *Dm* cells. We found that miRNAs, AGOs, GW182, the CCR4-NOT complex and DDX6/Me31B repress and degrade polyadenylated mRNA targets that are translated via scanning and eIF4A independent mechanisms in both human and *Dm* cells. Collectively, our results indicate that the CCR4-NOT complex is a major conserved downstream effector of silencing.

Results

The W-binding pockets of AGOs mediate binding to the GW182/TNRC6 proteins

Structural studies of human (*Hs*) AGO2 revealed the presence of tandem W-binding pockets (pockets P1 and P2) on the surface of the AGO2 PIWI domain opposite to the miRNA-binding site (Supplemental Fig. S1A; Schirle and MacRae 2012). These pockets represent potential binding sites for the GW182/TNRC6 proteins and are conserved in *Hs* AGO1, AGO3 and AGO4 as well as in *Dm* AGO1 (Supplemental Fig. S1B; Schirle and MacRae 2012). To determine whether AGOs exhibit silencing activity independently of GW182 proteins, we designed mutations to disrupt the W-binding pockets in *Hs* AGO2 and *Dm* AGO1 (mutants P1 and P2, Supplemental Fig. S1A,B and Table S1). The ability of the mutated proteins to interact with GW182/TNRC6 proteins was tested in coimmunoprecipitation assays.

Mutations in either of the two *Dm* AGO1 pockets abolished the interaction with endogenous *Dm* GW182 in Schneider cells (S2 cells; Fig. 1A, lanes 8 and 9 *vs*. 7). The mutant proteins were expressed at levels comparable to wild-type and associated with endogenous miR-2a, indicating that the mutations do not disrupt the fold of the PIWI domain (Fig. 1A). Similarly, combined mutations in the two pockets of *Hs* AGO2 abolished its interaction with TNRC6A, TNRC6B and TNRC6C in HEK293T cells (Fig. 1B–D, lanes 10 vs. 7). Mutations in only one of the two pockets disrupted the interaction of *Hs* AGO2 with TNRC6C but only reduced TNRC6A binding (Fig. 1B,D). The binding of TNRC6B was impaired by mutations in P2 but not in P1 (Fig. 1C). These results reveal differences in the binding properties of the three TNRC6 proteins. Importantly, the mutations in the *Hs* AGO2 W-binding pockets did not interfere with miR-16 loading (Fig. 1D). We concluded that the integrity of the W-

binding pockets is required for *Hs* AGO2 and *Dm* AGO1 to interact with GW182/TNRC6 proteins.

The silencing activity of AGOs requires the integrity of the W-binding pockets

Next, we examined the silencing activity of the AGO mutants using previously described λN- or MS2-based tethering assays (Pillai et al. 2004; Rehwinkel et al. 2005). Tethered *Dm* AGO1 and *Hs* AGO2 repressed translation and promoted degradation of polyadenylated mRNA reporters, as shown previously (Fig. 2A–D; Rehwinkel et al. 2005; Pillai et al. 2004; Eulalio et al. 2008; Chen et al. 2009; Piao et al. 2010). Mutations in P2 were sufficient to abolish the activity of the *Dm* and *Hs* AGOs in tethering assays (Fig. 2A–D). The activity of *Dm* AGO1 was also abolished by mutations in P1 (Fig. 2A,B).

Because the reporters were degraded, it was possible that the recruitment of deadenylases by GW182/TNRC6 masked any additional repressive activity that AGOs might have independently of these proteins. Therefore, we next tested the activity of the AGO mutants using mRNA reporters that are refractory to deadenylation and subsequent decay. In *Dm* cells, we used an mRNA reporter with a 3'-end generated by a self-cleaving hammerhead ribozyme (HhR). Immediately upstream of the ribozyme cleavage site, the reporter contains an internal poly(A) stretch of 95 residues followed by a poly(C) stretch of 7 residues, which blocks deadenylation (F-Luc-5BoxB-A_{95}-C_7-HhR; Zekri et al. 2013). Tethered *Dm* AGO1 repressed this reporter predominantly at the translational level (Fig. 2E,F). The mutations in either P1 or P2 abolished *Dm* AGO1 repressive activity (Fig. 2E,F). The protein mutants were expressed at levels comparable to wild-type (Fig. 2G).

In human cells, we used an R-Luc-5BoxB reporter containing the 3'-end of the MALAT1 non-coding RNA, which is processed by RNase P and thus lacks a poly(A)

tail (Wilusz et al. 2012). *Hs* AGO2 repressed the translation of this reporter without causing mRNA degradation (Fig. 2H–J). The repression was relieved by mutations in either of the two W-binding pockets (Fig. 2H–J). The *Dm* or *Hs* AGO proteins did not repress the corresponding reporters that lacked the BoxB sites (Supplemental Fig. S2A,B). Taken together, our results indicate that the activity of tethered AGO proteins depends on the integrity of the W-binding pockets.

Dm AGO1 requires the interaction with GW182 to silence miRNA targets

Because tethering assays bypass some steps in silencing, we next tested the activity of the AGO mutants in complementation assays in *Dm* cells, wherein miRNAs predominantly associate with AGO1. For these assays, we used previously characterized firefly luciferase reporters containing 3'-UTRs of natural miRNA targets (e.g., *par-6* and *cg5281*, silenced by miR-1 and miR-12, respectively; and *nerfin-1* silenced by miR-9b and miR-279; Eulalio et al. 2007). The depletion of endogenous *Dm* AGO1 suppressed the silencing of all reporters, as expected, and both F-Luc expression and mRNA levels were restored (Fig. 2K,L; Supplemental Fig. S2C,D).

In depleted cells, a siRNA resistant version of *Dm* AGO1 fully restored silencing of all reporters (Fig. 2K,L; Supplemental Fig. S2C,D). By contrast, the double P1+P2 mutant did not restore silencing. The single pocket mutants partially rescued silencing to different extents depending on the reporters (Fig. 2K,L; Supplemental Fig. S2C,D). Thus, the integrity of the W-binding pockets is also required for *Dm* AGO1 to silence miRNA targets in complementation assays.

AGOs, GW182/TNRC6s and CCR4-NOT share a common mechanism to degrade mRNAs

It is well established that GW182/TNRC6 proteins and AGOs induce mRNA degradation through the 5'-to-3' decay pathway (Rehwinkel et al. 2005; Behm-Ansmant et al. 2006, Eulalio et al. 2007; Chen et al. 2009; Piao et al. 2010). In this pathway, deadenylation precedes decapping. Consequently, mRNAs degraded through this pathway accumulate in a deadenylated form in cells in which decapping is inhibited (Eulalio et al. 2007).

To investigate whether GW182/TNRC6 AGOs and NOT1 all elicit first deadenylation and then decapping, we sought to inhibit decapping. To this end, we overexpressed a DCP1 mutant that inhibits decapping in a dominant negative manner (DCP1* mutant; Chang et al. 2014; Supplemental Table S1). Tethered *Dm* GW182, AGO1 and NOT1 degraded the F-Luc-5BoxB-poly(A) reporter (Fig. 2M, lanes 3, 5, 7 vs. 1). Overexpression of the DCP1 mutant prevented this degradation in S2 cells. The reporter accumulated as a fast migrating form (Fig. 2M, lanes 4, 6 and 8 vs. 2), which corresponds to the deadenylated decay intermediate. Thus, as observed previously for GW182 and AGOs, tethered NOT1 caused deadenylation-dependent decapping.

Likewise, in human cells, MS2-tagged TNRC6A-SD, AGO2 and NOT1 degraded a β-globin reporter containing 6 binding sites for the MS2 protein in the 3' UTR (Fig. 2N, lanes 3, 5 and 7 vs.1). This degradation was prevented in cells expressing a DCP2 catalytic inactive mutant (DCP2*), and the reporter accumulated in the deadenylated form (Fig. 2N, lanes 4, 6 and 8). Our results indicate that miRNAs, AGOs, GW182/TNRC6 proteins and the CCR4-NOT complex share a common mechanism to degrade target mRNAs.

AGOs, GW182/TNRC6s and CCR4-NOT silence mRNAs translated via a scanning-independent mechanism

It has been reported that miRNAs silence gene expression by interfering with ribosome scanning (Meijer et al. 2013; Ricci et al. 2013; Fukao et al. 2014; Fukaya et al. 2014). To test whether AGO, GW182/TNRC6 and CCR4-NOT all require ribosome scanning to repress translation, we generated reporters translated via a scanning-independent mechanism.

The reporter for expression in *Dm* cells was derived from the F-Luc-5BoxB-$A_{95}C_7$-HhR reporter but contained a 5'-UTR of only 6 nucleotides (6nt-F-Luc-5BoxB-A_{95}-C_7-HhR (Fig. 3A). Notably, the translation efficiency of this reporter (this means F-Luc activity normalized to mRNA levels) was reduced only 1.4-fold relative to the parental reporter containing a 107-nt 5'-UTR (Supplemental Fig. S3A–D). Given that F-Luc proteins lacking the N-terminal 3–10 amino acids are inactive (Supplemental Fig. S3E–G; Sung and Kang 1998), and considering that the translation efficiencies of the reporters with a short and a long 5'-UTR are comparable (Supplemental Fig. S3A-D), it is reasonable to assume that a significant fraction of ribosomes initiate translation at the first AUG (or minimally at codon 3) in the mRNA with a 6-nt 5'-UTR. Consequently, translation of the 6nt-F-Luc-5BoxB-$A_{95}C_7$-HhR occurs without scanning. Accordingly, when the F-Luc ORF was replaced by HA-GST, the HA-tagged protein could be detected by western blotting using anti-HA antibodies further validating the conclusion that a substantial fraction of ribosomes start translation at the first AUG (Supplemental Fig. S3H).

Remarkably, the reporter containing a 6-nt 5'-UTR was repressed by tethered AGO1, GW182 and NOT1 (Fig. 3B) in the absence of mRNA degradation due to the lack of a poly(A) tail (Fig. 3B,C; Supplemental Fig. S4A). The repression was comparable to that observed for the parental reporter containing a 107-nt long 5'-UTR as well as for the reporter also containing a poly(A) tail, which was consequently degraded (Fig. 3B,C; Supplemental Fig. S4A).

The observation that a reporter translated via a scanning-independent mechanism is nevertheless repressed in *Dm* cells was unexpected given previous reports (Meijer et al. 2013; Ricci et al. 2013; Fukao et al. 2014; Fukaya et al. 2014) and prompted us to reanalyze the requirement for 43S scanning in human cells. To this end, we replaced the 5'-UTR of the R-Luc-5BoxB-MALAT1 reporter with a TISU motif (Translation Initiator of Short 5'-UTR, Fig. 3D), which directs efficient cap-dependent translation initiation of very short 5'-UTRs via a scanning- and eIF4A-independent mechanism (Elfakess et al. 2011; Sinvani et al. 2015). The translation efficiency of the TISU reporter was 8-fold lower relative to the parental reporter containing a 219-nt long 5'-UTR and the MALAT1 3'-end (Supplemental Fig. S3I–L). Nevertheless, TNRC6A-SD, AGO2 and NOT1 repressed the expression of these two reporters and that of a corresponding polyadenylated reporter to comparable extents. The polyadenylated reporter was degraded, whereas the reporters containing the MALAT1 3'-end were resistant to degradation (Fig. 3E,F; Supplemental Fig. S4B). Notably, insertion of an HA-tag immediately downstream of the first AUG in the TISU reporter, enabled detection of R-Luc by western blotting using anti-HA antibodies (Supplemental Fig. S3M), confirming that TISU directs translation initiation at the first AUG, and therefore in the absence of scanning.

We further confirmed that translation of the TISU reporter was independent of scanning, and thus of eIF4A, using silvestrol, a compound that stimulates eIF4A1/2 RNA binding activity reducing the pool of the protein available for translation (Bordeleau et al. 2008; Cencic et al. 2009). Silvestrol inhibited cap-dependent translation of the *Renilla* luciferase, but the translation driven by the TISU sequence was not inhibited (Fig. 3G; Supplemental Fig. S4C), as expected (Elfakess et al. 2011).

Because the translation efficiency of the reporter containing the TISU sequence was strongly reduced, to investigate the dependence on eIF4A for silencing we generated reporters containing 5'-UTRs with different degrees of secondary structure, which were expected to exhibit different eIF4A requirements (Supplemental Tables S2 and S3). In particular, we generated a reporter containing a 5'-UTR consisting of 18 CAA repeats, which is unlikely to adopt secondary structures, and its translation is thought to be independent of eIF4A (Meijer et al. 2013). This 5'-UTR was also shown to confer resistance to silencing (Meijer et al. 2013). Unexpectedly, translation of this reporter was partially inhibited by silvestrol (Fig. 4A; Supplemental Fig. S5A). Furthermore, the reporter coimmunoprecipitated with eIF4A2 almost as efficiently as a reporter containing a 219-nt long 5'-UTR (Fig. 4B,C), indicating that the CAA repeats do not confer independence from eIF4A in a cellular context. As a control, the corresponding TISU-containing reporter was the least affected by silvestrol treatment and did not efficiently associate with eIF4A2 in coimmunoprecipitation assays (Fig. 4A–C; Supplemental Fig. S5A), further confirming that translation driven by TISU does not require eIF4A activity. We observed that TNRC6A-SD, AGO2 and NOT1 repressed the CAA reporter without causing mRNA degradation due to the presence of the MALAT1 3'-end (Fig. 4D,E).

We also tested a 5'-UTR that contains four 12-nucleotide guanine quartet $(CGG)_4$ motifs in tandem, and is predicted to form G-quadruplex structures and thus requires eIF4A for translation (Cencic et al. 2009; Wolfe et al. 2014). Accordingly, the translation of this reporter was sensitive to silvestrol treatment (Fig. 4A; Supplemental Fig. S5A), and the reporter was efficiently coimmunoprecipitated with eIF4A2 (Fig. 4B,C). TNRC6A-SD, AGO2 and NOT1 repressed the CGG reporter to an extent comparable to that of the CAA reporter (Fig. 4F,G vs. Fig. 4D,E) as well as to the corresponding reporters containing a TISU motif or a 219-nt long 5'-UTR

(Supplemental Fig. S5B,C). The repression caused by the tethered proteins was not influenced by differences in the translation efficiencies of the reporters (Supplemental Fig. S5D–G).

In sum, AGO, GW182/TNRC6s and NOT1 silence mRNA targets independently of whether their translation requires ribosome scanning or eIF4A activity and independently of the 5'-UTR secondary structure.

eIF4A2 binding to mRNAs does not correlate with silencing efficiency

eIF4A2 was reported to be either recruited to or dislodged from silenced miRNA targets (Meijer et al. 2013; Fukao et al. 2014; Fukaya et al. 2014). To resolve this discrepancy, we investigated eIF4A2 association with the R-Luc-6MS2-A_{95}-MALAT1 reporter containing a 5'-UTR of 219-nt. This reporter associates with eIF4A2 and its translation is sensitive to silvestrol treatment (Fig. 4A–C). The reporter was silenced to different extents by tethered AGO2, TNRC6A-SD or NOT1 (Fig. 4H). Nevertheless, eIF4A2 associated with the reporter to comparable levels (Fig. 4I,J). Moreover, the association was comparable to that observed for the unrepressed reporter in cells expressing the MS2 protein alone (Fig. 4I,J). The possibility that the observed eIF4A2 binding is unspecific and occurs upon cell lysis is unlikely, as eIF4A2 did not associate with the TISU reporter (Fig. 4B,C). Thus, eIF4A2 association with mRNAs correlates with their sensitivity to silvestrol treatment but is neither enhanced nor reduced by silencing.

Ribosome scanning is not required for mRNA degradation caused by tethered AGOs, GW182/TNRC6s and NOT1

It has been reported that ribosome scanning is also required for miRNAs to degrade their targets (Meijer et al. 2013). Given our observations that translational repression

occurs independently of scanning, we next analyzed whether AGO, NOT1 and GW182/TNRC6 degraded polyadenylated mRNA reporters that are translated via a scanning-independent mechanism. In *Dm* cells, a polyadenylated reporter containing a 6-nt 5'-UTR was degraded by tethered AGO1, GW182 and NOT1 (Fig. 5A,B). Similarly, the TISU-R-Luc-6MS2-poly(A) reporter was also degraded by AGO2, TNRC6A-SD and NOT1 in human cells (Fig. 5C,D). Thus, in the absence of scanning, deadenylation and subsequent mRNA decay still occur.

We also investigated whether a β-globin reporter containing a 114-nt 5'-UTR could be degraded in the presence of silvestrol. This reporter was selected because it is very efficiently degraded by tethered AGO2, TNRC6A-SD and NOT1 in human cells. This degradation was not prevented in the presence of silvestrol (Fig. 5E–G), although translation of a cotransfected R-Luc reporter was inhibited 2.5-fold (Fig. 5E). Taken together, our results indicate that mRNA degradation induced by tethered AGO, GW182 and NOT1 does not require eIF4A activity or prior ribosomal scanning.

miRNAs silence reporters translated via a scanning independent mechanism

Next, we investigated whether miRNAs (as opposed to tethered silencing factors) also repress reporters translated via a scanning independent mechanism. To this end, we generated F-Luc-*nerfin-1* and F-Luc-*par6* reporters containing a 6nt 5'-UTR. These reporters were efficiently silenced by the corresponding miRNAs as the parental reporters containing 107-nt long 5'-UTR (Fig. 6A–D). Furthermore, the *nerfin-1* reporter was repressed predominantly at the translational level whereas the *par-6* reporter was predominantly degraded independently of the length of the 5'-UTR (Fig. 6A–D).

For expression in human cells, we generated a polyadenylated R-Luc reporter containing the TISU motif or a 219-nt 5'-UTR and eight *let-7* miRNA binding sites in the 3'-UTR. Both of these reporters were efficiently silenced and degraded by endogenous *let-7* independently of the length of the 5'-UTR (Fig. 6E,F). We conclude that miRNAs also silence mRNA reporters translated via scanning-independent mechanisms in both human and *Dm* cells.

The CCR4-NOT complex requires DDX6 to represses translation

We and others have proposed that the RNA helicase DDX6 acts downstream of the CCR4–NOT complex to mediate translational repression and stimulate decapping in human cells (Chen et al. 2014; Mathys et al. 2014; Rouya et al. 2014). To further confirm that DDX6 function lies downstream of CCR4-NOT we used tethering assays to analyze the repressive activity of a NOT1 mutant that is strongly impaired in the interaction with DDX6 (Fig. 6G, NOT1 Mut; Supplemental Table S1). The NOT1 mutant failed to repress the translation of the R-Luc-5BoxB-MALAT1 mRNA, which is not degraded (Fig. 6H,I). These results indicate that full length NOT1 requires interaction with DDX6 to repress translation of a reporter that is resistant to deadenylation. However, the NOT1 mutant was active when tethered to the corresponding polyadenylated reporter and the reporter was degraded (Fig. 6J,K). Thus, the deadenylase subunits degrade mRNA poly(A) tails independently of whether DDX6 is bound to NOT1.

Additionally, DDX6 depletion suppressed NOT1-mediated silencing of the R-Luc-5BoxB-MALAT1 reporter in human cells (Supplemental Fig. S6A,B), further validating the conclusion that NOT1 requires DDX6 to repress translation. In contrast to the results obtained in human cells, depletion of Me31B in S2 cells had a modest effect on the silencing activity of AGO1, GW182 and NOT1 tethered to a reporter

that is not degraded (Supplemental Fig. S6C,D). These results suggest the existence of alternative silencing mechanisms in these cells. Alternatively, the residual amounts of Me31B in depleted cells (<10% of control) might still be sufficient for silencing (Supplemental Fig. S6D).

DDX6 represses translation initiation independently of 43S scanning

If DDX6/Me31B act downstream of AGOs, GW182/TNRC6 and CCR4-NOT, it is expected that they also repress reporters translated via an eIF4A-independent mechanism. Consistent with this expectation, tethered DDX6 repressed the expression of all reporters containing the MALAT1 3'-end, including the TISU and CAA reporters in human cells (Fig. 7A–D). Thus, DDX6 represses translation in the absence of 43S scanning and deadenylation. DDX6 activity was only slightly impaired by the mutations that prevent binding to NOT1, consistent with the notion that DDX6 acts downstream of the CCR4-NOT complex (Fig. 7A–E). Similarly, Me31B repressed the F-Luc-5BoxB-A_{95}-C_7-HhR reporter independently of the length of the 5'-UTR (Fig. 7F), indicating that the ability to repress translation in the absence of scanning is conserved among DDX6 orthologs.

In yeast, Dhh1 (the DDX6 ortholog) was shown to repress translation at initiation (Coller and Parker 2005) or at elongation (Sweet et al. 2012). To help to resolve this discrepancy, we analyzed the association of the R-Luc-6MS2-A_{95}-MALAT1 reporter with polysomes upon repression by DDX6. Sucrose gradient analyses indicated that tethered DDX6 changed the distribution of the reporter in the polysome profile toward lighter polysomes/nonpolysomal fractions, indicating that DDX6 represses translation initiation in human cells (Fig. 7G,H; Supplemental Fig. S6E,F).

Discussion

AGOs require interaction with GW182/TNRC6 to mediate silencing

Previous studies reported that *Dm* AGO1 can repress miRNA targets independently of GW182/TNRC6 proteins and of the CCR4-NOT complex (Fukaya and Tomari 2012; Wu et al. 2013; Fukaya et al. 2014). Here we show that amino acid substitutions in the two W-binding pockets present on the surface of the PIWI domain of *Dm* AGO1 and *Hs* AGO2 (Schirle and MacRae 2012) abolish the binding of AGOs to GW182/TNRC6 proteins without disrupting miRNA loading. These mutations also abolish the silencing activity of AGOs in both tethering and complementation assays. The most parsimonious explanation for our results is that AGOs require interaction with GW182/TNRC6 proteins to mediate silencing. Although we cannot rule out the possibility that AGOs interact with another, yet-unidentified, W-containing protein using a mode of interaction similar to that used with GW182/TNRC6, we consider this possibility unlikely because AGOs, like GW182/TNRC6, NOT1 and miRNAs, degrade polyadenylated mRNA targets via the 5'-to-3' decay pathway. Furthermore, all three proteins as well as miRNAs repress the translation of mRNA targets that are refractory to deadenylation. Finally, we show that all three proteins and miRNAs repress and/or degrade mRNA targets that do not require eIF4A and 43S ribosomal scanning for translation. These results point to a common mechanism used by these proteins and miRNAs to mediate silencing.

eIF4A2 is unlikely to act as a repressor in the miRNA pathway

We and others have previously reported that human NOT1 interacts with DDX6 but not with eIF4A2, arguing against specific recruitment of eIF4A2 by NOT1 (Chen et al. 2014; Mathys et al. 2014; Rouya et al. 2014). Rather, eIF4A2 was shown to bind to

eIF4G and to stimulate translation (Chen et al. 2014; Mathys et al. 2014; Rouya et al. 2014; Fukao et al. 2014). Furthermore, although it has been reported that eIF4A2 is recruited to silenced mRNAs (Meijer et al. 2013), our results demonstrate that eIF4A2 efficiently associates with reporter mRNAs in the absence of silencing. The only mRNA reporter that did not associate efficiently with eIF4A2 was the reporter containing the TISU motif, as expected given that the translation of this reporter is insensitive to silvestrol treatment. Collectively, these observations suggest that recruitment of eIF4A2 by NOT1 is unlikely to represent a repressive mechanism acting in the miRNA pathway.

Ribosomal scanning is not a prerequisite for silencing

A previous study reported that mRNAs with highly structured 5'-UTRs, which depend on eIF4A for translation, are susceptible to silencing whereas mRNAs with unstructured 5'-UTRs are refractory to silencing in human cells (Meijer et al. 2013). By contrast, Ricci et al. failed to detect a correlation between silencing on 5'-UTR secondary structure in rabbit reticulocyte lysates. Like Ricci et al. (2013), we found no evidence for the requirement of structured 5' UTRs for silencing in either human or *Dm* cells. Our conclusions are based on the use of reporters that have very short 5'-UTRs (in *Dm* cells) or contain the TISU motif (human cells). These reporters direct translation independently of scanning. We could also not confirm that a reporter containing 18 CAA-repeats in the 5'-UTR is resistant to silencing as reported by Meijer et al. (2013). Furthermore, the CAA reporter was sensitive to silvestrol treatment and associated with eIF4A2, indicating that it partially depends on eIF4A activity for translation as reported by Pestova and Kolupaeva (2002).

In summary, all reporters tested in our study were partially degraded when they contained a poly(A) tail or were repressed predominantly at the translational level

when they contained 3' termini that conferred resistance to deadenylation. Similar results were obtained for tethered human AGO2, TNRC6, NOT1, DDX6 and their *Dm* orthologs as well as for miRNAs in the absence of tethering, indicating that 43S scanning is not a prerequisite for translational repression, deadenylation and decay of miRNA targets. The reasons for the differences from the results reported by Meijer et al. (2013) remain unclear, but one possible explanation is that Meijer et al. (2013) performed RNA transfections of the CAA reporter whereas our reporters were transcribed in the cells. Furthermore, RNA transfections preclude conclusions regarding changes in mRNA levels because of the inherent difficulty in estimating the fraction of the transfected mRNA that enters the cytoplasm and is ultimately assembled into functional RNPs and translated (Barreau et al. 2006).

Silencing does not require eIF4A activity

Previous studies made use of eIF4A inhibitors (hippuristanol, silvestrol or pateamine A) to demonstrate a role for eIF4A in silencing. However, this approach has yielded conflicting results, as these drugs were reported either to have no effect (Petersen et al. 2006) or to partially inhibit miRNA-mediated silencing (Meijer et al. 2013; Fukao et al. 2014). These discrepancies most likely result from the difficulty of finding appropriate normalization controls that are not affected by the treatment. By contrast, our conclusion that eIF4A activity is not required for silencing is based on the results obtained with the reporters containing a very short 5'-UTR (in *Dm* cells) or the TISU motif (human cells), which are not subjected to the normalization problem linked to the use of translational inhibitors. Using these reporters we determined that 43S scanning and eIF4A activity are not required for silencing.

We further confirmed the conclusion that eIF4A is not required for silencing through the analysis of mRNA levels, which in principle is not subject to

normalization caveats because eIF4A inhibitors do not cause global mRNA destabilization (Cencic et al. 2009). We observed that AGO2, GW182/TNRC6 and NOT1 degrade polyadenylated reporters in the presence of silvestrol. These results indicate that silencing complexes assemble and degrade the mRNA target also when translation and eIF4A activity are inhibited. In accordance with these results, we also show that miRNAs, AGO, GW182/TNRC6 and NOT1 degrade polyadenylated reporters that do not require scanning for translation.

Moreover, because eIF4A2 did not efficiently bind to the TISU-containing mRNA, our results indicate that miRNAs can repress translation by a mechanism that is independent of eIF4A2 and does not involve either eIF4A2 dissociation or recruitment. The observation that eIF4A1,2 dissociate from silenced mRNAs is based on studies performed in cell-free extracts, wherein the coupling between deadenylation and decapping is disrupted, as in these systems mRNAs are deadenylated but not further degraded (Fukao et al. 2014; Fukaya et al. 2014). Therefore, it is possible that the assembly and/or composition of silencing complexes varies when the relative abundance and/or activity of the factors involved is altered, resulting in different functional outcomes. Alternatively, our results with the reporters containing very short 5'-UTRs may have revealed the existence of a mechanism that acts independently of eIF4A or downstream of eIF4A dissociation.

The role of DDX6 in silencing

Our data together with previous studies indicate that human DDX6 is required for translational repression mediated by the CCR4-NOT complex in human cells (Chen et al. 2014; Matthys et al. 2014; Rouya et al. 2014). The contribution of DDX6 to this repression becomes apparent in particular for reporters that lack a poly(A) tail and hence are not degraded. In the presence of a poly(A) tail the dominant effect of the

CCR4-NOT complex is deadenylation and decay in human and *Dm* cells. mRNA destabilization is observed even when the NOT1-DDX6 interaction is disrupted, suggesting that the recruitment of decapping factors and XRN1 still occurs. Therefore, it is possible that in addition to DDX6, other factors are involved in coupling deadenylation to decapping. For example, the decapping activator Pat interacts with the CCR4-NOT complex (Jonas and Izaurralde 2013) and can also facilitate the recruitment of decapping factors to mRNAs undergoing deadenylation.

A question that remains unanswered is how DDX6 represses translation. Our polysome profiles indicate that DDX6 inhibits translation predominantly at initiation in human cells. Furthermore, we found that DDX6-mediated repression does not require ribosomal scanning, suggesting that DDX6 may interfere with eIF4E or eIF4G function. In this context, it is interesting that DDX6 interacts with the eIF4E-transporter protein (4E-T; Kamenska et al. 2014), an eIF4E-binding protein that competes with eIF4G for binding to eIF4E and represses translation initiation. However, depletion of 4E-T only partially alleviates silencing (Kamenska et al. 2014; D.K.O., D.B. and E.I. unpublished results), which implies that DDX6 may employ additional mechanisms to repress translation that are thus far unknown.

Through its interaction with the CCR4-NOT complex, DDX6 is likely to be involved in the repression of many mRNAs in addition to miRNA targets. Indeed the CCR4-NOT complex is recruited to specific mRNAs by numerous RNA-associated proteins, including Bicaudal-C, Smaug, CUP, Nanos, Pumilio and tristetraprolin (TTP; Barckmann and Simonelig 2013; Fabian et al. 2013). Thus, elucidating the precise mechanism by which DDX6 represses translation is expected to provide valuable insight into a widespread post-transcriptional repressive mechanism operating in eukaryotic cells.

Materials and Methods

DNA constructs

Plasmids for expression of λN-HA- and MS2-tagged proteins in *Dm* S2 and human cells, as well as miRNA reporters and luciferase reporters for tethering assays have been previously described (Rehwinkel at al. 2005; Eulalio et al. 2007; Eulalio et al. 2008; Braun et al. 2011; Zekri et al. 2013; Chen et al. 2014). We generated *Hs* AGO2 and *Dm* AGO1 mutants via site-directed mutagenesis. Protein mutants used in this study are listed in Supplemental Table S1. The reporters lacking the 5' UTR or containing the TISU motif, the $(CAA)_{18}$ repeats and the 12-nucleotide guanine quartet $(CGG)_4$ were generated by site-directed mutagenesis using the corresponding parental plasmids as template. The sequences of the corresponding 5'-UTRs are listed in Supplemental Table S3. Additional constructs used in this study are described in the Supplemental Material and Table S2.

Cell culture and transfections

The S2 cells were transfected in 6-well plates using Effectene transfection reagent (Qiagen). The human cells were transfected using Lipofectamine 2000 or TurboFect reagents (Life Technologies). In all experiments, firefly and *Renilla* luciferase activities were measured using the Dual-Luciferase Reporter Assay System (Promega), three days after transfection of the S2 cells and 48 hrs after transfection of the human cells. Total RNA was isolated from the S2 and human cells using TriFast (Peqlab Biotechnologies) and analyzed as described previously (Behm-Ansmant et al. 2006). All western blots were developed using the ECL western blotting detection system (GE Healthcare). Antibodies used in this study are listed in Supplemental Table S4. Silvestrol (MedChem Express, HY-13251) was resuspended in DMSO at 1 mg/ml concentration and added to the cells at a final concentration of 0.25 μM. The

treatment was for 16 hrs.

Tethering, complementation and coimmunoprecipitation assays

The interaction of AGO (wild-type or mutants) with endogenous miRNAs and GW182/TNRC6 was tested as described previously (Rehwinkel et al. 2005; Eulalio et al. 2008). Tethering assays in S2 cells and human cells were performed as described before (Braun et al. 2011). Detailed protocols can be found in the Supplemental Material. AGO1 complementation assays in S2 cells were performed as described previously (Huntzinger et al. 2013).

Polysome profiling in HEK293T cells

HEK293T cells (9×10^6/15-cm dish) were transfected with Lipofectamine 2000. The transfection mixtures contained 20 μg of the R-Luc-6xMS2-$(A)_{95}$-MALAT1 reporter, 4 μg of the pEGFP-N3-F-Luc transfection control and 6 μg of a plasmids expressing MS2-HA or MS2-HA-DDX6. Cells were treated with cycloheximide 48 hrs after transfection at a final concentration of 50 μg/ml for 30 min. Cell lysis and sucrose gradients were performed as described in the Supplemental Materials.

RNA immunoprecipitation in HEK293T cells

To study the association of eIF4A2 with mRNA reporters in HEK293T cells, cells (4×10^6/10-cm dish) were transfected with Lipofectamine 2000. The transfection mixtures contained 5 μg of pEGFP-N3-F-Luc transfection control reporter and any one of the following reporters: pCIneo-R-Luc-6xMS2-A_{95}-MALAT1 (10 μg), pCIneo-TISU-R-Luc-6xMS2-MALAT1 (8 μg), pCIneo-CAA-R-Luc-6xMS2-A_{95}-MALAT1 (15 μg) or pCIneo-CGG-R-Luc-6xMS2-A_{95}-MALAT1 (8 μg). A detailed description of the precipitation procedure in found in the Supplemental Material.

Supplemental Material

Supplemental Material includes five Figures, four tables, Supplemental Methods and Supplemental References.

Acknowledgements

We thank A. Boland for designing the Argonaute mutants. This work was supported by the Max Planck Society and by grants from the Deutsche Forschungsgemeinschaft (DFG, FOR855 and the Gottfried Wilhelm Leibniz Program awarded to E.I.).

REFERENCES

Ameres SL, Zamore PD. 2013. Diversifying microRNA sequence and function. *Nat Rev Mol Cell Biol* **14:** 475–488.

Barckmann B, Simonelig M. 2013. Control of maternal mRNA stability in germ cells and early embryos. *Biochim Biophys Acta* **1829:** 714–724.

Barreau C, Dutertre S, Paillard L, Osborne HB. 2006. Liposome-mediated RNA transfection should be used with caution. *RNA* **12:** 1790–1793.

Bawankar P, Loh B, Wohlbold L, Schmidt S, Izaurralde E. 2013. NOT10 and C2orf29/NOT11 form a conserved module of the CCR4-NOT complex that docks onto the NOT1 N-terminal domain. *RNA Biol* **10:** 228–244.

Behm-Ansmant I, Rehwinkel J, Doerks T, Stark A, Bork P, Izaurralde E. 2006. mRNA degradation by miRNAs and GW182 requires both CCR4:NOT deadenylase and DCP1:DCP2 decapping complexes. *Genes Dev* **20:** 1885–1898.

Bordeleau M-E, Robert F, Gerard B, Lindqvist L, Chen SMH, Wendel H-G, Brem B, Greger H, Lowe SW, Porco JA, et al. 2008. Therapeutic suppression of translation initiation modulates chemosensitivity in a mouse lymphoma model. *J Clin Invest* **118:** 2651–2660.

Braun JE, Huntzinger E, Izaurralde E. 2013. The role of GW182 proteins in miRNA-mediated gene silencing. *Adv Exp Med Biol* **768:** 147–163.

Braun JE, Huntzinger E, Fauser M, Izaurralde E. 2011. GW182 proteins directly recruit cytoplasmic deadenylase complexes to miRNA targets. *Mol Cell* **44:** 120–133.

Cencic R, Carrier M, Galicia-Vazquez G, Bordeleau M-E, Sukarieh R, Bourdeau

A, Brem B, Teodoro JG, Greger H, Tremblay ML, et al. 2009. Antitumor activity and mechanism of action of the cyclopenta[b]benzofuran, silvestrol. *PLoS ONE* **4:** e5223.

Chang C-T, Bercovich N, Loh B, Jonas S, Izaurralde E. 2014. The activation of the decapping enzyme DCP2 by DCP1 occurs on the EDC4 scaffold and involves a conserved loop in DCP1. *Nucleic Acids Res* **42:** 5217–5233.

Chekulaeva M, Mathys H, Zipprich JT, Attig J, Colic M, Parker R, Filipowicz W. 2011. miRNA repression involves GW182-mediated recruitment of CCR4–NOT through conserved W-containing motifs. *Nat Struct Mol Biol* **18:** 1218–1226.

Chen C-YA, Zheng D, Xia Z, Shyu A-B. 2009. Ago-TNRC6 triggers microRNA-mediated decay by promoting two deadenylation steps. *Nat Struct Mol Biol* **16:** 1160–1166.

Chen Y, Boland A, Kuzuoğlu-Öztürk D, Bawankar P, Loh B, Chang C-T, Weichenrieder O, Izaurralde E. 2014. A DDX6-CNOT1 complex and W-binding pockets in CNOT9 reveal direct links between miRNA target recognition and silencing. *Mol Cell* **54:** 737–750.

Chu C-Y, Rana TM. 2006. Translation Repression in Human Cells by MicroRNA-Induced Gene Silencing Requires RCK/p54. *PLoS Biol* **4:** e210.

Coller J, Parker R. 2005. General translational repression by activators of mRNA decapping. *Cell* **122:** 875–886.

Cooke A, Prigge A, Wickens M. 2010. Translational repression by deadenylases. *J Biol Chem* **285:** 28506–28513.

Eichhorn SW, Guo H, McGeary SE, Rodriguez-Mias RA, Shin C, Baek D, Hsu S-

H, Ghoshal K, Villén J, Bartel DP. 2014. mRNA destabilization is the dominant effect of mammalian microRNAs by the time substantial repression ensues. *Mol Cell* **56:** 104–115.

Elfakess R, Sinvani H, Haimov O, Svitkin Y, Sonenberg N, Dikstein R. 2011. Unique translation initiation of mRNAs-containing TISU element. *Nucleic Acids Res* **39:** 7598–7609.

Eulalio A, Rehwinkel J, Stricker M, Huntzinger E, Yang S-F, Doerks T, Dorner S, Bork P, Boutros M, Izaurralde E. 2007. Target-specific requirements for enhancers of decapping in miRNA-mediated gene silencing. *Genes Dev* **21:** 2558–2570.

Eulalio A, Huntzinger E, Izaurralde E. 2008. GW182 interaction with Argonaute is essential for miRNA-mediated translational repression and mRNA decay. *Nat Struct Mol Biol* **15:** 346–353.

Eulalio A, Huntzinger E, Nishihara T, Rehwinkel J, Fauser M, Izaurralde E. 2009. Deadenylation is a widespread effect of miRNA regulation. *RNA* **15:** 21–32.

Fabian MR, Sonenberg N. 2012. The mechanics of miRNA-mediated gene silencing: a look under the hood of miRISC. *Nat Struct Mol Biol* **19:** 586–593.

Fabian MR, Cieplak MK, Frank F, Morita M, Green J, Srikumar T, Nagar B, Yamamoto T, Raught B, Duchaine TF, et al. 2011. miRNA-mediated deadenylation is orchestrated by GW182 through two conserved motifs that interact with CCR4–NOT. *Nat Struct Mol Biol* **18:** 1211–1217.

Fabian MR, Frank F, Rouya C, Siddiqui N, Lai WS, Karetnikov A, Blackshear PJ, Nagar B, Sonenberg N. 2013. Structural basis for the recruitment of the human CCR4-NOT deadenylase complex by tristetraprolin. *Nat Struct Mol Biol* **20:**

735–739.

Fukao A, Mishima Y, Takizawa N, Oka S, Imataka H, Pelletier J, Sonenberg N, Thoma C, Fujiwara T. 2014. MicroRNAs trigger dissociation of eIF4AI and eIF4AII from target mRNAs in humans. *Mol Cell* **56:** 79–89.

Fukaya T, Tomari Y. 2012. MicroRNAs Mediate Gene Silencing via Multiple Different Pathways in Drosophila. *Mol Cell* **48:** 825–836.

Fukaya T, Iwakawa H-O, Tomari Y. 2014. MicroRNAs block assembly of eIF4F translation initiation complex in Drosophila. *Mol Cell* **56:** 67–78.

Guo H, Ingolia NT, Weissman JS, Bartel DP. 2010. Mammalian microRNAs predominantly act to decrease target mRNA levels. *Nature* **466:** 835–840.

Hendrickson DG, Hogan DJ, McCullough HL, Myers JW, Herschlag D, Ferrell JE, Brown PO. 2009. Concordant regulation of translation and mRNA abundance for hundreds of targets of a human microRNA. *PLoS Biol* **7:** e1000238.

Huntzinger E, Izaurralde E. 2011. Gene silencing by microRNAs: contributions of translational repression and mRNA decay. *Nat Rev Genet* **12:** 99–110.

Huntzinger E, Kuzuoğlu-Öztürk D, Braun JE, Eulalio A, Wohlbold L, Izaurralde E. 2013. The interactions of GW182 proteins with PABP and deadenylases are required for both translational repression and degradation of miRNA targets. *Nucleic Acids Res* **41:** 978–994.

Jackson RJ, Hellen CUT, Pestova TV. 2010. The mechanism of eukaryotic translation initiation and principles of its regulation. *Nat Rev Mol Cell Biol* **11:** 113–127.

Jonas S, Izaurralde E. 2013. The role of disordered protein regions in the assembly

of decapping complexes and RNP granules. *Genes Dev* **27:** 2628–2641.

Kamenska A, Lu W-T, Kubacka D, Broomhead H, Minshall N, Bushell M, Standart N. 2014. Human 4E-T represses translation of bound mRNAs and enhances microRNA-mediated silencing. *Nucleic Acids Res* **42:** 3298–3313.

Mathys H, Basquin J, Ozgur S, Czarnocki-Cieciura M, Bonneau F, Aartse A, Dziembowski A, Nowotny M, Conti E, Filipowicz W. 2014. Structural and Biochemical Insights to the Role of the CCR4-NOT Complex and DDX6 ATPase in MicroRNA Repression. *Mol Cell* **54:** 751–765.

Meijer HA, Kong YW, Lu WT, Wilczynska A, Spriggs RV, Robinson SW, Godfrey JD, Willis AE, Bushell M. 2013. Translational Repression and eIF4A2 Activity Are Critical for MicroRNA-Mediated Gene Regulation. *Science* **340:** 82–85.

Nishihara T, Zekri L, Braun JE, Izaurralde E. 2013. miRISC recruits decapping factors to miRNA targets to enhance their degradation. *Nucleic Acids Res* **41:** 8692–8705.

Pestova TV, Kolupaeva VG. 2002. The roles of individual eukaryotic translation initiation factors in ribosomal scanning and initiation codon selection. *Genes Dev* **16:** 2906–2922.

Petersen CP, Bordeleau M-E, Pelletier J, Sharp PA. 2006. Short RNAs Repress Translation after Initiation in Mammalian Cells. *Mol Cell* **21:** 533–542.

Piao X, Zhang X, Wu L, Belasco JG. 2010. CCR4-NOT deadenylates mRNA associated with RNA-induced silencing complexes in human cells. *Mol Cell Biol* **30:** 1486–1494.

Pillai RS, Artus CG, Filipowicz W. 2004. Tethering of human Ago proteins to

mRNA mimics the miRNA-mediated repression of protein synthesis. *RNA* **10:** 1518–1525.

Presnyak V, Coller, J. 2013. The DHH1/RCKp54 family of helicases: an ancient family of proteins that promote translational silencing. *Biochim Biophys Acta* **1829:** 817–823.

Rehwinkel J, Behm-Ansmant I, Gatfield D, Izaurralde E. 2005. A crucial role for GW182 and the DCP1:DCP2 decapping complex in miRNA-mediated gene silencing. *RNA* **11:** 1640–1647.

Ricci EP, Limousin T, Soto-Rifo R, Rubilar PS, Decimo D, Ohlmann T. 2013. miRNA repression of translation in vitro takes place during 43S ribosomal scanning. *Nucleic Acids Res* **41:** 586–598.

Rouya C, Siddiqui N, Morita M, Duchaine TF, Fabian MR, Sonenberg N. 2014. Human DDX6 effects miRNA-mediated gene silencing via direct binding to CNOT1. *RNA* **20:** 1398–1409.

Schirle NT, MacRae IJ. 2012. The crystal structure of human Argonaute2. *Science* **336:** 1037–1040.

Sinvani H, Haimov O, Svitkin Y, Sonenberg N, Tamarkin-Ben-Harush A, Viollet B, Dikstein R. 2015. Translational Tolerance of Mitochondrial Genes to Metabolic Energy Stress Involves TISU and eIF1-eIF4GI Cooperation in Start Codon Selection. *Cell Metab* **21:** 479–492.

Sung D, Kang H. 1998. The N-terminal amino acid sequences of the firefly luciferase are important for the stability of the enzyme. *Photochem Photobiol* **68:** 749–753.

Sweet T, Kovalak C, Coller J. 2012. The DEAD-box protein Dhh1 promotes

decapping by slowing ribosome movement. *PLoS Biol* **10:** e1001342.

Wilusz JE, JnBaptiste CK, Lu LY, Kuhn C-D, Joshua-Tor L, Sharp PA. 2012. A triple helix stabilizes the 3' ends of long noncoding RNAs that lack polyA tails. *Genes Dev* **26:** 2392–2407.

Wolfe AL, Singh K, Zhong Y, Drewe P, Rajasekhar VK, Sanghvi VR, Mavrakis KJ, Jiang M, Roderick JE, Van der Meulen J, et al. 2014. RNA G-quadruplexes cause eIF4A-dependent oncogene translation in cancer. *Nature* **513:** 65–70.

Wu P-H, Isaji M, Carthew RW. 2013. Functionally diverse microRNA effector complexes are regulated by extracellular signaling. *Mol Cell* **52:** 113–123.

Zekri L, Kuzuoğlu-Öztürk D, Izaurralde E. 2013. GW182 proteins cause PABP dissociation from silenced miRNA targets in the absence of deadenylation. *EMBO J* **32:** 1052–1065.

FIGURE LEGENDS

Figure 1. The W-binding pockets are required for AGOs to bind GW182/TNRC6 proteins. (*A*) Lysates from S2 cells expressing HA-tagged versions of MBP or AGO1 (wild-type or pocket mutants) were immunoprecipitated using an anti-HA antibody. Inputs (1% for the HA-tagged proteins and 2.5% for GW182) and immunoprecipitates (20% and 35%, respectively) were analyzed by western blotting using an anti-HA antibody. Endogenous GW182 was detected using anti-GW182 antibodies. The association between HA-AGO1 and endogenous miR-2a was analyzed by northern blotting. $tRNA^{Ala}$ served as a loading control. (*B–D*) Lysates from HEK293T cells expressing HA-tagged AGO2 (wild-type or pocket mutants) and GFP-tagged TNRC6 proteins were immunoprecipitated using an anti-HA antibody. HA-tagged MBP served as a negative control. Inputs (1.5% for the HA-tagged proteins and 2% for the GFP-tagged proteins) and immunoprecipitates (20% and 35%, respectively) were analyzed by western blotting using the corresponding antibodies. The presence of endogenous miR-16 in the immunoprecipitates was determined by northern blotting (D). $tRNA^{Ala}$ served as a loading control. AGO mutants are described in Supplemental Fig. S1 and Table S1.

Figure 2. The silencing activity of AGOs depends on the integrity of the W-binding pockets. (*A,B*) Tethering assay using the F-Luc-5BoxB-poly(A) reporter and λN-HA-AGO1 (wild-type or pocket mutants) in S2 cells. A plasmid expressing R-Luc served as a transfection control. (A) F-Luc activity and mRNA levels were normalized to those of the R-Luc transfection control and set to 100% in cells expressing the λN-HA peptide. (B) Northern blot of representative RNA samples. (*C,D*) Tethering assay

using the R-Luc-5BoxB-poly(A) reporter and λN-HA-AGO2 (wild-type or mutants) in human HEK293T cells. A plasmid expressing F-Luc served as a transfection control. R-Luc activity and mRNA levels were normalized to those of the F-Luc transfection control and analyzed as described in panels (A,B). (*E,F*) Tethering assay using the F-Luc-5BoxB-A_{95}-C_7-HhR reporter and λN-HA-AGO1 (wild-type or mutants) in S2 cells. Samples were analyzed as described in panels (A,B). (*G*) Western blot analysis showing the equivalent expression of the λN-HA-AGO1 proteins used in the tethering assays shown in panels (A,B,E,F). (*H,I*) Tethering assay using the R-Luc-5BoxB-MALAT1 reporter and λN-HA-AGO2 (wild-type or mutants) in HEK293T cells. (*J*) Western blot analysis showing the equivalent, expression of the λN-HA-AGO2 proteins used in the tethering assays shown in (C,D,H,I). (*K,L*) Complementation assays using F-Luc-*par6* reporter in S2 cells depleted of endogenous AGO1. Plasmids encoding HA-AGO1 (wild-type or mutants) or HA-MBP (as negative control) were included in the transfection mixtures as indicated. For each condition, firefly luciferase activities and mRNA levels were normalized to those of the *Renilla* luciferase transfection control and set to 100% in the absence of miR-1 (100% values are only shown for control cells). (K) Normalized firefly luciferase activities and mRNA levels. (L) Northern blot of representative RNA samples. In all panels bars represent mean values and error bars represent standard deviations from at least three independent experiments (see also Supplemental Fig. S2). (*M*) A tethering assay using the F-Luc-5BoxB-poly(A) reporter was performed in S2 cells. The transfection mixtures included plasmids expressing GFP or GFP-DCP1* as indicated. The panel shows a northern blot of representative RNA samples. The positions of the polyadenylated (An) and deadenylated (A_0) mRNA reporter are indicated on the right. (*N*) A tethering assay using the β-globin-6xMS2 reporter and MS2-tagged proteins was performed in

HEK293T cells. The transfection mixtures contained plasmids expressing wild-type DCP2 (-) or the catalytic DCP2* mutant (+). The panel shows a northern blot of representative RNA samples.

Figure 3. AGO, GW182/TNRC6 and NOT1 silence mRNA reporters translated via a scanning independent mechanism. (*A*) Schematic representation of the *Dm* reporters used in panels (B,C). (*B,C*) Tethering assay using the F-Luc-5BoxB reporters shown in panel (A) and λN-HA-tagged GW182, AGO1 and NOT1 in S2 cells. F-Luc activity and mRNA levels were normalized to those of the R-Luc transfection control and analyzed as described in Fig. 2A,B. Quantification of the corresponding northern blots is shown in Supplemental Fig. S4A. (*D*) Schematic representation of the reporters used in panels (E–G). (*E,F*) Tethering assay using the R-Luc-5BoxB reporters shown in panel (D) and λN-HA-tagged TNRC6A-SD, AGO2 and NOT1 in HEK293T cells. R-Luc activity and mRNA levels were normalized to those of the F-Luc transfection control and analyzed as described in Fig. 2C,D. The corresponding quantification of mRNA levels is shown in Supplemental Fig. S4B. (*G*) Human HEK293T cells were transfected with the R-Luc reporters shown in (D). A F-Luc reporter whose translation was dependent on the Hepatitis C virus (HCV) IRES was included as a control. One day after transfection, cells were treated with DMSO or Silvestrol. R-Luc activity in Silvestrol treated cells was normalized to that measured in control cells. The corresponding values for the HCV IRES-F-Luc reporter are shown in Supplemental Fig. S4C. In all panels, bars represent mean values and error bars standard deviations from at least three independent experiments.

Figure 4. eIF4A2 binding to mRNAs is not influenced by silencing. (*A*) HEK293T cells were transfected with the R-Luc-MS2-A_{95}-MALAT1 reporters containing the

indicated 5'-UTRs and HCV IRES-F-Luc control. Silvestrol treatment was performed as described in Fig. 3G. The corresponding values for HCV IRES-F-Luc reporter are shown in Supplemental Fig. S5A. (*B,C*) Lysates from HEK293T cells expressing the indicated R-Luc-MS2-A_{95}-MALAT1 reporters and a F-Luc transfection control were immunoprecipitated (IP) using anti-eIF4A2 antibodies. The RNAs coimmunoprecipitating with eIF4A2 were analyzed by northern blot. R-Luc mRNA levels were normalized to those of the F-Luc control. The normalized values in the IP were divided by those in the input and set to 100 for the reporter containing a 219-nt 5'-UTR. (*D–G*) Tethering assays using the indicated R-Luc-MS2-A_{95}-MALAT1 reporters and MS2-HA-tagged TNRC6A-SD, AGO2 and NOT1 in human cells. R-Luc activity and mRNA levels were normalized to those of the F-Luc transfection control and set to 100 in cells expressing MS2-HA. (E,G) Northern blots of representative RNA samples. (*H–J*) Lysates from HEK293T cells expressing R-Luc-MS2-A_{95}-MALAT1 reporter and MS2-HA tagged proteins were immunoprecipitated using anti-eIF4A2 antibody as described in panels (B,C). (H) Normalized R-Luc activities. (I) Representative western and northern blot of input and IP fractions. (J) The efficacy of the immunoprecipitation was analyzed as described in (B,C). Error bars represent standard errors from at least three independent experiments. Translation efficiencies for the reporters used in this figure are shown in Supplemental Fig. S5D–G.

Figure 5. Ribosome scanning is not required for degradation of silenced mRNAs. (*A,B*) Tethering assay using the 6nt-F-Luc-5BoxB-poly(A) reporter in S2 cells. Firefly luciferase activities and mRNA levels were normalized to those of the *Renilla* luciferase and analyzed as described in Fig. 2A,B. (*C,D*) Tethering assay using the TISU-R-Luc-6MS2-poly(A) reporter in human HEK293T cells. Samples were

analyzed as described in Fig. 2C,D. (*E–G*) Tethering assay using the β-globin-6MS2-poly(A) reporter in human HEK293T cells treated with Silvestrol or DMSO. Panel E shows the inhibitory effect of silvestrol on the translation of a cotransfected R-Luc reporter. In panels (F,G), samples were analyzed as described in Fig. 2C,D.

Figure 6. Ribosome scanning is not required for miRNA target degradation. (*A–D*) S2 cells were transfected with polyadenylated F-Luc-*nerfin-1* or F-Luc-*par6* reporters containing a 6-nt or 107-nt 5'-UTR and the corresponding miRNAs. A plasmid expressing *Renilla* luciferase (R-Luc) served as transfection control. Firefly luciferase activities and mRNA levels were normalized to those of the *Renilla* luciferase and set to 100 in the absence of miRNAs. Panels (A) and (C) show normalized firefly luciferase activities and mRNA levels. Northern blot analysis of representative RNA samples are shown in (B) and (D). (*E,F*) HEK293T cells were transfected with plasmids expressing the indicated R-Luc-*let-7* reporters or the corresponding reporters carrying mutations in the *let-7* binding sites and a plasmid expressing F-Luc as a transfection control. *Renilla* luciferase activities were normalized to those of the F-Luc and set to 100 in cells transfected with the reporter lacking the *let-7* binding sites and analyzed as described in (A–D). (*G*) Interaction of GFP-NOT1 (wild-type or a mutant that does not bind DDX6, Mut) with HA-DDX6 in human cells. (*H–K*) Tethering assay using the R-Luc-5BoxB reporters containing the MALAT1 3'-UTR (H,I) or a poly(A) tail (J,K) and λN-HA-NOT1 (wild-type or Mut). R-Luc activity and mRNA levels were normalized to those of the F-Luc transfection control and analyzed as described in Fig. 2C,D. See also Supplemental Fig. S6A–D.

Figure 7. DDX6 represses translation independently of ribosome scanning. (*A–D*) Tethering assay using the R-Luc-6xMS2-A_{95}-MALAT1 reporters containing the

indicated 5'-UTRs and MS2-HA-tagged DDX6 or a DDX6 mutant (DDX6*) that does not bind to NOT1 in human cells. R-Luc activity was normalized to that of the F-Luc control and analyzed as described in Fig. 2C,D. (*E*) Western blot showing the interaction of DDX6 or DDX6* with GFP-NOT1 in HEK293T cells. (*F*) Tethering assay using the F-Luc-5BoxB-A_{95}-C_7-Hhr reporters containing a 6-nt or a 107-nt 5'-UTR and λN-HA-Me31B in S2 cells. F-Luc activity and mRNA levels were analyzed as described in Fig. 2A,B. (*G,H*) Tethering assay using the R-Luc-6xMS2-A_{95}-MALAT1 reporter and MS2-DDX6 in human cells. In panel (G) Luciferase activity was analyzed as described in Fig. 2C. The association of the R-Luc reporter and the F-Luc control with polysomes was analyzed by sedimentation through a sucrose gradient. Panel (H) shows the amount of the R-Luc mRNA in each fraction normalized to the total amount across all fractions in cells expressing MS2 (black curve) or MS2-DDX6 (red curve). Lower panels show representative northern blots. Data corresponding to the F-Luc control and the corresponding ribosomal RNA profiles are shown in Supplemental Fig. S6E,F.

Kuzuoğlu-Öztürk et al. Fig. 1

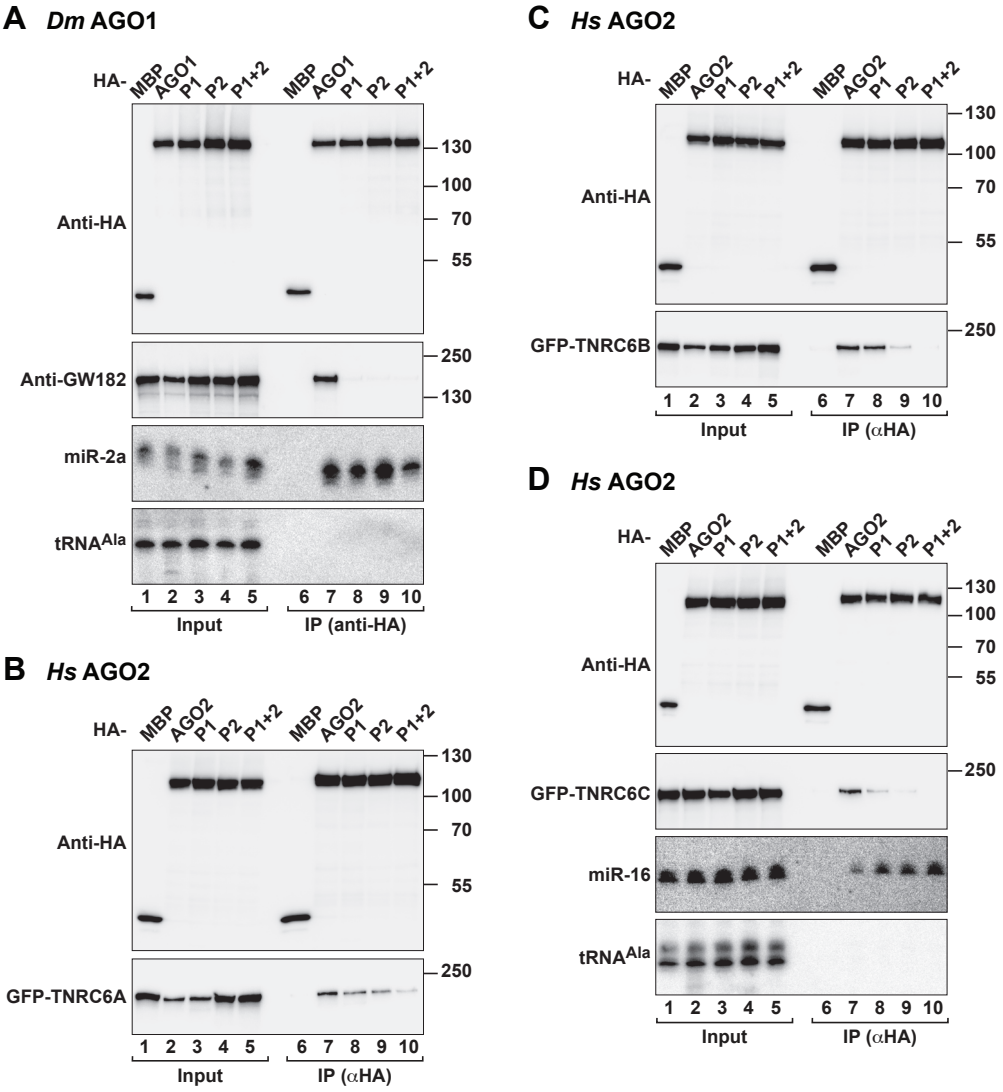

Kuzuoğlu-Öztürk et al. Fig. 2

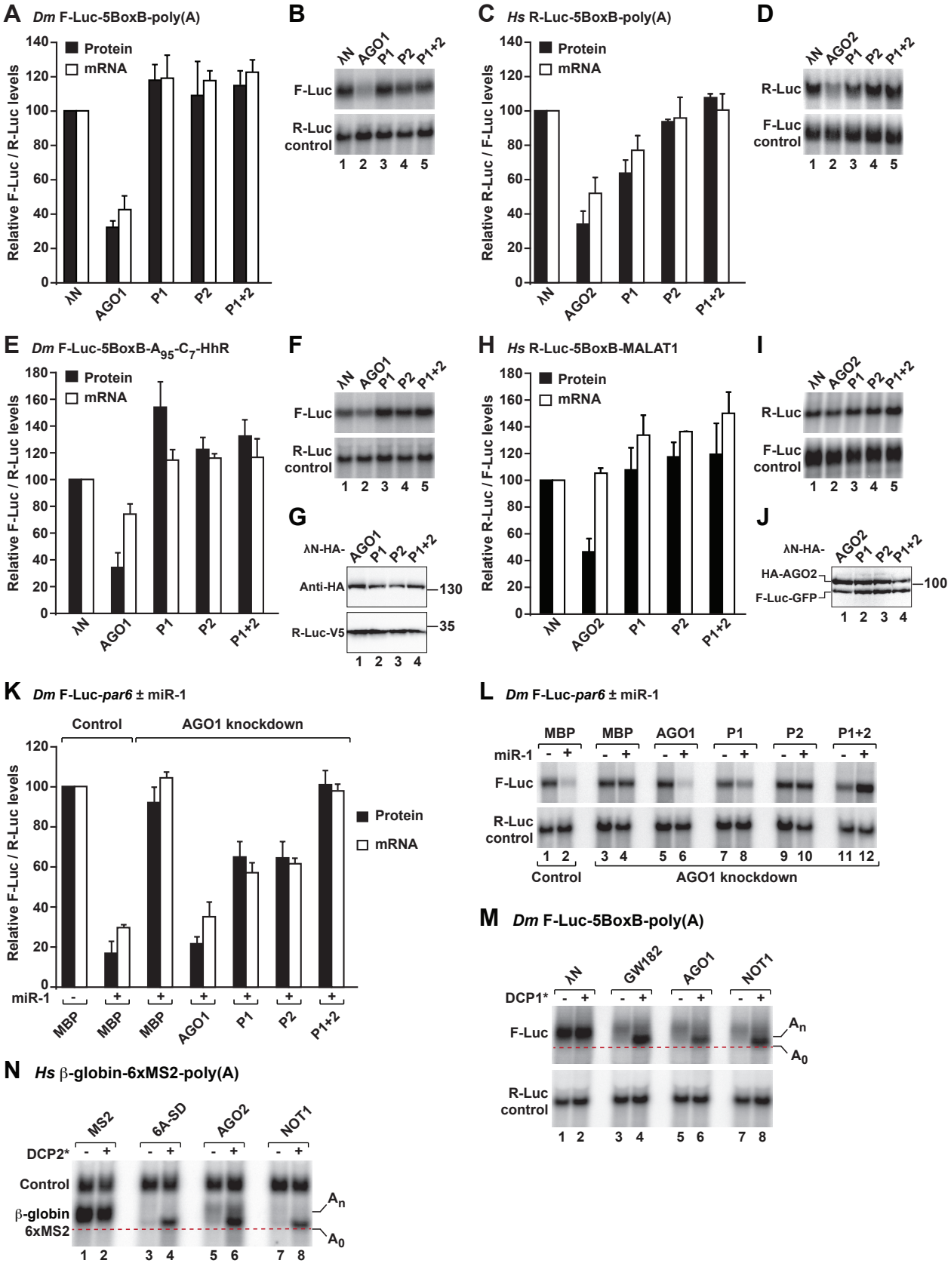

Kuzuoğlu-Öztürk et al. Fig. 3

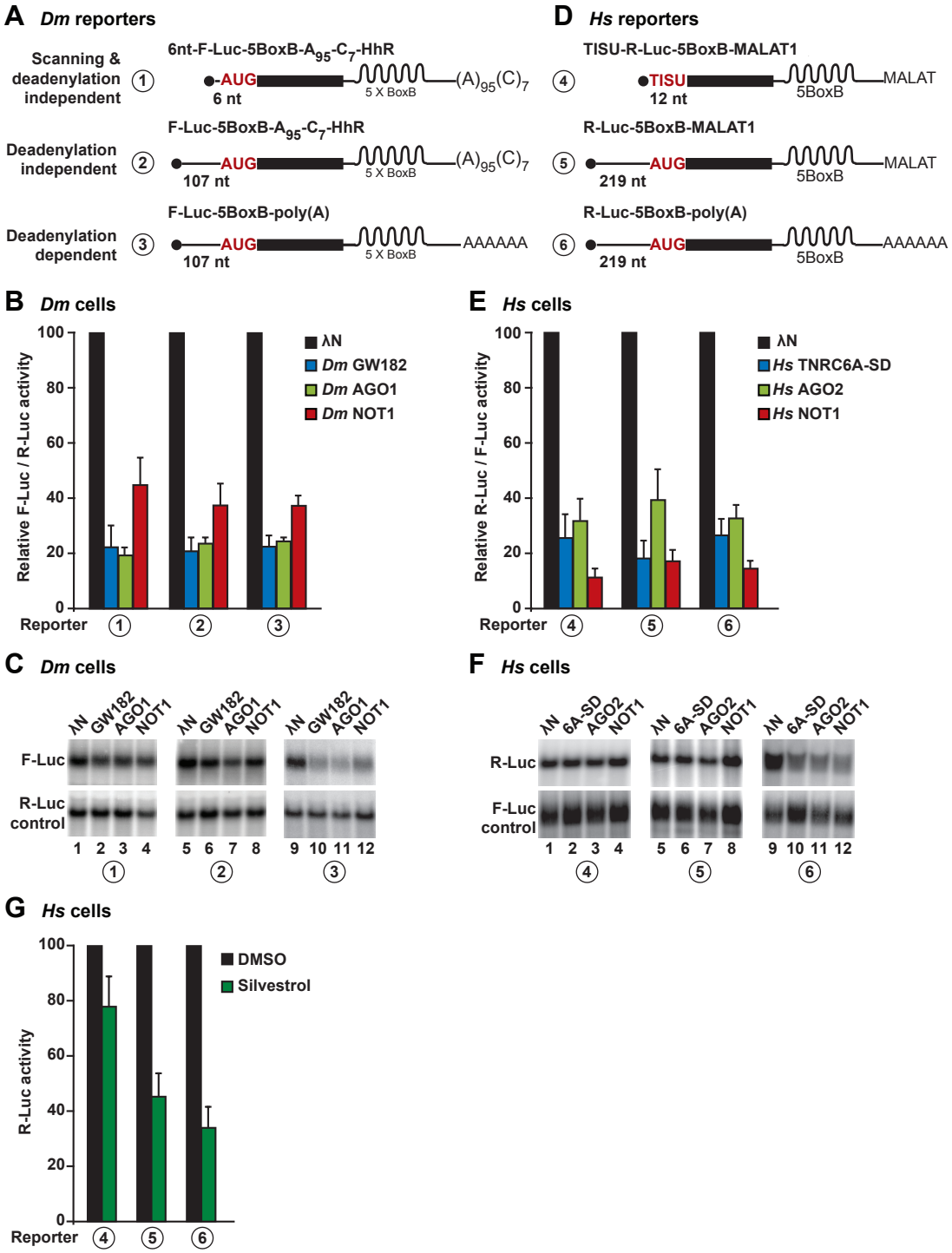

Kuzuoğlu-Öztürk et al. Fig. 4

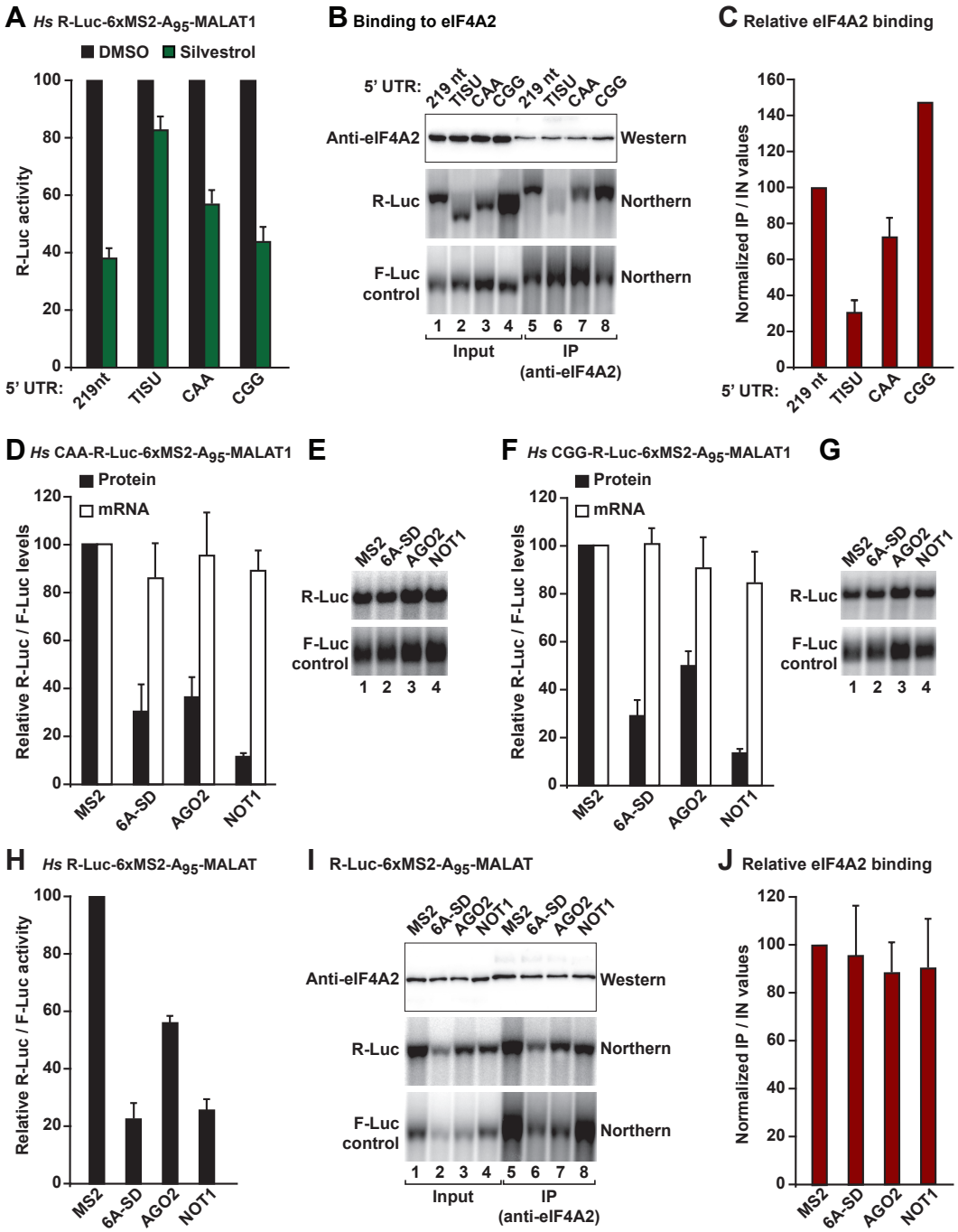

Kuzuoğlu-Öztürk et al. Fig. 5

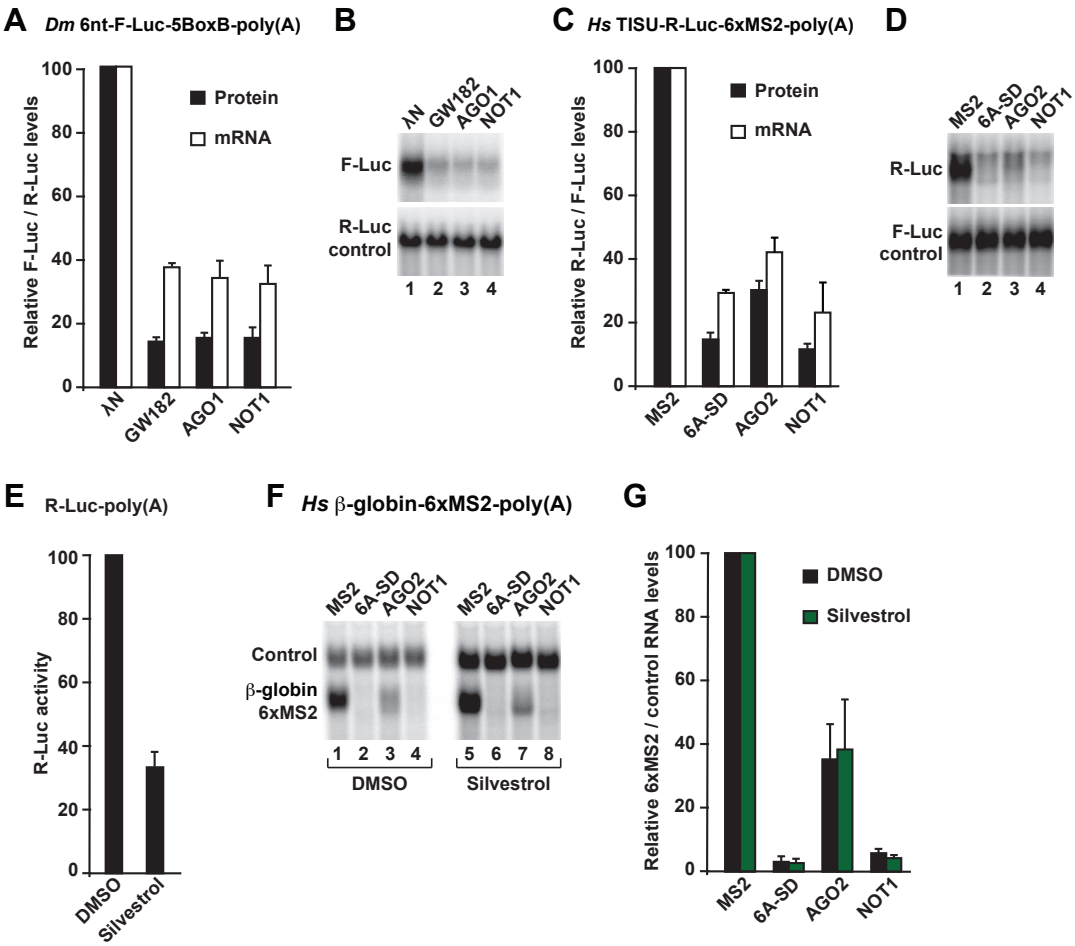

Kuzuoğlu-Öztürk et al. Fig. 6

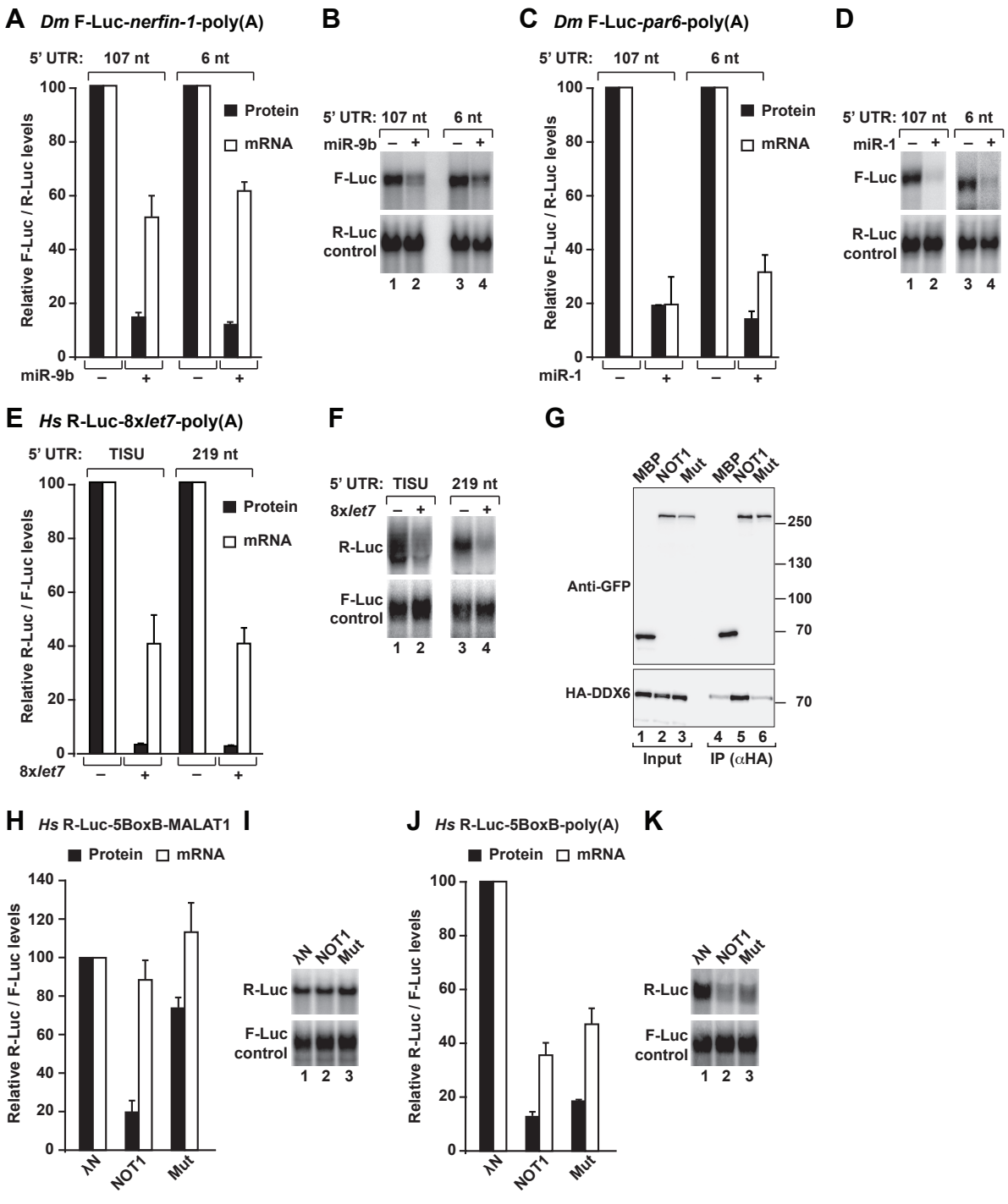

Kuzuoğlu-Öztürk et al. Fig. 7

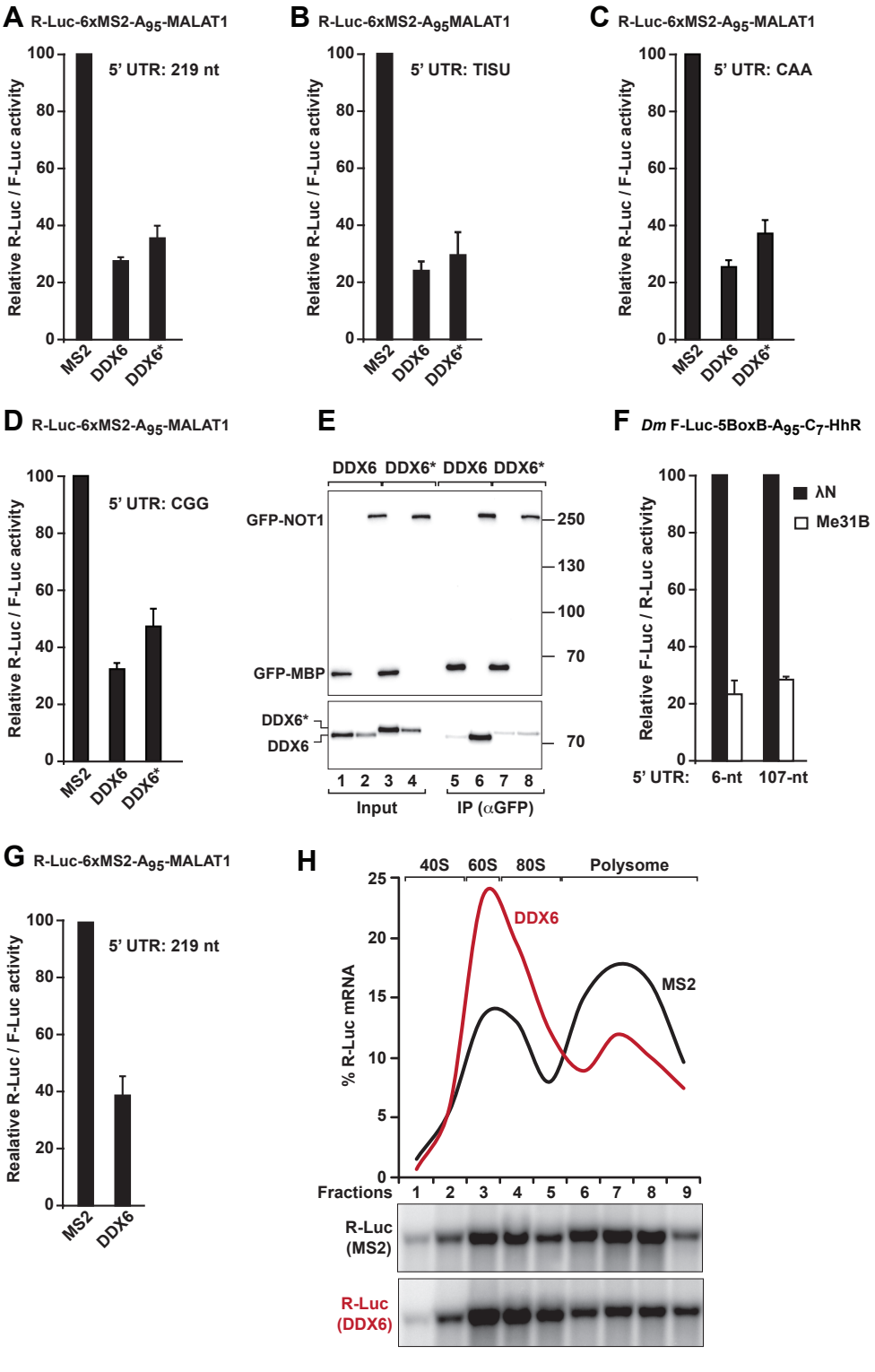

Supplemental Material

Supplemental Methods

DNA constructs

The plasmids for expression of the β-globin-6xMS2 and the control β-globin-GAP mRNAs in human cells were kindly provided by Dr J. Lykke-Andersen and were described previously (Lykke-Andersen et al. 2000). The plasmid for expression of the R-Luc-5BoxB-poly(A) reporter in human cells was kindly provided by Dr W. Filipowicz and was described previously (Pillai et al. 2004). The reporter containing the MALAT1 3'-end was generated as described in Bhandari et al. (2014). All constructs were fully sequenced to confirm the presence of the mutations and the absence of additional mutations. Protein mutants used in this study are listed in Supplemental Table S1.

Coimmunoprecipitation assays in S2 cells

The interaction of AGO1 (wild-type or mutants) with endogenous miRNAs and GW182 was tested as described previously (Rehwinkel et al. 2005; Eulalio et al. 2008). Briefly, 2.5×10^6 cells were seeded per well in 6-well plates and transfected with 1.5 µg HA-tagged proteins (MBP and AGO1 wild-type or mutants). Three days after transfection, the cells from 8 wells were pooled and resuspended in 2 ml of NET buffer (50 mM Tris-HCl (pH 7.5), 150 mM NaCl, 1 mM EDTA, 0.1% Triton X-100 and 10% glycerol) supplemented with protease inhibitors (Roche-EDTA free protease-inhibitor cocktail tablet). The cells were lysed by sonication (3 times 30 sec followed by 30 sec on ice) and incubated for 15 min on ice. Cell debris were removed by 15 min centrifugation at 16,000 *g* at 4°C. Aliquots for western (2.5%) and northern (5%) blot analysis were taken and the remaining cell lysate was incubated with anti-

HA antibody (8 µg, Covance) for 1 hour at 4°C. Next, protein G-Sepharose beads (GammaBind G-Sepharose, GE Healthcare) were added to the lysate (100 µl of a 50% slurry) and incubated for an additional hour. Beads were washed three times with NET buffer. An aliquot of beads (20%) was directly resuspended in SDS-PAGE sample buffer for western blot analysis. The remaining beads were resuspended in 200 µl of buffer containing 50 mM Tris-HCl (pH 8.0), 300 mM NaCl, 5 mM EDTA pH 8.0 and 0.5% SDS and treated with proteinase K (1.5 mg/ml) for 2.5 hours at 50°C. RNA isolation and analysis was performed as described by Rehwinkel et al. (2005). miR-2a and $tRNA^{Ala}$ were detected using radioactively labeled antisense oligonucleotide probes (miR-2a: GCTCATCAAAGCTGGCTGTGATA, $tRNA^{Ala}$: CTCACATGCTAAGCGAGCGCTCTAC).

Coimmunoprecipitation assays in HEK293T cells

To test the interaction of AGO2 (wild-type or mutants) with endogenous miRNAs and GFP-tagged TNRC6s, HEK293T cells (4×10^6/10-cm dish) were seeded one day before transfection using Turbofect (Thermo Scientific). The transfection mixtures contained plasmids expressing λN-HA tagged MBP (4 µg) or AGO2 [either wild-type (9 µg) or mutant (12 µg)] and 8 µg of plasmid expressing GFP-tagged TNRC6s. Cells were harvested 48 hours after transfection. Cells corresponding to 4 dishes were pooled, washed with PBS and lysed on ice for 15 min in 1 ml of NET buffer. Immunoprecipitations were performed as described for S2 cells. The oligonucleotide probes used for detection of miR-16 and $tRNA^{Ala}$ were as follows: CGCCAATATTTACGTGCTGCTA (miR-16) and CTCTACCGCTTGAGCTAATTCCCC ($tRNA^{Ala}$).

RNA immunoprecipitation in HEK293T cells

HEK293T cells (4×10^6/10-cm dish) were seeded 24 hours before transfection with Lipofectamine 2000. The transfection mixtures contained 5 µg of pEGFP-N3-F-Luc transfection control reporter and any one of the following reporters: pCIneo-R-Luc-6xMS2-A_{95}-MALAT1 (10 µg), pCIneo-TISU-R-Luc-6xMS2-MALAT1 (8 µg), pCIneo-CAA-R-Luc-6xMS2-A_{95}-MALAT1 (15 µg) or pCIneo-CGG-R-Luc-6xMS2-A_{95}-MALAT1 (8 µg). Cells were washed with ice-cold PBS and lysed in 500 µl of NET buffer for 15 min on ice. The cell debris were removed by a 15 min centrifugation at 16,000 *g* at 4°C. Aliquots (5%) were taken for western and northern blot analysis. The remaining lysate was incubated with 3 µg of anti-eIF4A2 antibody (Abcam, ab31218) for 2 hours at 4°C. Next, protein G-Sepharose beads were added to the lysate (100 µl of a 50% slurry) and incubated for additional 2 hours. After 2 hours incubation, beads were washed 3 times with NET buffer and resuspended in 1 ml NET buffer without detergent. An aliquot (20%) of the bead suspension was directly resuspended in SDS-PAGE sample buffer for western blot analysis. The remaining beads were used for RNA isolation using TriFast (Peqlab Biotechnologies). At this stage, samples were spiked with 4 µg of double stranded RNA. RNA samples were treated with DNase I (Turbo DNA-free kit, Ambion, AM1907). Input and precipitated fractions were analyzed by western and northern blotting. Note that the protein G-Sepharose beads used for RNA immunoprecipitation were preincubated with yeast RNA (250 µg of yeast RNA /100 µl of 50% slurry) and washed with PBS before use.

Tethering assays

For tethering assays in S2 cells, the transfection mixtures contained 0.1 µg of Firefly luciferase reporter plasmid (or 0.3 µg for the reporter containing a 6-nt 5'-UTR), 0.4

μg of *Renilla* luciferase transfection control and 4 ng of plasmids expressing the λN-HA tagged proteins. In the experiment described in Fig. 2M, the transfection mixtures contained in addition 0.95 μg of plasmids expressing GFP or GFP-DCP1 GSSG mutant (Chang et al. 2014). For tethering assays in human cells, HEK293T cells (0.8 × 10^6/well in six-well plates) were transfected using Lipofectamine 2000 (Life technologies). The transfection mixtures contained 0.25 μg of *Renilla* luciferase reporter plasmids, 0.25 μg of the pEGFP-N3-F-Luc transfection control and 0.1–1 μg of plasmids expressing λN-HA or HA-MS2 tagged proteins (0.1 μg for TNRC6A-SD, AGO2 and DDX6 and 1 μg for NOT1).

In the experiment described in Fig. 2N and Fig. 5E–G, the transfection mixtures contained 0.5 μg of the control plasmid (β-globin-GAP), 0.5 μg of the plasmid encoding the β-globin-6xMS2, plasmids expressing the MS2-HA tagged proteins (0.2 μg for TNRC6A-SD, 0.1 μg for AGO2 and 2 μg for CNOT1). In Fig. 2N, the transfection mixtures contained in addition plasmids expressing HA-tagged DCP2 (either wild-type or catalytically inactive DCP2* mutant; 1 μg).

Polysome profiling in HEK293T cells

HEK293T cells (9 × 10^6/15-cm dish) were seeded one day before transfection with Lipofectamine 2000 (Life Technologies). The transfection mixtures contained 20 μg of the R-Luc-6xMS2-$(A)_{96}$-MALAT1 reporter, 4 μg of the pEGFP-N3-F-Luc transfection control and 6 μg of a plasmids expressing MS2-HA or MS2-HA-DDX6. Cells were treated with cycloheximide 48 hrs after transfection at a final concentration of 50 μg/ml for 30 min. Cells were washed once with ice-cold PBS (containing 50 μg/ml cycloheximide), and lysed in 300 μl of ice-cold buffer containing 10 mM Tris-HCl (pH 7.4), 10 mM NaCl, 1.5 mM $MgCl_2$, 0.5% Triton X-

100, 2 mM DTT, 1 U/µl RiboLock RNase inhibitor, 0.5% Na-deoxycholate and 50 µg/ml cyclohexamide for 10 min on ice. The cell debris were removed by a 10 min centrifugation at 10,000 *g* at 4°C. The supernatants were layered on top of a linear 10–50% (w/v) sucrose gradient (prepared using Gradient Master 107ip Biocomp) in 10 mM Tris-HCl (pH 7.4), 75 mM KCl, 1.5 mM $MgCl_2$, and 50g/ml cycloheximide. Centrifugation was carried out in a Beckmann, SV55Ti rotor at 41,000 r.p.m. for 2 hours at 4°C.

Fractions were collected using a density-gradient fractionation system (Teledyne Isco), and polysome profiles were monitored by absorbance of light at 254 nm. Fractions were spiked with 10 µg of double-stranded RNA and treated with proteinase K (0.1 mg/ml, in 10 mM Tris-HCl (pH 8.0), 5 mM EDTA, 0.5% SDS) for 30 min at 42°C. Total RNA was isolated by two rounds of phenol:chloroform extraction followed by one chloroform extraction. RNA samples were treated with DNase I and analyzed by northern blotting.

Supplemental references

Bhandari D, Raisch T, Weichenrieder O, Jonas S, Izaurralde E. 2014. Structural basis for the Nanos-mediated recruitment of the CCR4-NOT complex and translational repression. *Genes Dev* **28:** 888–901.

Cope CL, Gilley R, Balmanno K, Sale MJ, Howarth KD, Hampson M, Smith PD, Guichard SM, Cook SJ. 2014. Adaptation to mTOR kinase inhibitors by amplification of eIF4E to maintain cap-dependent translation. *J Cell Sci* **127:** 788–800.

Lykke-Andersen J, Shu MD, Steitz JA. 2000. Human Upf proteins target an mRNA for nonsense-mediated decay when bound downstream of a termination codon. *Cell* **103:** 1121–1131.

Miyoshi K, Okada TN, Siomi H, Siomi MC. 2009. Characterization of the miRNA-RISC loading complex and miRNA-RISC formed in the Drosophila miRNA pathway. *RNA* **15:** 1282–1291.

Okamura K, Ishizuka A, Siomi H, Siomi MC. 2004. Distinct roles for Argonaute proteins in small RNA-directed RNA cleavage pathways. *Genes Dev* **18:** 1655–1666.

Supplemental Table S1. Mutants used in this study.

Protein	**Name of the construct**	**Mutations**
Dm AGO1 NM_166020.1	P1	P714G + A744F
	P2	L819Y
	P1+2	P714G + A744F + L819Y
Hs AGO2	P1	P593A + A623F
	P2	L697Y + K663A
	P1+2	P593A + A623F + L697Y + K663A
Dm DCP1 NM_137998.2	DCP1* (GSSG)	R70G + L71S + N72S + T73G
Hs DCP2 AY135173.1	DCP2*	E148Q
Hs NOT1 EF553522.1	NOT1 Mut	F1101S + N1105A + K1114A + R1138A + N1144A + F1145A + K1276A + F1281A + E1284A
Hs DDX6 NM_004397.3	DDX6*	R94E + F101D + Q322A + N324A + R375A
Hs TNRC6A AY035864.1	TNRC6A-SD	Residues 1272–1709

Supplemental Table S2. Reporters used in this study.

Organism	Name of the Reporter	Vector
Dm	F-Luc-5BoxB-poly(A)	pAc5.1C
	F-Luc-5BoxB-A_{95}-C_7-HhR	pAc5.1C
	6nt-F-Luc-5BoxB-A_{95}- C_7-HhR	pAc5.1C
	6nt-F-Luc-5BoxB-poly(A)	pAc5.1C
	F-Luc-poly(A)	pAc5.1C
	F-Luc-*par6*-poly(A)	pAc5.1C
	6nt-F-Luc-*par6*-poly(A)	pAc5.1C
	R-Luc- A_{95}-HhR	pAc5.1C
	F-Luc-*Nerfin-1*-poly(A)	pAc5.1C
	6nt-F-Luc-*Nerfin-1*-poly(A)	pAc5.1C
	F-Luc-*cg5281*-poly(A)	pAc5.1C
Hs	R-Luc-5BoxB-poly(A)	pCI-neo
	R-Luc-5BoxB-MALAT1	pCI-neo
	TISU-R-Luc-5BoxB-MALAT1	pCI-neo
	R-Luc-poly(A)	pCI-neo
	R-Luc-6xMS2	pCI-neo
	R-Luc-6xMS2-MALAT1	pCI-neo
	R-Luc-6xMS2-A_{95}- MALAT1	pCI-neo
	TISU-R-Luc-6xMS2- MALAT1	pCI-neo
	TISU-R-Luc-6xMS2	pCI-neo
	CAA-R-Luc-6xMS2-A_{95}-MALAT1	pCI-neo
	CGG-R-Luc-6xMS2bs-A_{95}-MALAT1	pCI-neo
	β-Globin-GAPDH (Control)	pcDNA3.1
	β-Globin-6xMS2-poly(A)	pcDNA3.1
	F-Luc	pEGFP-N3
	R-Luc-8xlet7	pCI-neo
	R-Luc-Scramble	pCI-neo
	TISU-R-Luc-8xlet7	pCI-neo
	TISU-R-Luc-Scramble	pCI-neo

Supplemental Table S3. Sequence of 5'-UTRs used in this study.

Organism	Reporter	Sequence
Dm	107nt-F-Luc	aucacuaccguuugaguucuugugcuguguggauacuccucccgacacaaagccgcucc aucagccagcagucgucuaauccagagaccccggaucgggguaccaac**AUG**GCU
	6nt-F-Luc	aucacu**AUG**GCU
Hs	219nt-R-Luc	gucagaucacuagaagcuuuauugcgguaguuuaucacaguuaaauugcuaacgcaguc agugcuucugacacaacagucucgaacuuaagcugcagugacucucuuaagguagccuu gcagaaguuggucgugaggcacugggcagguguccacucccaguucaauuacagcucuu aaggcuagaguacuuaauacgacucacuauaggcuagccacc**AUG**GCU
	TISU-R-Luc	gucagauccaag**AUG**gcggcaGCU
	CAA-R-Luc	gucagauccaacaacaacaacaacaacaacaacaacaacaacaacaacaacaacaacaacaa gccacc**AUG**GCU
	CGG-R-Luc	gucagauccuagguugaaaguacuuugacggcggcggcggucaaucuuacggcggcgg cggacauagauacggcggcggcgguagaaacuacggcggcggcggauuagaauaguaaa gccacc**AUG**GCU

Residues in red indicate the transcription start site. There are 3 potential start sites for the *Dm* reporters. The first AUG is indicated in bold and underlined.

Supplemental Table S4. Antibodies used in this study.

Antibody	**Source**	**Catalog Number**	**Dilution**	**Monoclonal/ Polyclonal**
Anti-HA-HRP (For western blots)	Roche	12 013 819 001	1:5,000	Monoclonal
Anti-HA (for immunoprecipitations)	Covance	MMS-101P		Mouse Monoclonal
Anti-GFP (for Western blotting)	Roche	11 814 460 001	1:2,000	Mouse Monoclonal
Anti-GFP (for immunoprecipitations)	In house			Rabbit polyclonal
Anti-tubulin	Sigma Aldrich	T6199	1:10,000	Monoclonal
Anti-mouse IgG-HRP	GE Healthcare	NA931V	1:10,000	Sheep Polyclonal
Anti-rabbit IgG-HRP	GE Healthcare	NA934V	1:10,000	Donkey Polyclonal
Anti-*Hs* DDX6	Bethyl Laboratories	A300-461A	1:3,000	Rabbit polyclonal
Anti-*Hs* PABP	Abcam	ab21060	1:5,000	Rabbit polyclonal
Anti-*Dm* GW182	In house		1:2,000	Rabbit polyclonal
Anti-*Dm* NOT1	Kind gift from E. Wahle		1:1,000	Rabbit polyclonal
Anti-*Dm* AGO1	Abcam	Ab5070	1:1,000	Rabbit polyclonal
Anti-*Dm* Me31B	In house		1:3,000	Rabbit polyclonal
Anti-*Hs* TNRC6	Bethyl Laboratories	A302-329A	1:1000	Rabbit polyclonal
Anti-*Hs* eIF4A2 (for immunoprecipitations)	Abcam	Ab31218		Rabbit polyclonal
Anti-*Hs* eIF4A2 (for Western blotting)	In house		1:1,000	Rabbit polyclonal
Anti-V5	AbD Serotec	MCA1360GA	1:5,000	Mouse Monoclonal

Figure S1. The W-binding pockets are conserved in the AGO proteins that interact with GW182/TNRC6 proteins. (*A*) Ribbon representation of *Hs* AGO2 (PDB ID: 4OLB) showing the position of the tryptophan-binding pockets. Residues lining the pockets are shown as green sticks or as red sticks when the residues were mutated. The tryptophan residues are shown as blue sticks. (*B*) Structure-based sequence alignment of the PIWI domain of human AGO1, AGO2, AGO3 and AGO4, *Drosophila melanogaster* AGO1 and AGO2, *Neurospora crassa* (*Nc*) QDE2, *Schizosaccharomyces pombe* AGO1 and the human PIWI-like clade. Residues lining the tryptophan-binding pockets 1 and 2 are shaded in pale green and orange, respectively. Residues forming the catalytic tetrad are highlighted in red. Residues mutated in this study are marked with a red asterisk. Residues lining the W-binding pockets are conserved in *Hs* AGO1, AGO3 and AGO4 as well as in *Dm* AGO1, which is the AGO protein dedicated to the miRNA pathway in *Dm* (Okamura et al. 2004; Schirle and MacRae 2012). By contrast, these residues are less conserved in the PIWI clade of Argonaute proteins and in *Dm* AGO2, which do not interact with GW182 (Behm-Ansmant et al. 2006; Miyoshi et al. 2009). To abolish the interaction of *Hs* AGO2 and *Dm* AGO1 with GW182 proteins, we substituted a proline residue in pocket 1 with glycine to prevent hydrophobic stacking interactions with tryptophan residues and an alanine with a bulky phenylalanine to block tryptophan binding (mutant P1). In pocket P2, we substituted a leucine residue with a bulky tyrosine to block the pocket and a lysine residue with alanine to prevent hydrophobic stacking interactions (mutant P2). See Supplemental Table S1.

Kuzuoğlu-Öztürk et al. Fig. S2

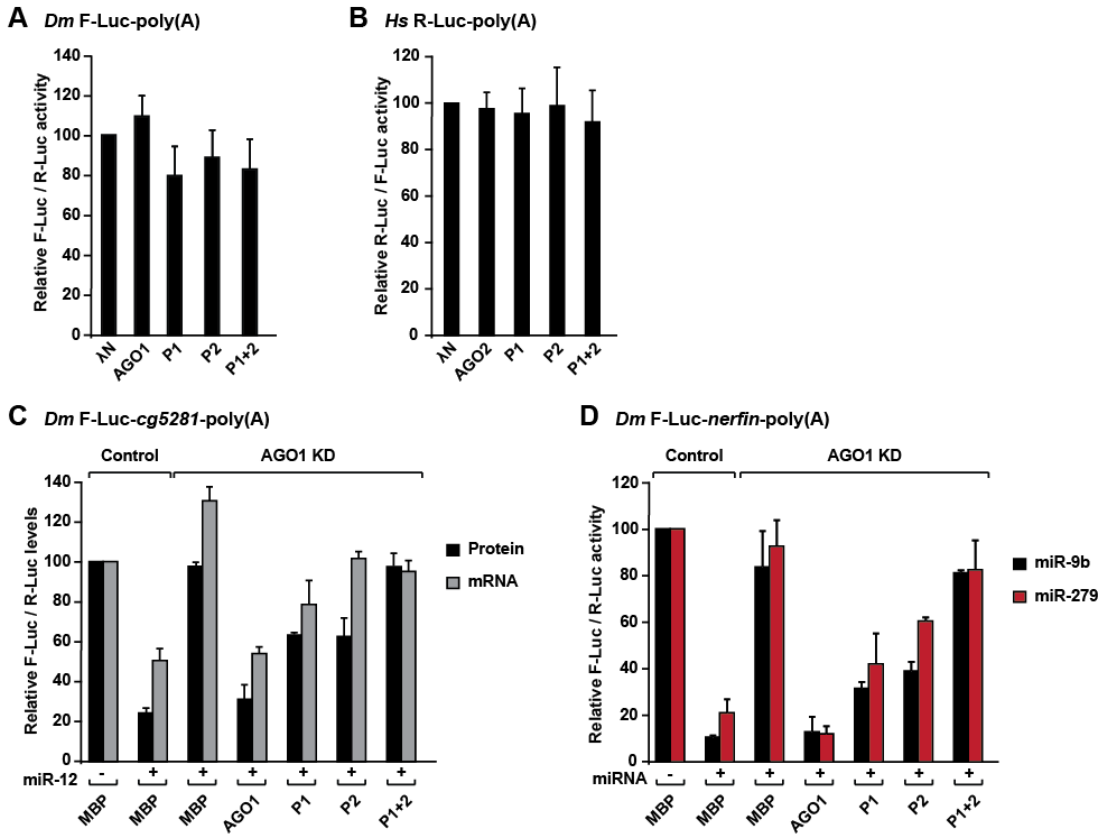

Figure S2. The silencing activity of AGOs depends on the integrity of the W-binding pockets. (*A,B*) Tethering assay using the indicated luciferase reporters lacking the 5BoxB sites in *Dm* and human cells expressing λN-HA-tagged *Dm* AGO1 and *Hs* AGO2 (wild-type or mutants), respectively. The assays with the corresponding reporters containing 5BoxB sites are shown in Fig. 2A–D. Samples were analyzed as described in Fig. 2. (*C*) Complementation assay. Control S2 cells (treated with β-Gal siRNA) or cells depleted of endogenous AGO1 were transfected with a mixture of three plasmids: one expressing the F-Luc-*cg5281* reporter; another expressing miR-12 primary transcript or the corresponding empty vector; and a third expressing *Renilla* luciferase (R-Luc). Plasmids encoding HA-AGO1 (wild-type or the indicated pocket mutants) or HA-MBP (as negative control) were included in the transfection mixtures as indicated. For each condition, firefly luciferase activities and mRNA

levels were normalized to those of the *Renilla* luciferase transfection control and set at 100% in the absence of the miR-12. Panel (C) shows normalized firefly luciferase activities and mRNA levels. Error bars represent standard deviations from at least three independent experiments (see also Fig. 2K,L). (*D*) A complementation assay was carried out using the F-Luc-*nerfin-1* reporter and miR-9b or miR-279. F-Luc activity was analyzed as described in (C).

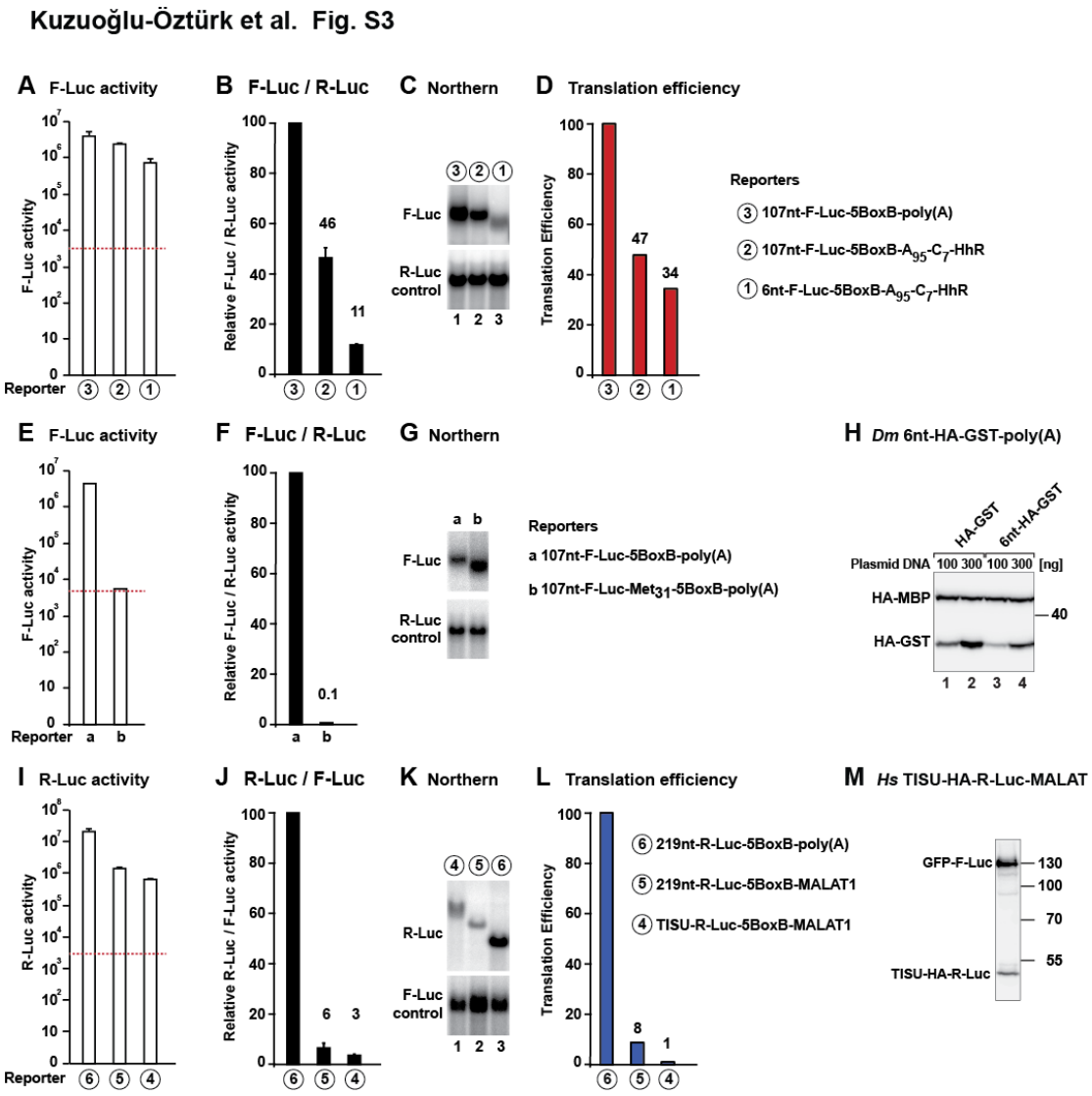

Figure S3. Translation efficiencies of the reporters used in Fig. 3. (*A–D*) S2 cells were transfected with the F-Luc-5BoxB reporters shown in Fig. 3A. (A) Absolute

values of luciferase activity (not normalized). Background levels are indicated by a dashed red line. (B) Luciferase activity normalized to that of the R-Luc transfection control and set to 100 for the polyadenylated reporter containing a 107-nt 5'-UTR. (C) Northern blot of representative RNA samples. (D) The translation efficiency for each reporter was calculated by dividing the normalized values for F-Luc activity shown in (B) by the normalized mRNA levels, shown in (C). Translation efficiencies were set to 100 for the polyadenylated reporter containing a 107-nt 5'-UTR. Note that although the translation efficiency of the reporters lacking a poly(A) tail is reduced, the absolute F-Luc values are three orders of magnitude greater than background levels (panel A). (*E–G*) A 107-nt-F-Luc-5BoxB-poly(A) reporter containing a N-terminally truncated F-Luc ORF starting at Met31 is expressed but no F-Luc activity is detected above background (red dashed line). These results indicate that F-Luc activity will not be detectable if ribosomes bypass the first AUG and start translation at the first in-frame Met. (*H*) Western blot analysis showing the expression of HA-GST reporters containing 5'-UTRs of 107-nt (lanes 1 and 2) and 6-nt (lanes 3 and 4). Transfection mixtures contained either 100 or 300 ng of reporter plasmids. HA-MBP served as a transfection control. (*I–L*) HEK293T cells were transfected with R-Luc-5BoxB reporters shown in Fig. 3D. R-Luc activity, mRNA levels and translation efficiencies were analyzed as described in (A–D). (*M*) Western blot analysis showing the expression of TISU-HA-R-Luc. F-Luc-GFP served as a transfection control. In all panels, the mean values are indicate above the corresponding bars.

Kuzuoğlu-Öztürk et al. Fig. S4

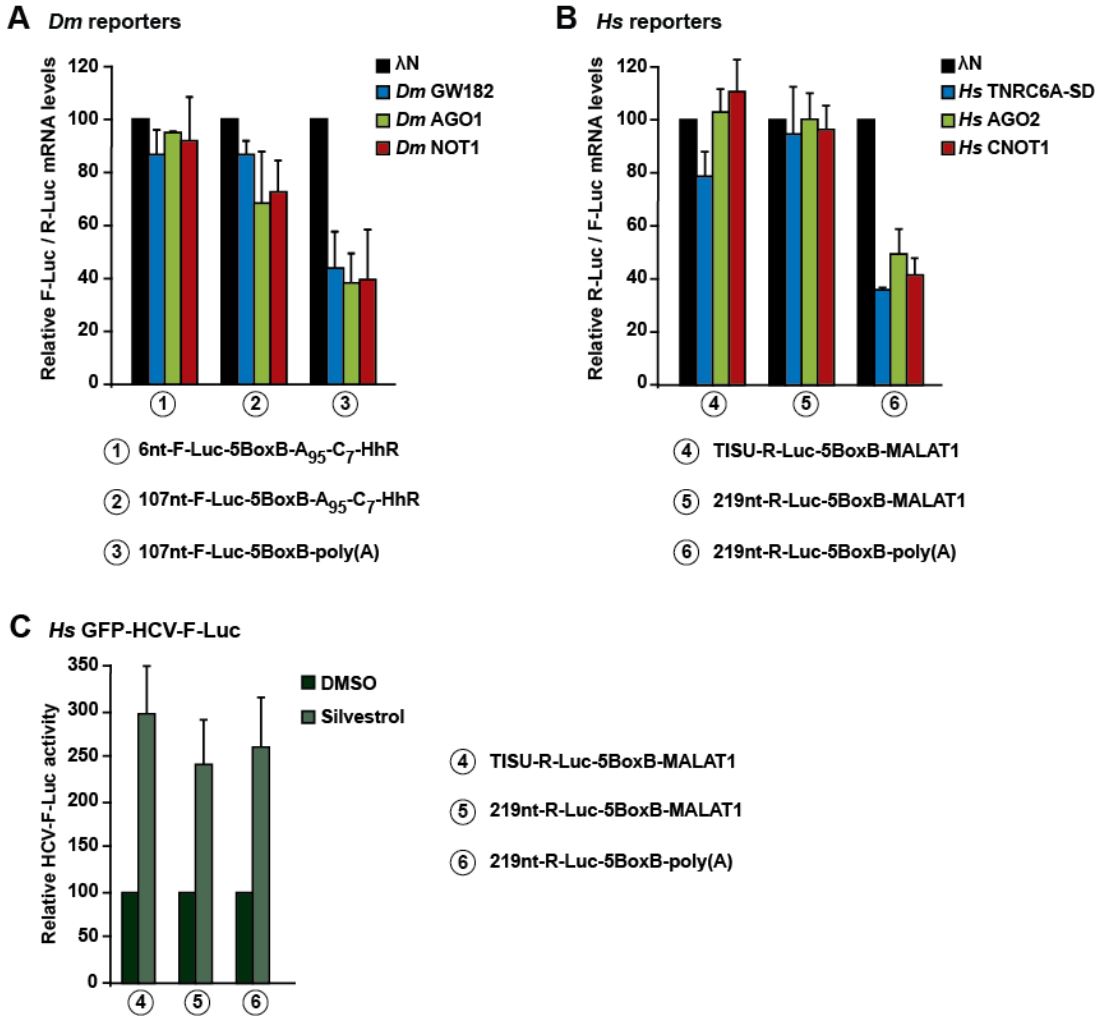

Figure S4. AGO, GW182/TNRC6 and NOT1 silence mRNA reporters translated via a scanning independent mechanism. (*A,B*) Normalized luciferase mRNA levels corresponding to the experiment shown in Fig. 3B and Fig. 3E, respectively. Error bars represent standard deviations from at least three independent experiments. (*C*) Luciferase activity for a bicistronic GFP-IRES$_{HCV}$-F-Luc reporter, which served as a transfection control in the experiment shown in Fig. 3G. Note that when cap-dependent translation is inhibited by silvestrol treatment, IRES-mediated translation increases, as reported before (Cope et al. 2014), which precludes the use of IRES reporters as normalization controls. Therefore, R-Luc and F-Luc activities measured in silvestrol treated cells were normalized to the respective values obtained in control

cells treated with DMSO.

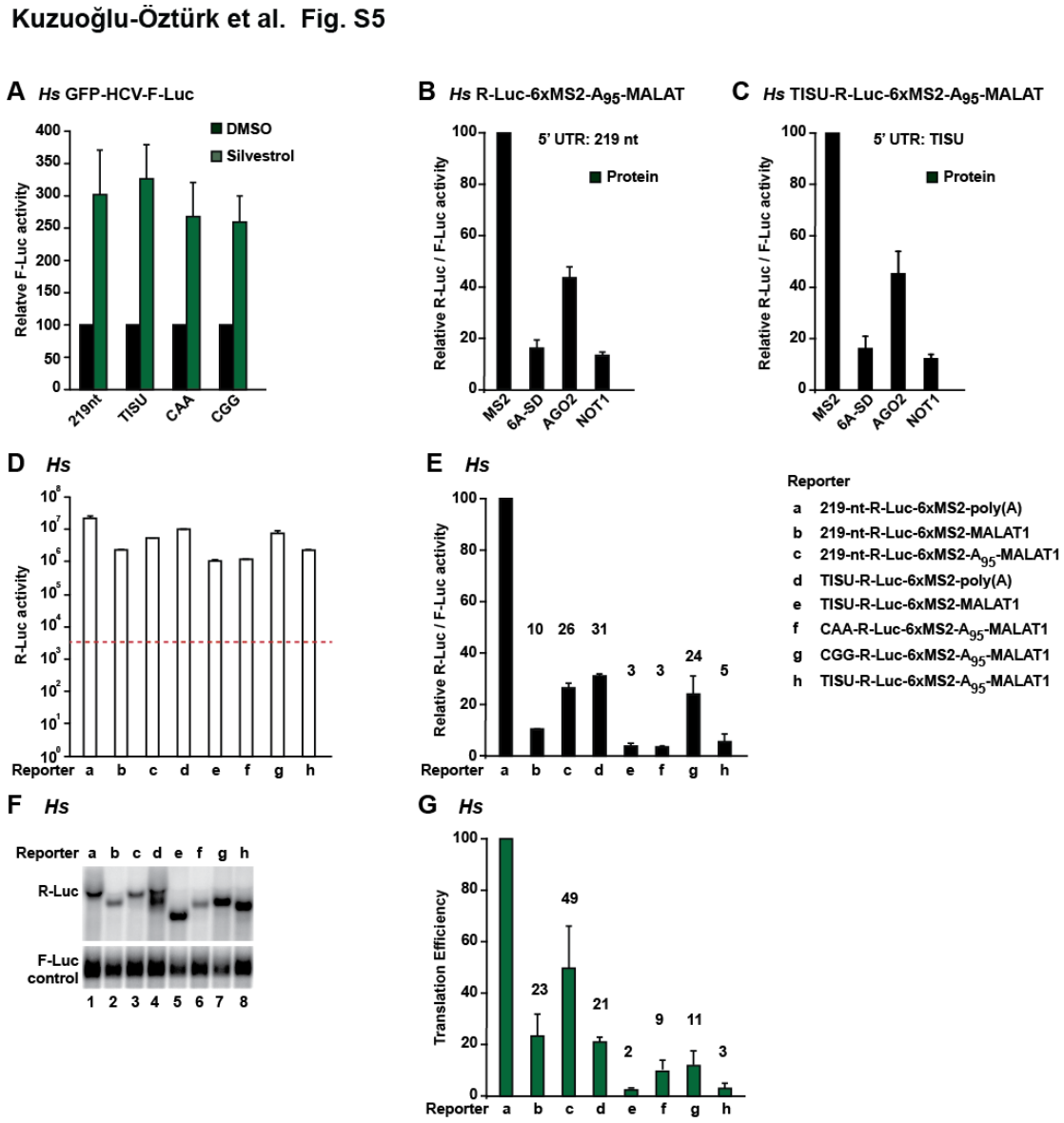

Figure S5. AGO, GW182/TNRC6 and NOT1 silence mRNA reporters independently of mRNA secondary structure in the 5'-UTR. (*A*) Luciferase activity for a bicistronic GFP-IRES$_{HCV}$-F-Luc reporter, which served as a transfection control in the experiments shown in Fig. 4A. F-Luc activities measured in silvestrol treated cells were normalized to the respective values obtained in control cells treated with DMSO as described in Supplemental Fig. S4C. (*B,C*) Tethering assays using the indicated R-Luc-MS2-A$_{95}$-MALAT1 reporters and MS2-HA-tagged TNRC6A-SD, AGO2 and

NOT1 in human cells. R-Luc activity was normalized to that of the F-Luc transfection control and set to 100 in cells expressing MS2-HA. (*D–G*) The translation efficiency of the MS2 reporters shown in Fig. 4 was analyzed as described in Supplemental Fig. S3A–D. Note that although the translation efficiency of the TISU reporters is very low, the absolute R-Luc values are 2–3 orders of magnitude greater than background levels (panel D). In all panels bars represent mean values, which are indicated above the bars.

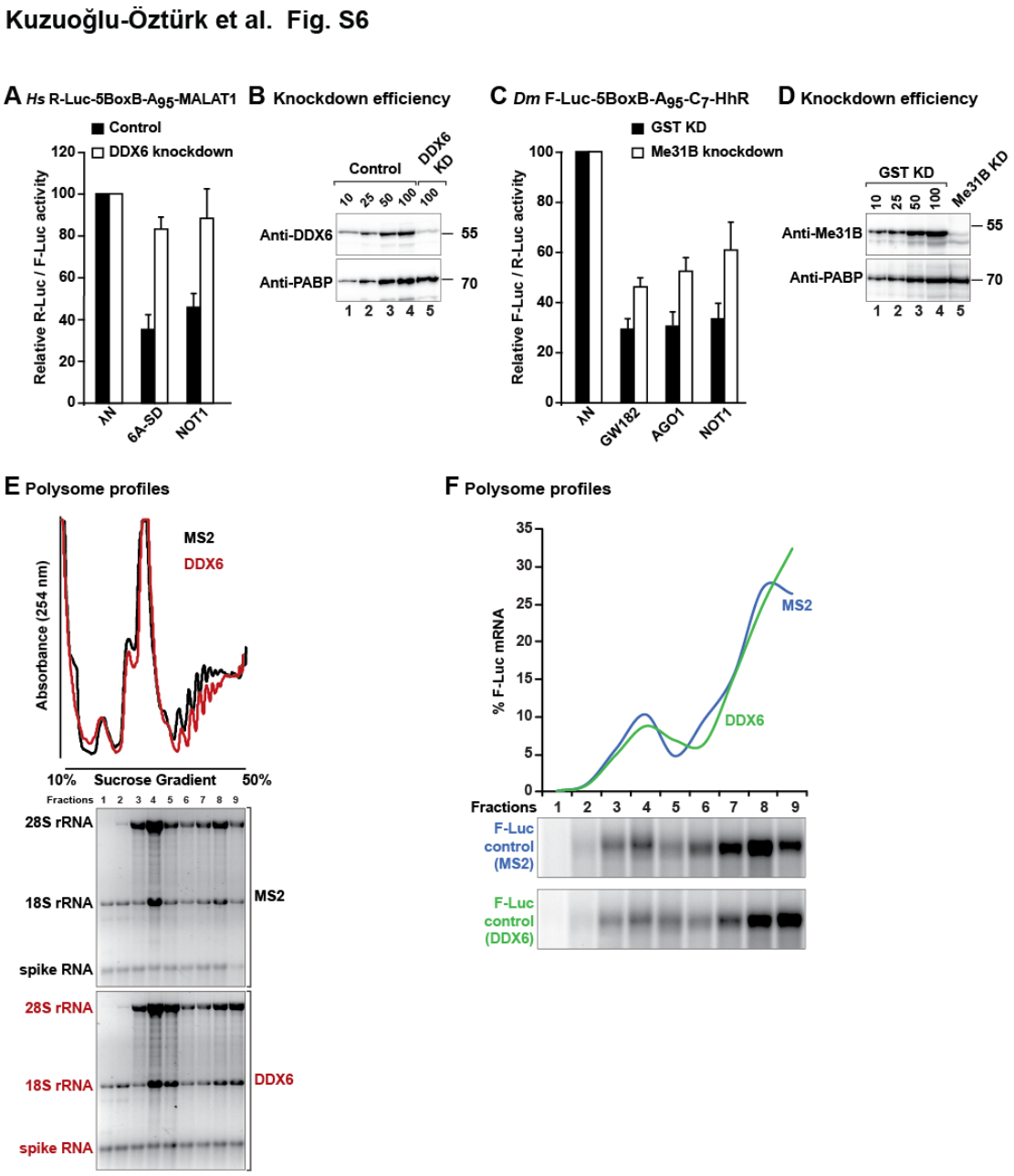

Figure S6. DDX6 represses translation initiation. (*A*) Tethering assay using the R-Luc-5BoxB-A_{95}-MALAT1 reporter and λN-HA tagged TNRC6A-SD and NOT1 in control HeLa cells or cells depleted of DDX6. Samples were analyzed as described in Fig. 2. (*B*) Western blot showing DDX6 knockdown efficiency. Dilutions of control cell lysates were loaded in lanes 1–4 to estimate the efficacy of the depletion. PABP served as a loading control. (*C*) Tethering assay using the F-Luc-5BoxB-A_{95}-C_7-HhR reporter and λN-HA tagged GW182, AGO1 and NOT1 in control S2 cells or cells

depleted of Me31B. Samples were analyzed as described in Fig. 2. (*D*) Western blot showing Me31B knockdown efficiency. Dilutions of control cell lysates were loaded in lanes 1–4 to estimate the efficacy of the depletion. PABP served as a loading control. (*E*) Polysome profiles corresponding to Fig. 7G. The absorbancy at 254 nm of each fraction was quantitated and normalized to the total intensity across all fractions. The presence of 18S and 28S rRNAs in each fraction was analyzed on denaturing agarose gels. The spike RNA added to the fractions prior RNA isolation indicated. (*F*) The amount of F-Luc control reporter corresponding to Fig. 7G was quantify in each fraction of the gradient and normalized to the total amount across all fractions.